Author:
Gallio, Andrea E

Title:
A framework for the investigation of heme homeostasis through genetically encoded heme sensors

A framework for the investigation of heme homeostasis through genetically encoded heme sensors

Andrea Eugenio Gallio

A dissertation submitted to the University of Bristol in accordance with the requirements for award of the degree of Doctor of Philosophy in the Faculty of Science

School of Chemistry
United Kingdom
June 2023

Word count: 27,176

Abstract

To meet the logistical needs of supply and demand for heme, organisms need to make it, move it to the right place, and degrade it when necessary. More specifically, the provision and distribution of heme must be coupled with the synthesis of heme proteins and meticulously regulated so that heme-tuned cellular pathways are only activated on demand. However, how cells handle heme to meet transient cellular requirements is yet to be clarified and represents a long-lasting question in bioinorganic chemistry. This study deploys a genetically encoded heme sensor (mAPXmEGFP) and Fluorescence Lifetime Imaging Microscopy to investigate the cellular mechanisms controlling heme bioavailability. The analysis is paired with the contextualisation of the data within the intricate network of regulation that oversees the levels of key proteins (*i.e.* ALAS1, HO-1, HO-2, and GAPDH) and their coordination with an intracellular heme buffering system that ensures heme homeostasis. Further, the implications and possible drawbacks deriving from the deployment of genetically encoded sensors in live cells is discussed and explored.

Author's declaration

I declare that the work in this dissertation was carried out in accordance with the requirements of the University's *Regulations and Code of Practice for Research Degree Programmes* and that it has not been submitted for any other academic award. Except where indicated by specific reference in the text, the work is the candidate's own work. Work done in collaboration with, or with the assistance of, others, is indicated as such. Any views expressed in the dissertation are those of the author.

Signed:
Date: 9^{th} June 2023

School of Chemistry
University of Bristol
Bristol
BS8 1TS
United Kingdom

Acknowledgements

I would like to thank my supervisor Prof. Emma Raven for her unconditional support through conventional and less-conventional times as well as the countless invaluable opportunities she put within my reach.

I gratefully acknowledge Prof. Andrew J. Hudson (University of Leicester) for the numerous exciting exchanges of ideas and his selfless guidance.

I am grateful for the very good friends I made along the way. Noa, you make every day interesting.

Finally, the tireless support of my family. Francesco, Barbara, and Alessia. I would be nowhere without you being there for me.

This work is dedicated to Nonna Maria

Contents

List of figures

List of tables

List of abbreviations

Chemicals and materials

CO - Carbon monoxide

NO - Nitric oxide

CN^- - Cyanide

IPTG - Isopropyl β-D-1-thiogalactopyranoside

LB - Lysogeny broth (growth medium)

SDS - Sodium dodecyl sulfate

TB - Terrific broth (growth medium)

Tris - Tris(hydroxymethyl)aminomethane

SDS - Sodium dodecyl sulphate

SA - Succinylacetone

hemin - Fe(III)-protoporphyrin IX chloride

ZnPP - Zn(II)-protoporphyrin IX

PVDF - Polyvinylidene difluoride

NAD(H) - Nicotinamide adenine dinucleotide

P_i - Inorganic phosphate

FBS - Fetal bovine serum

$\alpha\alpha$ - 1% (v/v) Penicillin-Streptomycin solution

ATP - Adenosine triphosphate

OPD - *o*-phenylenediamine dihydrochloride

EDTA - Ethylenediaminetetraacetic acid

DTT - Dithiothreitol

PBS - Phosphate Buffer Saline

DMSO - Dimethyl sulfoxide

***o*-PD** -*o*-phenylenediamine dihydrochloride

2,3-DAP - 2,3-diaminophenazine

Rh6G - Rhodamine 6G

Proteins

ALAS-1 - δ-aminolevulinic acid synthase 1

preALAS - Cytosolic precursor of δ-aminolevulinic synthase 1

HO-1 - Heme oxygenase-1

HO-2 - Heme oxygenase-2

HO-3 - Heme oxygenase-3

Mb - Myoglobin

gMb - Green myoglobin (*i.e.* sperm whale myoglobin (H64Y/V68F)

HBPs - Heme binding protein(s)

HRMs - Heme regulatory motif(s)

IDO - Indoleamine 2,3-dehydrogenase

GAPD(H) - Glyceraldehyde 3-phosphate dehydrogenase

HRP - Horse radish peroxidase

GFP - Green fluorescent protein

EGFP - Enhanced green fluorescent protein

mEGFP - Monomeric enhanced green fluorescent protein

***s*APX** - Soybean ascorbate peroxidase

mAPX - Monomeric ascorbate peroxidase

EYFP - Enhanced yellow fuorescent protein

ECFP - Enhanced cyan fuorescent protein

mKATE2 - Monomeric katushka 2

iNOS - Inducible nitric oxide synthase

sGC - Soluble guanylate cyclase

Per2 - Period circadian protein homolog 2

CLOCK - Circadian locomoter output cycles protein kaput

IRP2 - Iron responsive protein 2

Techniques

FLIM - Fluorescence lifetime imaging microscopy

TCSPC - Time-correlated single photon counting

FCS - Fluorescence correlation spectroscopy

SDS-PAGE - Sodium dodecyl sulphate polyacrylamide gel electrophoresis

UV-visible - Ultraviolet-visible

BCA assay - Bicinchoninic acid assay

MTT assay - 3-(4,5-dimethylthiazol-2-yl)-2,5-diphenyl-2H-tetrazolium bromide assay

Amino acids

G - Glycine - Gly, **P** - Proline - Pro

A - Alanine - Ala, **V** - Valine - Val

L - Leucine - Leu, **I** - Isoleucine - Ile

M - Methionine - Met, **C** - Cysteine - Cys

F - Phenylalanine - Phe, **Y** - Tyrosine - Tyr

W - Tryptophan - Trp, **H** - Histidine - His

K - Lysine - Lys, **R** - Arginine - Arg

Q - Glutamine - Gln, **N** - Asparagine - Asn

E - Glutamic Acid - Glu, **D** - Aspartic Acid - Asp

S - Serine - Ser, **T** - Threonine - Thr

Miscellaneous

a.u. - Absorbance units

DNA - Deoxyribonucleic acid

RNA - Ribonucleic acid

mRNA - Messenger RNA

RET - Resonance energy transfer

FRET - Förster resonance energy transfer

RNAi - RNA interference

siRNA - Small interference RNA

HEK293 - Human embryonic kidney 293 cells

HEK-mAPXmEGFP - HEK293 cell line stably expressing mAPXmEGFP

HeLa - Henrietta Lacks cells

ET - Electron transfer

O.D. - Optical density

PDB - Protein data bank

PROTEX - Protein expression laboratory (University of Leicester)

GRE - Glucocorticoid response element

AP-1 - Activator protein-1

NFKB - Nuclear factor kappa B

ER - Endoplasmic reticulum

kDa - Kilo Dalton

VR - Vibrational Relaxation

IC - Internal Conversion

HMOX1 - Human heme oxygenase-1 gene

HMOX2 - Human heme oxygenase-2 gene

CP - Cysteine-proline motif

HRM - Heme regulatory motif

EMBL-EBI - European molecular biology laboratory-european bioinformatics institute

PDB - Protein Data Bank

R - Molar gas constant = $R = 8.315\ J \cdot mol^{-1} \cdot K^{-1}$

T - Temperature

***d*$\mathbf{H_2O}$** - Deionised water

Part I

Introduction

Chapter 1

The study of heme dynamics in biology

Heme is a macrocyclic complex of iron, with the metal ion coordinated equatorially to the four nitrogen atoms of an electronically delocalised protoporphyrin IX ring (Figure 1.1A) and to one or two axial ligands [1]. The term "heme" is used widely, and often interchangeably, to refer to different types of iron Fe-protoporphyrin IX (*e.g.* heme A, heme B, heme C, heme D). When one of these heme structures is bound to a protein, the two axial ligation positions are normally occupied by donor ligands provided by protein amino acids and by molecules of substrate, solvent, or gas (Figure 1.1A-B). Heme ligation to the side chains of histidine (H), cysteine (C), methionine (M), tyrosine (Y), lysine (K), and glutamic acid (E) residues is known [2, 3]. In binding to a protein in this way, the heme becomes either 5- or 6-coordinated (Figure 1.1B). By convention, the proximal position, which is most commonly a histidine, is assigned as the 5^{th} ligand and is normally shown below the heme when visualising heme structures. The 6^{th} ligand, if there is one, is then drawn above the heme on the so-called distal side. This proximal/distal terminology dates back at least as far as the crystallography studies of Kendrew and Perutz [4,5]. The distal position can be occupied by a protein amino acid; by a diatomic gas (*e.g.* O_2, NO, CO); by water, hydroxide or another small molecule ligand (*e.g.* H_2S, CN^-); or it can be vacant giving a 5-coordinate heme species.

The reactivity of the heme is controlled in part by the number and identity of these ligands at the proximal and distal positions, while stabilisation of the heme molecule is further controlled by the heme binding pocket via hydrophobic interactions with the porphyrin ring and vinyl groups, and hydrogen bonds between the

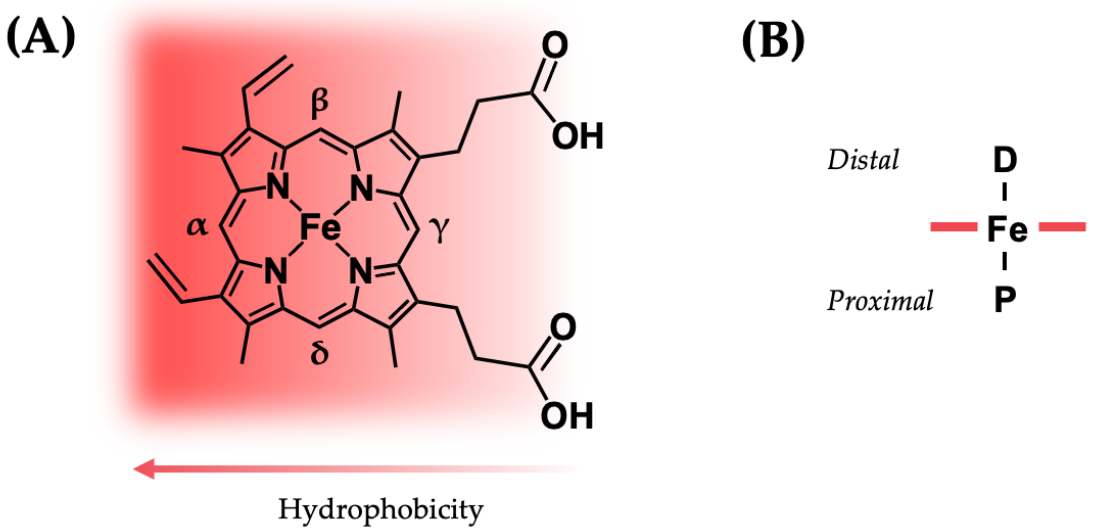

Figure 1.1: (A) The structure of heme B. While heme is mostly hydrophobic, the carboxylate groups enable hydrogen-bonding interactions between the heme group and other molecules, including assisting the binding of heme to a protein. The α, β, δ, and γ positions of the heme (*i.e.* edges) are labeled [7]. (B) The heme group is classified as containing distal and proximal sides, which are conventionally drawn above and below the plane of the ring, respectively. In heme proteins, the proximal side is usually bound to an amino acid residue provided by the protein; this helps to control its reactivity as a redox centre and its properties as a gas-binding molecule for storage and signaling.

propionate groups and the solvent [6]. The role of the protein can thus be envisaged as solubilising the hydrophobic heme molecule, and in doing so controlling the reactivity of the heme group for biological purposes.

1.1 The emerging roles of heme

Most of what has been learned about the traditional roles of heme in biology relates to binding of heme to individual proteins such as those involved in oxygen transport (*e.g.* myoglobin, hemoglobin, cytoglobin, neuroglobin) [8], bioenergetics (*e.g.* cytochrome *c*, cytochrome *c* oxidase) [6, 9–13], metabolism and catalysis driven by the insertion of oxygen (*e.g.* cytochrome P450, indoleamine 2,3-dioxygenase) [6], peroxidase catalysis [14], formation of nitric oxide [15] and lipid metabolism (COX-2) [16].

The non-traditional roles of heme started to emerge as far as back as 1975 when heme was shown as a regulator of the synthesis of δ-aminolevulinic acid synthase 1

(ALAS-1) - the enzyme that catalyzes the first of the 8 steps of the heme biosynthesis pathway (Chapter 3.1.1) [17]. Heme is now recognised as a regulator of many cellular activities [18–20], including transcriptional regulation and gas sensing [20–22], degradation of the p53 protein [23], regulation of the circadian clock [24–43], immune response [44, 44], aging [45], and the gating of numerous ion channels [46–60].

Despite its toxicity and lack of solubility, at least two chemical features make heme suitable as a regulator. The first is that heme is redox active and can respond to the redox status of the cell by modulating its oxidation state. The second is that the production and modulation of the reactivity of key cell signalling gases (*i.e.* O_2, NO, CO) is linked to the presence of heme. Gases like O_2, NO, and CO, can bind rapidly and sometimes reversibly to heme. Carbon monoxide is itself produced via degradation of heme by the O_2-dependent heme oxygenase enzyme [61,62], and NO is produced by the heme- and O_2-dependent NO synthase enzyme [15]. Overall, the redox state of heme, heme-binding to proteins and nucleic acids, and the production of signalling gases and their binding to heme may all be interconnected. This suggests multiple layers of regulatory control as a versatile but intricate mechanism for cell signalling.

1.2 Heme descriptors

The literature on the roles of heme in cells addresses different forms of heme using a bewildering range of terminologies where phrases such as “labile heme”, “regulatory heme”, “free heme”, and “heme pool” are often used interchangeably [63]. While the need to discriminate between the different types of heme in cells is obvious, it is challenging to provide a precise description of each type. What does “labile heme” mean? How can “free heme” exist in the cell, given that heme is cytotoxic and poorly soluble? Does the phrase “regulatory heme” describe a supply of heme dedicated exclusively for regulatory purposes, or might it be used for other purposes? Does it actually make sense to talk about “pools” of heme when current estimates for heme concentration are in the nM to μM range [64–68]? The lack of precise descriptions

for the nature of different types of heme can lead to confusing or contradictory interpretations. Hence, a commentary on the use of such terminology is provided here.

The phrase "regulatory heme" has been used in disciplines that vary from blood disorders like porphyria [69, 70], gene expression [71, 72], and heme biosynthesis [73–75]. Regulatory heme refers to a small portion of the total heme content of the cell that is present in a regulatory capacity in an intracellular heme pool. These terms originate from early papers [71, 72, 75–78], where it was also suggested that the nature of regulatory heme was likely to be as free molecules of heme. The existence of a form of regulatory heme is conceptually useful, and because of this its nature has been debated as long ago as 1975 when new roles for heme – above and beyond the traditional roles in oxygen binding, electron transfer and catalysis – were identified by Granick [75]. In Granick's work, the regulation of heme biosynthesis was proposed as being controlled by fluctuations in the concentrations of heme in a dedicated heme pool where heme was envisaged as being weakly associated to an ensemble of cytosolic proteins [75, 79]. These weak binding interactions were considered key for heme to be readily exchangeable [75, 78]. The term regulatory heme was then later adopted by scientists in multiple fields [46, 69, 80–90].

"Free heme" was introduced in the 1970s [72, 77, 91] and was interpreted as an intracellular population of free heme molecules either on their own (free) or all together (in a pool, but not bound to a protein). These early papers noted the difficulties associated with the idea of a pool of free heme, but, nevertheless, the concept and the terms "free heme" and "pool of free heme" became engrained in the literature [77, 84, 86, 87, 92, 93]. Although broadly adopted, the term "free heme" has rarely been precisely defined but only taken to imply a heme molecule that is not bound to anything else. Long and co-workers have recently denoted free heme as "heme that is not bound to proteins, either because it is newly synthesised and not yet incorporated into hemoproteins or it has been released from hemoproteins during oxidative stress" [88, 94]. However, there are difficulties with the concept of

free heme, especially in large amounts, because heme is cytotoxic through Fenton chemistry and radical formation [84, 86, 88, 95–97]. Heme is also a hydrophobic molecule and poorly soluble, so presumably cannot exist in cells without being solubilised by binding to a protein, cellular membrane [98], or nucleic acids [45, 99]. Moreover, heme needs to be ligated at the 5^{th} and 6^{th} ligation position, otherwise it will stack to form dimers or higher multimers in solution [100, 101]. This is problematic for cellular handing because, in a dimeric or multimeric form, heme could not be delivered to proteins that require only one molecule per binding site. Thus, free molecules of heme are envisaged as only existing transiently in cells.

In more recent years the term "labile heme" has appeared [44,67,88,98,102–113]. The use of this term allows a distinction to be made between the proportion of the total heme content that is available for mobilisation, and the proportion that is unavailable (or, more precisely, inert for exchange) because it is bound with a high affinity, and therefore irreversibly, to proteins. Ideas on what the concepts of labile heme actually means mimic the early ideas on regulatory heme [75, 79]. Labile heme is envisaged as being continuously engaged in transient binding to intracellular proteins that exist to actively buffer heme concentrations in the cell. Since some heme is unavailable for distribution in cells, labile heme is thus envisaged as an intermediary through which heme can move and be distributed through the cell [98, 103–105]. The term labile heme probably finds its origins as an adaptation of "labile iron pool" that pre-dated it [114]. The use of the term lability, above, to distinguish a more mobile fraction of the total heme from that which is permanently (irreversibly) embedded into heme proteins is similar in concept to the kinetic lability of ligands in inorganic metal complexes [115–117]. Labile ligands exchange very fast whereas inert ligands exchange slowly. But the availability and distribution of heme will be defined not just by the kinetic lability of the ligands bound to the heme, but also by thermodynamics. This is because cascades of heme exchange events down a thermodynamic gradient (dictated by heme binding affinity) will control the overall distribution of heme. Hence, it has been proposed that "exchangeable heme"

is a more precise term to convey the concept that both kinetic and thermodynamic processes are relevant when considering the bioavailability of heme [66, 78, 89, 118, 119]. In this thesis, the following working set of definitions is used:

Total heme, $\mathbf{H}_t$ - The total heme content of a cell. This includes the fraction of heme that is bound irreversibly to heme proteins and thus not available for other purposes (defined here as H_p), and the fraction of exchangeable heme (which includes small quantities of free heme, see below).

Protein heme, $\mathbf{H}_p$ - The fraction of heme that is irreversibly bound to heme proteins (including membrane and cytosolic proteins).

Exchangeable heme, $\mathbf{H}_e$ - A fraction of the total heme that is reversibly bound to proteins or small ligand molecules (*e.g.* free amino acids, H_2O). Exchangeable heme can be considered as a reservoir that provides an accessible supply of heme to the cell.

Free heme, $\mathbf{H}_f$ - Molecules of heme that are not bound to a protein but weakly co-ordinated with water molecules. Free heme is expected to exist in vanishingly small quantities.

In principle, $H_t = H_p + H_e + H_f$, where H_e and H_f account for cellular heme bioavailablity.

1.3 Quantification of cellular heme to understand heme distribution

The fundamental requirement for heme across virtually all organisms – both in catalytic and regulatory roles – means that cells need mechanisms to manage heme supply and demand. Supply of heme is regulated by the well-studied heme biosynthesis pathway [61,74,120–122]. At the other end of the heme lifecycle, surplus heme (when it exists) is degraded by the O_2-dependent heme oxygenase enzyme [62, 123].

But while the enzymatic machinery for making heme – heme synthesis – and removing heme – heme degradation – is well established, what happens in between is almost completely unknown. It has long been recognised that cells need a supply of heme to respond to cellular demands [71, 72], but until quite recently tools to examine this question have been lacking. Granick speculated in the 1970s [75, 79] that the concentration of exchangeable heme in the cytosol was in the range 10-100 nM. This value is remarkably close to recent measurements (Table 1.1). In the past, the cellular heme concentration had to be inferred from the amount of heme measured in soluble cell lysis extracts determined using either fluorometric approaches [124] or enzymatic reconstitution techniques [64, 81, 89, 125]. These methods are likely to report a concentration that lies somewhere between that for exchangeable heme (H_e) and the total amount of heme present in the cell (H_t) because the denaturing methods lead to release of heme from many heme proteins, not just those involved in regulation. In order to selectively measure concentrations of exchangeable heme, it is necessary to use a method that is compatible with live cell fluorescence imaging or spectroscopy [126]. Such an approach is possible by the design and application of genetically-encoded heme sensors which can be expressed recombinantly in different cell lines.

1.3.1 Development and applications of heme sensors

This Section provides an historical overview of the different fluorescent heme sensors that appeared in the literature. Heme concentrations reported from these studies vary, and are summarised in Table 1.1. A discussion on the mechanisms underlying the sensing capacity of fluorescent heme sensors is given in Section 2.1.

In the early 2000s, Takeda *et al.* provided the first proof-of-concept for a heme sensing technology to deploy in cells. The sensor comprised an EGFP-cytochrome b_{562} fusion protein [127] which was later improved for enhanced resonance energy transfer (RET) between EGFP and cytochrome b_{562} [128] by optimising the linker ligating the two proteins.

Reporter	Heme probe	Fluorescent tag(s)	$K_{d,heme}$ (nM)[a,b]	Measured heme concentration (nM)	Quantification method	Tested in	Ref.
CYSDY-9	IsdX1, IsdC	ECFP, EYFP	63.5 ± 14.3	Cytosol 26.6 ± 5.5 Mitochondria 23.3 ± 4.9 Nucleus 31.0 ± 7.0 ER 5.4 ± 1.4[c]	FRET	HeLa	[65]
HS1	cytochrome b_{562}	EGFP, mKATE2	3 (ferric), <1 (ferrous)	Cytosol 20-40 Mitochondria <2.5 Nucleus <2.5	FRET	*S. cerevisiae*	[68]
CHY	*P. falciparum* Histidine Rich Protein	ECFP, EYFP	250	Cytosol 1600	FRET	*P. falciparum*	[67]
apo-HRP	Horseradish Peroxidase	-	-	600	Reconstitution of catalytic activity[d]	Human lung fibroblasts (IRM90)	[63, 89]
apo-HRP	Horseradish Peroxidase	-	-	2100 ± 2	peroxidase activity[d]	Human erythrocytes	[64]
apo-HRP	Horseradish Peroxidase	-	-	2100 ± 2	peroxidase activity[d]	HEK293	[129]
mAPXmEGFP[e]	Ascorbate Peroxidase	mEGFP	22	4	FRET	HEK293	[66]

Table 1.1: Summary of genetically encoded heme sensors reported in the literature. [a]The heme affinity, frequently expressed as the dissociation constant, $K_{d,heme}$, is a key parameter in heme quantitation. $K_{d,heme}$ values should be close to the physiological concentrations of heme (in the nM to μM range), to ensure prompt response of the sensor to changes in [heme] but also avoiding the sensor from becoming either fully saturated or fully unsaturated (which is essential to study dynamic cellular processes). $K_{d,heme}$ defines the fraction of total cellular heme which is available for donor−acceptor heme exchange (acceptor = *apo*-heme sensor). Heme sensors with the highest heme affinities will accept heme from a larger ensemble of heme donors, and vice versa. Caution is needed when comparing heme concentrations obtained with different sensors, as the sensors with lower $K_{d,heme}$ will draw heme from a larger number of donors. [b]For ferric heme unless otherwise stated. [c]A relatively low concentration of heme was measured in the endoplasmic reticulum of HeLa cells compared to other cell lines (mouse melanoma B16, human HCT116 colon cancer cell, human PANC-1, hamster kidney fibroblast BHK-21, and CHO), which was interpreted as due to the high expression levels of heme oxygenase-1 in the endoplasmic reticulum surface of HeLa cells. [d]*holo*-HRP was formed by mixing *apo*-HRP with HEK293 lysates. The reconstitution of the catalytic activity of the HRP reporter by its binding to cellular heme was then used to measure heme concentration. [e]mAPX = monomeric APX; mEGFP = monomeric EGFP.

Fluorescently labelled variants of heme oxygenase-1 (K18C [130] and D140H [131] variants) have also been used to detect heme *in vitro*. These sensors were a step forward in terms of heme quantification, but were not deployed in cells for real-time monitoring of heme concentrations.

The first genetically encoded heme sensor, CISDY-9 [65], was designed to exploit the natural dimerisation of a pair of bacterial chaperones (IsdX1 and IsdC). Tagging each chaperone with a fluorescent probe and linking them with a short peptide tether produced an intracellular Föster resonance energy transfer (FRET) reporter which was used to analyse heme populations in HeLa cells (Table 1.1). With the exception of the endoplasmic reticulum, heme concentrations were found to be evenly distributed across the cytosol, the mitochondria and the nucleus, which is different from reported measurements in yeast [68].

Cytochrome b_{562} was later engineered with EGFP and mKATE2 fluorescent tags. This created a sensor that could be deployed in cells [68] in which the fluorescence intensity of EGFP was quenched (via FRET) on heme binding; the intensity of mKATE2 was unchanged providing a means of assessing heme concentration by ratiometric analysis. A somewhat heterogeneous distribution of heme throughout yeast cells was reported (Table 1.1), and the behaviour of the sensor in cells [105] supported the concept of a (buffered) reservoir of exchangeable heme that is readily available for regulatory roles and crucial in the overall physiology of yeast. The same sensor was then utilised to demonstrate that heme delivery from mitochondria – the place of heme biosynthesis – to the nucleus was 25% faster than to the cytosol and the mitochondrial inner matrix. The authors suggested direct membranes contacts between mitochondria and the ER as a possible pathway for heme delivery to the nucleus [132, 133].

A genetically encoded (FRET-based) heme sensor based on histidine rich protein 2 has been used to quantify heme concentrations in the parasite *P. falciparum* [67]. In this case, heme concentrations are higher (*ca.* 1.6 μM), but this is not completely unexpected considering that 80% of the amount of heme contained in a human body

is synthesised by red blood cells [63].

Peroxidase-based fluorescent sensors, based on horseradish peroxidase and ascorbate peroxidase, were first used to measure dynamic heme fluxes in *C. elegans* [129]. Ascorbate peroxidase has also been used in this work and in published work [66] to monitor heme concentrations and distributions in live cells using Fluorescence Lifetime Imaging Microscopy. In this case, miniscule concentrations (a few nM) of free heme were measured - corresponding to one molecule or less per cellular compartment. These observations are consistent with a system that sequesters free heme.

Heme sensors can be used beyond the determination of heme concentrations. A GFP-labelled version of cytochrome *c* peroxidase has been recently developed and used to study heme protein maturation by heme insertion [112]. In this design, the percentage of the heme-bound sensor in yeast cells was revealed by the relative amplitudes of exponential-decay components in the emission measured by fluorescence lifetime imaging. This provides a forward-looking approach to establish, in real-time, the dynamic processes involved in the folding process that accompanies the formation of heme proteins.

Heme sensor design has also relied on synthetic approaches. Promising examples include the use of the antimalarial 4-aminoquinoline probe [134] and peptide-based fluorescent probes [135]. However, synthetic sensors have not found, as yet, widespread adoption for *in cellulo* measurements.

1.4 Aims of this work

The aim of this work is to provide a methodological framework for the study of heme dynamics in the cellular environment through the use of genetically encoded heme sensors. To meet the transient cellular demands for heme, a readily available supply is required, but we know little about how heme is mobilised to respond to particular cellular needs in specific places. Where and in what concentrations is heme located? How do heme distributions vary under different cellular conditions? What are the

key players in maintaining cellular heme homeostasis? To answer these questions, this thesis explores the capabilities of a novel heme sensor (mAPXmEGFP) that, for the first time, reports on heme bioavailability through changes in mean fluorescence lifetime rather than fluorescence intensity. In doing so, the two major limitations of previously reported sensors - due to photobleaching and inner-filtering (Section 2.2) - are surpassed.

Part II

Results

Chapter 2

A fluorescence lifetime-based method to report on heme bioavailability

2.1 Introduction

Genetically encoded sensors for heme comprise a heme-binding protein conjugated to one or more fluorescent proteins where the fluorescence output is modulated by heme binding (Figure 2.1). There are different mechanisms that can lead to suitable modulation of the fluorescence output through heme binding: (i) FRET between the fluorescent protein and a bound molecule of heme; (ii) FRET between a pair of fluorescent proteins; and (iii) modulation of the fluorescence anisotropy (*i.e.* polarisation).

FRET between the fluorescent protein and a bound molecule of heme can only occur if (i) the heme-binding pocket of the sensor is located in close proximity to the chromophore-forming amino acids in the fluorescent protein; and (ii) the emission spectrum of the fluorescent protein is overlapped with either the Soret or Q absorption bands of heme [136]. In this case, resonance-energy transfer provides a non-radiative decay pathway for the photo-excited state of the chromophore, via the heme moiety, that competes with the radiative-decay pathway responsible for the fluorescence signal (Figure 2.1A). If the distance between the chromophore-forming amino acids on the fluorescent protein and the heme-binding pocket, r, is much less than the Förster distance, R_0 (calculated from the spectral overlap integral [136]),

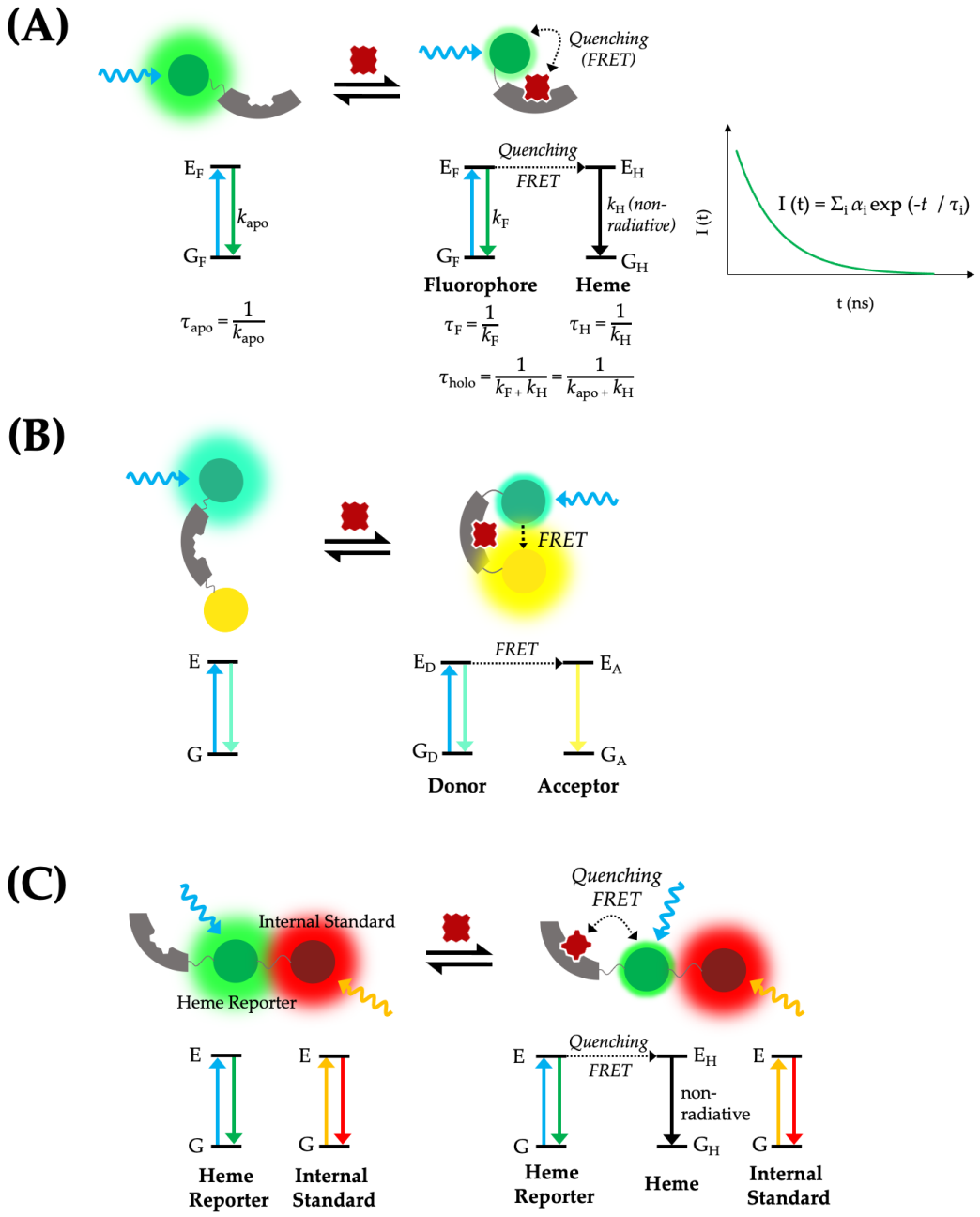

Figure 2.1: Basic principles of fluorescent heme sensor designs. (A) FRET between the fluorescent tag and a bound molecule of heme: heme-binding to this type of sensor introduces an additional relaxation pathway for the electronic excited state of the fluorophore. The mean fluorescence lifetime of the probe changes between the limiting values of τ_{apo} to τ_{holo} for the pure *apo*- and *holo*-forms of the sensor dependent on heme concentration [66]. (B) FRET between a pair of fluorescent tags: the heme-binding domain of the sensor undergoes a conformational change that brings two fluorophores into close proximity to one another. In this example, Förster energy transfer results in a decrease in the emission of a green fluorophore and an increase in emission of a yellow fluorophore. Hence changes in the relative emission intensities of the two fluorophores can be used to determine heme concentration [65]. Multiple heme-binding sites may be present in the heme-binding domain [67]. (C) A FRET sensor (similar to that shown in (A)) that incorporates an additional fluorophore in order to measure a ratiometric intensity. The sensor is composed of two fluorophores, but heme-binding triggers the selective quenching of the fluorescence of only one of them. The unperturbed tag can then be used as an internal reference to monitor the changes in the intensity of emission for the quenched fluorophore, providing a method for precise heme quantification [68, 105]. Figure adapted from Gallio *et al.* [118].

then the efficiency of FRET in the *holo*-sensor will be near to 100%. On the other hand, the fluorescence quantum yield of the *holo*-sensor (*i.e.* the sensor with heme bound to it) will be near to 0% and the presence of heme can be inferred from the quenching of the intensity of the fluorescence emission. Alternatively, if the distance r is close to the R_0, then there will be an intermediate efficiency for FRET in the *holo*-sensor given by Equation 2.1 [136, 137].

$$FRET_{Efficiency} = \frac{1}{1 + (\frac{r}{R_0})^6} \times 100\% \tag{2.1}$$

Heme induced FRET in a fluorescent heme sensor can also be inferred from a reduction in the fluorescence lifetime. A change in the fluorescence lifetime can be observed by Time-Correlated Single Photon Counting (TCSPC), where the proportions of the *apo*- and *holo*- forms of the sensor can also be deduced by determining the relative amplitudes of functions in the fitting of an exponential decay model.

When Förster resonance-energy transfer (FRET) is used to detect heme, heme binding induces a conformational change that brings the chromophore-forming amino acids of a couple of fluorescent proteins (*i.e.* a donor and an acceptor, respectively) into close proximity (Figure 2.1B). In this case, resonance-energy transfer between the donor and acceptor leads to subsequent radiative decay from the acceptor. Hence, the binding of a molecule of heme is detected by the attenuation of the short wavelength emission band of one of the fluorescent proteins (the donor), and the appearance of the long wavelength emission band of the other fluorescent protein (the acceptor).

Heme binding may also modulate the fluorescence anisotropy (*i.e.* the photoselective excitation of fluorophores by polarised light [136]) of a heme sensor. However, anisotropy methods - which depend on the relation between the emission of fluorescent light and the rotational relaxation of molecules - have not yet been exploited for cellular heme sensing. This is likely due to the highly heterogeneous viscosity of the intracellular environment [140–142] which affects the local rotational relaxations and the fluorescence anisotropy of molecules [138, 139].

2.1.1 Aims of this chapter

The aim of this chapter is to build a new fluorescence lifetime-based heme sensor using GFP and a heme peroxidase. Following a description of the heme sensor, this chapter deals with its deployment in HEK293 cells to monitor heme bioavailability through live cell Fluorescence Lifetime Imaging Microscopy. The results are summarised and discussed in the context of a physiological interpretation of the microscopy data. This work is published [66].

2.2 The mAPXmEGFP heme sensor

For a genetically-encoded heme sensor, a measurement of a fluorescence lifetime decay profile has significant advantages over a measurement of fluorescence intensity: (i) the fluorescence lifetime decay can be used to determine the ratio of *holo*- to *apo*-forms of the sensor, but the intensity can only be used to detect the *apo*-form of the sensor (because the *holo*-form of the sensor is quenched); (ii) the quantitative accuracy of fluorescence lifetime imaging or spectroscopy is independent of sensor concentration, the inner filter effect (*i.e.* the attenuation of the excitation beam due to high concentration of absorbing chromophores which results in fluorescence being not uniformly distributed in the sample), and photobleaching of the fluorescent protein (the photon-induced chemical damage of a fluorophore that determines loss of its ability to fluoresce) [66, 67, 112, 118, 136, 137]; and (iii) fluorescence lifetime measurements imply simplified sensor designs because quantitative measurements that rely on fluorescence intensity quenching require an additional tag to normalise the signal (Figure 2.1C).

A fluorescence lifetime-based FRET sensor was built following the design in Figure 2.1A by ligating enhanced green fluorescent protein (EGFP, Figure 2.2B) to the heme enzyme soybean ascorbate peroxidase (*s*APX) (Figure 2.2A). The design and photophysical characterisation of this sensor was carried out as part of Dr. Galvin Leung's PhD project in collaboration with Prof. Andrew Hudson at the

University of Leicester [66].

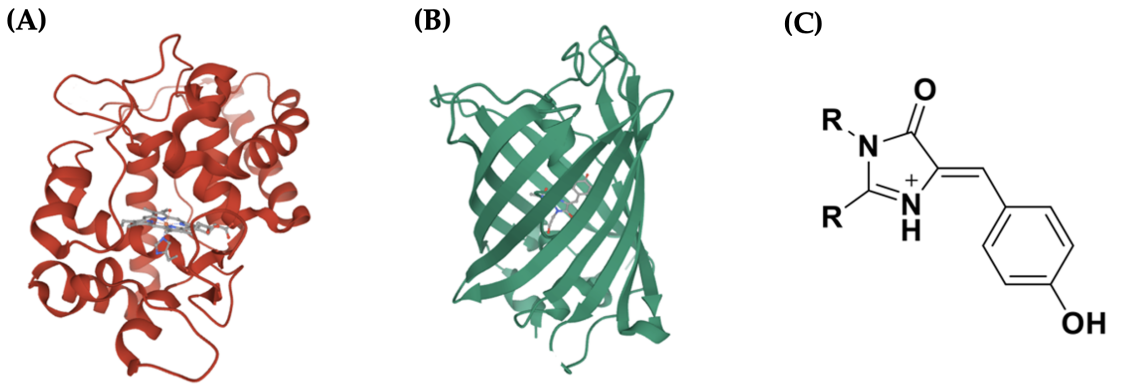

Figure 2.2: (A) Crystal structure of soybean ascorbate peroxidase (APX, *holo*-form; PDB entry: 1OAG) [143]. (B) β-barrel structure of an enhanced green fluorescent protein (EGFP, PDB entry: 4EUL) [144]. (C) Chemical structure of the chromophore responsible for the fluorescent properties of the GFP proteins family [145].

The elements of the fusion sensor were chosen by taking into account both convenience and available knowledge to minimise uncertainties during characterisation. *s*APX is a well-known protein [6, 146, 147] that has found applications in imaging and proteomics [112, 129, 148]. *s*APX exhibits a mid-range affinity for heme (K_d = 40-400 nM) [149], weaker than those of, for example, globins, cytochromes, and catalase, which have heme dissociation constants that are typically in the 0.001-1 pM range [129]. From a design standpoint, the ideal heme responsive element in a heme sensor should possess a K_d value close to the concentration of heme in the measuring environment. The mid-range affinity of *s*APX for heme makes it well-suited to function as a heme responsive element because it is close to previous estimations of cellular heme concentration (Table 1.1). Such a feature would make the sensor sensitive to fluctuations in the population of heme, providing sensing capacity over a range of physiologically relevant concentrations [103] and avoiding the risks of being either easily saturated or not bound in extremely low heme concentration scenarios [150].

EGFP, besides having been thoroughly studied since the discovery of the green fluorescent protein (GFP) in *Aequorea victoria* [150–152], has been widely exploited as a cellular fluorescent reporter in genetically encoded sensors [153], displays greater

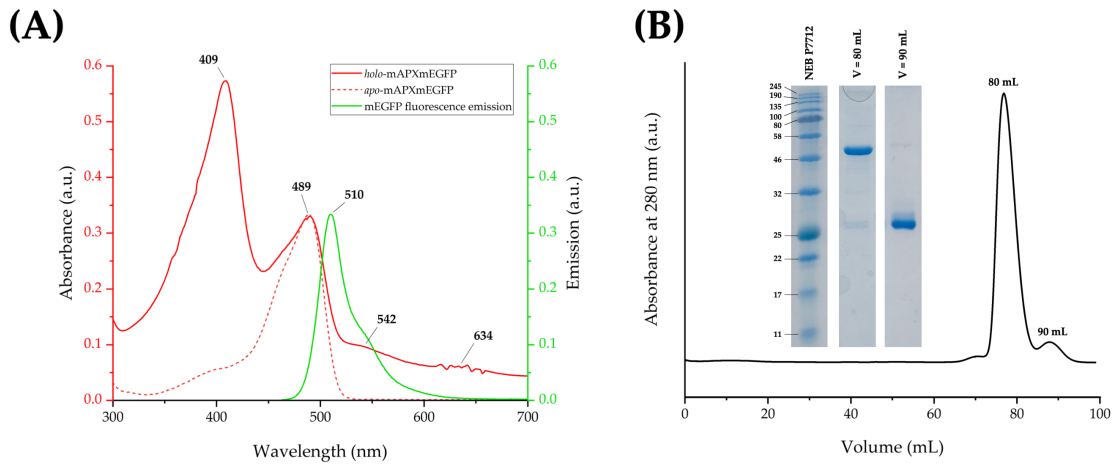

Figure 2.3: (A) UV-vis spectra of purified *apo*-mAPXmEGFP (dotted red trace), *holo*-mAPXmEGF (red trace), and emission of mEGFP (Fluorescent Protein Database) (300-700 nm). *holo*-mAPXmEGFP shows a strong Soret peak at 409 nm, mEGFP aborption band at 489 nm, and low intensity Q-bands at 542 nm and 634 nm, respectively. The mEGFP absorption is the predominant band showed by *apo*-mAPXmEGFP. Soret peak and Q-bands can be reconstituted in *apo*-mAPXmEGF through progressive additions of hemin. The emission spectrum of mEGFP overlaps with the Q-bands of *holo*-mAPXmEGF (B) Affinity chromatography elution profile of mAPXmEGFP HiLoad™Superdex™200 pg column (GE Healthcare) (Elution buffer: $[KPO_4]$ = 10 mM, [KCl] = 150 mM, pH = 7; T = 6 °C). A first group of aggregates is followed by the peak corresponding to mAPXmEGFP (at around V = 80 mL) and mEGFP (V = 90 mL). The SDS-PAGE gels of fractions corresponding to these latter peaks are shown in the inset.

fluorescence quantum yield than GFP, and its folding is generally more efficient [154]. Given the historical importance of GFP-based reporters, the description of the heme sensor mAPXmEGFP is accompanied with an overview on the development EGFP in the next paragraph.

The heme sensing capacity of a *s*APX-EGFP fusion protein through RET is given by the overlap between the absorption Q bands of heme-bound *sb*APX and the emission band of EGFP (Figure 2.3A and 2.4A). On this basis, mAPXmEGFP was developed, where complexities arising from homo-dimerisation of *s*APX and EGFP were avoided by introducing point mutations in APX (K14D/E112K) [155] and EGFP (A206K) [156] to generate monomeric versions of each protein (mAPX and mEGFP; full sequences in Appendix A.1.2, Figure A.1). The K_d for heme binding to mAPXmEGFP was determined as 22 nM [66], within the same range of previously estimated concentrations of exchangeable heme (Table 1.1).

The development of EGFP

The discovery and isolation of the wild-type GFP (WT-GFP) from *Aequorea victoria* by Prof. Osamu Shimomura resulted in a Nobel Prize award for Chemistry in 2008, which was shared with Prof. Roger Tsien and Prof. Martin Chalfie for the further development and engineering of the protein. The green fluorescent protein was originally observed in the early 70's in jellyfish and other coelenterates as responsible for the conversion of the blue emission of a calcium-dependent aequorin to green luminescence. Since then, GFP has proven a versatile tool widely exploited in biochemistry and cell biology [151] as it does not require a unique jellyfish factor to fold into the fluorescent structure [157].

The tertiary structure of GFP is constituted by 11 beta strands arranged in a hollow beta barrel conformation containing a shorth helix that bears the protein chromophore. The chromophore is a *para*-hydroxybenzylideneimidazolinone (Figure 2.2C) [158, 159] resulting from a cyclisation reaction involving Ser65, Tyr66, and Gly67 [152, 160]. Briefly, the imidazolinone ring is formed by nucleophilic attack of the amide of Gly67 on the carbonyl of Ser65. Following a dehydration step, a dehydrogenation of Tyr66 conjugates the electronically delocalised imidazolinone ring into an extended aromatic system [152, 161].

WT-GFP has a two excitation bands ($\lambda_{Ex,1} = 400$ nm; $\lambda_{Ex,2} = 475$ nm) with λ_{Em} sitting just over 500 nm [162]. However, whilst the longer excitation band provides better photo-stability and is better suited for microscopy applications, it presents a relatively low fluorescent quantum yield [162, 163]. Moreover, the detection limit of WT-GFP was determined around 1 μM over cellular autofluorescence [157], a relatively high concentration for *in cellulo* applications.

Modern GFPs, adapted for improved brightness, photo-stability, and chromophore maturation dynamics, differ from WT-GFP for several key features. In particular, EGFP is an enhanced version of GFP that displays greater folding efficiency and a single excitation peak ($\lambda_{Ex} \sim 490$ nm) [144]. EGFP is generated through two key mutations, F64L and S65T [144, 160, 162, 163]. S65T is regarded responsible

for the suppression of the absorption maximum at 400 nm of WT-FP by modulating the ionised state of Glu222 – Glu222 is involved in hydrogen bonding with the chromophore-forming Ser65 in WT-GFP. On the other hand, F64L is thought of as responsible for improved folding efficiency [144, 154].

Both GFP and EGFP tend to form dimers with consequent concentration-dependent changes in the shape of their absorption spectrum. A further mutation in the EGFP (A206K) was introduced in this work to yield the monomeric variant mEGFP by replacing the hydrophobic residue Ala206 – positioned at the crystallographic interface of the dimer – with the positively charged Lys [156, 164].

2.2.1 Expression and purification of mAPXmEGFP

apo-mAPXmEGFP-(6×His) was expressed in *Escherichia coli* BL21(DE3) transformed with pLEICS45-mEGFPmAPX. A starter culture was grown in the presence of succinylacetone, a potent heme biosynthesis inhibitor [165]. Following expression, induction and cell harvest, the lysate was centrifuged, filtered, and *apo*-mAPXmEGFP was purified by affinity and size exclusion chromatography. The size exclusion elution profile is trimodal, with peaks in the 65 - 100 mL range. Fractions corresponding to a 54 kDa species were isolated as a purified product (*apo*-mAPXmEGFP-(6×His)) (Figure 2.3B). Sample purity was evaluated by UV-vis spectrophotometry and SDS-PAGE (Figure 2.3A-B). *holo*-mAPXmEGFP was prepared by incubation on ice of *apo*-mAPXmEGFP with 1.5 equivalents of hemin chloride solution. Successful reconstitution was checked by UV-Vis (Figure 2.3A). Excess heme was removed from the sample of *holo*-mAPXmEGFP with a second round of gel filtration. Full experimental details are outlined in Appendix A.1.2.

2.2.2 The lifetime of mAPXmEGFP reports on heme concentration

The fluorescence lifetime of mAPXmEGFP has been found to be sensitively influenced by heme binding, confirming its potential as a fluorescent lifetime-based

heme sensor [66]. This modulation reports on the population of heme bound to the sensor, thus making a lifetime-based sensor well suited for quantitative applications. Heme binding to mAPXmEGFP facilitates Resonance Energy Transfer (RET) from the excited states of mEGFP to the heme chromophore (Figure 2.4A) and consequently quenches the fluorescence lifetime τ of the sensor from τ_{apo} to τ_{holo} ($\tau_{\text{apo}} > \tau_{\text{holo}}$). In particular, the presence of heme introduces a competitive non-radiative relaxation pathway to the release of a photon by fluorescence from the exited states of mEGFP (Figure 2.1B). A more detailed description of the heme-induced quenching mechanism in mAPXmEGFP is provided in Figure 2.4 and summarised here. Biopolymers often display multi-exponential fluorescence decays [136]. mEGFP in particular displays two possible energetically close electronic excited states, I^*, and B^* [66, 166, 167]. Following excitation from the mEGFP non-interacting deprotonated ground states, I and B, the relaxation mechanism from I^* or B^* is different when heme is bound or unbound to mAPX (Figure 2.4B). In particular, heme bound to the sensor introduces via FRET two additional relaxation pathways from I^* and B^*, respectively, that, overall, shorten the mean fluorescence lifetime of mAPXmEGFP (Figure 2.4C-D). The statistical nature of the concept of fluorescence lifetime implies that a defined population of excited fluorophores is composed of randomly emitting species. Following excitation at t_0, each emitted photon contributes to describing a probability distribution of emission time-lapses τ_i that defines the mean fluorescence fluorescence lifetime, τ_{Mean}, of mAPXmEGFP (Figure 2.4D), where the fluorescence intensity $I(t)$ traces a first order exponential decay as a linear combination of each contributing decay component, i [136] (Equation 2.2).

$$I(t) = \sum_i \alpha_i e^{-t/\tau_i} \tag{2.2}$$

2.2.3 Theoretical underpinnings of heme sensing through the use of mAPXmEGFP

The photophysical parameters for the description of the fluorescence lifetime decay of mAPXmEGFP in the *apo* and *holo* forms were determined in collaboration with Prof. Andrew Hudson (University of Leicester) using *apo*-mAPXmEGFP isolated and purified from *E. coli* [66] (Chapter 2.2.1). The fluorescence decay from excited *apo*-mAPXmEGFP consists of two components, τ_{Fast} and τ_{Slow}, due to the emission from the non-interacting excited states of mEGFP, I^* and B^* (Figure 2.4B). Thus, the lifetime decay of mAPXmEGFP is well described by a linear combinations of τ_{Slow} and τ_{Fast} weighted by the fractional pre-exponential factors (*i.e.* amplitudes) α_{Fast} and α_{Slow} where $(\alpha_{\mathrm{Fast}} + \alpha_{\mathrm{Slow}}) = 1$ (Equation 2.3).

$$I(t) = \alpha_{\mathrm{Slow}} e^{\frac{-t}{\tau_{\mathrm{Slow}}}} + \alpha_{\mathrm{Fast}} e^{\frac{-t}{\tau_{\mathrm{Fast}}}} \tag{2.3}$$

The pre-exponential factors α_{Fast} and α_{Slow} in Equation 2.3 report on the fraction of *holo*-mAPXmEGFP, f (*i.e.* the relative abundance of *holo*-mAPXmEGFP *versus* (*holo* + *apo*)-mAPXmEGFP) (Equation 2.4).

$$f = \frac{holo\text{-mAPXmEGFP}}{holo\text{-mAPXmEGFP} + apo\text{-mAPXmEGFP}} \propto \frac{\alpha_{\mathrm{Fast}}}{\alpha_{\mathrm{Fast}} + \alpha_{\mathrm{Slow}}} \tag{2.4}$$

Equation 2.4 is demonstrated in the following paragraphs. The biexponential fitting of the Time-Correlated Single Photon Counting (TCSPC) decay profiles for mixtures of *apo*- and *holo*-mAPXmEGFP provided time constants equal to 2.7 ns and 1.3 ns [66]. In *apo*-mAPXmEGFP, the lifetime value of I^* is shorter than that of B^*. Thus, τ_{I^*} and τ_{B^*} can be reconciled with $\tau_{\mathrm{Fast}} = 1.3$ ns and $\tau_{\mathrm{Slow}} = 2.7$ ns, respectively. Heme binding to the sensor introduces - via Resonance Energy Transfer (RET) - non-radiative relaxation pathways (*i.e.* vibrational relaxation, VR, and internal conversion, IC) to the ground state of the heme chromophore that competes with the emission of photons through fluorescence (Figure 2.4 B). Thus, τ_{Fast} and τ_{Slow}

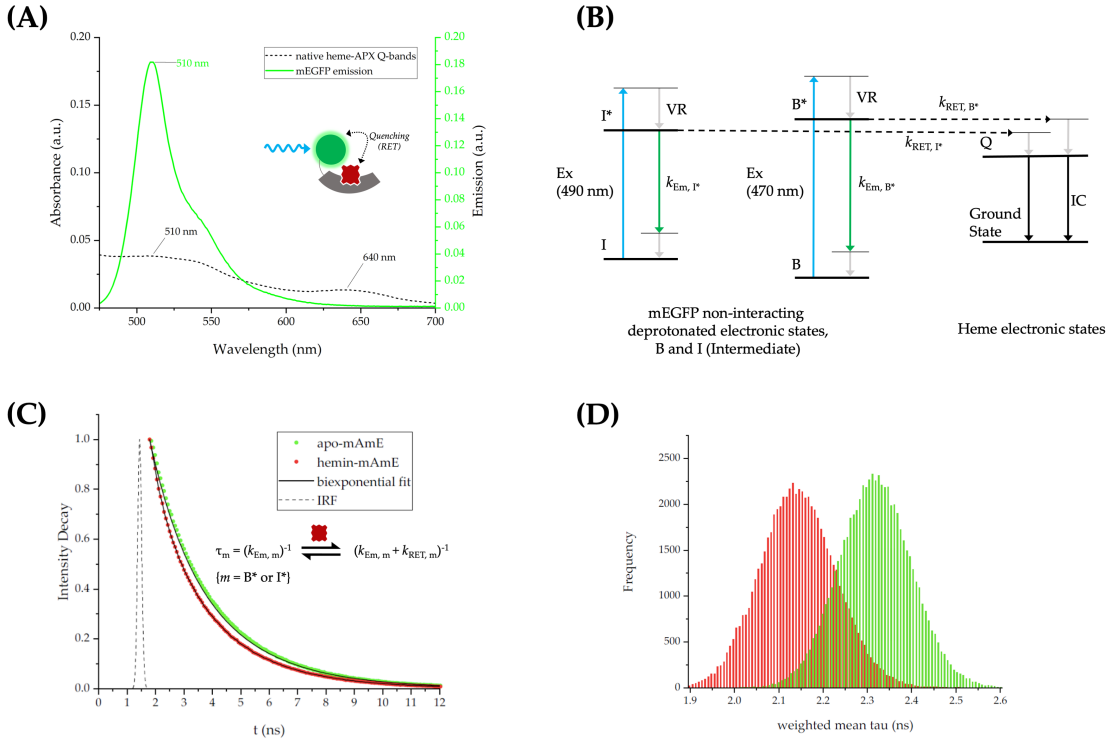

Figure 2.4: (A) The overlap between mEGFP emission (green trace) and heme-APX Q-bands (dotted trace) satisfies the energy match requirement for Resonance Energy Transfer to occur between the electronic excited states of mEGFP and the heme chromophore in mAPXmEGFP (inset). (B) Jablonski diagram describing RET from mEGFP electronic excited states [167] to heme (*c.f.* mEGFP emission and heme Q band for overlap) with rate constants, k_{RET,B^*} and k_{RET,I^*}, respectively, followed by vibrational relaxation (VR) and internal conversion (IC) to the ground state of heme. (C) Time-correlated single-photon counting, from *apo*- (green) and *holo*-mAPXmEGFP (red) (λ_{Ex}, 475 nm; λ_{Em}, 510 nm; 37 °C) fitted to a bi-exponential decay function, *I(t)* (Equation 2.3), with time constants of 2.7 (τ_{Slow}) and 1.3 ns (τ_{Fast}) (χ^2 values were typically between 0.8 and 1.7 for both *apo*- and *holo*-mAPXmEGFP. No significant improvement in χ^2 could be achieved by inclusion of more decay components) [66]. The instrument response function (IRF) is indicated as a dotted trace. (D) Histograms comparing the distribution of mean fluorescence lifetimes for the *apo*-mAPXmEGFP (green) and the *holo*-mAPXmEGFP (red). The median is shifted towards shorter lifetime values in *holo*-mAPXmEGFP compared to *apo*-mAPXmEGFP.

decrease when heme is bound to the sensor (Figure 2.4C-D).

Assuming that $k_{RET,I^*} = k_{RET,B^*} = 2.5\times10^8 s^{-1}$, τ_{I^*}(holo) and τ_{B^*}(holo) are estimated equal to 1.0 ns and 1.6 ns, respectively [66]. The difference between τ_{I^*}(holo) = 1.0 ns, τ_{B^*}(holo) = 1.6 ns, and τ_{I^*}(apo) = 1.3 ns is not easily resolved from fluorescence decay profiles. Hence, the fast component of a fitted biexponential decay function τ_{Fast} is interpreted as the result of the emission from I*(holo), B*(holo), and B*(apo). Overall, $\tau_{\text{Slow}} = \tau_{B^*}$(apo) = 2.7 ns whilst τ_{Fast} = Mean{τ_{I^*}(holo), τ_{B^*}(holo), τ_{I^*}(apo)}.

The fluorescence quantum yields for each of the excited states I* and B* relative

to *apo*- and *holo*-mAPXmEGFP are described by Equations 2.5-8, where ϵ is the probability of photoexcitation to B^*, $(1-\epsilon)$ is the probability of photoexcitation to I^*, and f is the fraction of mAPXmEGFP bound to a molecule of heme as defined in Equation 2.4.

$$Q_{B^*}(apo) = k_{Em,B^*}\tau_{\text{Slow}} \times \epsilon \times (1-f) \tag{2.5}$$

$$Q_{I^*}(apo) = k_{Em,I^*}\tau_{\text{Fast}} \times (1-\epsilon) \times (1-f) \tag{2.6}$$

$$Q_{B^*}(holo) = k_{Em,B^*}\tau_{\text{Fast}} \times \epsilon \times f \tag{2.7}$$

$$Q_{I^*}(holo) = k_{Em,I^*}\tau_{\text{Fast}} \times (1-\epsilon) \times f \tag{2.8}$$

Since the integrated intensities of fast and slow decay emissions are $\alpha_{\text{Fast}}\tau_{\text{Fast}}$ and $\alpha_{\text{Slow}}\tau_{\text{Slow}}$, then:

$$\frac{\alpha_{\text{Fast}}}{\alpha_{\text{Slow}} + \alpha_{\text{Fast}}} = \frac{Q_{I^*}(apo) + Q_{B^*}(holo) + Q_{I^*}(holo)}{Q_{B^*}(apo)} \tag{2.9}$$

It follows that the relationship between f and measured values of α_{Fast} and α_{Slow} is given by Equation 2.10 ($C = \frac{k_{Em,B^*}}{k_{Em,I^*}}(\frac{1}{\epsilon}-1)$) by substituting Equations 2.5-2.8 into Equation 2.9.

$$\frac{\alpha_{\text{Fast}}}{\alpha_{\text{Slow}} + \alpha_{\text{Fast}}} = \frac{f + C}{1 + C} \tag{2.10}$$

The value of C can be estimated from the mean value of $\frac{\alpha_{\text{Fast}}}{\alpha_{\text{Slow}}+\alpha_{\text{Fast}}}$ for purely *apo*-mAPXmEGFP. To this aim, the value of $C = 0.264$ was obtained for $f = 0$ by expressing mEGFP alone in HEK293, because mEGFP is unable to bind heme. The expression of mEGFP in HEK293 provides a baseline measurement for *in cellulo* experiments in which mEGFP emission is not perturbed by the presence of heme.

Once C was determined from images of HEK cells expressing mEGFP alone, the fraction of *holo*-mAPXmEGFP $f(i,j)$ in each pixel with coordinates (i,j) in 2D lifetime images of HEK293 cells expressing mAPXmEGFP is given by Equation

2.11 by rearranging Equation 2.10.

$$f(i,j) = \frac{\alpha_{\text{Fast}}}{\alpha_{\text{Slow}} + \alpha_{\text{Fast}}}(1 + C) - C \tag{2.11}$$

Then, using the heme dissociation constant of mAPXmEGFP ($K_{\text{d}} = 22$ nM [66]), the heme concentration $[Heme]$ can be determined from the values of $f(i,j)$ with Equation 2.12, to calculate maps of equilibrium concentration of heme, $[Heme]$, from 2D distributions of lifetime in images of live HEK293 (see below and Figure 2.5).

$$[Heme] = \frac{K_{\text{d}}}{\frac{1}{f(i,j)} - 1} \tag{2.12}$$

2.2.4 Measurement of heme concentration in HEK293 cells

The capacity of mAPXmEGFP to measure heme concentration was tested in live HEK293 cells to establish a reporter of changing levels of heme bioavailability. A stable HEK293 cell line expressing mAPXmEGFP (HEK-mAPXmEGFP) was generated by antibiotic selection (Appendix A.4.2) and cultured, prior to FLIM, to produce heme-depleted, normal heme level, and heme-rich conditions. To achieve this, images of HEK-mAPXmEGFP cells were cultured for 24 hours before imaging in α-Minimum Essential Medium (Sigma Aldrich; α-MEM), α-MEM supplemented with 1 mM succinylacetone (SA, Sigma Aldrich) - a heme biosynthesis inhibitor - and α-MEM supplemented with 10 μM hemin (Merck), respectively (Appendix A.6.2-FLIM). The resulting maps of intensity-weighted mean fluorescence lifetime (τ_{Mean}) showed distributions of lifetimes shifted towards longer values under heme depleted conditions ($\tau_{\text{Mean,SA}} = 2.33$ ns) and shorter values under heme rich conditions ($\tau_{\text{Mean,H}} = 2.19$ ns) when compared to those measured in the control ($\tau_{\text{Mean,αMEM}} = 2.25$ ns) [66]. The change in lifetime reports on heme bioavailability and mimicks the abundance of heme either supplied to the media or reduced by chemical inhibition of heme biosynthesis.

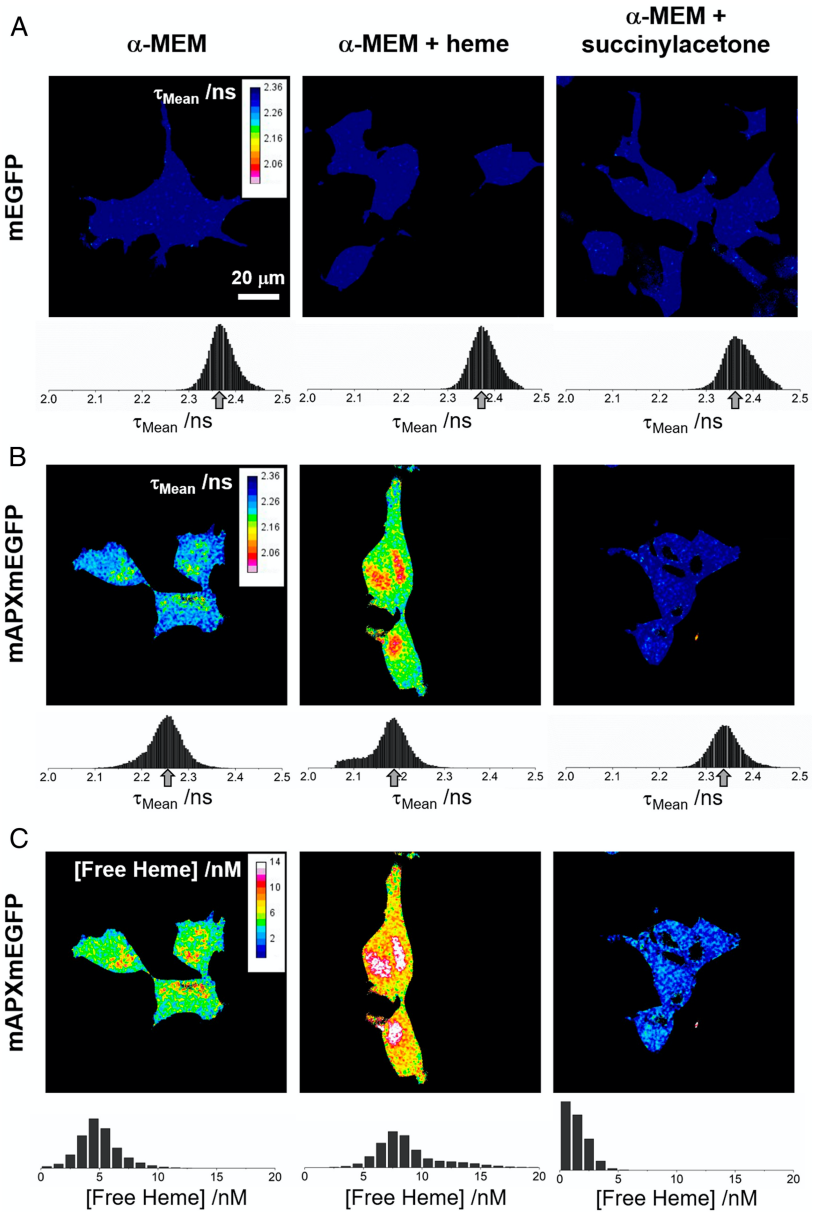

Figure 2.5: Colour maps of intensity-weighted mean fluorescence lifetime and free heme concentration. The intensity-weighted mean fluorescence lifetime, τ_{Mean}, are displayed for HEK293 cells expressing either (A) mEGFP alone or (B) mAPXmEGFP and cultured under different conditions (λ_{Ex}, 488 nm; $\lambda_{Em} > 495$ nm). (Left) α-MEM (with 10% fetal bovine serum); (Middle) α-MEM supplemented with heme (10 μM; 24 h prior to imaging); (Right) α-MEM depleted of heme following addition of succinylacetone (1 mM; 24 h prior to imaging). Images of representative cell clusters are shown. Typically, 10 images per condition were acquired in duplicate. Each of the colour maps in A and B is accompanied by a histogram showing the frequencies for which particular values of τ_{Mean} occur in the spatial distribution of pixels for the images of cells under different conditions. An arrow indicates the modal pixel value of τ_{Mean}. (C) The concentration of free heme calculated from the relative amplitudes, α_{Slow} and α_{Fast}, in the images shown in B using the heme-dissociation constant, K_{d}, for mAPXmEGFP determined in [66] (22 nM at 37°C). Each of the colour maps for free heme concentration is accompanied by a histogram showing the frequencies for which particular values of [Heme] occur in the spatial distribution of pixels for the images of cells under different conditions. Dr. Galvin C.-H. Leung and Dr. Dominic Alibhai are gratefully acknowledged for the acquisition of this data. Figure adapted from Leung *et al.* [66].

2.3 Discussion

The value of mean fluorescence lifetime of mAPXmEGFP for all the conditions explored corresponds to a miniscule concentration of measured exchangeable heme ($[\mathrm{H}]_{\alpha MEM}$ = 4-5 nM, $[\mathrm{H}]_{SA}$ = <1 nM, $[\mathrm{H}]_{H}$ = 8-9 nM; Figure 2.5C). Sub-nanomolar concentrations of heme represent a few molecules or less than one molecule (in the presence of SA) of heme per fL. This is consistent with the low solubility in water and cytotoxicity of free heme [84, 86, 88, 95–97, 100, 101] but invalidates the idea of pools of free heme and implies that heme must be made available through alternative mechanisms. In particular, it highlights that heme mobilisation might occur one molecule at a time from a diffuse cellular heme buffer that binds heme transiently, limiting its concentration and maintaining its bioavailability by releasing it judiciously. The transient nature of the interaction between heme and the buffer - presumed to be comprised of a poly-dispersed ensemble of low-affinity heme-binders - would represent the key feature that defines an exchangeable heme pool. Such mechanisms would contribute to maintaining heme bioavailability and biocompatibility by overseeing heme supply to downstream proteins and preventing heme-induced cytotoxicity, respectively. Heme exchange from the buffer might occur through predissociation of free heme or via inter-protein interaction between a heme donor and a heme acceptor. Thus, a network of heme transfer equilibria would be at least partially responsible for meeting cellular heme demands. In this scenario, heme is allocated to downstream heme proteins by molecules that bind heme transiently, according to thermodynamic gradients dictated by heme affinity. This suggests a scale of heme bioavailability affected by the expression levels of both traditional heme proteins and the proteins that putatively constitute the heme buffer. In support of this view, the enzymatic activity of indoleamine 2,3-dehydrogenase (IDO) was found to decrease in the presence of an *apo*-myoglobin mutant as a consequence of heme release to myoglobin (Mb) [168]. While the great affinity of Mb for heme (K_{d} = 100 pM) [168] accounts for the thermodynamic stabilisation due to the transfer of heme, IDO shows how heme-binding to heme proteins can prove more dynamic

and reversible than traditionally thought, indicating how they actively buffer heme alongside their primary heme-dependent functions.

It is worth noting that altering the oxidation state of the heme iron centre has the potential of severely affecting the thermodynamics and kinetics of the heme transfer. In particular, an increased transfer efficiency would be achieved whenever the redox shift decreases the heme affinity of the buffer component, from which it would be more easily mobilised. Iron mobilisation from the iron-storage protein ferritin is based on a similar strategy. In ferritin, iron is stored as Fe(III) in a crystal ferrihydrite inorganic structure and labilised via reduction to Fe(II), which enhances the solubility of the metal leading to its coordination to cytosolic ligands and chaperones [169]. Moreover, the d^6 high-spin electronic configuration of Fe(II) makes it more labile towards ligand substitution reactions, translating into increased bioavailability. Incidentally, the ferrous form represents the vast majority of the labile iron pool [170], a state that is likely maintained by the low cytosolic redox potential [171]. Conversely, exchangeable heme is thought as largely oxidised in the ferric heme form [172]. Thus, direct comparisons between heme and metal ions in cells requires due precaution. Even though the redox state of the heme iron centre does not severely affect the overall solubility of the complex, the bulkiness of the tetrapyrrole limits the number of species capable of efficiently binding heme through the unoccupied axial positions, sufficiently stabilising it, and preventing it from aggregations and precipitation.

Kinetics can also play a role in making heme bioavailable. From a mechanistic point of view, the description of heme transfer between two heme-binding molecules might cover a range of degrees of pre-dissociation, spanning from a purely dissociative pathway [111] to a purely associative one, with dissociative- and associative-interchange in the middle. The donor-acceptor couple would define the transfer mechanism (Figure 2.6). As the exchange process gravitates more towards an associative type of transfer, the extent to which a heme sensor can probe exchangeable heme shrinks, because it implies a decreased amount of free heme available to be

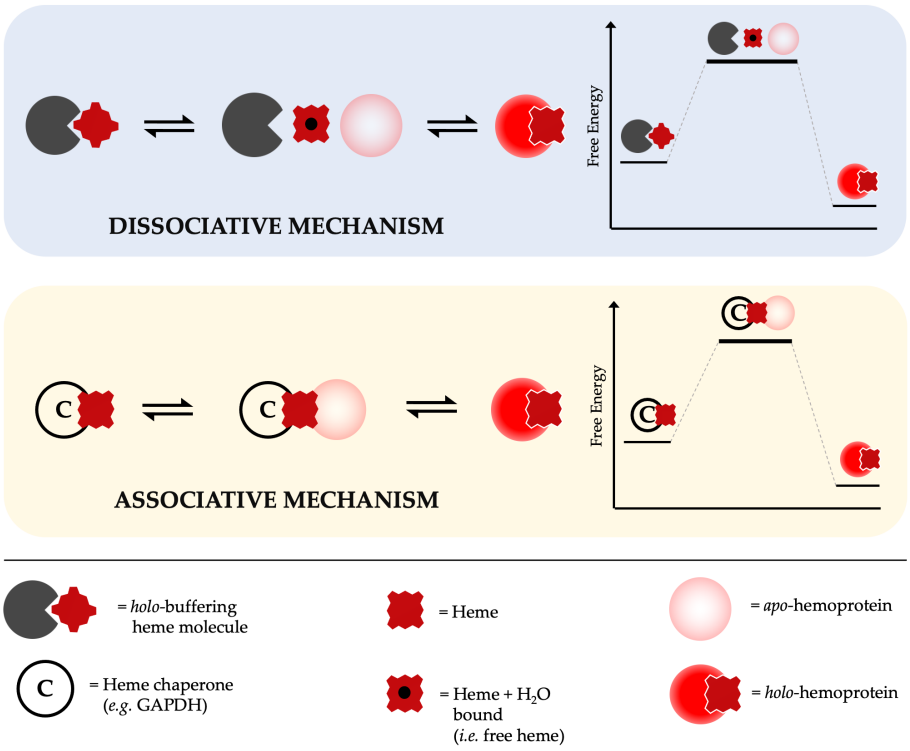

Figure 2.6: Heme-binding partners (dark gray pacmans) are envisaged as transferring heme to heme proteins (red circles) by dissociative (pale gray box) or associative (pale yellow box) pathways, resembling classical ligand exchange mechanisms in coordination chemistry. In a dissociative pathway, a free molecule of heme (assumed to be coordinated by a water molecule) is formed transiently following dissociation from a heme-binding partner, and is intercepted by an *apo*-heme protein (faded red circles). Alternatively, an associative exchange of heme is possible and is shown here for the example of heme delivery by chaperones (C, circles). This latter mechanism may provide better selectivity toward the target heme protein. However, this is not envisaged as being exclusive to chaperones, but a mechanism which, in principle, is available to be used by heme-binding partners as well in delivering heme to *apo*-heme proteins. The different mechanisms of heme exchange may help to fine-tune the delivery of heme to specific acceptors.

measured. This means that sampling heme bioavailability via free heme quantification would prove particularly difficult when the acceptor heme protein binds heme with a great affinity (*e.g.* Mb). Such acceptors might be regarded as "heme sponges" that leave no detectable free heme. Similarly, an associative heme transfer mechanism where there is a direct and cooperative exchange between donor and acceptor would limit the amount of detectable heme, regardless of the heme affinity of the acceptor. Arguably, heme delivered by a chaperone is a process falling into this latter category (Figure 2.6). Nevertheless, a heme sensor like mAPXmEGFP is well suited to probe exchangeable heme whenever the transfer process is delivered through a dissociative mechanism, but also as a general reporter of heme bioavala-

bility changes in the cellular environment, sampling free heme from a wide variety of chemical equilibria.

2.4 Conclusions

The need for a tool to interrogate exchangeable heme has led to the development of the fluorescent heme sensor mAPXmEGFP. The sensor was deployed in live HEK293 cells as a reporter of heme bioavailability which, arguably, is capable of detecting changing levels of free heme, dissociated from a pool of exchangeable heme. For the conditions examined, a diffuse network of heme buffering proteins is thought to maintain heme bioavailability. However, fluctuating levels of heme binding proteins are expected to tune heme bioavailabilty in response to environmental changes and throughout the cell cycle, according to changing requirements of cellular heme. Thus, the measurement of heme concentration in the matrix of intact cells can only be relevant in a relative capacity because: (i) the nature of exchangeable heme levels is dynamic and susceptible to the health and life cycle stage of the cell; and (ii) the portion of exchangeable heme accessible to a given sensor is dictated by the heme binding affinity and concentration of the sensor and the proteomic profile of heme binding proteins (HBPs) when heme concentration is measured. These concepts are explored in later chapters.

Chapter 3

Exploring the roles of HO-1, HO-2, ALAS-1, and GAPDH in maintaining cellular heme homeostasis

3.1 Introduction

Heme biosynthesis, heme trafficking and delivery, and heme degradation must coordinate to maintain heme bioavailability [118]. Together, these pathways oversee the lifecycle of cellular heme (Figure 3.1). Such control likely relies on the interplay between the regulation of the enzymatic activities and the levels of at least four proteins: δ-aminolevulinic acid synthase 1 (ALAS-1, the enzyme catalysing the rate determining step of heme biosynthesis [61,74,93,120,122,173,174]), glyceraldehyde 3-phosphate dehydrogenase (GAPDH, a glycolytic protein that moonlights as a heme chaperone [106,175–177]), heme oxygenase-1 (HO-1, the inducible form of the heme degrading enzyme heme oxygenase [123, 178, 179]), and heme oxygenase-2 (HO-2, the constitutive form of the heme degrading enzyme heme oxygenase [180–182]). To begin the discussion, Sections 3.1.1-3.1.3 provide an overview of the roles and properties of ALAS-1, GAPDH, HO-1, and HO-2 in the context of heme biology.

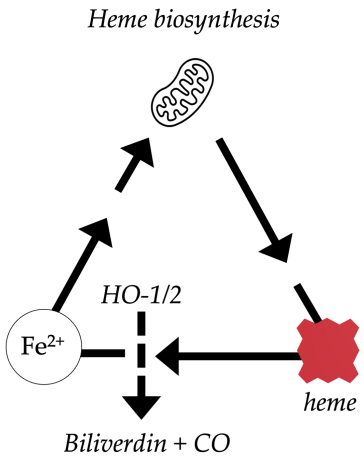

Figure 3.1: The life cycle of heme in cells starts with its biosynthesis in the mitochondria and ends with its degradation by heme oxygenase-1 (HO-1; inducible isoform) and heme oxygenase-2 (HO-2; constitutive isoform). Heme oxygenase generates Fe^{2+} which can be recycled for the synthesis of new heme molecules. A balance between synthesis and degradation contributes to controlling heme bioavailability in cells. Modified from Gallio *et al.* [118].

3.1.1 ALAS-1

ALAS-1 catalyses the first step of heme biosynthesis (Figure 3.2) [61, 122, 183]. Two genes encode δ-aminolevulinic acid synthase: ALAS-1 and ALAS-2. ALAS-1, the housekeeping form, is ubiquitously expressed, whereas ALAS-2 is solely found in erythrocytes and erythroid precursor cells [184–186]. This thesis focuses on ALAS-1 because no cells of the latter group are involved in the present study. ALAS-1 catalyses the condensation between glycine and succinyl-coenzyme A to form δ-aminolevulinic acid (Equation 3.1). This reaction represents the first and rate determining step of the heme biosynthetic pathway [184] (Figure 3.2).

$$\text{glycine} + \text{succinyl-coenzyme A} \xrightarrow{ALAS-1} \delta\text{-aminolevulinic acid} \tag{3.1}$$

A cytosolic precursor of ALAS-1 (preALAS) is post-translationally transported into the mitochondrial matrix where it is proteolitically processed into the mature enzyme. The regulation of ALAS-1 levels is mediated by heme through negative feedback at three different levels: (i) preALAS-1 mRNA synthesis inhibition; (ii) inhibition at post-transcriptional steps; and (iii) inhibition of the transport of preALAS-1 from the cytosol into the mitochondria [73]. Whilst the transport of ALAS-1 into the

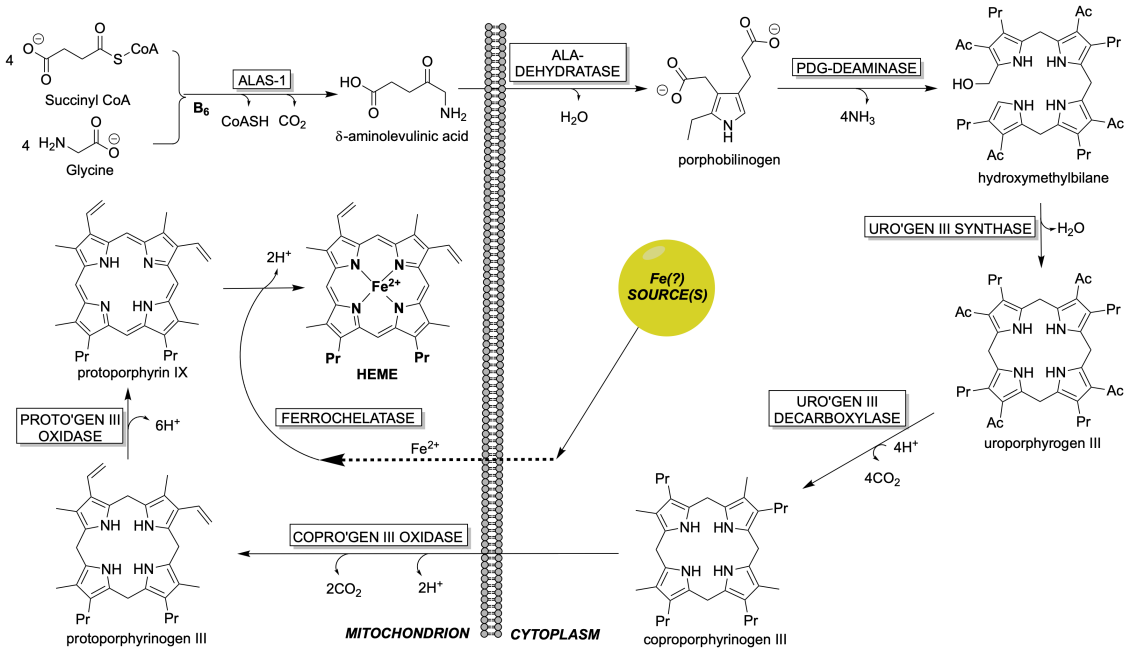

Figure 3.2: Heme biosynthesis is an eight-step enzymatic pathway partially occurring in the mitochondria and the cytoplasm. The first and rate determining step is the condensation of succinyl CoA and glycine to form δ-aminolevulinic acid, a reaction catalysed ALAS-1 (ALA-synthase). A series of consecutive cyclisations and decarboxylations leads to protoporphyrin IX and the insertion of iron - mediated by ferrochelatase - to form heme.

mitochondrial matrix is regulated through heme binding to the cysteine of a heme regulatory motif (HRM) of preALAS-1 [187], further molecular details for the post-translational regulation of heme biosynthesis are required [188]. Thus, the regulation of heme biosynthesis through tuning of ALAS-1 levels is linked to the "regulatory heme pool", as referred to in the literature (see Section 1.2) [73,184,187–189]. A decrease in the regulatory heme pool levels induces an increase in ALAS-1. Conversely, increased regulatory heme levels are associated with a decrease in ALAS-1 [184,189]. On the other hand, ALAS-1 can be easily induced with the administration of protoporphyrinogenic drugs. Cellular iron levels are also likely to be involved. Interestingly, freshly-generated heme in the mitochondria does not affect the activity of ALAS-1 [189], indicating a possible mechanism for the sequestration of mitochondrial heme.

3.1.2 GAPDH

The primary function of glyceraldehyde 3-phosphate dehydrogenase (GAPDH, Figure 3.3) is to catalyse the 6th step of glycolysis (Equation 3.2) [190].

$$\text{Glyceraldehyde 3-phosphate} + \text{NAD}^+ + \text{Pi} \xrightarrow{GAPDH} \text{1,3-Bisphosphoglycerate} + \text{NADH} + \text{H}^+ \tag{3.2}$$

However, GAPDH moonlights to execute a varied spectrum of roles (*e.g.* mRNA stabilisation, DNA damage and repair control, regulation of transcriptional expression, signal transduction, apoptosis, and mitochondrial membrane potential modulation) [176, 177, 191, 192]. Emerging evidence also points to GAPDH as central for the uptake and transport of heme and its insertion into heme proteins [175]. In particular, GAPDH mediates heme delivery by acting as heme chaperone to a growing list of proteins: iNOS [106, 193, 194], HAP1 [106], cytochrome P450s and catalase [195], sGCβ [107], IDO1 and TDO [196, 197], Mb and Hbα, β, and γ [198], and HO-2 [199]. To date, GAPDH is the only heme chaperone that satisfies the following requirements: (i) it is capable of binding and sequestering heme in cells; (ii) its heme binding properties are linked to downstream heme deliveries; and (iii) it can associate with *apo*-heme proteins [175]. However, from the list of proteins proposed

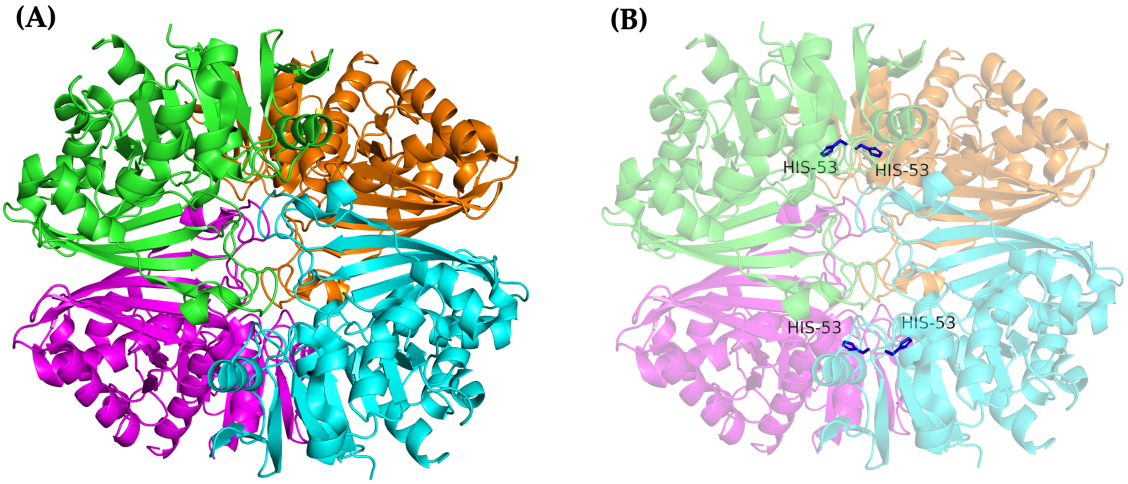

Figure 3.3: (A) Crystal structure of GAPDH (tetramer; PDB: 1ZNQ). (B) The proposed heme binding site in GAPDH is His53, which lies in between the subunits of the tetramer [106]. Further details on the identification and modelling of the GAPDH heme-binding site was provided by Sweeny *et al.* [106].

over the years as possible heme chaperones [118], few have been thoroughly studied. The need to uncover new heme binding proteins that may act as heme chaperones is a current challenge that is further elaborated in Chapter 4.

3.1.3 HO-1 and HO-2

The heme oxygenase system catalyses the degradation of heme into biliverdin, CO, and Fe^{2+} [180, 181]. There are three known isozymes of heme oxygenase: heme oxygenase-1 (HO-1), heme oxygenase-2 (HO-2), and heme oxygenase-3 (HO-3). HO-3 has exclusively been detected in mice, therefore the discussion in this thesis is focused on HO-1 and HO-2. HO-1 and HO-2 exhibit different structures [200, 201] (Figure 3.4), regulation [202], and tissue distribution [180, 181]. Most notably, the HO-1 gene displays consensus sequences for several regulatory elements in its promoter region (*e.g.* heat-shock factor, AP-1, NFKB, metal regulatory elements). The shared feature of the different stimuli that induce HO-1 expression is the ability to cause oxidative stress, including excess heme. Thus, excess heme induces its own degradation through gene expression of HO-1 [203, 204]. In contrast, a single glucocorticoid response element (GRE) is known in the HO-2 promoter gene. Generally speaking, HO-1 and HO-2 are regarded as isozymes and, more specifically, as the inducible and the constitutive forms, respectively. In HEK293 cells (the model system in this study) and, more generally, in the cardiovascular system, HO-2 is the predominant form under normal conditions. HO-2 possesses heme regulatory motifs (HRMs) that aid heme transfer to the catalytically active binding site [111] but do not affect its expression levels. Rather, these are post-translationally down-regulated by lowered heme occupancy in the active site of HO-2 which triggers its chaperone-mediated autophagy [205]. Overall, whilst HO-2 degrades heme under physiological conditions, it aids the restoration of heme levels when low. Hence, HO-2 is gaining increasing recognition as a key player in the maintenance of physiological levels of cellular heme as it degrades heme constitutively when heme is present in excess, but is degraded under heme deficient conditions. Moreover, in the absence of excess

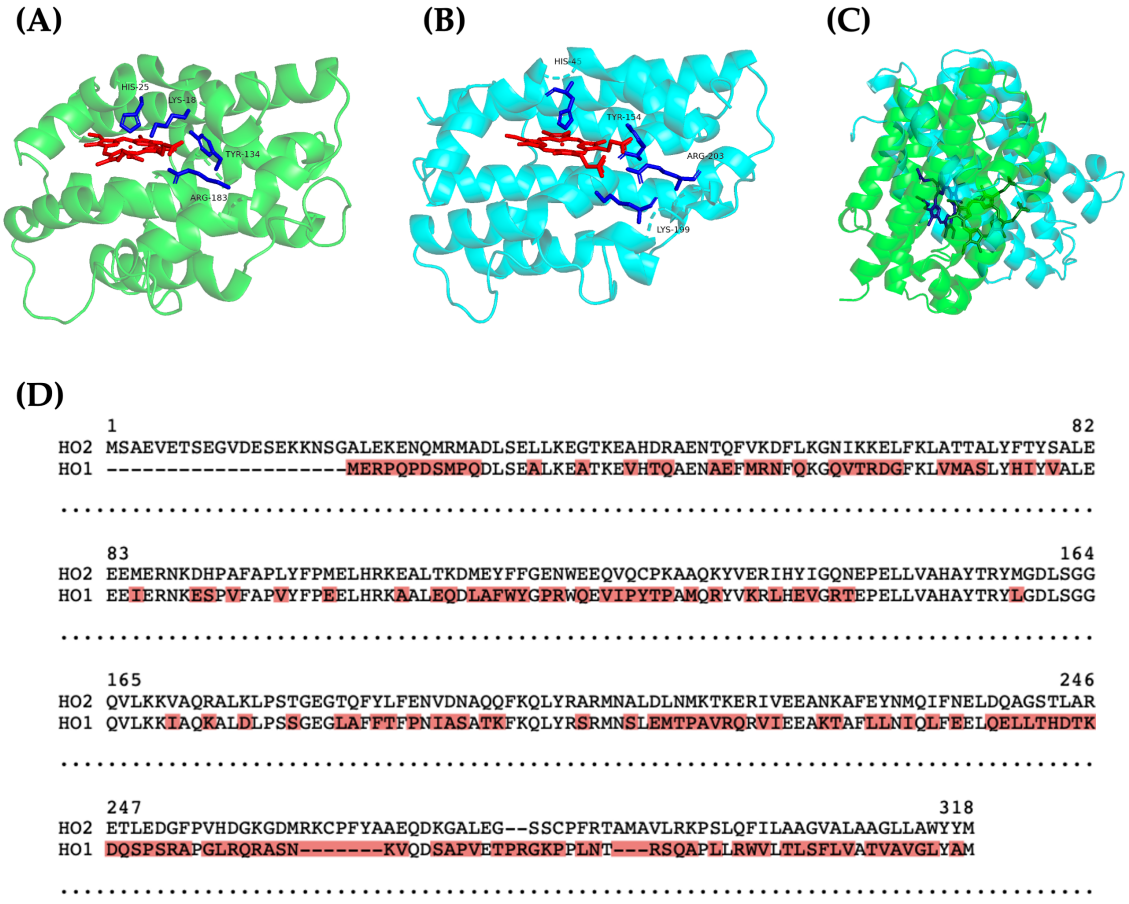

Figure 3.4: Although HO-1 and HO-2 catalyse the same reaction, they differ in primary structure, 3D structure, and regulation, suggesting different roles in the maintenance of heme homeostasis. (A) Crystal structure of *holo*-HO-1 (PDB: 1N45 [201]; residues involved in heme binding in blue). (B) Crystal structure of *holo*-HO-2 (PDB: 2QPP [200]; residues involved in heme binding in blue). (C) Alignment of the structures in (A) and (B), respectively (green: HO-1; blue: HO-2). (D) Alignment between the primary sequence of human HO-1 (P09601) and HO-2 (P30515). Mismatches in the alignment of the amino acid sequences of HO-1 and HO-2 are highlighted in red.

heme, endogenous heme concentration is regarded as too limiting to observe any HO-2 activity. In this scenario, HO-2 would act as a heme buffering factor that contributes to maintaining heme bioavalability [172]. Hence, when heme is within the boundaries of physiologically supported concentration (undefined), *holo*-HO-2 is a passive source of exchangeable heme.

3.1.4 Aims of this chapter

Provided that ALAS-1, GAPDH, HO-1, and HO-2 play key roles in controlling cellular heme levels, it is desirable to understand how the cell responds to tailored perturbations of these systems and to verify the existence of an interplay between

them. The study of these cellular pathways is carried out in HEK293-mAPXmEGFP cells by means of two strategies: (i) by inhibiting heme biosynthesis and the activity of HO-1, and HO-2; and (ii) by using RNA interference (RNAi) to downregulate the protein levels of ALAS-1, GAPDH, HO-1, and HO-2. The relative levels of these key proteins is estimated by quantitative immunoblotting. Alongside this analysis, bioavailable heme is estimated by measuring the fluorescence lifetime output of the mAPXmEGFP sensor. Given the ambiguity generated by the interpretation of vanishingly low concentrations of heme previously measured with mAPXmEGFP (Section 2.2.4), a new concept for the interpretation of the lifetime microscopy results is introduced and deployed: "heme accessibility". In particular, heme accessibility allows more intuitive reporting on fluctuating relative levels of cellular heme bioavailability. This is discussed below.

3.2 A new concept of heme accessibility

It can be unclear which type(s) of heme (*i.e.* total heme, protein heme, exchangeable heme, or free heme - as defined in Section 1.2) a heme sensor is measuring. This uncertainty is emphasised by the generally vanishingly low concentration of heme reported by heme sensors, mAPXmEGFP included (Table 1.1). Thus, given the absolute need to supply enough heme throughout the cell, interpreting the results in this form is particularly difficult. Because independent studies measured intracellular heme concentration in the nanomolar range (Table 1.1) [65, 66, 68], it has been hypothesised that free heme is the type of heme being reported on [66, 118], consistent with the requirement of keeping its concentration low due to its cytotoxicity. However, it is problematic to reconcile miniscule amounts of detected cellular heme with the logistical needs of heme supply and demand to gain physiologically relevant insights into heme biology. Therefore, how we interpret the output of the mAPXmEGFP sensor measurements requires revision.

As outlined in Section 2.1, a genetically-encoded heme sensor is normally constituted by an *apo*-heme protein and a fluorescent tag. The chemical and physical

properties of the heme-binding moiety specifies the kind(s) of heme the sensor is reporting on and the mechanism through which heme binding to the sensor occurs (as elaborated in Section 2.3 and in Figure 2.6). For example, a heme sensor where the selected heme binding domain is a protein naturally allocated with heme through GAPDH (*e.g.* IDO, HO-2, sGC; Section 3.1.2) would be well suited to study the maturation of such protein mediated by its GAPDH-dependent heme delivery. However, with no other heme chaperones confirmed yet (with the possible exception of HRG9 [206]) and with little or no information as to how the majority of heme proteins are loaded with heme, we can only attempt to reverse-engineer which kind(s) of heme any given heme sensor is measuring. For the expression of mAPXmEGFP in mammalian cells such as HEK293, because mAPX is an exogenous protein (from soybean; protein sequence in Appendix A.1.2, Figure A.1), no dedicated means of heme acquisition are arguably in place. Instead, mAPXmEGFP must rely on heme binding from reservoirs of exchangeable heme, which include free heme and heme loosely bound to other biomolecules (Section 1.2). It follows that mAPXmEGFP can probe exchangeable heme to a degree that depends on its heme affinity constant - because the higher the affinity the more heme can be drawn to the sensor from an exchangeable reservoir - but also according to how the cells tunes heme bioavailability by adapting to environmental changes or as heme bioavailability requirements change during the cell cycle. Further, it is possible that heme provision might have to be localised to specific regions of the cell, at different rates and times. Keeping these complications in mind, mAPXmEGFP can be used as a reporter of changing levels of heme bioavailability when its *access* to exchangeable heme changes. This notion defines the concept of *heme accessibility* and can be generalised as referring to the amount of heme available and accessible to any given heme protein, according to its chemistry, cellular locus, and other relevant factors.

Overall, the concept of heme accessibility contextualises heme measurements in the cellular milieu, acknowledging the complexities therein, and recognising that the reported bioavailability, as measured by a probe, is intrinsically relative to the probe

deployed for the measurement.

3.2.1 mAPXmEGFP heme accessibility can be quantified

In the case of mAPXmEGFP, heme accessibility as outlined above can be quantified as the degree of access that the sensor has to exchangeable heme. In particular, as discussed in Section 3.2, the access of mAPXmEGFP to cellular heme will be determined by cellular *loci*, sensor heme binding affinity, and the specific profile of heme-binding protein levels - all of which define the nature of exchangeable heme at the time of the measurement.

A quantitative description of the fluorescence decay of mAPXmEGFP and how this is affected by heme binding was provided in Section 2.2. As shown, the shorter lifetime of *holo*-mAPXmEGFP compared to *apo*-mAPXmEGFP and, in particular, the values of the pre-exponential factors α_{Fast} and α_{Slow}, can be used to determine the fraction of *holo*-mAPXmEGFP ($f(i,j)$; *i.e.* the ratio between *holo*- and *total*-mAPXmEGFP, as defined by Equation 2.11). Allowing f_C as the fraction of *holo*-mAPXmEGFP measured in a control experiment, and f as that measured in an experimental test condition, the percentage heme accessibility change, $\%H_{acc}$, of mAPXmEGFP is given by Equation 3.3.

$$\%H_{acc} = 100\% \times \frac{f - f_C}{f_C} \tag{3.3}$$

$\%H_{acc}$ represents the percentage change in the fraction of *holo*-mAPXmEGFP $f(i,j)$ for a particular experimental condition, f, compared to that of a control, f_C, and provides an expression for determining the heme accessibility of mAPXmEGFP, quantifying the relative amplitude of this change. $\%H_{acc}$ is an adimensional index that reports on increased or decreased access to heme of mAPXmEGFP. In particular, changes to heme accessibility of mAPXmEGFP are interpreted as corresponding to increased or decreased cellular heme bioavailability, respectively. When heme bioavailability increases, $\%H_{acc} > 0$; on the other hand, when heme bioavailability

decreases $\%H_{acc} < 0$.

3.3 Interference of the activity of ALAS-1, HO-1, and HO-2.

HEK293-mAPXmEGFP cells were treated with 1 mM SA, 10 μM hemin, and 10 μM ZnPP respectively 24 hours prior to analysis. In this Chapter, although no significant changes have been implemented to the experimental procedure for the supply of SA and hemin compared to the previous Chapter, the two chemicals are used with the specific aim of interfering with ALAS-1 activity (SA), downregulate ALAS-1 expression (hemin), induce HO-1 expression (hemin), and modulate HO-2 degradation (hemin) [111, 205]. In addition, ZnPP was separately supplied to compete with heme for the occupancy of the active site of HO-1 and HO-2 and inhibit the activity of the intracellular heme degradation machinery [207]. For each of these conditions, heme accessibility of mAPXmEGFP was obtained through FLIM analysis and the relative protein levels of ALAS-1, HO-1, HO-2, and GAPDH were measured by fluorescence immunoblotting (experimental details in Appendix A.5).

3.3.1 Analysis of mAPXmEGFP heme accessibility

To measure how the heme accessibility of mAPXmEGFP changes in HEK293-mAPXmEGFP when heme biosynthesis is inhibited, hemin is supplemented, or the activity of HO-1 and HO-2 is inhibited, HEK293-mAPXmEGFP cells were cultured in the presence of 1 mM SA or 10 μM hemin or and 10 μM ZnPP and imaged by FLIM. The detailed experimental methodology that was developed for these experiments is presented in Figure 3.5. The measured fluorescence decays in each case were fitted to biexponential models (Equation 2.3) to calculate the distribution of intensity-weighted mean lifetimes (Figure 3.5A-D). The distribution of the pre-exponential factors α_{Slow} and α_{Fast} were also plotted to represent the quantitative distribution of *holo*- and *total*-mAPXmEGFP in the cells (Figure 3.5E).

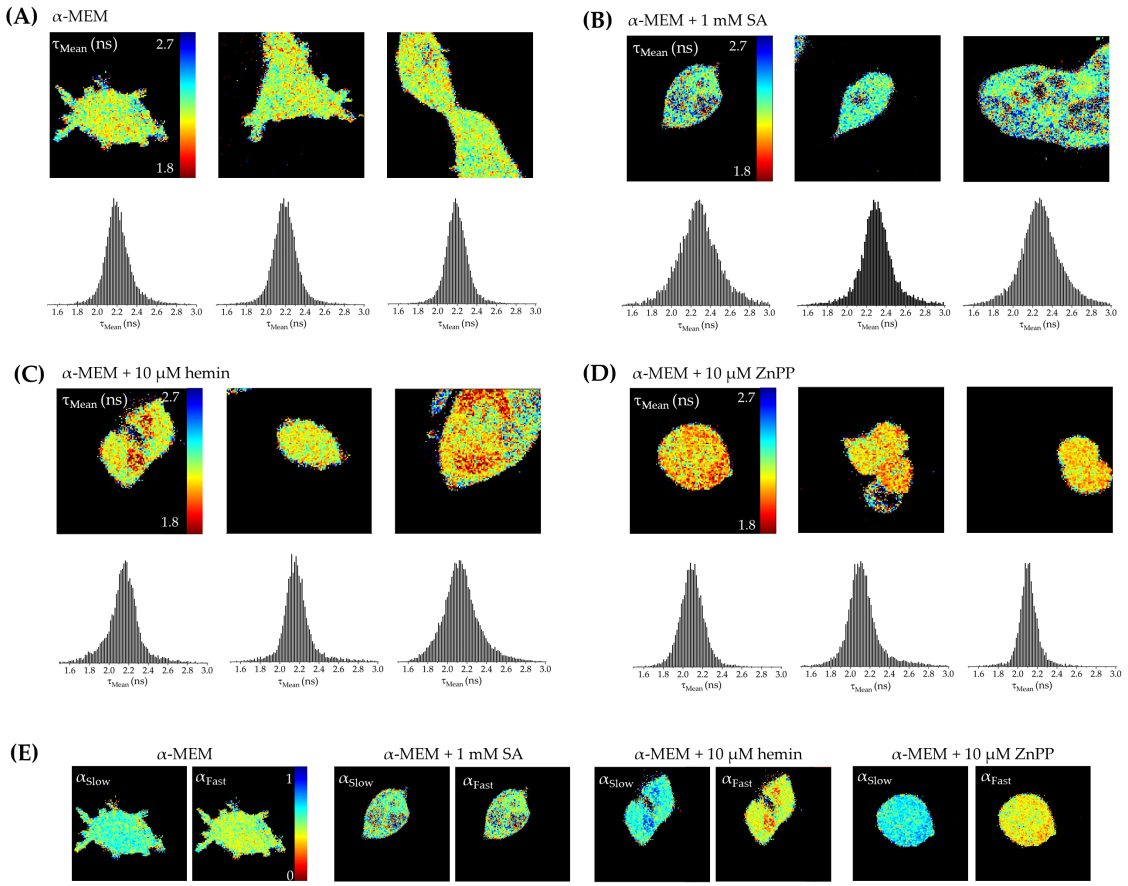

Figure 3.5: HEK293-mAPXmEGFP cells were cultured until 70% confluent in separate microscopy dishes. 24 h prior to imaging, the minimal growth medium (α-MEM, αα, 10% FBS) was refreshed and different dishes were supplemented with the following additives: 1 mM SA, or 10 μM hemin, or 10 μM ZnPP. In a control experiment, the medium was refreshed with no supplementation. Images of three cell clusters representative for each condition are shown: (A) Cells grown in α-MEM (control): (B) Cells grown in α-MEM + 1 mM SA; (C) Cells grown in α-MEM + 10 μM hemin; and (D) Cells grown in α-MEM + 10 μM ZnPP. At least seven images per condition were acquired. Each of the colour maps is accompanied by a histogram (below) showing the distribution of frequencies for which particular values of τ_{Mean} occur within the corresponding cluster. FLIM images were acquired as outlined in Appendix A.6. (E) Examples of the colour-coded representation of the fast (α_{Fast}) and slow (α_{Slow}) lifetime fluorescence decay components of mAPXmEGFP determined for each condition.

The values of $\%H_{acc}$ were calculated with reference to a control where cells were cultured in minimum essential medium (α-MEM, αα, 10% FBS). $\%H_{acc}$ values are listed in Table 3.1 (bottom row) with other parameters obtained through fitting of the 2D lifetime images acquired. mAPXmEGFP heme accessibility is, respectively, lowered and increased by approximately ±10% when cells are cultured in the presence of 1 mM SA or 10 μM hemin. These results show that the amount of exchangeable heme mAPXmEGFP has access to can be varied within a range that

spans 20% of the sensor response range through the use of SA and hemin. However, the concentrations of 1 mM SA and 10 μM hemin lie in the upper limit of concentrations used in the literature for similar purposes and can compromise cell viability (Figure 3.9) and modify the normal proteomic profile. These variations could affect cellular and heme homeostasis to an extent that would affect a truthful interpretation of the results.

	1 mM SA	**Control**	**10 μM hemin**	**10 μM ZnPP**
$\boldsymbol{\tau_{Mean}(ns)}$	2.30±0.02	2.25±0.01	2.20±0.03	2.10±0.06
$\boldsymbol{\alpha_{Slow}}$	0.535	0.495	0.457	0.398
$\boldsymbol{\alpha_{Fast}}$	0.465	0.505	0.543	0.602
$\boldsymbol{f(i,j)}$	0.324	0.374	0.422	0.497
$\boldsymbol{\%H_{acc}}$	-14%	-	+13%	+33%

Table 3.1: Summary of relevant parameters obtained from the fitting of the fluorescence lifetime decay measured for mAPXmEGFP in HEK293-mAPXmEGFP cells grown in the presence of 1 mM SA, or 10 μM hemin, or 10 μM ZnPP. Lifetimes are expressed as the modal values of lifetime distributions and averaged over at least seven clusters of cells for which separate images were acquired - representative examples are shown in Figure 3.5. The pre-exponential factors α_{Slow} and α_{Fast} were used to calculate the overall ratio between *holo*- and *total*-mAPXmEGFP, $f(i,j)$ (Equation 2.11), and the corresponding $\%H_{acc}$ (Equation 3.3) in reference to the control experiment where cells were cultured in minimum essential medium only.

Interestingly, heme accessibility change is markedly increased by around 30% when ZnPP was used for the incubation. In order to quantify the binding of ZnPP to mAPXmEGFP, *in vitro* experiments show that ZnPP binds to mAPXmEGFP and satisfies the energy match requirement for resonance energy transfer with mEGFP (Figure 3.6A-B). However, ZnPP binding to mAPXmEGFP was found to not affect the lifetime of the sensor when mEGFP is excited by a pulsed laser light at 490 nm (Figure 3.6C-D). This can be accounted for by hypothesising that ZnPP binds unspecifically and away from the mEGFP chromophore - thus impeding FRET due to excessive distance between the chromophores - or because of a misalignment between the dipole transition moments of mEGFP and ZnPP [136, 137]. Another possible disruption induced by the presence of ZnPP would be the intrinsic fluorescence of ZnPP itself (λ_{Em} = 589 nm [208]). However, when a solution of ZnPP was excited with laser light at 490 nm - the excitation wavelength of mEGFP - no fluorescence signal was detected, indicating that ZnPP would not affect the measurement

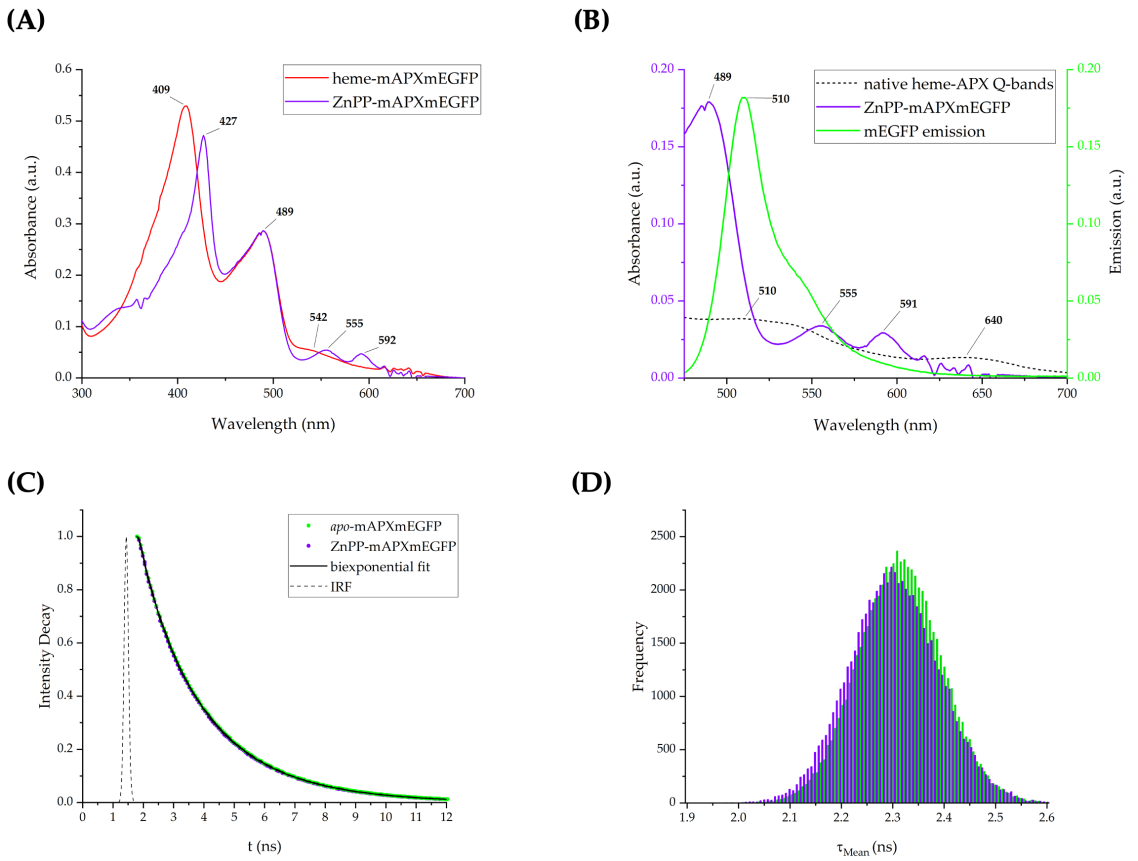

Figure 3.6: ZnPP binding to mAPXmEGFP. (A) Comparison between the UV-vis spectra of *heme*-mAPXmEGFP (red trace) and *ZnPP*-mAPXmEGFP (purple trace). (B) Overlap between the Q-bands of ZnPP-mAPXmEGFP (purple trace) (555 nm; 591 nm) and the emission band of mEGFP (green trace). The Q bands of native heme-APX (dotted trace) are also reported as a reference. (C) Although ZnPP binds to mAPXmEGFP and the resulting Q-bands overlap with mEGFP emission, no change in the fluorescence lifetime decay of *apo*-mAPXmEGFP was measured after incubation with ZnPP ($\chi^2_{apo-mAPXmEGFP} = 1.07$; $\chi^2_{ZnPP-mAPXmEGFP} = 0.97$). (D) The distributions of the τ_{Mean} of *apo*-mAPXmEGFP (green) and ZnPP-mAPXmEGFP (purple) measured in HEK293-mAPXmEGFP are superimposed.

of mAPXmEGFP lifetime. Thus the effects of ZnPP in HEK293-mAPXmEGFP are discussed in this Chapter assuming that the lifetime of mAPXmEGFP was not influenced by the presence of ZnPP in the incubation media.

3.3.2 Analysis of protein levels

To contextualise the change in the heme accessibility, $\%H_{acc}$, of mAPXmEGFP measured for the conditions explored in Section 3.3.1, the relative levels of the proteins ALAS-1, HO-1, HO-2, and GAPDH were measured by fluorescence western blotting (detailed methodology can be found in Appendix A.5) in whole cell lysates of HEK293-mAPXmEGFP cultured in minimum essential medium (α-MEM, αα, 10% FBS; control) and in the presence of 1 mM SA, 10 μM hemin, and 10 μM ZnPP, respectively. The percentage changes of ALAS-1, HO-1, HO-2, and GAPDH are summarised in Table 3.2 and shown in Figure 3.7. The results are discussed in the following paragraphs of this Section.

Incubation	**ALAS-1**	**HO-1**	**HO-2**	**GAPDH**	$\%H_{acc}$
1 mM SA	+340%	-40%	-20%	+5%	-14%
10 μM Hemin	-80%	+300%	-20%	+20%	+13%
10 μM ZnPP	-100%	+1500%	-40%	+30%	+33%

Table 3.2: Summary of the measured normalised fold change in the levels of ALAS-1, HO-1, HO-2, and GAPDH in HEK293-mAPXmEGFP lysates following 24 h incubation with 1 mM SA, 10 μM hemin and 10 μM ZnPP. The fold change was measured by densitometry and normalised using β-actin detection (Appendix A.5 for full experimental detail). The table reports the mean values measured for each incubation (refer to Figure 3.7 for more details). Protein level changes are colour-coded in green (positive change) and red (negative change). The calculated values of mAPXmEGFP $\%H_{acc}$ - as defined in Section 3.2 - are also reported on the last column for each incubation.

Incubation with SA

ALAS-1 is upregulated significantly when cells are incubated with SA (+340%). At the same time HO-1 and HO-2 are downregulated by -40% and -20%, respectively. This indicates that when heme biosynthesis is impeded cells compensate for this disruption by upregulating ALAS-1 – and thus increasing their own heme biosynthetic capacity - whilst decreasing the degradation of heme by HO-1 - the inducible isoform of heme oxygenase - and HO-2 – the degradation of which is triggered by lowered heme occupancy in its active site [205]. Such effect suggests a mechanism of compensation to face the reduced regime of heme production due to the presence of SA. The slight increase (+5%) in GAPDH is within the standard deviation

measured for the replicates relative to the untreated cells (control; Figure 3.7).

This scenario is accompanied by a lower level of $\%H_{acc}$ detected by mAPXmEGFP (Table 3.1), highlighting that, overall, cellular heme bioavailability decreases. In this case, the changes in protein levels is consistent with a mechanism that compensates for the lowered production of heme due to heme biosynthesis inhibition. It is worth noting though that the upregulation in ALAS-1 analysed over a longer experimental time-frame (*e.g.* 48 hours incubation instead of 24 hours) might fully compensate, or over-compensate for the fraction of it inhibited by SA, and regenerate completely bioavailable heme levels. In this scenario, mAPXmEGFP $\%H_{acc}$ would be similar to the control in Table 3.1 and thus reported as close to zero.

Incubation with hemin and ZnPP

The incubation of 10 μM hemin and 10 μM ZnPP generated the same regulation pattern of the four proteins ALAS-1, HO-1, HO-2, and GAPDH, differing only in the amplitude of their relative fold change, with ZnPP inducing enhanced effects (*cf.* hemin; Table 3.2 and Figure 3.7). The addition of exogenous hemin or ZnPP has increased the intracellular concentration of porphyrins decreasing the requirement for heme synthesis and leading to a drastic downregulation of ALAS-1 (-80%, hemin; -100%, ZnPP). In particular, 10 μM ZnPP downregulates ALAS-1 to the point that it was undetectable by immunoblotting (Figure 3.7E). On the other hand, the increased heme bioavailability - measured with the positive values of mAPXmEGFP $\%H_{acc}$ (+13%, hemin; +33% ZnPP) - was likely exceeding the buffering capacity of the cell and induced a dramatic upregulation of HO-1 (+300%, hemin; +1500% ZnPP). This speaks for the efficacy of ZnPP in inhibiting the heme oxygenase system but also in generating oxidative stress, which in turn induces HO-1 expression. As mentioned in Section 3.1.3, the HO-1 gene is induced by heme binding to its promoter. Thus, HO-1 upregulation can be regarded as a mechanism to cope with the increased concentration of heme. By analogy with the effect induced by the presence of SA, the reciprocal up/down-regulation of ALAS-1 and HO-1 indicates a compensation mechanism that aids the re-establishment of homeostatic cellular

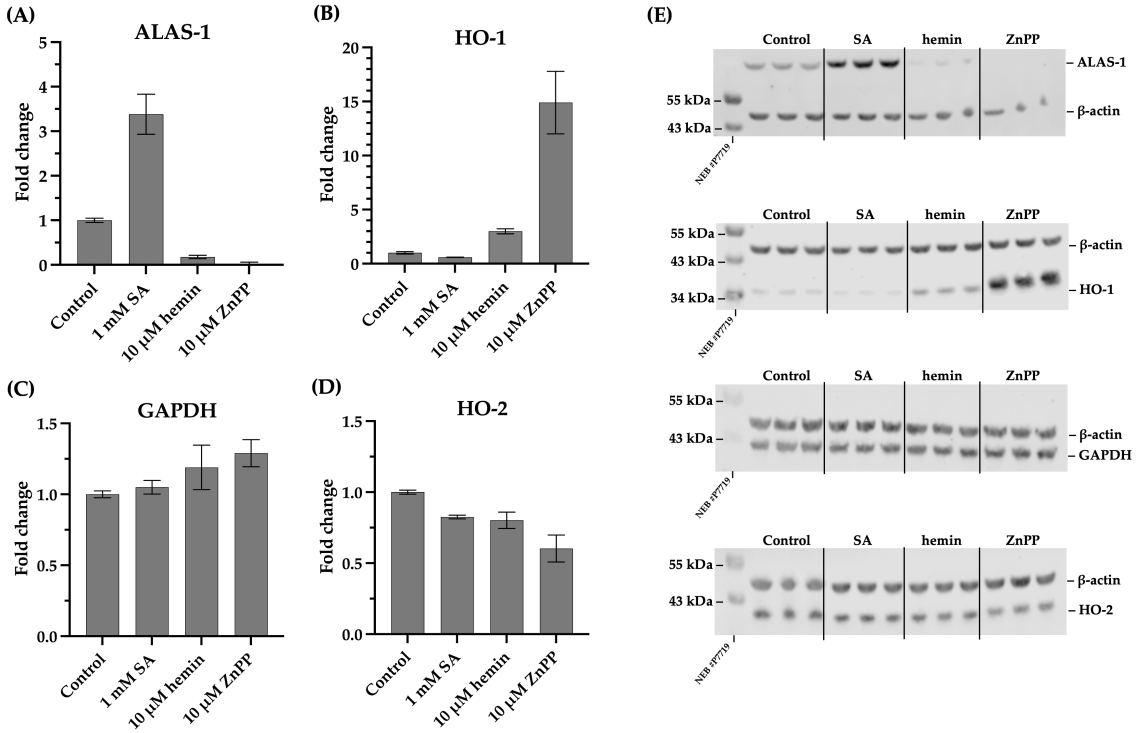

Figure 3.7: Quantitative immunoblotting of whole lysates of HEK293-mAPXmEGFP cultured for 24 h in the presence of 1 mM SA, 10 µM hemin, and 10 µM ZnPP highlights a reciprocal and opposite regulation of (A) ALAS-1 and (B) HO-1 levels, and (C) GAPDH and (D) HO-2 levels. Error bars show the standard deviation over triplicate measurements. (E) Representative immunoblots showing a comparison between the band intensities detected in cell lysates of HEK293-mAPXmEGFP grown in the presence of 1 mM SA (SA), 10 µM hemin (hemin), and 10 µM ZnPP (ZnPP). Each blot shows respectively (top to bottom) ALAS-1 detection, HO-2 detection, GAPDH detection, and HO-2 for the conditions explored. Band intensities was measured by densitometry and normalised using β-actin detection as an internal control. Membranes were imaged using a Licor Odyssey Fc. Analysis of band intensities was carried out with Empiria Studio® Software. Full experimental details in Appendix A.5.

heme levels in response to stimuli that disrupt it. The time-frame of the experiment (24 h) can once again explain why, despite the substantial up-regulation of HO-1, it was still possible to detect a positive change in the $\%H_{acc}$ of mAPXmEGFP. The reciprocal interplay between the levels of ALAS-1 and HO-1 can be visualised in Figure 3.7A-B.

HO-2 was down-regulated in the presence of hemin and ZnPP by -20% and -40%, respectively. As recently shown by Ragsdale and collaborators, HO-2 is degraded when heme occupancy in its active site is reduced [205]. This aligns with the notion that heme is not being produced (ALAS-1 downregulation) whilst HO-1 is over-expressed (increased heme degradation), making heme less available. However, it

clashes with the calculated $\%H_{acc} = +33\%$ measured for mAPXmEGFP when incubated with ZnPP. An interpretation of this effect is the following. A high regime of heme degradation (high level of HO- 1) and a low regime of heme production (low ALAS-1) generate cellular heme deficiency that leads to heme being released from the exchangeable heme reservoir, making heme, overall, transiently more bioavailable. In this scenario, the low occupancy in the active site of HO-2 – which triggers its degradation [205] - can be interpreted as a localised effect within the endoplasmic reticulum - the main locus of HO-1 and HO-2 [180, 181, 207] – where HO-1 is being highly expressed (+300%, hemin; +1500% ZnPP). In summary, whilst cellular heme bioavailability is on average increased because heme is being released from its exchangeable reservoir, the over-expression of HO-1 leads to low heme levels in the endoplasmic reticulum, and in turn, to the degradation of HO-2.

Interestingly, both hemin and ZnPP induced an increase in GAPDH levels (+20%, hemin; +30% ZnPP), which, in this context, could enhance the heme buffering capacity of the cell.

Overall, Table 3.2 and Figure 3.7 highlight two patterns of reciprocal regulation

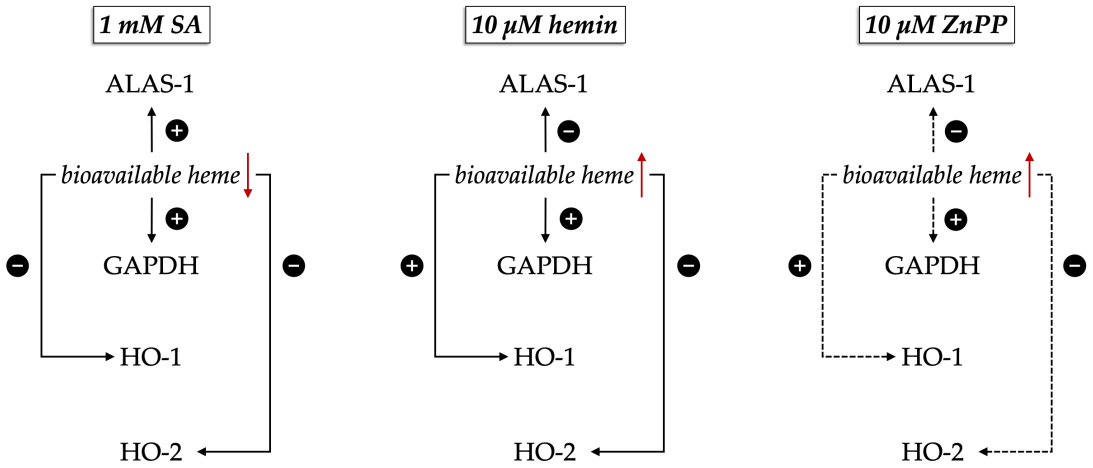

Figure 3.8: Schematic representation of the effects induced by incubation of HEK293-mAPXmEGFP for 24 h with 1 mM SA, 10 μM hemin, and 10 μM ZnPP, respectively. The red arrows represent increasing (upward-pointing) or decreasing (downward-pointing) levels of bioavailable heme. As a consequence of changing levels of bioavailable heme, the levels of ALAS-1, GAPDH, HO-1, and HO-2 are either up-regulated (plus signs) or down-regulated (minus signs). The arrows connecting bioavailable heme to the other proteins in the case of the 10 μM ZnPP incubation are dotted because it is not clear whether proteins level are directly affected by the level of bioavailable heme or by other unknown pathways induced by the presence ZnPP.

of (i) ALAS-1 and HO-1, and (ii) GAPDH and HO-2 levels, respectively. The incubation with ZnPP generated the most dramatic effects in terms for ALAS-1 down-regulation, HO-1 up-regulation, and the mAPXmEGFP $\%H_{acc}$. However, the sum of the downstream effects triggered by ZnPP - which are likely to outnumber heme-dependent cellular pathways - can be hard to predict and take into account. The observed pattern of regulation is represented in schematic form in Figure 3.8.

3.3.3 SA, hemin, and ZnPP affect the viability of HEK293 cells

The conditions explored in Section 3.3.2 can lead to complications due to unforeseen downstream effects or cytotoxicity. For example, cells were supplemented with ZnPP to inhibit the activity of HO-1 and HO-2, but ZnPP lacks specificity despite being selective. More specifically, ZnPP is a potent inhibitor of heme oxygenase activity by competing with heme for the occupation of the enzyme's active site [207], but it non-selectively binds HO-1 and HO-2, as well as being capable of modulating the activity of other enzymes such as cytochrome P450, inducible nitric oxide synthase (iNOS), and soluble guanylate cyclase (sGC) and acts as a transcription cofactor for several genes [179, 207]. Similar considerations also apply to hemin incubation and, to a minor extent to succinyl acetone when supplied as media additives to cells. This introduces complications that makes it difficult to draw confident physiological arguments to explain heme biology. Ultimately, the disruptions introduced by adding SA, hemin, and ZnPP to the growth medium reduces cell viability, as shown in Figure 3.9. Because of such complications, the interference with the functions of key proteins involved in heme biology is carried out in the next Section through with a more sophisticated approach, using RNA interference.

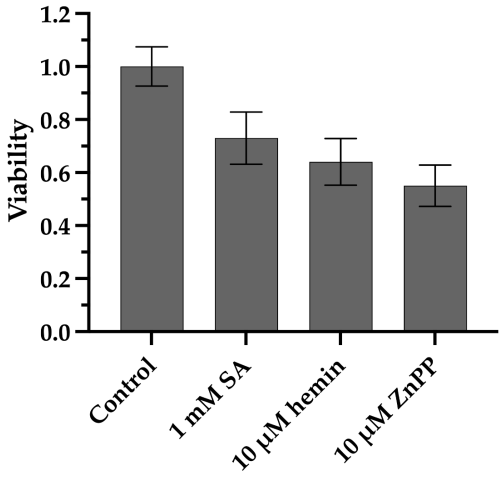

Figure 3.9: Relative viability of HEK293-mAPXmEGFP 24 h after the addition to minimal growth medium of 1 mM SA, 10 μM hemin, and 10 μM ZnPP. The relative viability was measured by means of a MTT assay (see Appendix A.4.3).

3.4 The use of RNA interference to study heme bioavailability

In this section, mAPXmEGFP and FLIM are used alongside gene silencing techniques to study cellular heme availability. Using a tailored gene silencing experiment, mAPXmEGFP and FLIM comprise a toolkit to analyse changes in bioavailable heme. This approach minimises the potential for side effects that may influence heme homeostasis in unpredictable ways. The proteins involved in this study are known to be involved in heme homeostasis (HO-1, HO-2, GAPDH, and ALAS-1)

A versatile tool to knockdown protein levels at the post-transcriptional stage is RNA interference (RNAi). RNAi is a natural mechanism for the post-transcriptional control of gene expression. Briefly, a double stranded RNA - or a hairpin RNA - is cleaved by Dicer (a RNAase) into a small interfering RNA duplex (siRNA, 21-26 nucleotides) that works as a template to recognise and bind homologous RNA sequence produced through the transcription of a given gene. The degradation of the RNA sequence by Dicer then determines the silencing of the gene that produced the RNA sequence. The design of siRNA to selectively silence genes has now become a potent tool in molecular biology [209].

In this study, the HMOX2 and the GAPDH genes were targeted using this

method. HMOX2 was chosen because the post-transcriptional regulation of HO-2 has recently been linked to the restoration of intracellular heme levels [205]. Similarly, GAPDH was selected in the light of its emerging roles in heme biology (Section 3.1.2). The silencing of HMOX2 and GAPDH in HEK239-mAPXmEGFP was accompanied with the measurement of distribution of lifetime of mAPXmEGFP through FLIM (Figure 3.10). Moreover, following the silencing of HO-2 (knocked down by 50%; Table 3.4) and GAPDH (knocked down by 42%; Table 3.4) the changes in the protein levels of ALAS-1, HO-2, HO-1, and GAPDH were measured by immunoblotting (full experimental details in Appendices A.4.4 and A.5).

siRNA knockdown of HO-2

A pair of siRNA sequences (HO-2 siRNA1, HO-2 siRNA2; Table 3.3) for the HMOX2 gene (human gene for HO-2) was designed to target respectively the nucleotide sequences in positions 528-548 and 529-279 of the HMOX2 gene (gene ID: HMOX2-NM_002134.4) as previously reported in the literature [210].

	Sequence 5'-3'	Overhang	Number of Bases	MW
HO-2 siRNA1	GCACACGACCGGGCAGAAA	UU	21	6144.83
HO-2 siRNA1_as	UUUCUGCCCGGUCGUGUGC	UU	21	5983.55
HO-2 siRNA2	GUACGUGGAGCGGAUCCAC	UU	21	6115.74
HO-2 siRNA2_as	GUGGAUCCGCUCCACGUAC	UU	21	6012.64

Table 3.3: Sequences and properties of the two siRNA designed to silence HMOX2 (siRNA1; siRNA2). Sense and anti-sense (as) strands are reported for each siRNA duplexes. Positions 528-548 and 529-279 of the HMOX2 gene (gene ID: HMOX2-NM_002134.4) were targeted.

A 50% knockdown of HO-2 (data shown in Appendix A.5) was followed by a slight increase in the level of HO-1 (+10%) and a more significant increase in GAPDH (+25%). The decrease in the HO-2 level was accompanied by the induction of HO-1 to counterbalance the reduced heme degradation regime due to limited HO-2 activity. At the same time, the induction of GAPDH may be interpreted as an attempt to make more heme available to HO-2 - because GAPDH is a heme chaperone for HO-2 [199] - by enhancing the activity of the population of the protein that is still being expressed (50%; *cf.* normal conditions). The increased level of GAPDH - which will effectively be buffering cellular heme to a major extent compared to nor-

mal conditions - also explains why the value of $\%H_{acc}$ for mAPXmEGFP changes only marginally (-0.2%).

On the other hand, the detected change in ALAS-1 when HO-2 is knocked down by siRNA was not significant, indicating that the reduced expression of HO-2 does not affect heme biosynthesis.

RNAi knockdowns	**ALAS-1**	**HO-1**	**HO-2**	**GAPDH**	$\%H_{acc}$
siRNA HO-2	unchanged	+10%	-50%	+25%	-0.2%
siRNA GAPDH	-28%	unchanged	+13%	-42%	+7%

Table 3.4: Normalised changes in the levels of ALAS-1, HO-1, HO-2, and GAPDH following knockdown of HO-2 (siRNA HO-2) and GAPDH (siRNA GAPDH) by RNAi. Protein levels were measured by densitometry and normalised using β-actin detection (the standard deviation for each value is typically estimated within a ±5% range; Appendix A.5 for experimental details and immunoblot images). Protein level changes are colour-coded in green (positive change) and red (negative change). The calculated values of the $\%H_{acc}$ of mAPXmEGFP obtained by FLIM are also reported in the last column for each incubation.

siRNA knockdown of GAPDH

A commercially available cocktail of siRNA sequences (ON-TARGETplus GAPD; Dharmacon) was deployed to knockdown GAPDH (43% knockdown; data shown in Appendix A.5). A slight increase in HO-2 levels was detected (+13%). This indicates increased heme occupancy in its active site, compared to the control, because not as much HO-2 degradation is triggered [205]. On the other hand, HO-1 levels do not change. However, a significant increase in the $\%H_{acc}$ of mAPXmEGFP was measured (+7%). Thus, the knockdown of GAPDH increases heme bioavailability to a small extent, or at least the access of mAPXmEGFP to bioavailable heme. This result consolidates the idea that GAPDH is a heme buffering component and a heme chaperone. It is plausible that heme loading to mAPXmEGFP is not mediated by GAPDH because the sensor is a non-native, exogenous protein to the HEK293 wild type milieu. Further, any heme bound to GAPDH is - to a certain extent - sequestered and not available (*i.e.* not accessible) to mAPXmEGFP. By knocking down GAPDH, whilst heme loading to proteins that rely on GAPDH for heme delivery might be compromised, heme becomes more accessible to mAPXmEGFP

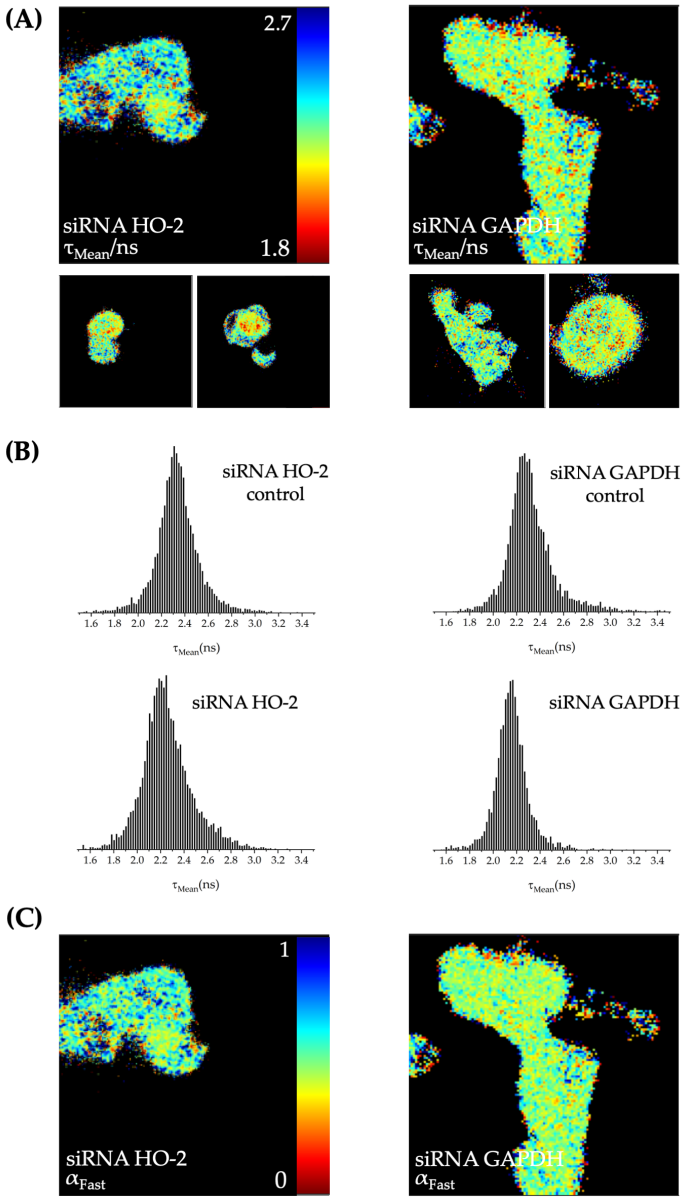

Figure 3.10: HEK293-mAPXmEGFP cells were cultured until 70% confluent in separate four-compartments microscopy dishes (CELLview). 48 h prior to imaging, minimal growth medium (α-MEM, αα, 10% FBS) was refreshed with α-MEM (serum-free, phenol red-free, antibiotic-free, αα-free) and cells were transfected with siRNA sequences to target HMOX2 and GAPDH, respectively (as outlined in Appendix A.4.4). (A) Representative distributions of the τ_{Mean} of mAPXmEGFP in three clusters of HEK293-mAPXmEGFP measured by FLIM when HMOX2 (top left; siRNA HO-2) and GAPDH (top right; siRNA GAPDH) were knocked down through RNAi. Typically, at least seven images per condition were acquired. (B) Histograms showing the distribution of τ_{Mean} for the two RNAi experiments compared to their relative control of untreated cells. (C) Fitting of the lifetime distribution of mAPXmEGFP in the two samples yielded the two lifetime decay components α_{Fast} and α_{Slow} ($\alpha_{\text{Fast}} + \alpha_{\text{Slow}} = 1$). The figure shows examples of the distribution of α_{Fast} - which reports on the fast decay component of τ_{Mean} (Equations 2.3-2.4) due to *holo*-mAPXmEGFP - in clusters of cells where HO-2 (left; siRNA HO-2) and GAPDH (right; siRNA HO-2) were knocked down. The comparison shows a prevalence of higher values of α_{Fast} in the sample where GAPDH was silenced, which indicates higher $\%H_{acc}$ (see text).

because some of it is being made bioavailable through alternative, less specific pathways than the GAPDH mediated trafficking (*e.g.* non-specific transient binding to other proteins that are not heme chaperones - *i.e.* another form of H_e - or free heme binding, H_f).

The increase in HO-2 (+13%) when GAPDH is knocked down might seem counter-intuitive, because GAPDH facilitates heme binding to HO-2 [175,199]. However, the general increase in heme bioavailability - indicated by the increased $\%H_{acc}$ of mAPXmEGFP (+7%) - seems to counterbalance the decrease in heme supply mediated by GAPDH, by increasing HO-2 heme occupancy. At the same time, such an increase is not reflected in any change in HO-1 levels indicating that heme, although generally more bioavailable, is managed by the cell sufficiently such that HMOX1 induction is not required.

This is aided by a reduction in the level of ALAS-1 (-28%), but also suggests the presence of an underlying heme buffering mechanism. In particular, HO-2 might be contributing to the buffering of heme as well as to its degradation, as recently suggested by Reddi and co-workers [172].

It is worth noting that a specific feature of the model system deployed here (HEK293-mAPXmEGFP) is that the buffering of heme might be mediated by mAPXmEGFP itself. Overall, such measures control the overall heme bioavailability and prevent the development of heme induced oxidative stress and the consequent induction of HO-1 expression.

The observed patterns of regulation following HMOX2 and GAPDH knockdown are summarised in schematic form in Figure 3.11.

siRNA knockdown of ALAS-1

Silencing of ALAS-1 was also attempted but cells could not survive without supplementing the incubation medium with hemin. The experimental conditions to accommodate ALAS-1 knockdown without hemin supplementation are currently being optimised. Hemin incubation is to be avoided to exclude from the analysis the competing effects that it triggers, which were explored and discussed in Section

3.3. It is interesting however, that whilst the cell appears to be equipped with a range of measures to cope with heme when in slight excess, the interference with ALAS-1 levels seems to irreversibly disrupt cell homeostasis.

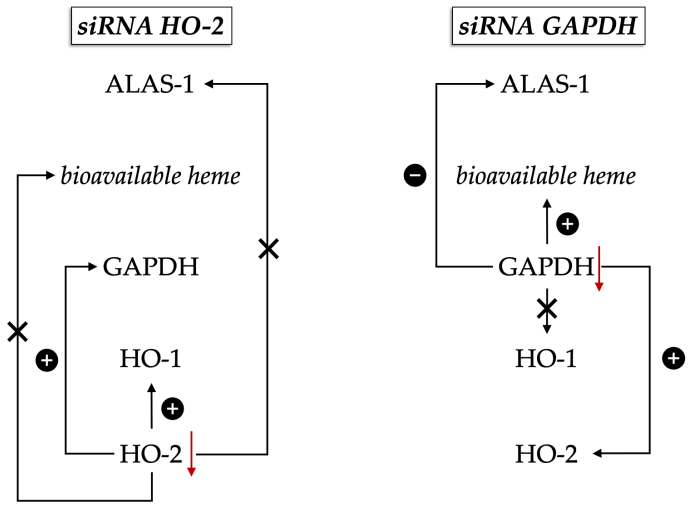

Figure 3.11: Schematic representation of the effects induced by siRNA HO-2 (left) and siRNA GAPDH (right) in HEK293-mAPXmEGFP. The red arrows represent increasing (upward pointing) or decreasing (downward pointing) levels of either HO-2 or GAPDH 48 h after transfection with suitable siRNA sequences (experimental details are in Appendix A.4.4). The knockdown of HO-2 or GAPDH led to different cellular responses in terms of bioavailable heme and the levels of ALAS-1, GAPDH, HO-1, and HO-2 which were are either up-regulated (plus signs) or down-regulated (minus signs).

3.5 Towards a compartment-selective analysis of the heme accessibility of mAPXmEGFP

Thus far, the $\%H_{acc}$ of mAPXmEGFP in live cells has been obtained through a global analysis averaged throughout whole cells imaged by FLIM. A current objective is to obtain a spatially-resolved, compartment-selective description of bioavailable heme and its fluctuations through lifetime measurement of mAPXmEGFP. This would allow, for example, identification of accumulation sites or locations that are particularly responsive to tailored cellular manipulations that affect the distribution of heme bioavailability.

To address this question, mAPXmEGFP sensors carrying signal peptides to tar-

get selected cellular *loci* were designed. Of particular interest are the following compartments: (i) mitochondria (main *locus* of the heme biosynthesis), (ii) the endoplasmic reticulum (main *locus* of HO-1 and HO-2), (iii) the peroxisomes (involved in the maturation of heme proteins), and (iv) the nucleus (where heme exerts its functions as a transcription co-factor) [21, 65, 129]. The required signal peptides to direct mAPXmEGFP to these locations are listed in Table 3.5 [129].

Target	**Signal peptide sequence**	**N-term**	**C-term**
Nucleus (NLS)	MDPKKKRKVDPKKKRKV	•	
Mitochondria (Mito)	MSVLTPLLLRGLTGSARRLPVPRAKIHSL	•	
Peroxisome (Per)	SKL		•
Endoplasmic reticulum (ER)	KDEL		•

Table 3.5: Signal peptides inserted either on the N-terminus or C-terminus of mAPXmEGFP. The construct for tagged-mAPXmEGFP sensors were obtained as outlined in Appendices A.2.2-A.2.3.

With mAPXmEGFP localised in specific compartments, it would be possible to probe cellular heme bioavailability in different regions of the cell. However, upon transient transfection of mAPXmEGFP constructs tagged with signal peptides at the C- or N-terminus as in Table 3.5, overexpression was found to be so pronounced that accurate co-localisation in the target organelles proved problematic. Figure 3.12 exemplifies this by showing the poor co-localisation of mAPXmEGFP directed to the nuclei and the mitochondria with nuclear (Hoechst 33342) and mitochondrial (Mitotracker) stains, respectively.

Transient DNA transfection is often associated with protein overexpression. Thus, the generation of stable HEK293 cell lines expressing the different peptide-tagged mAPXmEGFP constructs was attempted to verify whether the genome integration of the tagged-mAPXmEGFP genes would result in improved compartmental co-localisation due to reduced expression. However, following initial transfection, cells did not recover upon initiation of antibiotic selection (Appendix A.4.2). This suggests that the prolonged localisation of mAPXmEGFP in specific compartments is toxic. Under these conditions, the sensor is thought to act as a thermodynamic sink that deprives the compartment of heme - otherwise required for essential functions - and ultimately leading to cell death. Hence, the signal peptide approach towards

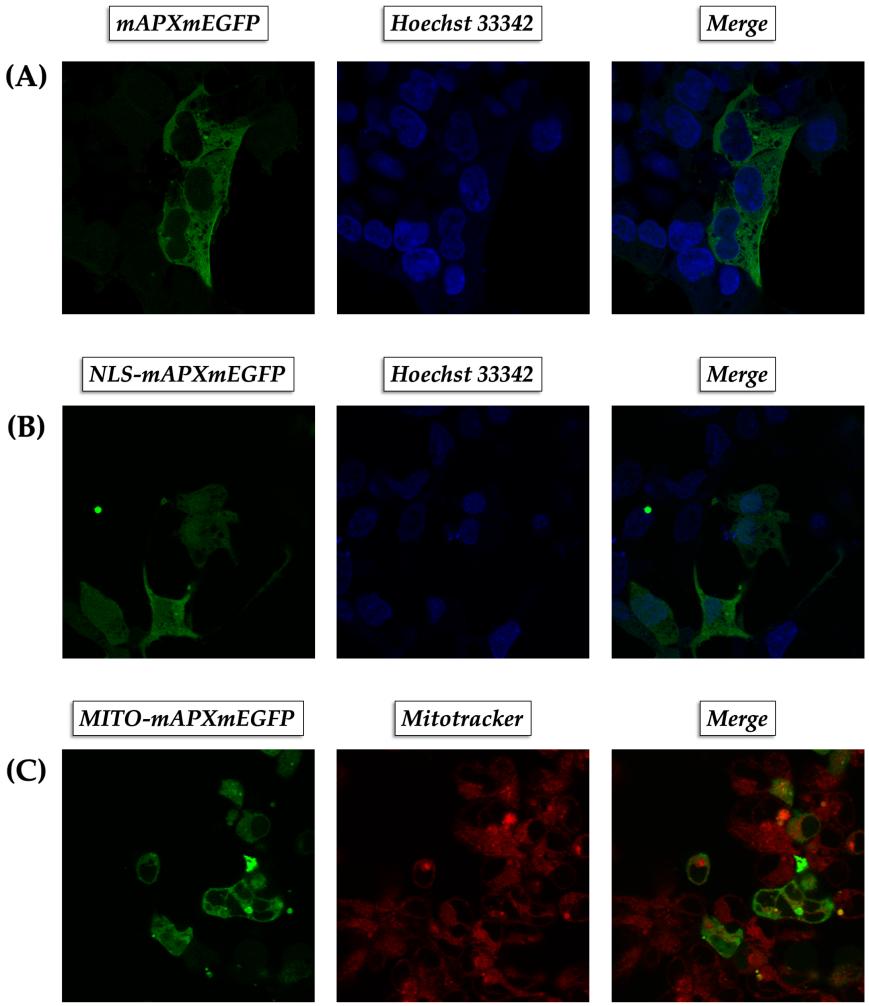

Figure 3.12: Confocal images of the fluorescence intensity signal of fixed HEK293 cells transiently transfected with constructs for the expression of mAPXmEGFP and mAPXmEGFP directed to the nucleus (NLS-mAPXmEGFP) and the mitochondria (MITO-mAPXmEGFP) through the respective signal peptides in Table 3.5. Immediately prior to imaging, cells were fixed in 4% *para*-formaldehyde (PFA) for 15 minutes at room temperature and washed with phosphate buffered saline (ThermoFisher). (A) mAPXmEGFP is unevenly distributed in the cellular environment. In particular, the nuclei appear to be scarcely populated of mAPXmEGFP. Left panel: mAPXmEGFP; middle panel Hoechst 33343 (nuclear stain); Right panel: merge. (B) NLS-mAPXmEGFP proved capable of co-localising in the nuclei with Hoechst 33343. However, NLS-mAPXmEGFP is significantly present in all other regions of the cell. (C) The distribution of MITO-mAPXmEGFP in HEK293 cells do not seem to be limited to the mitochondria. This can be seen by comparing the signal of MITO-mAPXmEGFP (left panel) with that of Mitotracker (middle panel) and merge (right panel).

a spatially-resolved, compartment-selective mAPXmEGFP signal output was abandoned. Instead, a segmentation strategy for the isolation of the lifetime signal of mAPXmEGFP was explored (Section 3.5.1).

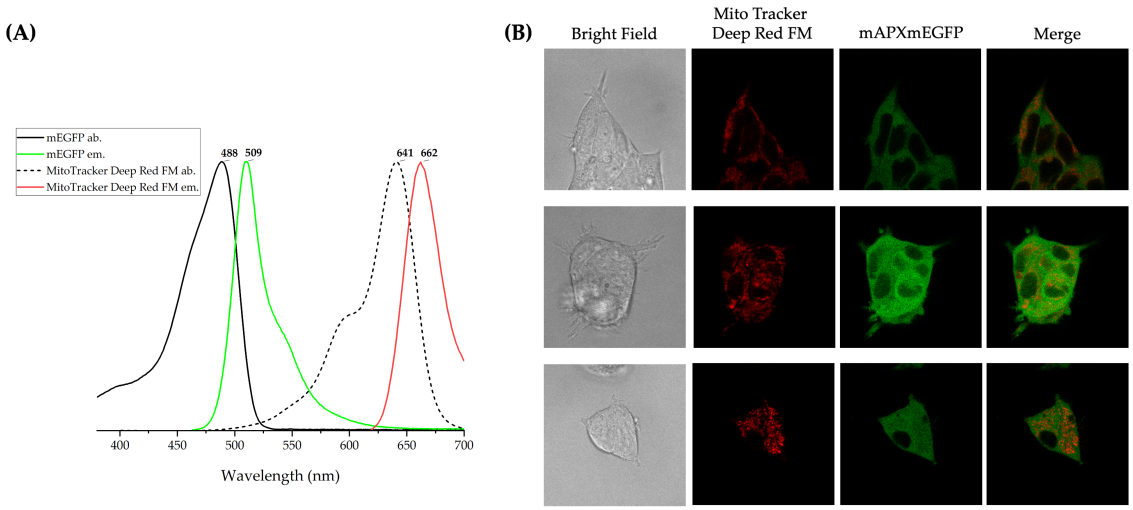

Figure 3.13: (A) Absorption and emission spectra of mEGFP and MitoTracker Deep Red FM displayed in the visible range (380-700 nm). The spectral shift between mEGFP emission (λ_{Em} = 488 nm) and MitoTracker Deep Red FM absorption (λ_{Exc} = 641 nm) avoids the mitochondrial stain being excited through RET by the emission of mEGFP. (B) Confocal images of HEK293-mAPXmEGFP stained with MitoTracker Deep Red FM. Bright-field (top left); MitoTracker Deep Red FM (top right); mAPXmEGFP (bottom left), merge (bottom right).

3.5.1 Segmentation of mAPXmEGFP lifetime through FLIM

HEK293-mAPXmEGFP cells were stained with Mito Tracker Deep Red FM immediately prior to FLIM following manufacturer's protocol (Thermo Fischer). MitoTracker Deep Red FM was chosen because its absorption and emission properties (λ_{Exc} = 641 nm, λ_{Em} = 662 nm) do not allow RET with mEGFP when the two fluorophores are co-localised and the sample is excited at the excitation wavelength of mAPXmEGFP (λ_{Exc} = 488 nm) (Figure 3.13). The lifetimes of the two fluorophores were measured through separate channels and the MitoTracker Deep Red FM channel images were then used to create segmentation images that were applied to the mAPXmEGFP channel. Thus, it was possible to isolate, in the mAPXmEGFP lifetime images, the regions occupied by the mitochondria and those outside of these compartments.

A global analysis of the lifetime traces corresponding to the pixels relative to the mitochondria, and the subtraction between whole cells and regions occupied by the mitochondria was then performed. Then, the fraction of *holo*-mAPXmEGFP in the mitochondria (f_{Mito}) compared to that corresponding to all other regions of the cell

(f_{NoMito}) were used to modify Equation 3.3 - expressing the explicit form of $\%H_{acc}$ - and obtain Equation 3.4.

$$\%H_{acc,Mito-NoMito} = 100\% \times \frac{f_{Mito} - f_{NoMito}}{f_{NoMito}} \tag{3.4}$$

A sample of HEK293-mAPXmEGFP allowed calculation of $\%H_{acc,Mito-NoMito}$ = -11% indicating that the heme accessibility of mAPXmEGFP in the mitochondria of HEK293 cells is 11% lower than in the remainder regions of the cell. This result aligns with the information provided by other studies (Table 1.1) where the mitochondria have been identified as heme deprived, compared to other regions. Because much of the heme biosynthesis occurs in the mitochondria, this is somehow surprising. On the other hand, it indicates that freshly produced heme might be sequestered or readily transported out of the mitochondria, explaining how newly synthesised heme does not affect ALAS-1 activity [189].

In HEK293-mAPXmEGFP cells where HO-2 was knocked down through RNAi a value for $\%H_{acc,Mito-NoMito}$ (siRNA HO-2) of -11% was obtained, showing that the knockdown of HO-2 does not affect mitochondrial heme - because $\%H_{acc,Mito-NoMito}$ (siRNA HO-2) is identical to that of untreated cells. On the other hand, knockdown of GAPDH yielded a value of $\%H_{acc,Mito-NoMito}$ (siRNA GAPDH) of -14%, showing that, compared to untreated cells, the $\%H_{acc,Mito-NoMito}$ of mAPXmEGFP decreases by 3% in the mitochondria. This contrasts with the global analysis (*i.e.* not segmented) for the siRNA GAPDH condition (Table 3.4) which shows a 6.5% increase. It follows that bioavailable heme has to be localised elsewhere in the cell as opposed to the mitochondria.

3.6 Conclusions

The difficulties encountered in the description of heme bioavailability through the deployment of heme sensors (introduced in Chapter 2 and discussed in Section 3.2) can be overcome by focusing on the portion of cellular heme that a given sensor has

access to. This led to the concept of heme accessibility, which was quantified for mAPXmEGFP ($\%H_{acc}$; Equation 3.3) and deployed to describe how heme bioavailability changed in response to a number of cellular stimuli aimed at inhibiting, inducing, or down-regulating key proteins in the maintenance of heme homeostasis (ALAS-1, GAPDH, HO-1, HO-2). Overall, the analysis highlighted a network of protein regulation that resists changes in intracellular heme levels. However, the interplay between the proteins considered in the present Chapter is complex, has consequences for the overall cell health when disturbed, and is likely connected to other key cellular pathways and HBPs yet to be discovered. Moreover, the need to obtain compartment-resolved information from mAPXmEGFP was tackled in Section 3.5 with a lifetime-based segmentation strategy. Although still in an early stage of development, this new and simple segmentation strategy - involving deep red stains commercially available for any cellular compartment - promises to provide insights towards a spatially-resolved description of cellular heme distribution.

Chapter 4

The prediction of heme binding sites to understand heme biology

4.1 Introduction

The combined regulation of ALAS-1, HO-1, HO-2, and GAPDH controls the overall concentration of cellular heme from its biosynthesis (ALAS-1) to its degradation (HO-1, HO-2), which is partially mediated by the heme chaperone GAPDH (Chapter 3). However, their interplay is complex and not all heme proteins are assisted by GAPDH during the process of acquiring heme. Thus, the regulation of heme levels is likely to involve additional pathways and heme binding partners yet to be discovered. In particular, the presence of a heme buffering system that binds heme transiently has been discussed in the literature [66,118] and is thought to constitute the majority of exchangeable heme, H_e. Such a buffer, thought of as being composed of soluble and membrane proteins, mediates heme loading into downstream heme acceptors and controls free heme cytotoxicity [84, 118].

A detailed description of exchangeable heme and the heme binding partners that constitutes the heme buffer requires the identification of the HBPs involved. Depending on the final destination of heme, multiple proteins are likely to be involved. It follows that the identification of such proteins is imperative to outline the molecular details of how heme is made bioavailable. Because of the transient nature of the interaction between heme and these unidentified HBPs, their iden-

tification is puzzling and elusive. To make progress, a combination of traditional methods ranging from homology modelling to mutational analysis and heme binding affinity studies will have to be coupled with the use of heme binding prediction tools and proteomics. The development of suitable heme binding prediction tools is particularly pressing because transient heme binding is likely non-conventional (*e.g.* heme binding to GAPDH; Figure 3.3), differing from traditional heme binding sites (Chapter 1; Figure 1.1).

Traditional heme binding sites have several common features: (i) a high heme-binding affinity; (ii) an abundance of alpha-helical structures in the heme binding sites [3]; (iii) the presence of two axial ligands (distal or proximal) on each side of the porphyrin ring that coordinate iron and/or stabilise the substrate (Figure 1.1); and (iv) a hydrophobic micro-environment with limited solvent exposure. Additional factors that finely-tune the variegated chemistry exerted by heme proteins include non-bonding side-chain backbone interactions with heme (*e.g.* hydrophobic interactions, π-π stacking, electrostatic interactions, and hydrogen bonds [211]) and the specific shape, size, and polarity of the heme binding pocket, which affects substrate selectivity [3, 212].

In contrast, research into the roles of heme as a regulator has uncovered unconventional low-affinity heme binding modes mediated by Heme Regulatory Motifs (HRMs; for example the cysteine-proline motif, CP, which is an important functional component of HO-2 [182] and Rev-Erb β [24]) [3, 21, 48]. HRMs are usually more solvent-exposed than traditional binding sites and can be located on the surfaces of proteins, in between subunits, (as in GAPDH; Figure 3.3), or in disordered regions (as the HRMs of HO-2, which contribute to the heme transfer to its own active site) [111, 199, 213, 214]. These low affinity binding modes are consistent with the requirement of bioavailable heme to be transiently bound in order to be exchanged with down-stream heme proteins.

Suspected but unconfirmed HBPs that might play a role in heme regulation include, among others, heat shock proteins such as Hsp70 [215], SapA [216] and

spermidine dehydrogenase, SpdH [217]. Identifying new HBPs would allow the discovery of novel aspects of heme biology. However, shortlisting plausible candidates is complicated by the ability of proteins to moonlight - as GAPDH does to chaperone heme (Section 3.1.2) - making them multitaskers that exert context-specific functions to fulfil complex biological behaviour [176, 177, 191, 218]. These secondary functions can be quite different from their primary role and makes the identification of proteins that moonlight to make heme bioavailable particularly challenging.

Several bioinformatics tools are available to study heme binding to proteins (*e.g.* HemeBind [219], HemeNet [220], TargetS, [221], HEMEsPred [222], HeMoQuest [223], AWSEM-heme [224]). However, they remain a niche in the field of bioinformatics, likely because they lack a structural output to visualise the heme binding site and generally only provide a list of protein residues with an associated likelihood of heme binding to those specific residues. Consequently, they have not been applied widely in the heme protein community.

4.1.1 Aims of this chapter

This Chapter addresses the problem of how unknown heme binding sites can be predicted and visualised in proteins yet to be structurally characterised. To do so, a combination of the bioinformatics tool ProFunc [225] and AlphaFold2 [226, 227] is explored. In particular, ProFunc is used to search for likely heme binding sites within models of protein structures generated with AlphaFold2. The use of ProFunc within AlphaFold2-generated structure also aims to compensate the current inability of AlphaFold2 to predict ligands, metal ions, and co-factors such as heme [228].

4.2 Using ProFunc to predict heme binding sites

ProFunc is a tool to predict the functions of proteins from their sequence and structural information retrieved from databases including the PDB, UniProt, and InterPro [3, 225, 229–231]. It works by performing alignments, searches for fold matches, conserved residues, surface cleft analysis, and 3D template searches to identify motifs or homologues [225]. ProFunc was developed by the Thornton group in 2005 at the EMBL-EBI and is accessible via its webserver (http://www.ebi.ac.uk/thornton-srv/databases/ProFunc/). In this Chapter, ProFunc is deployed to scan protein structures generated by AlphaFold2 and identify matches with amino acid templates. Templates consist of two to five amino acid residues in a specific 3D arrangement generated for heme with heterogeny, HET - a section of the PDB to search for non-identifiable residues, such as heme [229, 232]. The work presented in this Chapter was conceptualised and carried out with Noa Marson (BA, MRes) in collaboration with Dr Roman Laskowski (EMBL-EBI).

The heme binding sites of STEAP1, Rev-Erb β, PGRM1, HO-2, GAPDH, BACH1, BACH2, p53, Rev-Erb α, PER2, CLOCK, IRP2, NPAS2, and ALAS-1 were predicted. The proteins were selected to contain known and suspected heme binding proteins and divided in three categories: (i) heme proteins with characterised heme binding sites (STEAP1, Rev-Erb β, PGRMC1, and HO-2) to test the validity of this approach, with the results aligned with PDB-deposited crystals structures of the *holo*-proteins as a control; (ii) heme-binding proteins with available crystal structures only in the *apo*-form (GAPDH, BACH1, BACH2, p53, Rev-Erb α, PER2, CLOCK, and IRP2); and (iii) heme-binding proteins with no crystal structure available (NPAS2 and ALAS-1). ProFunc results include a heme binding score (Table 4.1) and a predicted binding site for each submitted protein. Predicted heme binding sites were then visualised using PyMOL and manually scanned near the heme ligand for cysteine and histidine residues.

Category	Protein*	Protein Function	UniProt ID	ProFunc Score
Heme-bound crystal structure available	STEAP1	Metalloreductase	Q9UHE8	218
	Rev-Erb β	Transcriptional regulator	Q14995	460
	PGRMC1	Progesterone-binding complex component	O00264	130
	HO-2	Heme metabolism	P30519	740
No heme-bound crystal structure	GAPDH	glycolytic enzyme/heme chaperone	P04406	160
	BACH1	Transcriptional regulator	O14867	116
	BACH2	Transcriptional regulator	Q9BYV9	130
	p53	Tumour suppressor	P04637	146
	Rev-Erb α	Transcriptional regulator	P20393	296
	PER2	Transcriptional regulator (circadian clock)	O15055	109
	CLOCK	Transcriptional regulator (circadian clock)	O15516	106
	IRP2	Post-transcriptional regulator (iron metabolism)	P48200	136
No heme-bound crystal structure	NPAS2	Transcriptional regulator (circadian clock)	Q99743	135
	ALAS-1	Synthesis of δ-aminolevulinic acide	P13196	157

Table 4.1: The table shows the name of the protein and its UniProt ID alongside its associated ProFunc score, an assessment of heme-binding. All proteins except HO-2 have low scores (≤460), meaning ProFunc has assigned heme as an unlikely ligand for the protein. However, there is evidence in the literature that all these proteins bind heme (see text). Whilst the scores for heme binding do not reflect what is known about heme proteins, a predicted binding site for each protein was generated and assessed (Sections 4.2.1-4.2.3).
*All listed proteins are human.

4.2.1 ProFunc predictions of heme binding sites in proteins with available heme-bound crystal structures

This Section analyses the ProFunc predicted heme binding sites in the AlphaFold2 models of STEAP1, Rev-Erb β, PGRMC1, and HO-2. The structures of these proteins in their *holo*-forms are available in the PDB - STEAP1 (PDB: 6Y9B; [233]); Rev-Erb β(PDB: 6WMQ; [35]), PGRMC1 (PDB: 4X8Y; [234]), HO-2 (PDB: 2QPP; [200]). The proteins were chosen as a test sample to assess the quality of the heme predicted heme binding sites in their AlphaFold2 model against their experimentally determined structures. The assessment was carried out by aligning the predicted binding sites with the corresponding crystal structure (Figure 4.1).

The correct heme binding site was identified for Rev-Erb β, PGRMC1, HO-2, and STEAP1 (Figure 4.1). This control sample of proteins suggests that ProFunc can predict heme binding sites accurately if provided with sufficient structural data. This results is promising for the application of ProFunc to generate reasonable heme binding sites in HBPs for which no heme binding site is crystallographically confirmed (Section 4.2.1) or no empirically determined crystal structure is available (Section 4.2.2).

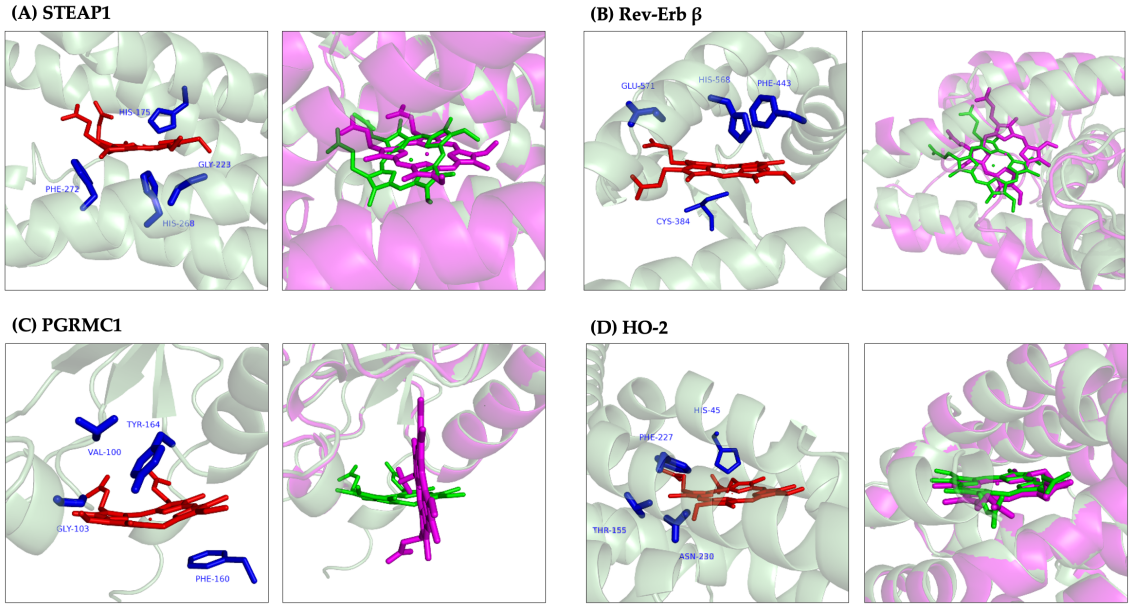

Figure 4.1: ProFunc predicted heme binding sites in the AlphaFold2 models of (A) STEAP1, (B) Rev-Erb β, (C) PGRMC1, and (D) HO-2. Each predicted structure (green, left panels) is aligned for comparison with the respective heme-bound crystal structures deposited in the PDB (purple, right panels). Protein structures alignments were performed using PyMOL.

4.2.2 ProFunc predictions of heme binding sites in proteins with available crystal structures without heme bound

To assess to ability of ProFunc to predict heme binding sites in proteins for which only the crystal structure without heme bound is available, the following proteins were chosen: GAPDH (PDB: 1ZNQ; [106]), BACH1 (PDB: 2IHC; [235, 236]), BACH2 (PDB: 3OHU; [235]), p53 (PDB: 3D09; [23, 237]), Rev-Erb α(PDB: 3N00; [37]), PER2 (PDB: 60F7; [238]), CLOCK (6QPJ; [29]), IRP2 (6VCD; [239]). The generated ProFunc models are shown in Figure 4.2. Below is a brief description of the results for each of the analysed proteins.

GAPDH

GAPDH has already been introduced in Section 3.1.2. Further structural details of the protein are provided here. The ProFunc model has identified a buried region of high secondary structure in the protein. This shows Thr153, Thr154 and Leu157 interacting with the heme α-hydrophobic edge of the heme (Figure 1.1A), as shown in

Figure 4.2A. His179 was identified as the closest histidine to heme, which could likely act as one of its axial ligands. Whilst this binding site is reasonable, another histidine (His53) was previously indicated by Stuehr and collaborators as the most likely heme binding residue through mutagenesis, spectroscopy, and modelling studies [106]. In particular, His53 lies in between the subunits of the GAPDH tetramer (Figure 3.3) and heme binds two His53 residues, each from different subunits. In the same study [106], His179 (shown by ProFunc in the heme binding site) was deemed unlikely to bind heme, as site directed mutagenesis to His179 did not affect the heme binding properties of GAPDH [106].

BACH1

The heme binding residues identified by ProFunc in BACH1 are Gln634, Gln636, Ile652 and Cys625 (Figure 4.2B). Whilst Gln634 and Gln636 are found in an alpha helix, Ile652 is located in a fairly disordered region. Cys625 was predicted in close proximity to the heme and may bind heme axially. BACH1 was previously indicated to bind heme through one of its six CP motifs, although which one exactly remains unknown [235, 236]. The six CP motifs include Cys224, Cys301, Cys438, Cys464, Cys495, and Cys649 [235, 236], none of which include the Cys625 predicted with ProFunc, which is not part of a CP motif.

BACH2

The ProFunc predicted heme binding residues in BACH2 include Thr83, Gly88, Leu90, and Cys112 (Figure 4.2C). The hydrophobic amino acids Gly88 and Leu90, part of an α-helix, interact with the δ-hydrophobic edge of heme (Figure 1.1A). The residue Thr83 points at one of the propionate groups of heme whilst Cys112 function as a possible axial ligand. Similarly to BACH1, of the five possible CP motifs in BACH2 [235] - all present in intrinsically disordered regions - none were identified involved in the heme binding site predicted by ProFunc.

p53

The ProFunc model of p53 shows heme binding via Pro98, Ser99, His168 and Ser269 (Figure 4.2D). All the residues are located in disordered regions with the exception of Ser269, which is on a β-sheet. In contrast, independent mutagenesis studies have shown that heme binding involves Cys275-Ala-Cys277 [23, 237].

Rev-Erb α

ProFunc identified Phe477, His602, and Glu604 in Rev-Erb α - all located on alpha helices (Figure 4.2C) as part of the predicted heme binding site. His602 was identified by independent mutagenesis studies as a heme binding residue [37]. As shown in Section 4.2.2, ProFunc was able to successfully predict the heme binding site of Rev-Erb β. Thus, the consistency between the ProFunc model of Rev-Erb α and the mutagenesis studies in the literature [37] may be a result of similarity between Rev-Erb α and Rev-Erb β proteins.

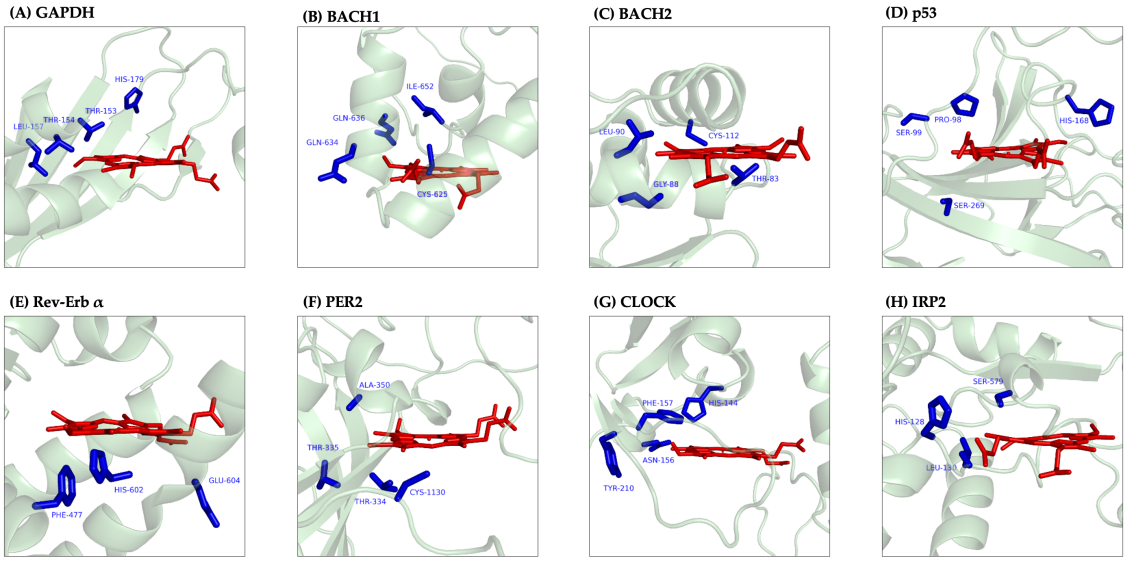

Figure 4.2: ProFunc predicted heme binding sites in the AlphaFold2 models of (A) GAPDH, (B) BACH1, (C) BACH2, (D) p53, (E) Rev-Erb α, (F) PER2, (G) CLOCK, and (H) IRP2.

PER2

For PER2, the identified binding residues were Thr334, Thr335, Ala350, and Cys1130 (Figure 4.2F). Again, in contrast to the ProFunc predicted binding site, a CP motif was identified in the literature as important for heme binding (Cys841-Pro842) [238].

CLOCK

ProFunc selected His144 as axial ligand - consistently with Freeman *et al.* [29] - while Asn156, Phe157 and Tyr210 face the α-hydrophobic edge of the heme (Figure 1.1A).

IRP2

Heme was placed by ProFunc in a disordered region of IRP2 with the binding site defined by the amino acids His128, Leu130 and Ser579 (Figure 4.2H). However, the residues Cys201-Pro-Phe-His204 have been previously identified as involved in heme binding [239] - this is in a region of low confidence in the AlphaFold2 model.

4.2.3 ProFunc predictions of heme binding sites in proteins with no available crystal structures

Where no deposited structural data is available, the use of structure prediction tools like AlphaFold is necessary in order to predict the heme binding structure through ProFunc. This Section describes the binding sites predicted by ProFunc in the AlphaFold2 model of NPAS2 - a protein involved in the regulation of the circadian clock [28, 30–32, 38, 39, 41, 42]- and ALAS-1 (Section 3.1.1), for which no empirical PDB entry is available.

ALAS-1

The binding site identified in the AlphaFold2 of ALAS-1 is located in between two α-helices of a well-folded region. The binding site consists of His259, Arg261 and

Ala265. Whilst His259 is axially positioned on top of the porphyrin ring and is aligned with the Fe atom, Arg261 points towards heme propionate groups and Ala259 interacts with heme δ-hydrophobic edge. Once again, mutagenesis studies have shown a CP motif as likely responsible for ALAS-1 heme binding (Cys108-Pro109) [187]. However, this motif is in a region of low or very low confidence in the AlphaFold model, so was unlikely to be identified by ProFunc (UniProt ID: P13196).

NPAS2

In the AlphaFold2 model submitted to ProFunc, the residues Val351, Asp355, Glu359 - shown to interact with the propionate groups of heme - and His348 were identified as heme binding residues (Figure 4.3B). However, NPAS2 is known to bind heme via either His119/Cys170 or His119/His171 [21,39,240]. The AlphaFold2 model shows two PAS-like domains in the NPAS2 protein. The binding residues implicated by the literature are found in one of these domains, and the binding residues from the ProFunc prediction are found in the other. Whilst the binding site predicted by ProFunc is not consistent with the literature [29], it is still found within the same type of domain (PAS domain).

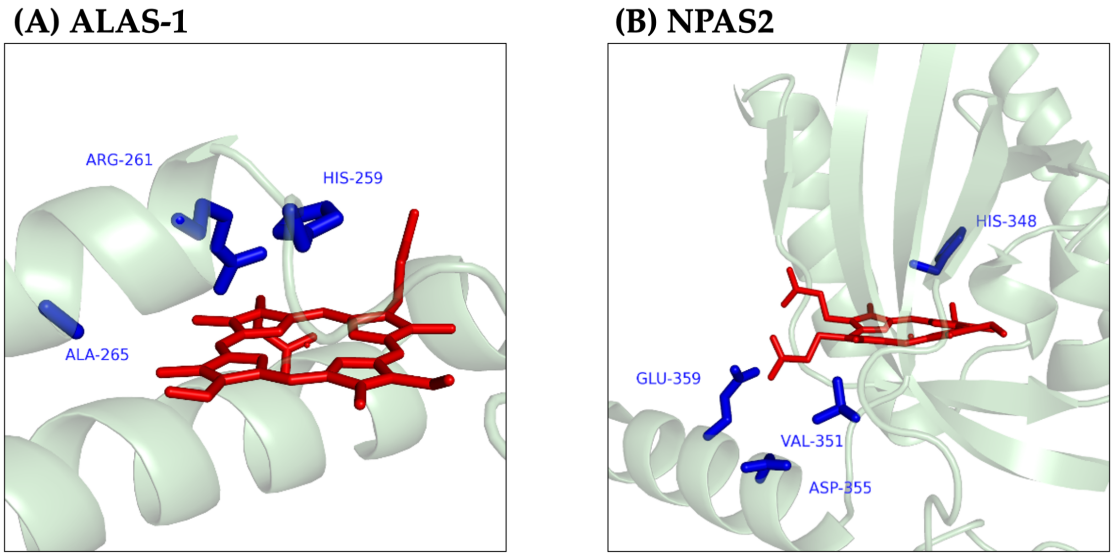

Figure 4.3: ProFunc predicted heme binding sites in the AlphaFold2 models of (A) ALAS-1 and (B) NPAS2. Although ProFunc has identified a region typical of a PAS domain within the AlphaFold2 model of NPAS2 [29], a β-sheet bisects the heme molecule. If the binding site is correct, heme would still bind to Val351, Asp355, Glu359, and His348 albeit in a different orientation.

4.3 Discussion

There are common features of heme binding sites, which have been used to identify potential binding sites. This includes the binding of histidine and cysteine to heme as axial ligands and the presence of structural motifs such as a PAS domain or a CP motif. Overall, histidine residues were identified by ProFunc in the predicted binding sites of five of the nine proteins with available crystal structures without heme bound (GAPDH, p53, Rev-Erb α, PER2 and CLOCK). Of these, two are consistent with results from mutagenesis studies (CLOCK [29] and Rev-Erb α [37]).

ProFunc was also able to identify the polar residues threonine and asparagine - interacting with the propionate groups of heme - in the predicted binding sites of BACH2 and CLOCK. Possible hydrophobic interactions were also recognised between GAPDH and BACH2 with leucine, BACH1 with isoleucine, BACH2 with glycine, p53 with proline, Rev-Erb α and CLOCK with phenylalanine, and PER2 with alanine.

BACH1, BACH2, Rev-Erb α, PER2, IRP2, and ALAS-1 were previously suggested to bind heme using CP motifs. However, CP motifs have not been identified in the ProFunc models. In some cases, for example ALAS-1 (Figure 4.4), this may be explained by the CP motifs being modelled by AlphaFold2 in regions of low confidence. It is possible that regulatory motifs such as these are harder to identify using template-based methods such as ProFunc, given that there are less *holo*-heme proteins that bind heme through CP motifs crystallographically characterised and deposited in the PDB.

Overall, the combination of AlphaFold2 and ProFunc shows that a template-based approach to predict heme binding sites can identify - albeit with varying accuracy - heme binding motifs. However, where the confidence of the AlphaFold2 model is low, the ProFunc predicted binding sites are less consistent with those suggested by traditional mutagenesis studies.

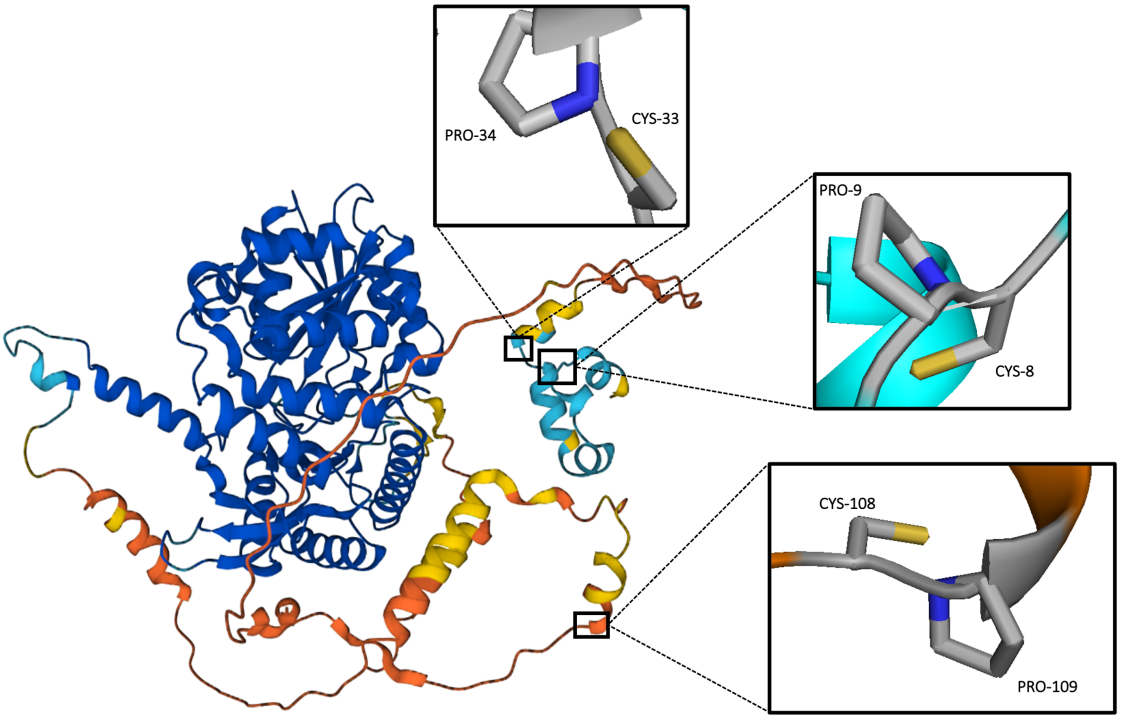

Figure 4.4: AlphaFold2 model of human ALAS-1 (UniProt ID: P13196). The model is colour-coded with regions of high confidence in blue and regions of low confidence in orange. ALAS-1 presents three CP motifs (enlarged). Heme binding to ALAS-1 was previously suggested to occur at the CP motif Cys108-Pro109 [187], unlike the binding site predicted with ProFunc (Figure 4.3A), which lies within the well-folded high-confidence region of the ALAS-1 AlphaFold2 model. In contrast, the ALAS-1 CP motifs are found in low confidence regions of the AlphaFold2 model. This might explain the discrepancy with the ProFunc prediction.

4.4 Conclusions

Looking forward, deploying ProFunc to predict heme binding sites can be used as a guide to identify binding residues in future screening studies for suspected heme-binders in an effort to identify further key players in the biology of heme. An example of such endeavour might include microarray analyses and application of proteomics techniques to simultaneously study expression level (mRNA), protein levels and their subcellular localisation, leading to a deeper understanding of the regulation involved in the control of heme homeostasis. Moreover, this information would also help contextualising further the data accessible through the deployment of genetically encoded heme sensors.

Chapter 5

Quantitative analysis of heme trafficking and heme sensors

5.1 Introduction

In the previous chapters, the use of the mAPXmEGFP heme sensor and bioinformatics tools were explored to further the understanding of cellular heme trafficking. In this chapter, the limitations associated with the deployment of genetically encoded heme sensors is discussed by focussing on the possible interference to heme homeostasis caused by their expression. These limitations will have to be taken into account when moving towards a unified rationalisation of cellular heme trafficking.

The logistics regulating heme movements in the cellular milieu is complex and is thought to involve chaperones as well as transient carriers that actively exchange heme to other binding partners. Taking into account all the possible modes of heme trafficking is essential to contextualise the deployment of genetically encoded heme sensors. In particular, the currently available views on possible mechanisms to explain how heme supply and demand is met in cells are found scattered in the literature: (i) a balance between heme biosynthesis and degradation; (ii) mediation by heme chaperones; (iii) trafficking through membrane contact sites; and (iv) involvement of a diffuse heme buffering system. Each of these concepts is presented in Figure 5.1 and Sections 5.1.1-5.1.4.

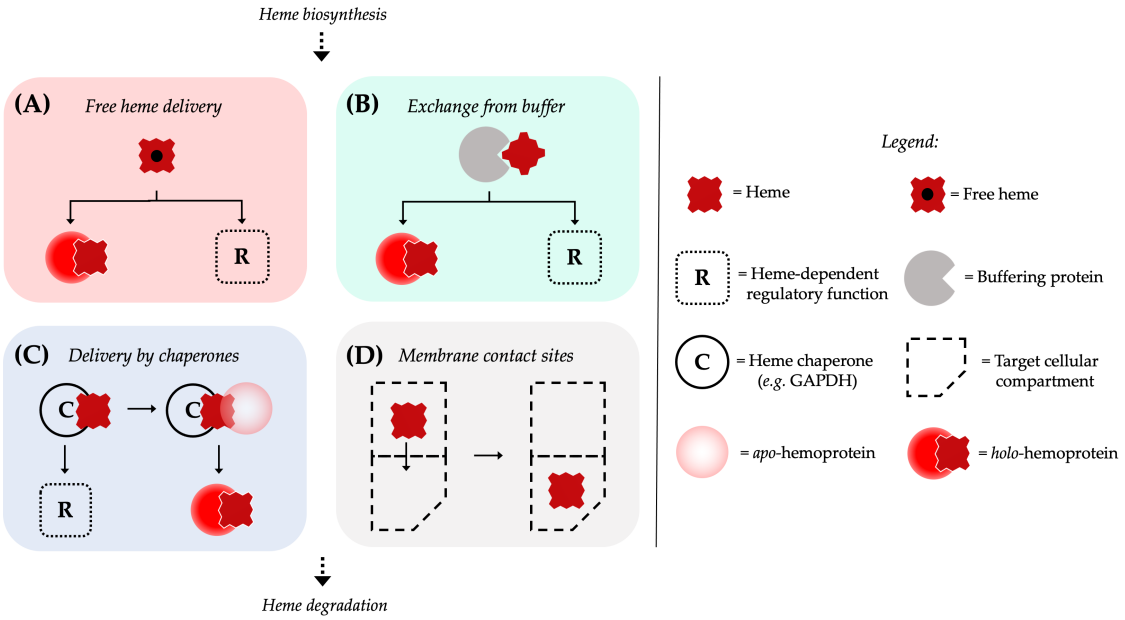

Figure 5.1: Representation of possible cellular heme delivery mechanisms to downstream heme proteins (a legend for the symbols used in the figure is on the right hand side). The balance and interplay between heme synthesis and degradation is mediated by four possible mechanisms of heme trafficking and delivery. (A) Direct incorporation of free heme into a heme protein. Free heme is envisaged as being present in limited concentrations [66]. By analogy with the problem of metalation (*i.e.* the binding of metal ion cofactors to metal-biding sites), it is possible that heme has to compete for its binding to heme binding sites with other metal compounds in the cell. However, molecules such as heme are thought as more easily discerned by proteins, because of its bulky protoporphyrin ring [241–243]. (B) Heme exchange from a buffering systems. Heme bound to heme-buffering proteins constitutes a body of exchangeable heme. Possible candidates for heme-binding proteins that have been suggested in the literature as putative buffering components are IDO, HBP22/23, SOUL, and albumin [104,168,244]. (C) Chaperone-mediated heme delivery to an *apo*-heme protein. (D) Distribution of heme via membrane contact sites between mitochondria - where heme is synthesised - to target other cellular compartments [133]. Figure adapted from [118].

5.1.1 The balance between heme biosynthesis and degradation

Cells need to maintain heme availability below the cytotoxic threshold [86, 90, 95]. HO-1 and HO-2, whose mechanism of degradation of heme into biliverdin and CO is well known [62, 123], play a crucial role in maintaining this balance by coordinating with heme biosynthesis and, in particular, with ALAS-1. This interplay has already been observed and discussed in Chapter 3.

5.1.2 The involvement of heme chaperones

The existence of biological chaperone systems is documented for other redox active transition metal ions (*e.g.* iron, copper, molybdenum, cobalt, nickel) [245–248]. Cells adopt strategies to tightly regulate the concentrations of different metals ions, ensuring suitable levels of bioavailability, effective physiological responses, and prevention of cytotoxicity [242, 247–262]. The concentration of transition metal ions in cells is kept at very low levels to avoid inappropriate activation of signalling pathways. For instance, the intracellular free copper concentration in *S. cerevisiae* is limited to less than one molecule per cell [247, 251]. Similarly, free zinc is estimated in the low femtomolar range in *E. coli* [247, 250]. Instead of being free to circulate around the cell, metal ions are stored, locked in an inaccessible state, and released to a network of chaperones or chelators that control their delivery, repurposing, and ensure fidelity in metalation when two competitive metals can bind to the same site [242, 248, 252–257]. By comparison, it is reasonable to presume that cells use similar principles for the movement and distribution of heme (Figure 5.1C).

The identification of heme chaperones with the specific role of transporting and selectively delivering heme to downstream proteins would thus clarify the picture considerably. But very few heme chaperones have been identified over the years. A notable example is the CcmE chaperone, part of the multi component Ccm membrane heme maturation machinery for heme translocation to cytochrome *c* in most proteobacteria, archaea, deinococcales, and plant mitochondria [263–265]. However, this is a special case as it speaks only to the need for formation of covalent links to heme in the specialised *c*-type cytochromes. GAPDH is perhaps the most compelling example of a heme chaperone so far identified [106–108, 175], introduced in Section 3.1.2. The interaction between GAPDH and heme was initially thought to occur to protect heme from degradation during its transport (which at the same time reduces its cytotoxicity) [194, 266]. However, GAPDH has since been found to be responsible for the delivery of heme to a number of downstream heme proteins (Section 3.1.2). Among these is to the nuclear transcription factor Hap1 [106] in *S.*

cerevisiae, to cytosolic iNOS in mouse macrophage cells [106], and to soluble guanylate cyclase in HEK293 cells [107]. The involvement of GAPDH in heme delivery in both yeast and mammalian systems is indicative of a broadly conserved strategy for heme transport [106]. GAPDH is primarily a glycolytic enzyme, and, therefore, its function as a heme chaperone looks to be opportunistic as far as the cell is concerned. This begs the question as to whether there are other as-yet unidentified heme chaperones lurking about the cell in disguise [118]. Moreover, if heme chaperones are used at all then more than one could be required to create an effective supply chain. Arguably, chaperones of chaperones might even exist [108]. But if heme binding can be opportunistic and does not need a specific heme binding motif – as GAPDH seems to indicate – then identification of heme chaperones needs to take into account non-canonical heme binding motifs [3, 267]. This issue was explored in Chapter 4.

Well-known heme binding proteins could be re-purposed for the task of cellular heme delivery under certain conditions. For example, IDO - for which heme delivery depends on GAPDH and is stimulated by NO [196, 197] - is capable of releasing its heme under certain conditions [168] and suggests the possibility that it could be used as a source of heme in specific regions of cells (discussed in Section 2.3; [268–271]).

The distribution of heme via chaperones can explain how heme moves from the mitochondria to other locations, and then subsequently to the endoplasmic reticulum for degradation by heme oxygenase. But the chaperone mechanism is ill-equipped to deal with rapid changes in heme availability. If increases or decreases in heme concentration are required then the rate-limiting steps are heme synthesis and degradation. Upregulation of heme synthesis, by expression of the ALAS-1 in response to low heme availability, could take at least 30 min [73], while induction of HO-1 for heme degradation could take hours [272]. Both of these mechanisms are too slow by far if rapid control of heme concentration is required, for example in the case of ion channel regulation which is necessary for appropriate cardiac function [50]. Hence, if the cell is solely reliant on heme chaperones, then it runs the risk of spikes in heme availability should there be a mismatch in timings between the delivery

and the removal of heme. Taken together, and bearing in mind the failure (so far) to identify large numbers of heme chaperones, complementary mechanisms will be required to regulate heme distribution, as elaborated below.

5.1.3 Trafficking through membranes

Evidence is emerging for the involvement of biological membranes as important factors in the trafficking of cellular heme. Heme has been shown to be capable of diffusing or even being retained by cellular lipid bilayers [273–275] and examples of putative membrane heme transporters have been identified, most notably the mitochondrial exporter Flvcr1b, which has been reviewed elsewhere [86, 276]. But while heme may or may not necessitate membrane transporters for its movement across compartments, the contribution of lipid bilayers to heme trafficking is still not completely clarified. A recent study has proposed that the trafficking of heme through membranes does not rely on transporters and is, in contrast, a chaperone-less pathway made possible by inter-organellar contact sites. This provides an elegant solution for the exchange of heme between compartments (Figure 5.1D) [132, 133].

5.1.4 Buffering of free heme concentration as a mechanism of control

An ability to store heme in cells would decrease the reliance of cells on heme synthesis and degradation and could be coupled to mechanisms to make heme more or less available, on-demand and at speed (Figure 5.1B). To date, there have been no proteins identified that have the dedicated function of storing heme, but there is evidence, from recent work [66], of a buffering capacity within cells that can accommodate changes in either the total concentration of heme (*i.e.* $[H_t]$), or the concentration of exchangeable heme (*i.e.* $[H_e]$), whilst maintaining the capability to mobilise heme as and when necessary. This could allow heme to travel from one place to another, where molecules of heme hitchhike across the cell by binding to

whichever protein(s) they can find *en route* to its final destination [118]. As indicated above, it is entirely possible that known heme proteins (such as IDO and GAPDH) participate in the buffering of free heme concentration (*i.e.* $[H_f]$) and protect the cell against increases or decreases in total, or exchangeable, heme concentrations. In this scenario for heme buffering, the ability of any given protein to acquire heme is based on how well it competes for heme (*i.e.* the heme affinity) against other proteins. Hence the availability of heme in the cell would be dependent entirely on the K_{d} and abundance of these buffering proteins. In this way, the concentration of free heme is buffered – or, in other words, the availability of heme is kept within a limited range – by the many heme-binding proteins in the buffer and would be distributed amongst those proteins according to their relative heme affinities.

5.1.5 The *in cellulo* measurement of heme bioavailability: the question of sensor interference

The expression of mAPXmEGFP in live cells introduces an additional heme binding species into the cellular milieu that may compete with other heme-binding proteins for molecules of exchangeable heme, dragging heme out of its natural distribution. Whilst there would be no issue with the sensor competing for heme with either heme-binding proteins or small molecules whose sole role is to buffer the concentration of free heme, it is critical that this competition does not significantly extend to *bona fide* heme-proteins (Figure 5.2). Heme binding to the sensor may result from the exchange of heme between a native heme binder to the sensor. Hence, to measure heme bioavailability the expressed sensor must integrate into the network of buffering partners, and its presence must not affect the physiological levels of exchangeable heme (H_e), free heme (H_f), or altering other phenotopic traits. In particular, heterogeneous distribution of mAPXmEGFP may revisit the natural topology of cellular heme distribution. It then becomes important to validate the heme bioavailability measurements obtained with mAPXmEGFP by ensuring that its expression is not disruptive.

5.1.6 Aims of this chapter

This chapter provides a quantitative basis for the expression of genetically encoded heme sensors in live cells, with a particular emphasis on mAPXmEGFP. In particular, it analyses the effects of (i) the heme binding affinity and (ii) the concentration of the deployed sensor. The repercussions deriving from these two parameters are discussed in Section 5.2 and 5.3, respectively.

5.2 The heme binding affinity of a heme sensor can affect heme bioavailability measurements

The concentration of cellular heme measured in this work (Chapter 2) and in the literature (see Table 1.1) is systematically low. Low concentration values for heme suggest that heme mobilisation might be occurring one molecule at a time. The presence of a heme buffer - composed of a poly-dispersed collection of proteins, or possibly even other biomolecules, binding heme non-specifically and with low affinity - can reconcile the need for having heme bioavailable and accessible to heme proteins whilst avoiding heme-induced oxidative stress. This feature of the buffer defines

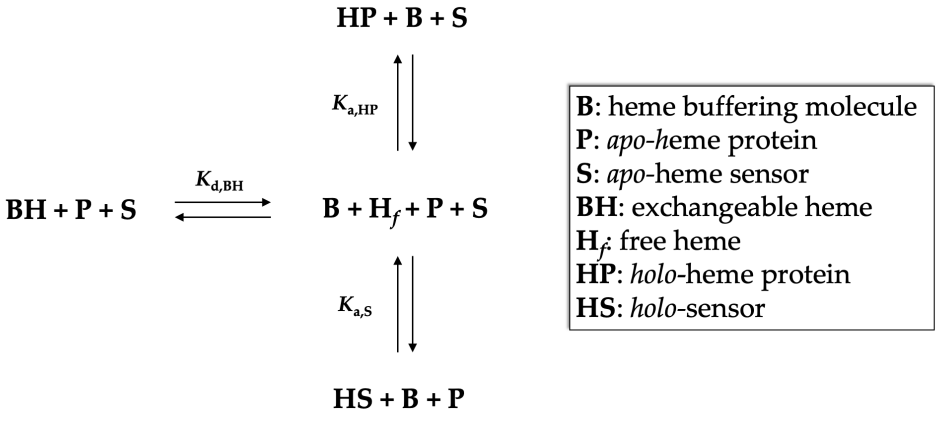

Figure 5.2: Interference introduced by a heme sensor to the heme exchange from the heme buffer (or chaperone) to a *bona fide* heme protein. The transfer of free heme from exchangeable heme (BH) to *apo*-heme proteins (P) involves dissociation of heme, to give free heme (H_f), from the exchangeable reservoir. A heme sensor (S) competes for free heme with the other heme proteins. The magnitude of this interference will depend on the heme binding affinity of the sensor and its cellular concentration.

what is meant by "exchangeable heme". Crucially, the low-affinity binding for heme ensures the capability of the buffer to make heme available readily by dissociation, leading to free heme. This mechanism can also prevent, to some degree, free-heme induced cytotoxicity because, once dissociated, it can promptly be incorporated either by *apo*-heme protein or a different component of the buffer. Hence, a network of chemical equilibria might account for heme bioavailability. Heme bioavailability can then be described as the result of heme exchange between a donor and an acceptor. In particular, the transfer of heme (H) from a buffering heme protein (B) to a *bona fide*-heme protein (P) can be formalised in two steps: (i) dissociation of heme from the buffer; and (ii) binding of heme to the heme protein (Equation 5.1).

$$\mathrm{BH} + \mathrm{P} \overset{K_{\mathrm{d,BH}}}{\rightleftharpoons} \mathrm{B} + \mathrm{H}_f + \mathrm{P} \overset{K_{\mathrm{d,HP}}}{\rightleftharpoons} \mathrm{B} + \mathrm{HP} \tag{5.1}$$

The heme transfer described in Equation 5.1 is quantified by the heme dissociation constants of the heme binding partners. The variation in free energy due to the dissociation of heme from a heme buffering molecule ($\Delta G^{\circ}_{\mathrm{d,BH}}$) can be obtained using the free energies of formation $\Delta G^{\circ}_{\mathrm{f}}$ of the species indicated in Equation 5.1. The explicit expression is given by Equation 5.2.

$$\Delta G^{\circ}_{\mathrm{d,BH}} = \Delta G^{\circ}_{\mathrm{f}}(B) + \Delta G^{\circ}_{\mathrm{f}}(H_f) - \Delta G^{\circ}_{\mathrm{f}}(BH) \tag{5.2}$$

Similarly, the variation in free energy due to the binding of heme to a heme protein is given by Equation 5.3.

$$\Delta G^{\circ}_{\mathrm{a,HP}} = \Delta G^{\circ}_{\mathrm{f}}(HP) - \Delta G^{\circ}_{\mathrm{f}}(H_f) - \Delta G^{\circ}_{\mathrm{f}}(P) \tag{5.3}$$

Overall, the free energies of dissociation from the heme buffer and binding to a heme protein ($\Delta G^{\circ}_{BH \to HP}$) are obtained by combining Equations 5.2-5.3 (Equation 5.4).

$$\Delta G^{\circ}_{BH \to HP} = \Delta G^{\circ}_{\mathrm{f}}(HP) + \Delta G^{\circ}_{\mathrm{f}}(B) - \Delta G^{\circ}_{\mathrm{f}}(BH) - \Delta G^{\circ}_{\mathrm{f}}(P) = \Delta G^{\circ}_{\mathrm{a,HP}} + \Delta G^{\circ}_{\mathrm{d,BH}} \tag{5.4}$$

Equation 5.4 can be re-arranged to calculate the values of $\Delta G^{\circ}_{BH \rightarrow HP}$ using the heme dissociation constants $K_{\mathrm{d,BH}}$ and $K_{\mathrm{d,HP}}$ (Equation 5.5).

$$\Delta G^{\circ}_{BH \rightarrow HP} = \Delta G^{\circ}_{\mathrm{a,HP}} + \Delta G^{\circ}_{\mathrm{d,BH}} = -RTln\frac{K_{\mathrm{d,BH}}}{K_{\mathrm{d,HP}}} \tag{5.5}$$

Equation 5.5 (where $R = 8.315\ J \cdot mol^{-1} \cdot K^{-1}$ and $T = 293.15\ K$) thus describes the stabilisation resulting from the transfer of heme from a heme donor (*e.g.* a heme buffering molecule, a heme chaperone) to a downstream heme protein or a heme sensor. For example, the $\Delta G^{\circ}_{BH \rightarrow mAPXmEGFP}$ for the transfer of heme from a heme binding protein (BH) for which $K_{\mathrm{d,BH}}$ is known to mAPXmEGFP can be calculated. This thought experiment allows us to visualise that the portion of accessible heme of mAPXmEGFP is influenced by the thermodynamic properties of both heme binding partners (Figure 5.3) - see Section 3.2 for the concept of heme accessibility. It follows

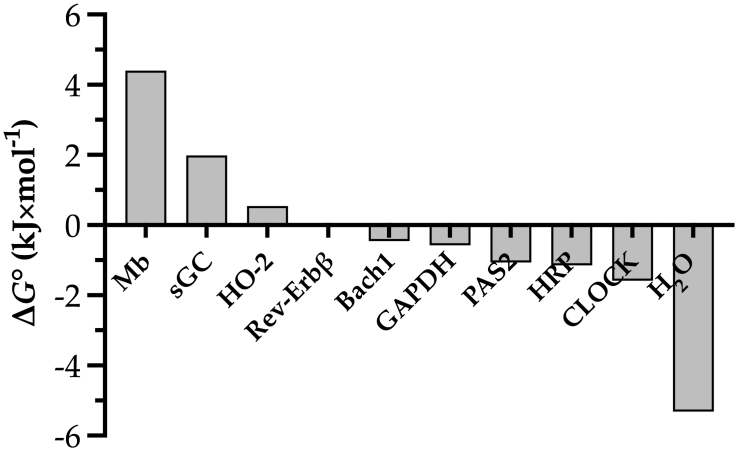

Figure 5.3: The bar chart shows the calculated $\Delta G^{\circ}_{BH \rightarrow mAPXmEGFP}$ for the exchangeable heme transfer from different heme binding molecules (BH: Mb, sGC, HO-2, Rev-Erbβ, Bach1, GAPDH, PAS2, HRP, CLOCK, and H_2O) to mAPXmEGFP. $\Delta G^{\circ}_{BH \rightarrow mAPXmEGFP}$ values were obtained using Equation 5.5 and the heme dissocation constants of the different BHs available in the literature ($R = 8.315\ J \cdot mol^{-1} \cdot K^{-1}$; $T = 293.15\ K$).

that there is no clear demarcation between putative components of the buffer and traditional heme proteins because the extent to which heme is bioavailable depends on its thermodynamic environment. As long as $K_{\mathrm{d,BH}} > K_{\mathrm{d,HP}}$ (*i.e.* the affinity for heme of the acceptor heme protein is greater than that of the heme donor buffer component) the free energy change will be negative, describing a thermodynamically

favoured process (Equation 5.5). This suggests a scale of bioavailability controlled by the heme binding affinity of the heme binding pairs involved in the exchange of heme. Figure 5.4 provides a colour-coded representation of such driving force.

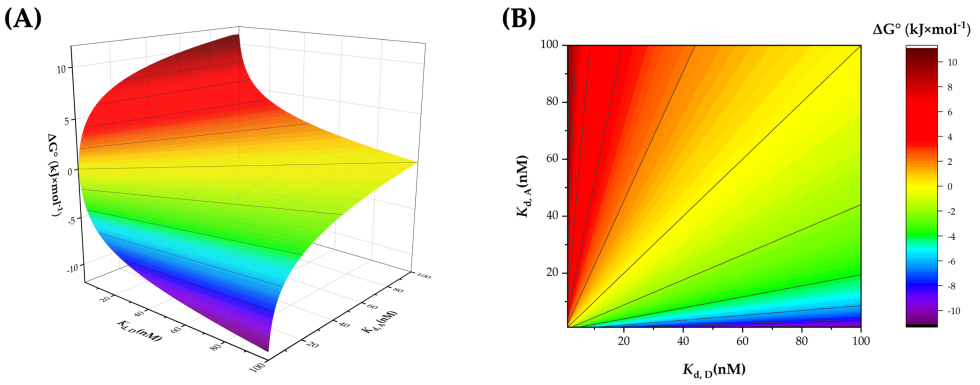

Figure 5.4: The $\Delta G^{\circ}_{D \rightarrow A}$ for the heme transfer from a hypothetical heme donor D (with associated $K_{\mathrm{D,d}}$) to a hypothetical heme acceptor A (with associated $K_{\mathrm{A,d}}$) was calculated for each donor-acceptor couple in the range 1 nM $< K_{\mathrm{d}} <$ 100 nM (using Equation 5.5 with $R = 8.315\ J \cdot mol^{-1} \cdot K^{-1}$ and $T = 293.15\ K$). The range of K_{d} values was chosen to be representative of traditional heme proteins. Warmer colours corresponds to less favoured heme transfer whereas colder colours correspond to favoured heme transfer according to the sliding colour scale on the right-hand side. (A) The 3D representation of $\Delta G^{\circ}_{D \rightarrow A}$ describes a heme exchangeability surface to visualise the thermodyanamic stabilisation due to heme transfer from a donor to an acceptor. In particular, low values of $K_{\mathrm{d,A}}$ (acceptor with high heme affinity) and high values of $K_{\mathrm{d,D}}$ (donor with lower heme affinity than the acceptor) identify the regions where the thermodynamic driving force for the transfer of heme from the donor to the acceptor is highest (blue-purple regions). For donor-acceptor couples with similar K_{d} the population of *holo*-donor *holo*-acceptor will be approximately equal (yellow region). Less favoured heme transfer is identified by the red region. (B) 2D projection of the heme exchangeability surface.

The transient nature of these interactions has likely been shaped by evolution into a delicate series of chemical equilibria where heme is being constantly exchanged and actively buffered by a pool of heme binders. Consequently, extemporaneous compositional changes in the proteomic profile of the heme binding proteins can tune cellular heme bioavailability and would provide a further layer of complexity in the cellular mechanisms that ensure heme heme bioavailability. Overall, the distribution of mitochondrial heme is influenced by *bona fide* heme proteins that evolved with a high heme affinity (*e.g.* globins, cytochromes, catalases) that provides the thermodynamic driving force towards the hierarchical equilibrium distribution of cellular heme [118, 175]. The next Section elaborates on the concept of heme sequestration by proteins with high heme-binding affinity.

5.2.1 Heme sequestration by high-affinity heme proteins can be visualised

The hierarchy of heme binding according to a thermodynamic gradient is defined by the heme binding affinity of heme proteins and would be responsive to changes in the relative composition of this ensemble. In other words, the heme accessibility to bioavailable heme of a given heme protein is tuned by the expression level of other co-localised heme proteins, particularly those with high heme binding affinity. As an example, upregulation of proteins in the heme buffer with high heme-affinity (*e.g.* a globin, or a cytochrome) would establish a "thermodynamic sink" where the high-affinity heme proteins act as heme sponges that sequester bioavailable heme by

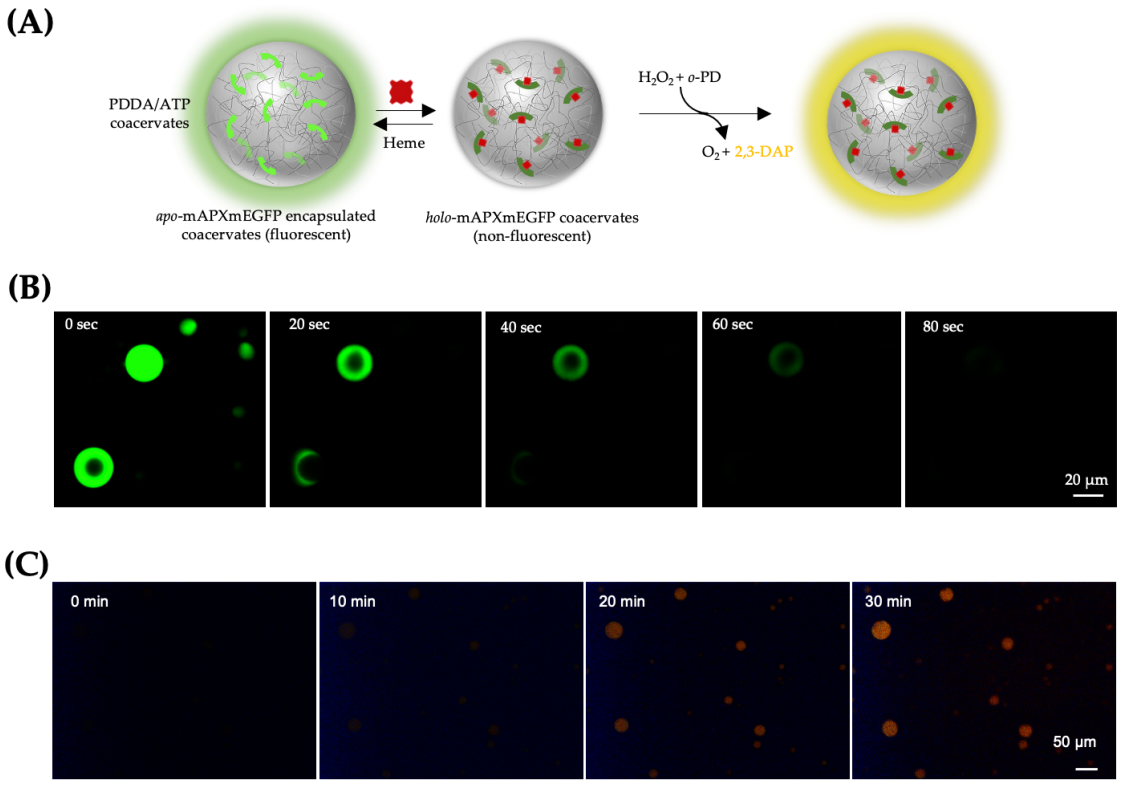

Figure 5.5: (A) Schematic representation of the of the coacervate-like structure built through liquid-phase separation of a suspension of poly-diallyldimethylammonium chloride (PDDA) cross-linked with ATP in aqueous solution. The structures self-assemble into coacervates where biopolymers can be encapsulated and co-localised, resembling a protocell environment that allow compartmentalisation. (B) *apo*-mAPXmEGFP was encapsulated in the coacervates and provided with hemin. The diffusion of hemin through the suspension determines a time-dependent quenching of the fluorescent signal of mAPXmEGFP. (C) Following the *in situ* reconstitution of mAPXmEGFP, the peroxidase activity of the sensor was observed through the conversion of *o*-PD into 2,3-DAP. Full experimental details can be found in Appendix A.3.1.

locking it into a thermodynamically inaccessible state.

To test this model, a method for the visualisation of heme sequestration by high affinity-heme binders was explored. *apo*-mAPXmEGFP was encapsulated in micro-droplets (*i.e.* coacervates) generated by liquid phase separation through the condensation of poly-diallyldimethylammonium chloride (PDDA) and ATP in aqueous solution [277] (Figure 5.5A). Upon reconstitution with hemin, the quenching of the fluorescence of mAPXmEGFP (Figure 5.5B) and the induction of peroxidase activity in the system can be observed with the reaction of H_2O_2 and *ortho*-phenylenediamine dihydrochloride (*o*-PD) - a water-soluble substrate for horseradish peroxidase (HRP) that produces the yellow-orange product 2,3-diaminophenazine; 2,3-DAP (Figure 5.5C).

Then, *apo*-mAPXmEGFP and *apo*-sperm whale myoglobin (H64Y/V68F) - also known as green myoglobin, gMb; K_d ~10 pM [278, 279] - were co-encapsulated, mimicking co-localisation in a protocell structure that simulates the compartmentalisation of the cellular environment. The *apo*-gMb probe was chosen as it is routinely used in a well-established heme exchange assay developed by Olson and coworkers [111, 278]. To visualise the heme sequestration capability of gMb and the subsequent impediment of the heme accessibility of mAPXmEGFP, the two encapsulated proteins were acoustically patterned in an ordered arrangement (Appendix A.3.1). Subsequently, the system was provided with hemin and the reaction with (*o*-PD) and H_2O_2 was induced to detect peroxidase activity (Figure 5.6). In this case no peroxidase activity and no quenching of the fluorescence of mAPXmEGFP was measured. In contrast, when *apo*-mAPXmEGFP was encapsulated alone in coacervate structures, reconstitution with hemin determines quenching of the fluorescence and the activation of peroxidase activity (Figure 5.5A-B). This result indicates that heme distribution is hierarchical and favours the highest affinity heme binder (*i.e.* gMb over mAPXmEGFP) in the confined coacervate environment.

.

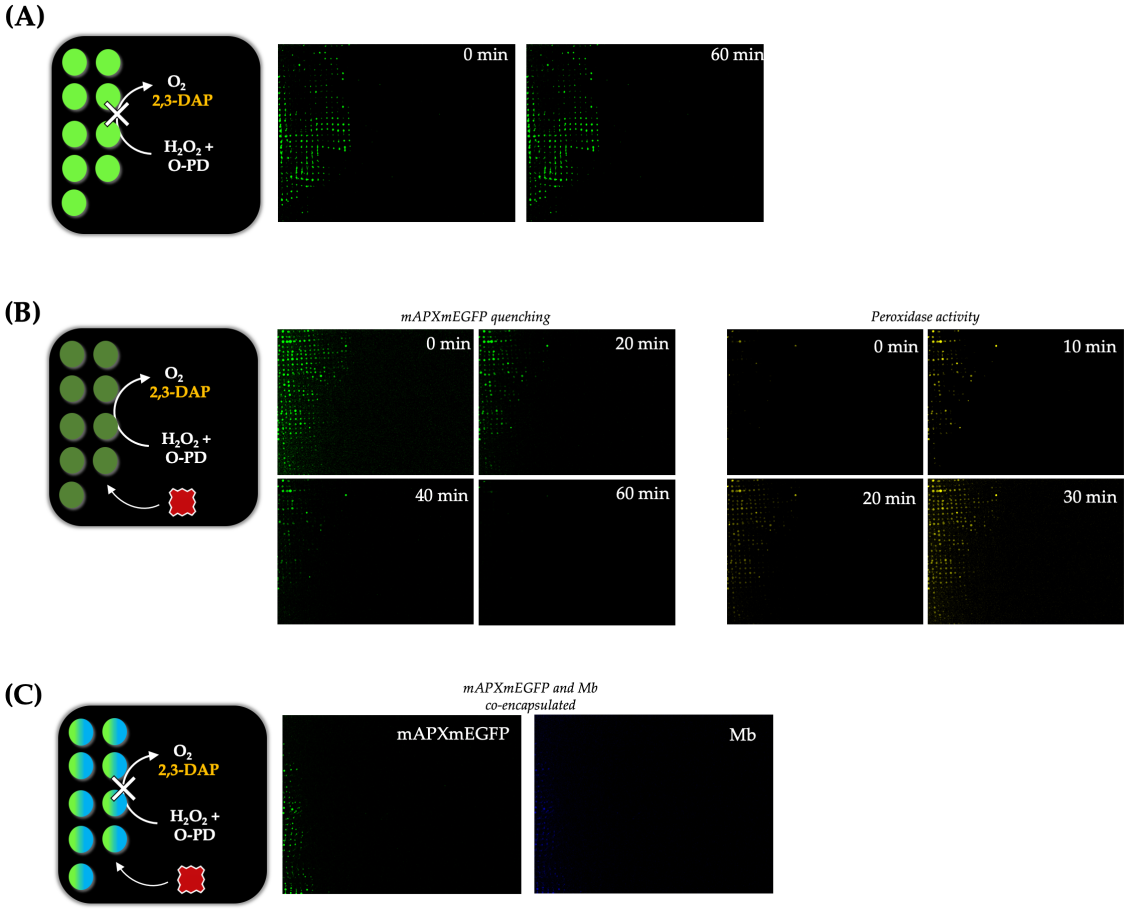

Figure 5.6: (A) Coacervates were patterned by means of sound waves and encapsulated with mAPXmEGFP. The coacervates are visible as green dots on the left-hand side of the images. (A) *apo*-mAPXmEGFP does not determine the conversion of *o*-PD into 2,3-DAP (2,3-diaminophenazine) and the fluorescence intensity of the sensor is unchanged after 60 minutes incubation. (B) When the patterned mAPXmEGFP is reconstituted with hemin it is possible to observe the time-dependet quenching of its fluorescence as well as the establishment of peroxidase activity (yellow signal). (C) When mAPXmEGFP was co-encapsulated with gMb (labelled with Dylight 405 (Thermo Fischer); blue dots), no peroxidase activity was detected, indicating that the supplied hemin is preferentially populating gMb over mAPXmEGFP.

5.3 The concentration of a heme sensor can affect heme bioavailability measurements

As discussed in Section 5.2, the heme binding affinity of heme proteins affects the equilibrium distribution of heme. Similarly, the proteomic profile of heme proteins will affect cellular heme as the relative protein content of the cell can favour the *holo*-form of the heme proteins that are more highly expressed. This is particularly relevant in the case of genetically encoded heme sensors because heme bioavailability measurements may be biased according to heme sensor abundance - which

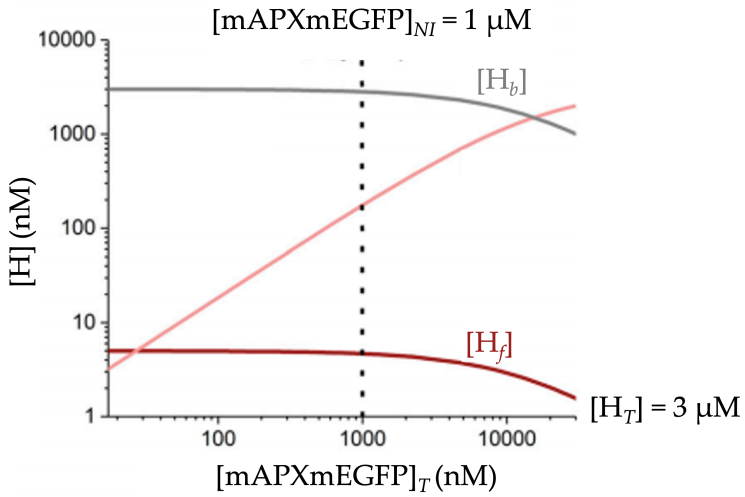

Figure 5.7: A computational model describing the interference to exchangeable heme induced by increasing concentrations of total mAPXmEGFP, $[\text{mAPXmEGFP}]_T$ (*apo-* + *holo*-mAPXmEGFP; horizontal axis). Exchangeable heme (H_e) is assumed to be mostly buffered through transient binding to heme binding partners, H_b. A smaller proportion of exchangeable heme is due to free heme existing as free molecules, H_f (red trace). At higher concentrations of mAPXmEGFP more exchangeable heme is transferred to the sensor. The concentration of *holo*-mAPXmEGFP is shown in pink, [*holo*-mAPXmEGFP]. To create the model, the total concentration of cellular heme, $[H_T]$, was assumed equal to 3 μM, as previously estimated [111, 213]. The concentration of free heme, $[H_f]$, was taken as equal to 5 nM (as obtained in Chapter 2) and the heme dissociation constant of mAPXmEGFP is 22 nM [66]. The total concentration of heme-binding partners was assumed to be 10 × $[H]_0$ to effectively buffer cellular heme. It can be seen that up to the non-interfering concentration of $[\text{mAPXmEGFP}]_{NI}$ = 1 μM cellular heme levels are not affected by $[\text{mAPXmEGFP}]_T$.

depends on the expression level and cellular distribution of the sensor itself, which may be compartment-specific. Such concerns represents possible limitations for the deployment of sensors like mAPXmEGFP in live cells.

Whilst unavoidable, the perturbation introduced by the expression of the sensor needs to be minimised by reducing its concentration below an interfering threshold, which, for mAPXmEGFP, was estimated to be around 1 μM (Figure 5.7). This result was obtained under three assumptions: (i) total heme concentration in HEK293 cells is equal to 3 μM [205]; (ii) the concentration of free heme in the absence of mAPXmEGFP under normal conditions is equal to 5 nM [66]; and (iii) the concentration of heme binding partners is 10 times higher than the total concentration of heme.

According to this model a concentration of mAPXmEGFP up to 1 μM is not expected to alter the bioavailability of cellular heme because it would not lower

the concentration of free heme, H_f, or heme bound to heme binding partners, H_b. Hence, it is paramount to maintain mAPXmEGFP within the non-interfering range of concentrations (up to 1 μM). It follows that accurate estimations of the working concentration of mAPXmEGFP are necessary to ensure that the expression of the sensor is not perturbing the homeostatic concentration of cellular heme.

In order to do this, mAPXmEGFP concentration was estimated in HEK293-mAPXmEGFP by fluorescence western blotting (Section 5.3.1) and, subsequently, by pairing FLIM with Fluorescence Correlation Spectroscopy (Section 5.3.2).

5.3.1 Determination of mAPXmEGFP concentration in HEK293 by immunoblotting

Using increasing amounts of purified mAPXmEGFP a calibration curve for the determination of sensor concentration of whole lysates of HEK293-mAPXmEGFP was obtained (Figure 5.8). A total of 2.5 million cells were lysed and the volume of each cell was assumed equal to 3 pL, as reported in the literature [205]. The average cellular concentration of sensor was determined by densitometry as ~ 80 nM (Figure 5.8), much below the 1 μM threshold estimated in Figure 5.7.

It is worth noting that immunoblotting is a semi-quantitative approach and can only provide an approximate figure for the overall average sensor concentration, averaged over the sum of the cells in the sample lysate. However, mAPXmEGFP is likely to show compartment localisation preferences leading to a heterogeneous distribution of its concentration.

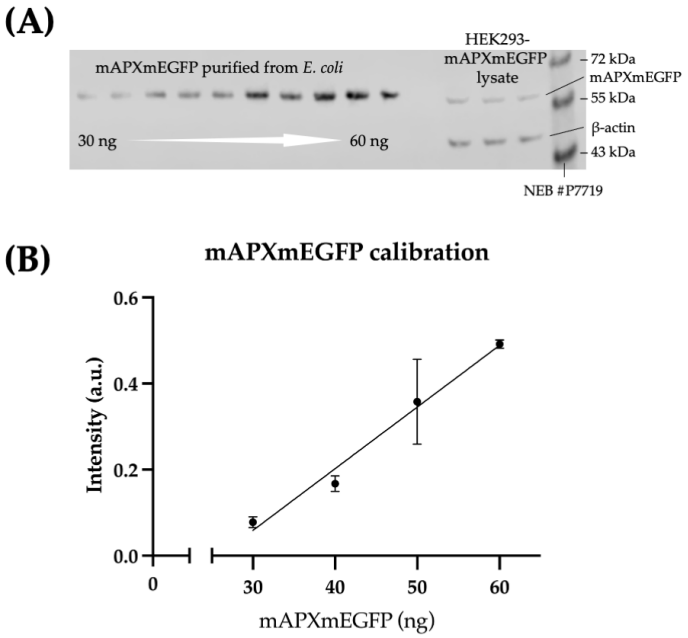

Figure 5.8: (A) Increasing amounts of purified mAPXmEGFP, following overproduction in *E. coli*, were loaded in replicates on a SDS-PAGE gel ranging from 30 ng to 60 ng of total protein alongside 5 µg of total cell lysate obtained from 2.5 million HEK293-mAPXmEGFP cells (total protein measured by BCA assay). Protein bands were transferred on a low-fluorescence PVDA membrane and band intensities detected by fluorescence immunoblotting using anti-GFP antibody (full experimental details in Appendix A.4.6). (B) Band intensities from the purified sensor were analysed by densitometry to build a calibration curve ($y = 0.014x - 0.37$; $R^2 = 0.98$) that was then used to calculate the estimated average concentration of mAPXmEGFP in HEK293-mAPXmEGFP cells using the intensities of the bands obtained from the whole cell lysates ([mAPXmEGFP] $\sim$ 80 nM).

5.3.2 Determination of mAPXmEGFP concentration and heme biovailability in live cells: pairing FLIM with Fluorescence Correlation Spectroscopy

It is possible to explore how different local cellular concentrations of mAPXmEGFP affect heme bioavailabilty by pairing FLIM with Fluorescence Correlation Spectroscopy (FCS), a powerful tool to study dynamic processes *in vitro*. Fluorescence Correlation Spectroscopy is a single molecule time-resolved technique that measures the fluorescence intensity of a probe diffusing through a confocal volume typically set at $V = 1$ fL [136, 280–284]. The fluorescence counts measured at $t = 0$ are then compared with those measured after a number of time lapses (generally within 10 s after $t = 0$) to generate a time-dependent correlation of the signal that describes a self-similarity trace. The autocorrelation trace is then fitted to different diffusion

models (chosen according to the type of environment the fluorophore is diffusing in) allowing us to obtain parameters that include the concentration and the diffusion coefficient of the fluorophore.

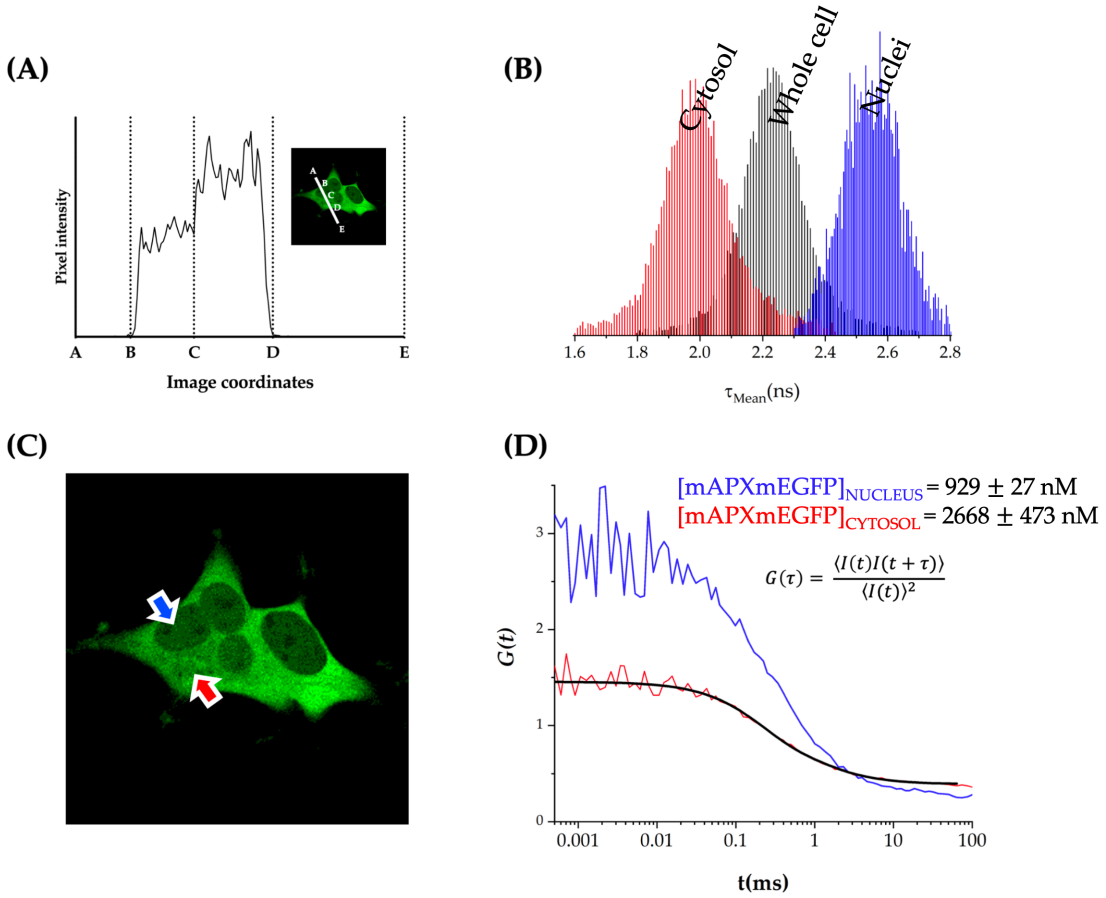

Figure 5.9: The FCS-FLIM approach allows measurement of heme bioavailability and mAPXmEGFP concentration in live cells. (A) The distribution of mAPXmEGFP in HEK293-mAPXmEGFP is not homogeneous. Fluorescence intensity in the confocal image of the cluster of cells shown in the inset identifies the nucleus as a region of lower sensor concentration compared to the cytosol. Pixel intensity analysis along the coordinates indicated in the white segment (inset A, B, C, D, E) is qualitatively shown in the plot. (B) Whole cell FLIM analysis of the cell cluster shows a distribution of mAPXmEGFP mean fluorescence lifetime (black histogram) that lies in between that of the nuclei (blue histogram) and the cytosol (red histogram). The faster mean fluorescence lifetime measured in the cytosol (red histogram) corresponds to higher heme bioavailability in this region compared to the nuclei (blue histogram). (C) FCS analysis was performed in the points indicated by the blue and red arrow respectively for which two separate autocorrelation traces were fitted to a self similarity model suited for the highly crowded cellular environment where the fluorophore is free to diffuse three-dimensionally (panel D; explicit fitting model in Appendix A.6.2-FCS). The measured concentrations at the two selected points are reported in the inset of panel (D).

By deploying FCS during live-cell confocal imaging, different regions of the cellular environment on the confocal plane can be separately studied. This technique was paired with FLIM in an FCS-FLIM approach that allows measurements within the

same microscopy session of both heme bioavailability (by FLIM) and mAPXmEGFP concentration (by FCS). The concentration of the sensor was observed to be heterogeneously distributed (Figure 5.9A) with an order of magnitude difference between the nuclear and the cytosolic regions ($[\text{mAPXmEGFP}]_{nucleus} = 929 \pm 27$ nM; $[\text{mAPXmEGFP}]_{cytosol} = 2668 \pm 473$ nM) (Figure 5.9D). These values are higher than the concentration measured by western blot from cell lysates ($\sim$ 80 nM; Section 5.3.1). It is worth noting that immunoblotting results are semi quantitative, averaged amongst the number of cells lysed, and do not account for possible expression level variations between different cells. On the other hand, FCS measures individual regions of single cells one at a time. The areas immediately surrounding the point analysed by FLIM were then isolated by segmentation in FLIM-fit for lifetime analysis to establish a possible correlation between sensor concentration and heme bioavailability. Interestingly, the area corresponding to the nucleus in the cluster of cells analysed (Figure 5.9C, blue arrow) showed distribution of longer mAPXmEGFP mean fluorescence lifetimes (Figure 5.9B, blue histogram) compared to the measured cytosolic area (Figure 5.9C, red arrow; Figure 5.9B red histogram). This indicates that higher heme bioavailability in the cytosol (shorter mean fluorescence lifetime) corresponds to higher mAPXmEGFP concentration, suggesting that the equilibria showed in Figure 5.2 may be shifted in the cytosol towards the *holo*-form of mAPXmEGFP due to its higher concentration.

This FCS-FLIM experiment was followed by the measurement of several self-similarity traces at a number of points in different cell clusters. However, in most cases no reliable autocorrelation of the mAPXmEGFP fluorescent signal could be consistently measured, as accurate FCS measurements rely on fluorophore concentrations in the nanomolar range [136, 280]. To further investigate the FCS-FLIM approach, limiting the expression level of mAPXmEGFP to establish a statistically relevant correlation between sensor and heme concentration is desirable.

5.3.3 Controlling sensor expression with inducible systems

Being able to exert control over the *in cellulo* population of mAPXmEGFP represents a current objective that would allow the minimisation of the potential drawbacks caused by high sensor expression regimes and deploy systematically the FCS-FLIM approach explored in Section 5.3.2. Towards this goal, a DNA fragment encoding mAPXmEGFP was inserted into a pMK240 vector [285] (Figure 5.10), which has a puromycin resistance gene encoding puromycin N-acetyltransferase (PAC) [286] with AAVS1 homologous arms [285, 287] and the expression of the sensor is under the regulation of the Tet-On operator [288, 289].

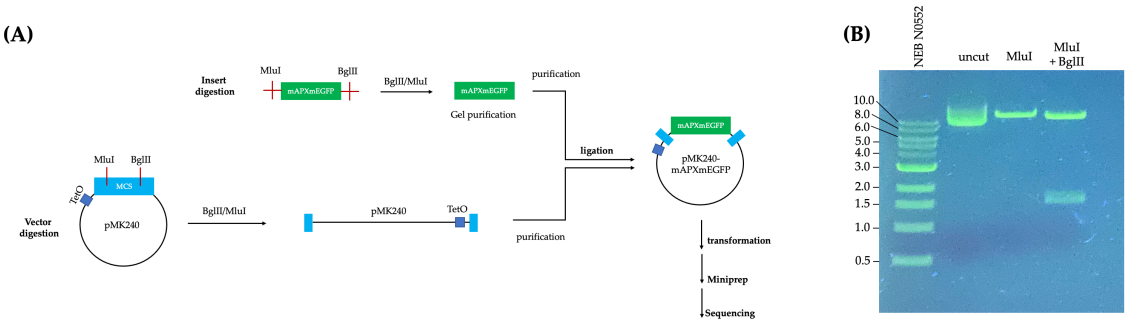

Figure 5.10: (A) Cloning strategy to obtain an inducible system for the controlled expression of mAPXmEGFP in mammalian systems. A traditional cut-and-paste approach was deployed. The pMK240 vector was developed by Prof Kayoko Tanaka and co-workers (University of Leicester) whereas the mAPXmEGFP fragment flanked by MluI and BglII restriction sites was purchased from TWIST bioscience. (B) The single and double digestion of the obtained construct show the linearised product (MluI) and the release of the insert mAPXmEGFP (1.5 kb; MluI + BglII) confirming successful cloning. See Appendix A.2.4 for further details.

HEK293 cells were co-transfected with pMK240-TWIST-mAmE and an AAVS1 targeting CRISPR-Cas9 construct (Addgene #72833) [287] (Figure 5.11). Integrated clones were selected with puromycin for 4 weeks. 11 monoclonal lines resistant to puromycin were isolated (experimental details in Appendix A.4.1-A.4.2) for further analyses. These lines are yet to be screened to identify the best performing clones based on their responsiveness to the induction of the expression of mAPXmEGFP by doxycycline. mAPXmEGFP expression levels are expected to increase proportionally to the concentration of doxycycline added to the medium. The performance of each clonal line, in terms of response to induction of sensor expression, will be evaluated by immunoblotting and FCS-FLIM. It will also be necessary to perform

genotyping to verify the correct insertion of the construct into the AAVS1 locus. The establishment of a reliable inducible system will clarify if and how different concentrations of mAPXmEGFP sensor provide different responses through the application of the FCS-FLIM approach introduced in Section 5.3.2. This work is yet to be explored.

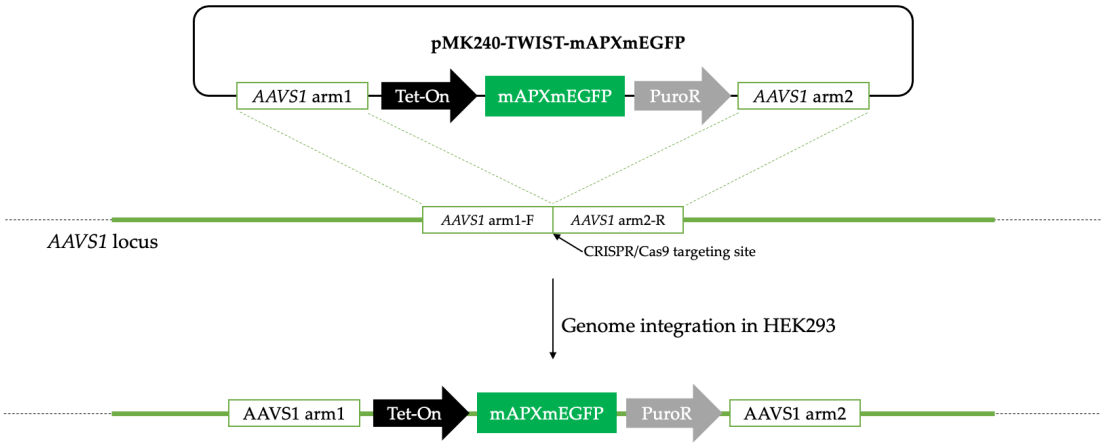

Figure 5.11: Schematic representation for the insertion of the donor plasmid pMK240-TWIST-mAPXmEGFP at the AAVS1 locus.

5.4 Conclusions and discussion

A key element to the successful deployment of the sensor technology is to ensure that normal heme homeostasis in the cell is not perturbed and that the sensor integrates seamlessly with the existing heme binders in the cellular environment. The possible limitations of the deployment of mAPXmEGFP as a tool to investigate heme trafficking derive from its heme binding affinity and its concentration. In Section 5.2, it was shown that the thermodynamics of heme binding to mAPXmEGFP is influenced by the heme binding affinity of neighbouring binding partners. In Section 5.3, the local cellular concentration of the sensor was suggested to be capable of biasing the measurements of heme bioavailability and a possible correlation between mAPXmEGFP concentration and measured heme bioavailability. Thus, such parameters need to be carefully contextualised when applying a heme sensing technology to understand its cellular trafficking. However, improving on these aspects

is not an easy task. The heme binding affinity can only be tuned by designing, optimising and characterising new heme sensors that will likely report on different fraction of exchangeable heme compared to that accessible to mAPXmEGFP. On the other hand, controlling the concentration of a given heme sensor will be important for advanced application to minimise the impact and interference introduced by the expression of an exogenous protein in cells. The effect of different sensor concentration regimes below the non-interference threshold can be monitored through FCS-FLIM, a yet unexplored approach which has been introduced in this Chapter.

These observations suggest that differently designed sensors deployed in different concentrations give access to information regarding different aspects of heme biology. For example, a heme sensor designed to measure heme using GADPH as heme binding probe will be well suited to study heme trafficking mediated by GAPDH. On the other hand, a hypothetical heme sensor based on a traditional heme protein (*e.g.* Mb, cytochrome *c*) will provide information on heme loading to such proteins. Finally, deploying a sensor like mAPXmEGFP - where mAPX is not naturally expressed in the cell line used as a model (*i.e.* HEK293) - can only provide data relative to the portion of exchangeable heme (the total amplitude of which is unclear, but could involve the entire hemome) accessible to the sensor itself. Hence, obtaining a description of cellular heme trafficking through the use of heme sensor technologies that reconciles the mechanisms introduced in Sections 5.1.1-5.1.4 will likely require different kinds of sensors designed to probe selectively each of the above mentioned pathways: (i) a balance between heme biosynthesis and degradation; (ii) mediation by heme chaperones; (iii) trafficking through membrane contact sites; and (iv) involvement of a diffuse heme buffering system. Moreover, the heme synthesis and degradation regimes at the time of each measurement will always have to be taken into account by measuring the relative increase or decrease of ALAS-1, HO-1, and HO-2 protein levels.

Chapter 6

Summary and future work

Overall, this thesis proposes a framework for the systematic study of heme homeostasis through the deployment of genetically encoded heme sensors. It takes into account the complexities of the cellular environment, the intricate network of regulatory pathways heme is involved in, and the possible repercussions due to the expression of heme sensors. The main results can be summarised as follows:

- The mAPXmEGFP sensor was successfully deployed in live HEK293 cells (Chapter 2) to report on changing levels of heme concentration through the analysis of its lifetime decay.

- The concept of heme accessibility, $\%H_{acc}$, was elaborated in Chapter 3 to better describe how sensor-measured heme bioavailability depends on the relative access a given heme sensor has to exchangeable heme.

- The analysis of the $\%H_{acc}$ of mAPXmEGFP in Chapter 3 for cells grown under different conditions where ALAS-1, GAPDH, HO-1, and HO-2 (all of which play key roles in heme homeostasis) were inhibited, induced, or down-regulated highlighted a complex network of protein regulation that resists changes in cellular heme levels. In particular, the reciprocal regulation of ALAS-1 and HO-1 suggested that the balance between heme biosynthesis and degradation is likely the major contributor to heme homeostasis, albeit not the only one.

- A lifetime-based methodology for the isolation of the mitochondrial signal of

mAPXmEGFP through organelle staining with Mito Tracker Deep Red FM was also developed in Chapter 3. This method can be used to quantitatively map the relative distribution of cellular heme using mAPXmEGFP and Deep Red stains selective for each cellular compartment.

- The need to provide tools to uncover key HBPs - which may play hitherto concealed roles in meeting the logistical requirements of cellular heme trafficking - was tackled in Chapter 4 by combining ProFunc with AlphaFold2 in order to predict heme binding sites within AlphaFold2-generated protein structures.

- The influence of thermodynamics and sensor concentration on the binding of heme to mAPXmEGFP was quantitatively addressed in Chapter 5. In turn, the combination of FCS and FLIM to study of heme bioavailability in live cells was adopted for the first time to monitor both sensor concentration and heme bioavailability.

The logistics for the distribution of heme in cells have yet to be fully revealed. The dynamic requirements of cellular supply and demand may be complex and perhaps there is no single mechanism for the movement of heme within cells that dominates. Chaperones, buffer proteins, membranes, and transporters are likely to work together in a concerted way, and could provide contingencies for heme supply under conditions where the cell needs to react quickly to changes in heme demand. All of these mechanisms are normally considered individually but are likely cooperating with each other. Thus, the interplay between heme biosynthesis, degradation, transcriptional and post-transcriptional regulation of heme buffering proteins, are all envisaged as jointly contributing to the maintenance of heme bioavailability in cells (Figure 6.1).

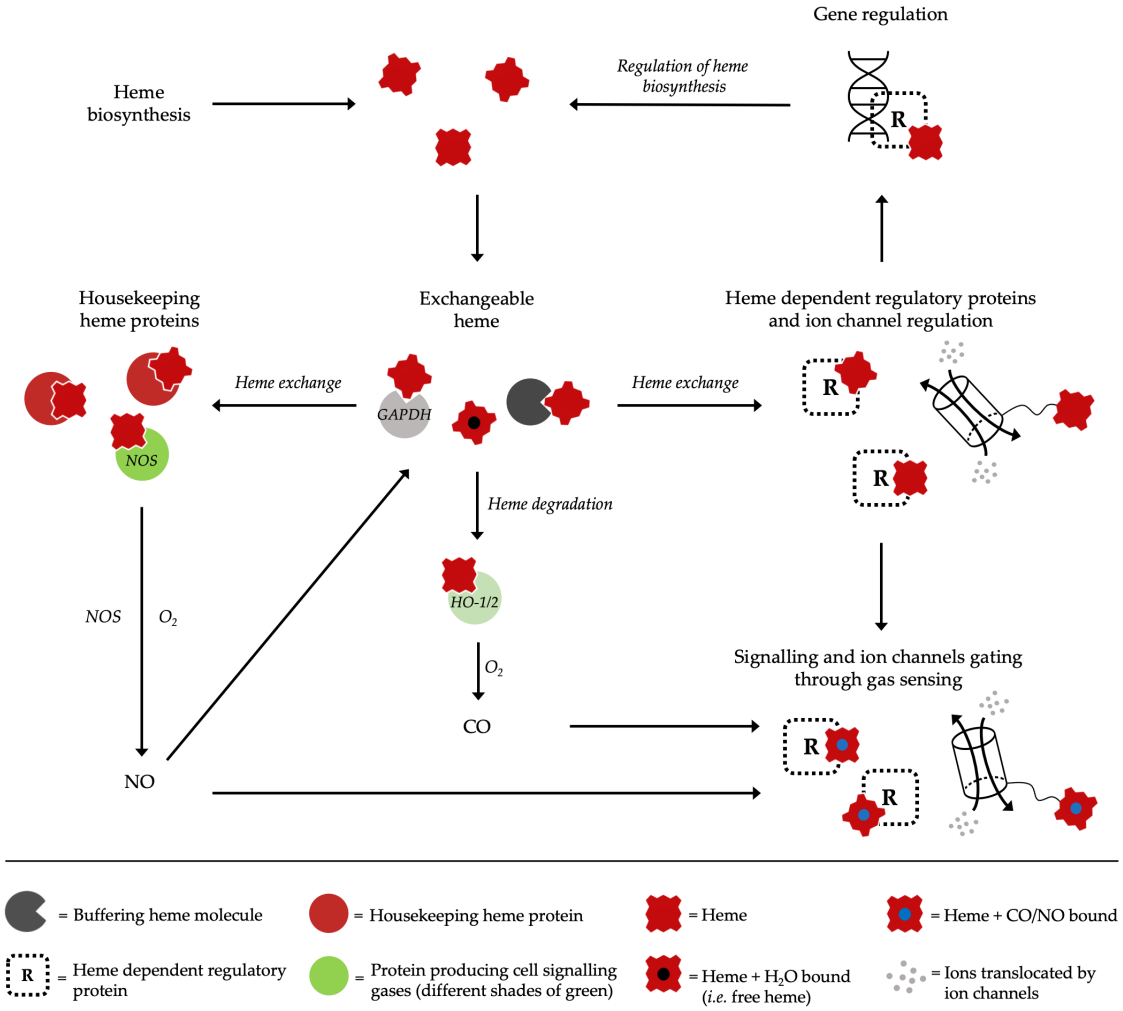

Figure 6.1: The possible interconnected pathways for the movements of heme in cells, and the links to signaling gases such as CO and NO. Heme biosynthesis provides cellular heme (top). A proportion of this is bound irreversibly to heme-binding housekeeping proteins (red circles). It is worth noting that inducers of ALAS-1 have also been observed inducing the expression of cytochrome P450 [184] and globins [189,290], suggesting that heme production might be accompanied by the expression of proteins that bind heme with high affinity, providing a thermodynamic drive that keeps heme levels low. At the same time, a body of exchangeable heme is envisaged to make heme available for regulatory proteins (R; right) by binding heme reversibly or through chaperones like GAPDH. These heme-binding partners constitute an exchangeable reservoir that can provide a flexible supply of heme and protect against changes in heme concentration. Once formed, heme-bound regulatory proteins can serve in regulatory roles by, for example, binding to DNA for transcriptional control (top right; including the regulation of heme biosynthesis, circadian rhythm, and ion channels) [23, 27, 29, 48, 50, 61, 291–293]. The green circles indicate the proteins that produce cell signaling gases - NOS (left) and HO-1/2 (middle). The synthesis of NO by NOS, and the production of CO by the heme degrading HO enzyme, add multiple layers of complexity to the picture by coupling the formation of cell signaling gases to heme-dependent processes [34,180,181]. For example, GAPDH-mediated heme delivery is highly dependent on NO fluxes for the maturation of heme proteins [175,193,195–197,294–298] and the regulation of heme biosynthesis has been found reciprocal to that of the circadian clock and genes that encode heme proteins such as NOS, sGC, and other key regulators of physiological cascades [29,204,299–302]. Figure adapted from Gallio *et al.* [118].

6.1 Future work

Many aspects of heme trafficking have remained unstudied for decades due to the lack of appropriate tools to address the problem. A renewed interest - which remained dormant since the pioneering studies of Granick and collaborators [75, 79] - was sparked in the past decade by the continuous emergence of heme-dependent regulatory roles [21,118], the discovery of the heme chaperone GAPDH [106,108,175, 194], and the development of genetically encoded heme sensors like mAPXmEGFP as in this work. However, many challenging questions are still awaiting an answer which will contribute to a unified description of heme homeostasis. A few examples of open questions that will need to be addressed in the future are introduced below.

Obtaining highly-diffracting crystals of *holo*-mAPXmEGFP would help to validate heme-fluorophore distances and provide a structural framework for the communication through FRET between the two chromophores. mAPXmEGFP has proven difficult to crystallise; over 230 crystallisation conditions were screened for the sensor both in the *apo*- and *holo*- forms, mostly unsuccessfully. Only one particular set of conditions has proved promising for *holo*-mAPXmEGFP (Appendix A.3). However, crystals of suitable size for X-ray analysis have not, thus far, been obtained. More trials and optimisation are required.

It would be desirable to analyse the movements of heme between cellular locations. This could be achieved by deploying a combination of heme-binding scaffolds, signal peptides and fluorescent tags to report on the simultaneous changes in heme concentrations within two (or more) subcellular compartments in cells expressing more than one of the heme-reporters directed to different compartments.

It will be increasingly important to develop methods to study the time-resolved response of the cells to tailored perturbations such as the up/down-regulation of ALAS-1, GAPDH, and HO-1/2. To access this information by using fluorescent heme sensors, long and repeated laser exposures - which are normally lethal to the cells - will be required. Thus, there is a need to develop less invasive methodologies to maintain cells viability during measurements. A solution may be represented by

multiphoton-FLIM, which requires significantly red-shifted λ_{Ex} and would minimise phototoxicity [136, 137].

Little information is currently available on the balance between the redox states of heme in cells, even though this is a critical aspect of its biological functions. Thus, there is a need to discriminate between reduced (ferrous) and oxidised (ferric) heme in heme-sensing experiments.

Finally, it will be important to establish a link between cellular heme levels and those of its metabolites (*i.e.* biliverdin and bilirubin) as increasing evidence points at an interplay between the biological pathways involving these three tetrapyrroles [303–309]. This can be achieved by integrating fundamental studies on heme bioavailability - like the one presented in this thesis - with the rich biology of its catabolites.

The multi-decade quest to uncover the underlying mechanisms that make heme bioavailable - with all its ramifications - is far from over.

.

Part III

Appendix

Appendix A

Materials and methods

A.1 Recombinant DNA Techniques

A.1.1 General procedure for the transformation of competent *E. coli* cells

100-200 mL of BL21(DH3) or DH5α competent *E. coli* cells from glycerol stocks (100-200 µL) were thawed at 0 °C and 1 µL of DNA at 100 µM was subsequently added. The mixture was gently mixed and incubated at 0 °C for 30 minutes. Then, a heat shock treatment at 42 °C for 45 seconds was followed by incubation at 0 °C for 2 minutes. The mixture was transferred to 1 mL of lysogeny broth (LB) and incubated at 37 °C for 45 minutes in a shaking incubator (150 rpm). The small growth (100 µL) was plated on an LB-agar Petri dish - supplemented with suitable antibiotic - and incubated overnight at 37 °C. The growth of single colonies proves the transformation under antibiotic control to be successful. A single colony was picked from the plate and grown overnight in 10 mL in LB in the presence of suitable antibiotic (37 °C, 150 rpm). Cell stocks were created in 50% glycerol and stored at -80 °C.

A.1.2 Expression and purification of mAPXmEGFP

The mAPXmEGFP expression construct is contained in the pLEICES45 vector. The DNA construct was provided by PROTEX (University of Leicester). The amino acid sequence of mAPXmEGFP is provided in Figure A.1. *apo*-mAPXmEGFP was expressed in *E. coli* BL21(DE3) cells transformed with pLEICS45-mAPXmEGFP. A starter culture was grown overnight in LB medium supplemented with 100 μg/mL ampicillin (Sigma Aldrich) at 37 °C in an orbital shaker (150 rpm). The starter culture was diluted 1:100 with LB medium ([Ampicillin] = 100 μg/mL) in 2 L baffled Erlenmeyer flasks and re-incubated (37 °C, 150 rpm) until the optical density at 600 nm was between 0.4-0.7. Expression was induced with 0.5 mM isopropyl β-D-1-thiogalactopyranoside (IPTG) and by dropping the temperature to 23 °C. Cells were harvested 20 h post-induction (10 minutes, 4000 rpm, 4 °C) and resuspended in lysis buffer (10 mM KPO_4, 150 mM KCl, pH = 7) supplemented with deoxyribonuclease I (Sigma Aldrich), EDTA-free protease inhibitor cocktail (Roche), and lysozyme (Sigma Aldrich). The suspension was sonicated on ice (4 bursts, 50%, 30 seconds on/off cycles) and the lysate was clarified by centrifugation (19000 rpm, 30 minutes, 4 °C). The homogenate was filtered (0.2 μm pores filter) and its volume was reduced to approximately 10 mL using a 50 kDa cut-off filter. mAPXmEGFP was purified by loading the lysate onto a nickel affinity column (HisTrap excel 5 mL; Washing buffer: [KPO_4] = 10 mM, [KCl] = 150 mM, [Imidazole] = 100 mM, pH = 7; Elution buffer: [KPi] = 10 mM, [KCl] = 150 mM, [Imidazole] = 500 mM, pH = 7; T = 6 °C). The eluate was de-salted with a PD10-G25 column (GE Healthcare) following the manufacturer's protocol and further purified by gel filtration on HiLoad Superdex 16/600 200 pg column (GE Healthcare) (Elution buffer: [KPO_4] = 10 mM, [KCl] = 150 mM, pH = 7; T = 6 °C).

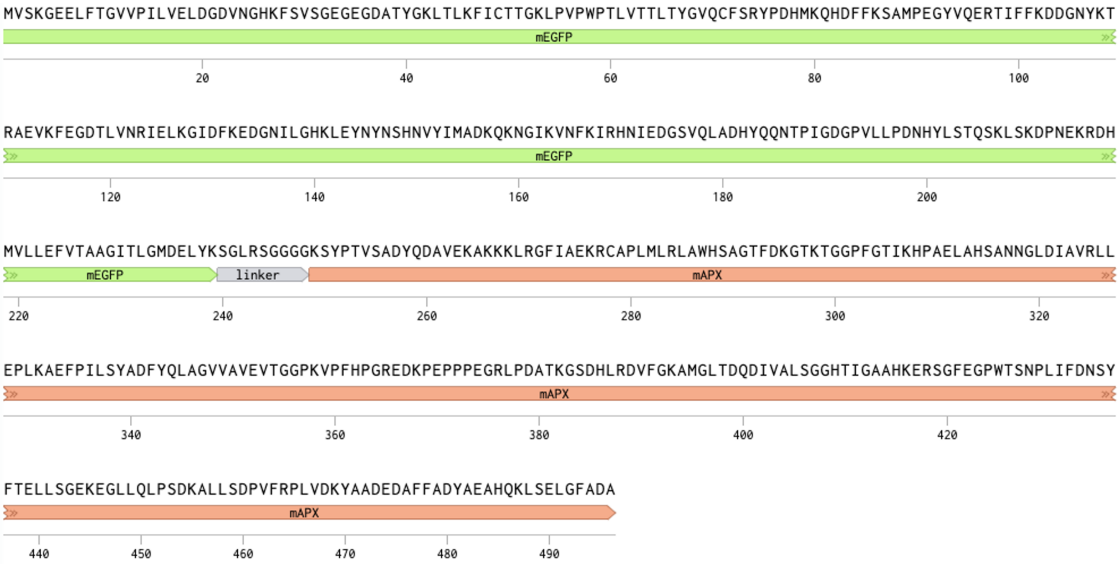

Figure A.1: Amino acid sequence of mAPXmEGFP. The colour-coded annotations identify the different domains of the fusion protein. Green: mEGFP; red: mAPX; gray: linker.

A.1.3 Expression and purification of sperm whale myoglobin H64Y/V68F (gMb)

The gMb (sperm whale myoglobin H64Y/V68F) expression construct is contained in the pEMBL19 vector (pEMBL19-gMb). The construct was originally developed by Olsen and co-workers [278]. The amino acid sequence of gMb is provided in Figure A.2. The expression protocol was adapted from the methods previously reported in the literature [278,310]. *E. coli* BL21(DE3) cells were transformed with pEMBL19-gMb. A starter culture was grown overnight in LB medium supplemented with 200 µg/mL ampicillin (Sigma Aldrich) at 37 °C in an orbital shaker (150 rpm). The starter culture was diluted 1:100 with LB medium ([Ampicillin] = 200 µg/mL) in 2 L baffled Erlenmeyer flasks and re-incubated (37 °C, 150 rpm) for 21 h. Cells were harvested 20 h post-induction (10 minutes, 4000 rpm, 4 °C) and resuspended in lysis buffer (50 mM Tris, 1 mM EDTA, 0.5 mM DTT) supplemented with deoxyribonuclease I (Sigma Aldrich), EDTA-free protease inhibitor cocktail (Roche), lysozyme (Sigma Aldrich). The suspension was sonicated on ice (4 bursts, 50%, 30 seconds on/off cycles) and the lysate was clarified by centrifugation (19000 rpm, 30 minutes, 4 °C). The homogenate was first enriched in gMb in a two-stage salting

purification. Ammonium sulfate (Fischer Bioreagent) was slowly added 40% m/V and the suspension incubated at 4 °C for 2 h. The suspension was centrifuged (4000 rpm, 10 min) and further ammonium sulfate was slowly added to the supernatant to 20% m/V (concentration zeroed to the previous addition). The suspension was incubated at 4 °C for 2 h and centrifuged (4000 rpm, 10 min). The supernatant was dialysed overnight twice using 14 kDa cut-off dialysis tubes (20 mM Tris, 1 mM EDTA, pH8). The dialysed sample was concentrated using a 10 kDa cut-off filter and further filtered through 0.2 µm pores. Gel filtration was performed on the sample using a HiLoad 16/600 Superdex 75 column (elution buffer: 20 mM Tris, 1 mM EDTA, pH 9). Fractions containing gMb were identified by SDS-PAGE, pooled, concentrated, and applied to a DEAE-Sepharose (Sigma) ion exchange column equilibrated in 20 mM Tris, 1 mM EDTA, pH 8.4. A dark green solution was obtained. gMb purity was assessed by SDS-PAGE and UV-Vis. The gel filtration elution profile and UV-vis spectra of gMb are shown in Figure A.3.

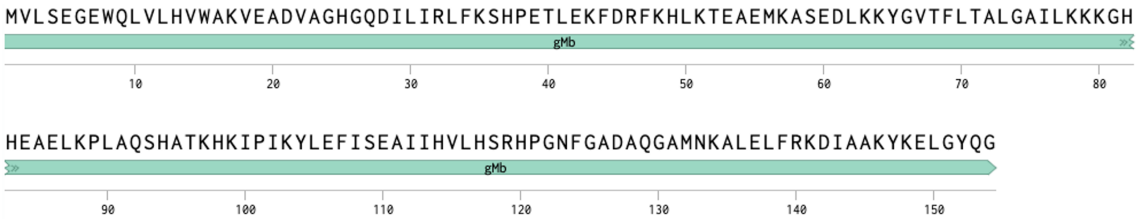

Figure A.2: Amino acid sequence of gMb.

Extraction of heme from gMb to obtain *apo*-gMb

The procedure was adapted from Teale's method [311]. In a glass test tube, an ice-cold 1 mL aliquot of ∼100 µM gMb was acidified by addition of 0.1 M HCl drop-by-drop until the dark green solution turns bright pink. Approximately 1 mL of ice cold butanone was added. The organic and aqueous phases were shaken and the test tube incubated at 0 °C for 10 min. A pink butanone layer was obtained over a colourless aqueous layer. The aqueous layer containing *apo*-gMb was isolated and dialysed against H_2O to remove traces of ketone. Successful heme extraction was confirmed by UV-Vis (Figure A.3).

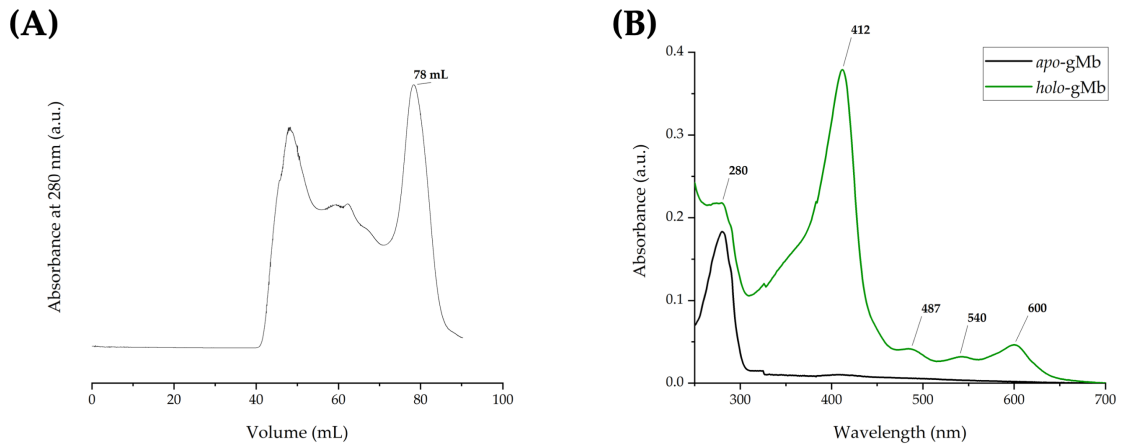

Figure A.3: (A) Gel filtration and (B) UV-vis spectra of gMb (the spectra of *apo*-gMb (black trace) and *holo*-gMb (green) are compared).

A.1.4 SDS-PAGE

Discontinuous polyacrylamide gels (10%) containing 0.1% SDS and polyacrylamide stacking gels (5%) were used. A Bio-Rad gel system with 0.75 mm gel thickness was used (materials in Table A.1). Samples were prepared by adding an equal volume of sample and sample buffer (100 mM Tris-HCl, pH 6.8, 4% SDS, 20% w/v glycerol, 0.002% bromophenol blue, 25 mM DTT) then boiled for 5 min. The gels were run in SDS running buffer (25 mM Tris-HCl, 192 mM glycerine, 0.5% w/v SDS) at 180 V until the dye front reached the end of the gel. Gels were soaked in InstantBlue™ Coomassie stain (Expedeon) for 1 h before destaining with distilled water by leaving the gels to gently shake on a rocker overnight.

Solution components	10% Resolving gel (mL)	5% Stacking gel (mL)
H_2O	4.0	6.8
30% acrylamide mix	3.3	1.7
1 M Tris (pH 6.8)	2.5	1.25
10% SDS	0.1	0.1
10% ammonium persulfate	0.1	0.1
TEMED	0.004	0.01

Table A.1: Materials and required to prepare 10 mL solutions Tris-glycine SDS-PAGE gels.

A.1.5 Titration of *apo*-heme proteins with hemin

Using a double beam Perkin Elmer Lambda 40 UV/VIS spectrometer, sequential equal amounts of the hemin titrating solution prepared as in Appendix A.1.6 were added both to the sample cuvette (containing the protein dissolved in 10 mM potassium phosphate, and 150 mM KCl at pH 7) and the reference cuvette, recording a spectrum after 3 minutes of equilibration following each addition (tipically in the 700-250 range nm). A representative example is shown if Figure A.4.

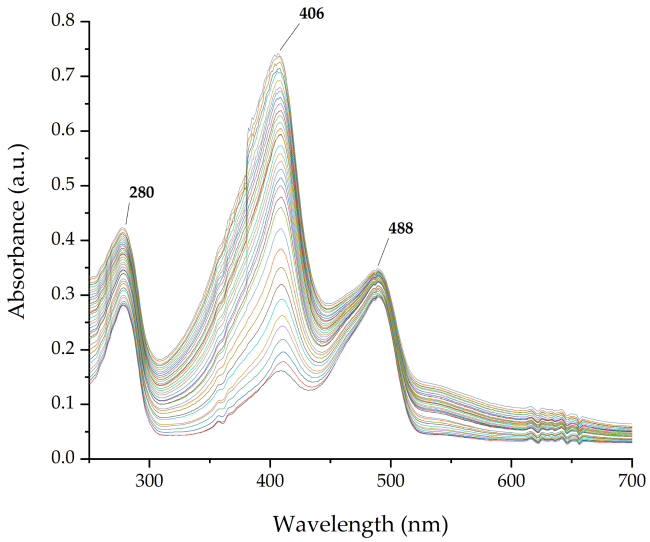

Figure A.4: A purified sample of 5 µM mAPXmEGFP was titrated with sequential amounts of 100 µM hemin titrating solution prepared as outlined in Section A.1.6. While the 280 nm absorption is due to aromatic side-chain amino acids, the relative band intensities at 406 nm and 488 nm arise from heme incorporated by the mAPX (Soret band) moiety and mEGFP in the fusion protein, respectively. Each subsequent addition of hemin led to an increase in the relative *holo*-protein concentration shown by the increment of the intensity of the Soret band. An absorbance ratio value A_{Soret}/A_{280} approaching 2 has been previously used as a parameter to assess protein purity [312].

A.1.6 General procedure to dissolve hemin and ZnPP in acqueous solutions

Hemin

A microspatula tip full of hemin chloride (Sigma Aldrich) was suspended in 1.5 mL centrifuge tube by adding 50 µL of 0.1 M NaOH (VWR). The suspension was diluted with 1 mL of $d\mathrm{H_2O}$ and centrifuged (13000 rpm; 30 s). The supernatant was

removed (500 µL) and diluted 1:1 with $d\mathrm{H_2O}$ in a clean tube. Centrifugation and dilutions were repeated until a clear solution was obtained. The solution of hemin was sterilised by filtration using a 0.2 µm pores membrane. The concentration of the sample was measured from the absorbance at 385 nm, and using ϵ_{385} = 58400 $\mathrm{M^{-1}cm^{-1}}$. The UV-vis spectrum of hemin is shown in Figure A.5.

ZnPP

ZnPP (25 mg; Sigma) was diluted with 25 mL of DMSO to make a 25 mg/mL stock. From the 25 mg/mL ZnPP, 4 µL was diluted with 4 µL of 0.1 M NaOH (VWR). The suspension was diluted with 750 µL of $d\mathrm{H_2O}$ and centrifuged (13000 rpm; 1 min). The supernatant was removed (500 µL) and diluted 1:1 with $d\mathrm{H_2O}$ in a clean tube. Centrifugation was repeated and the supernatant filtered (0.2 µm pores). The absorbance of the sample at 412 nm was measured by UV-Vis spectroscopy using ϵ_{412} = 87400 $\mathrm{M^{-1}cm^{-1}}$. The UV-vis spectrum of ZnPP is shown in Figure A.5.

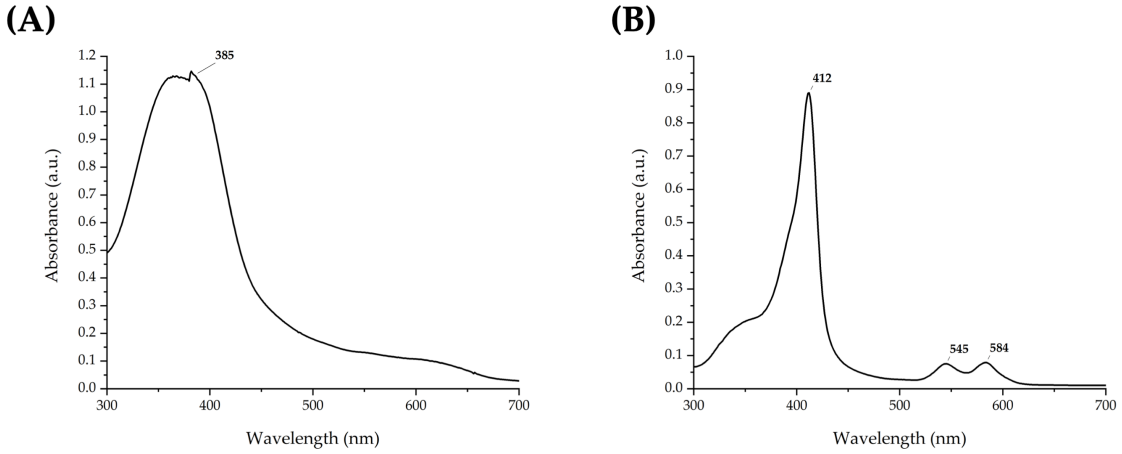

Figure A.5: UV-Vis spectra of (A) hemin and (B) ZnPP.

A.2 Molecular cloning

A.2.1 Agarose gel electrophoresis

Agarose was dissolved in 1× TAE buffer (40 mM Tris/0.4 mM EDTA pH 8/20 mM acetic acid) to a concentration of 0.5-1%. The suspension was briefly microwaved

(950W) at 30 second intervals to obtain a clear solution. The solution was left to cool slightly before the addition of peqGREEN, and then left to set. DNA samples (10 ng) were mixed with loading dye (Qiagen). The samples were loaded onto the gel alongside a DNA ladder and the gel was run at 80 V for 30 minutes in TAE buffer. The gel was then visualised under UV-light. The DNA ladders used were 1 kb Plus DNA Ladder and Quick-Load Purple 1 kb DNA Ladder (New England BioLabs, NEB).

A.2.2 Site-directed mutagenesis on pEGFP-C1-Cyto-APX, pEGFP-C1-Mito-APX, and pEGFP-C1-NLS-APX

The mutations K14D and A206K on the APX domain, and E112K on EGFP are required in order to express *in-vivo* the monomeric sensor mAPXmEGFP. The plasmids pEGFP-C1-Cyto-APX, pEGFP-C1-Mito-APX, and pEGFP-C1-NLS-APX expressing EGFP-APX (pEGFP-C1-Cyto-APX) and EGFP-APX, including signal peptides for the localisation of the sensor in the mitochondria (pEGFP-C1-Mito-APX) and nucleus pEGFP-C1-NLS-APX respectively were kindly donated by Prof. Iqbal Hamza [129] (see Table 3.5 for peptide sequences). Site-directed mutagenesis was performed on the plasmids that encode mAPXmEGFP. PCR tubes were prepared by mixing 12.5 µL of Primestar enzyme mix (Takara), 1 µL of forward primer (F) 10 µM, 1 µL of reverse primer (R) 10 µM, 1 µL of plasmid DNA template 10 ng/µL, and 9.5 µL of sterile deionised H_2O. Primers and PCR conditions for each point mutation are listed below (mutations sites are underlined):

K14D

F (5'-3'): TGATTACCAG<u>GAC</u>GCCGTTGAGAAG

R (5'-3'): GCACTCACAGTTGGGTAAG

PCR program:

98 °C for 2 min (hot start); Touch down 11 times (68-58 °C); Cycle 20 times (denaturation: 98 °C, 10 s, annealing: 60 °C, 5 s; elongation: 72 °C, 45 s); final elongation

(72 °C, 5 min)

E112K

F (5'-3'): GGGTGGACCTAAAGTTCCATTCC

R (5'-3'): GTGACCTCAACGGCAACA

PCR program:

98 °C for 2 min (hot start); Touch down 11 times (74-64 °C); Cycle 20 times (denaturation: 98 °C, 10 s, annealing: 60 °C, 5 s; elongation: 72 °C, 45 s); final elongation (72 °C, 5 min)

A206K

F (5'-3'): CACCCAGTCCAAACTGAGCAAAGAC

R (5'-3'): CTCAGGTAGTGGTTGTCG

PCR program:

98 °C for 2 min (hot start); Touch down 11 times (66-56 °C); Cycle 20 times (denaturation: 98 °C, 10 s, annealing: 60 °C, 5 s; elongation: 72 °C, 45 s); final elongation (72 °C, 5 min)

The PCR products were treated with KLD enzyme mix (Kinase, Ligase, and DpnI, New England BioLabs® *Inc.*) for phosphorylation, ligation/re-circularisation and template removal following the manufacturer's protocol. Subsequently, DH5-α competent cells were transformed separately with each of the obtained constructs. The KLD reaction mixtures were added to the cells, which were incubated at 0 °C for 30 minutes, followed by a 45 seconds heat shock at 42 °C, and further 2 minutes of incubation at 0 °C. Cells were reconstituted in SOB medium for 2 h at 37 °C, plated on an LB-agar Petri dish and incubated overnight at 37 °C. A single colony was picked, inoculated in LB ([Kanamycin] = 50 μg/mL) and incubated overnight at 37 °C. Cells were pelleted by centrifugation (4000 rpm) and the plasmid DNA constructs

extracted using a QIAprep Spin Miniprep Kit following the manufacturer's protocol. The new constructs were respectively labelled pEGFP-C1-Cyto-mAPXmEGFP, pEGFP-C1-Mito-mAPXmEGFP, and pEGFP-C1-NLS-mAPXmEGFP.

A.2.3 Insertion into pEGFP-C1-Cyto-mAPXmEGFP of the signal peptide sequences for localisation in the peroxisomes and endoplasmic reticulum respectively

C-term insertion of KDEL sequence to target the endoplasmic reticulum

F (5'-3'): GACCTGTAAGGATCCACCGGATCTAG

R (5'-3'): GTCCTTGGCSTCAGCAAACCCAAG

C-term insertion of SKL sequence to target the peroxisomes

F (5'-3'): ACTGTAAGGATCCACCGGATCTAG

R (5'-3'): TTGCTGGCATCAGCAAACCCAAG

PCR program (for both insertions):

98 °C for 2 min (hot start); Touch down 11 times (72-62 °C); Cycle 20 times (denaturation: 98 deg, 10 s, annealing: 62 °C, 15 s; elongation: 72 °C, 135 s); final elongation (72 °C, 120 s). The PCR products were digested and purified following the procedure reported above. The new constructs were respectively labelled pEGFP-C1-ER-mAPXmEGFP, pEGFP-C1-Per-mAPXmEGFP.

A.2.4 pMK240-mAPXmEGFP

pMK240-mAPXmEGFP was obtained through insertion of a mAPXmEGFP encoding gene in modifying pMK240 [285] (Figure A.6A-B). A DNA fragment encoding the fusion protein mAPXmEGFP was purchased from TWIST Bioscience. The codon sequence was optimised for mammalian expression to encode the mAPXmEGFP amino acid sequence in Figure A.2 and MluI and BglII restriction sites were added respectively at the 5' and 3' ends. Internal MluI and BglII cut sites were avoided. pMK240 and the insert were digested with MluI and BglII. Then, the insert was

pasted in between the Mlu I-Bgl II sites in the multi-cloning site of pMK240 using Quick Ligation™ (New England Bioscience M2200) using a 1:3 molar ratio vector:insert. The ligation product was used to transform DH5α*E. coli* cells. pMK240-mAPXmEGFP (Figure A.6B) was purified and isolated using a QIAprep Spin Miniprep Kit following the manufacture's protocol.

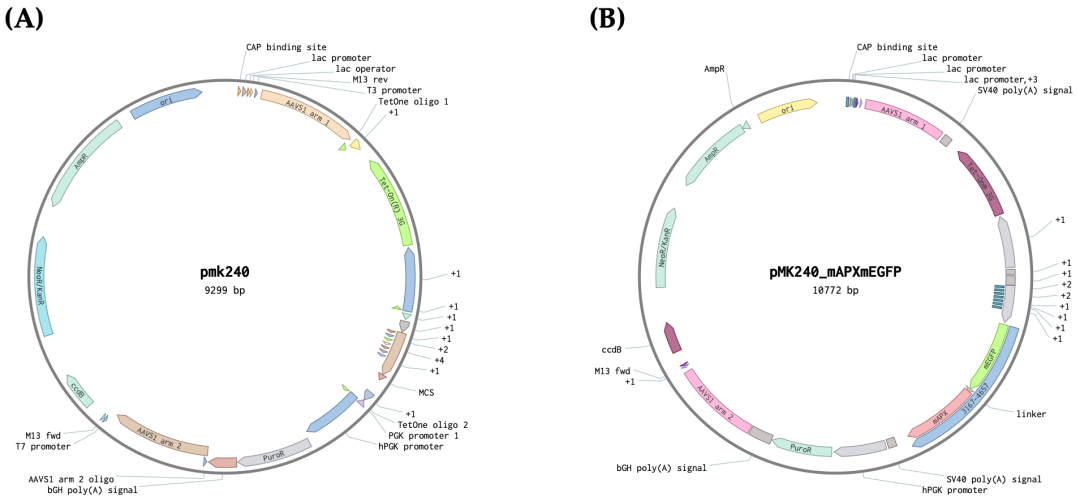

Figure A.6: (A) pMK240 and (B) pMK240-mAPXmEGFP plasmid maps.

A.3 Crystallisation screen for mAPXmEGFP

A precipitant was identified from the MORPHEUS protein crystallisation screen [313] that led to small crystals of *holo*-mAPXmEGFP (Figure A.7A): 12.5% w/v PEG 1000, 12.5% w/v, PEG 3350, 12.5% v/v MPD; Additives: 0.003 M of each NPS; Buffer: 0.1 M bicine/Tris base pH 8.5. Obtaining a crystal structure of the sensor will allow to experimental determination of the Förster distance in the sensor. The AlphaFold2 model of mAPXmEGFP shows a disordered, low-confidence region separating mAPX (rich in α-helices) and mEGFP (β-barrel) (Figure A.7B).

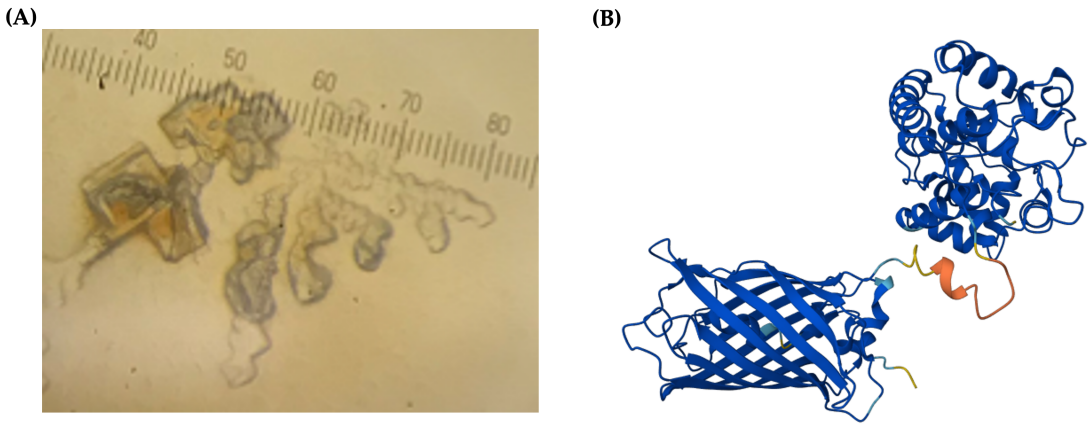

Figure A.7: (A) Picture of crystals of *holo*-mAPXmEGFP obtained in a small-scale crystallisation trial. (B) AlphaFold2 model of mAPXmEGFP. The model is colour-coded with regions of high confidence in blue and regions of low confidence in orange.

A.3.1 Encapsulation of mAPXmEGFP and gMb in coacervates

The work described in this Section was carried out with Dr. Ananya Mishra (University of Bristol).

Fluorescence microscopy

Fluorescence imaging was performed using a Leica DFC 310FX and dye molecules and protein were excited by using specific filters with the following excitation (λ_{Ex}) and emission (λ_{Em}) wavelength cutoffs. mAPXmEGFP, λ_{Ex} = 450 - 490 nm and λ_{Em} = 510 nm; 2,3-DAP, λ_{Ex} = 515 - 560 nm and λ_{Em} = 580 nm. All glass slides used for the imaging were functionalised with PEG-TMS.

Acoustic Trapping of coacervates

For 2D array formations of PDDA/ATP coacervate microdroplets the orthogonal transducer pairs were run at slightly different frequencies during the trapping process. They were operated at the third harmonic frequency (6.76/6.78 MHz and 10 V). Patterned PDDA/ATP coacervate micro-droplets were prepared in situ by adding an aqueous solution of ATP (150 µL, 50 mM, pH 8) to an aqueous solution of PDDA (300 µL, 25 mM monomer, 100-200 kDa, pH 8) in the presence of the two orthogonal acoustic standing waves generated from opposing transducer pairs.

The mixtures were kept standing for 30 mins to ensure homogeneous formation of the coacervate droplets by continuous coalescence in the square chamber resulting in a 2D microdroplet array. mAPXmEGFP/gMb encapsulation was carried out by addition of the protein into the sample chamber prior to introducing ATP to trigger the formation of spontaneous mAPXmEGFP/gMb captured micropatterned coacervates. The supernatant in the acoustic chamber was carefully removed and exchanged with $d\mathrm{H_2O}$ water three times under the same acoustic force field. Fluorescent microscope images were recorded at the centre of the trapping chamber within the observation window.

Acoustic device

A custom-built acoustic trapping device based on a square arrangement of four piezoelectric transducers (Noliac, NCE 51, L15 x W2mm x T1 mm) was used. The opposing transducer pairs were wired in series, driven by two signal generators (Agilent 33220a-001), and connected to an oscilloscope (Agilent DSOX2014A). A PEG functionalised glass coverslip was attached to the bottom of the device using an adhesive.

A.4 Tissue culture techniques

A.4.1 Cell culture

HEK293 cells were purchased from the European Collection of Authenticated Cell Cultures and maintained in α-MEM (Gibco) supplemented with 10% foetal bovine serum (Gibco) and 1% (v/v) penicillin-streptomycin (αα; Gibco, 15140-122) at 37 °C and 5% CO_2 in T75 or T25 flasks (Greiner). Cells expressing mAPXmEGFP were maintained in α-MEM (Gibco) supplemented with 10% foetal bovine serum (Gibco) and 200 µg/mL geneticin (Gibco) at 37 °C and 5% CO_2 in T75 or T25 flasks (Greiner) or 10 cm Petri dishes (Nunc). Cells were sub-cultured once approximately 80% confluence was reached and trypsinised using TrypLE (Gibco).

A.4.2 General procedure to generate a new stable HEK293 cell line

HEK293 cells from a confluent T75/25 flask were used to seed 2 mL cultures in polystyrene-coated 6-well plates (Greiner) and cultured until 70-80% confluent. Typically, 200-500 ng of DNA were used for each transfection using Lipofectamine 3000 (Invitrogen) as per manufacturer's instruction in serum-free medium. After 24-48 h the medium was changed to a complete formulation and cell cultured until confluent. Cells were sub-cultured onto a 10 cm Petri dish for antibiotic screening by refreshing the medium containing a suitable antibiotic every second day over a period of approximately four weeks. Cells transfected with pLEICS138-mAPXmEGFP were screened with 500 μg/mL geneticin (G418, Thermo Fischer Scientific). Cells transfected with pMK240-mAPXmEGFP were screened with 1 μg/mL puromycin. Antibiotic selection was continued until single clones started to appear. Clones were isolated with the agarose method (Lindeberg's method) and individually sub-cultured for functional tests. Cell stocks of successful clones were prepared by harvesting confluent cultures and resuspending them in maintenance medium with 5% DMSO. At least 1 million live cells were aliquoted in 1 mL cryo-tubes and incubated overnight in an *iso*-propanol bath at -80 °C. Cryo-tubes were then put under liquid nitrogen for long-term storage.

A.4.3 MTT assays for cellular viability

HEK293-mAPXmEGFP cells were seeded in a 96 well plate (Greiner) and cultured by refreshing the medium every second day (medium: α-MEM, 10% bovine serum albumin; 200 μg/mL geneticin). Upon reaching 80% confluence, the medium was refreshed and supplemented with 10 μM ZnPP, 10 μM hemin, or 1 mM succinyl acetone respectively (each condition repeated on separate wells for a total of 12 replicates). Cells were incubated for 24 h and MTT assay was performed following manufacturer's protocol (Biotium).

A.4.4 RNA interference

The knockdown of HO-2 and GAPDH was accompanied by the following control conditions: (i) untreated cells; (ii) cells transfected with ALLstar siRNA as a negative control (Qiagen); and (iii) cells transfected with siRNA-GAPDH (smart POOL, Dharmacon) as a positive control.

HO-2

Two consecutive rounds of siRNA transfection were carried out. HEK293 cells were plated in 6-well plates and cultured until 90% confluent. Immediately prior to transfection cells were washed 1x with warm transfection medium (T-medium; serum-free and antibiotics-free α-MEM (Gibco)) and supplemented with 1 mL of T-medium. 200 pg RNA transfection master mixes were prepared by mixing 10 µL of 10 µM siRNA1 with 10 µl of 10 µM siRNA2 and 20 µL of Lipofectamine 3000 diluted 1:25 with T-medium (siRNA1 and siRNA2 sequences are reported in Table 3.4). Transfection master mixes were incubated 30 min at room temperature and then quantitatively added to the 1 mL cultures in the 6-well plates. Transfection cultures were incubated overnight, sub-cultured quantitatively into a 10 cm dish and incubated again. On the next day, a 200 pg siRNA transfection was carried out as above in the 10 cm dishes. Cells were lysed for immunoblotting or harvested for further analysis 24 h after the second round of transfection .

GAPDH

ON-TARGETplus GAPD control siRNA (Dharmacon D-009630-00-0005) was used. This cocktail of siRNA sequences is normally used as positive control. Transfection was carried out according to the manufacturer's protocol with modifications. Briefly, HEK293-mAPXmEGFP cells were plated in a 10 cm Petri dish and cultured in complete medium (α-MEM, $\alpha\alpha$, 10% FBS) until there was 50%-70% confluency. Solutions of 5 µM RNA mix were prepared by diluting 100 µM siRNA stock with RNAse free H_2O. The transfection mix was prepared by mixing 3.3:1 the 5 µM ON-TARGETplus GAPD solution with DharmaFECT reagent (Dharmacon)

as per manufacturer's instruction using serum-free and antibiotic-free media. Prior to transfection, cells were gently washed with 1×PBS and media was replaced with 6.4 mL serum-free and antibiotic-free α-MEM supplemented with 1 mM sodium pyruvate. Transfection mix was added to the cells to a final volume of 8 mL and incubated for 48 h prior to further analysis.

A.4.5 Lysis of HEK293 cells

Cells were cultured in either a 6-well plate (Greiner Bio-one) or 10 cm dishes (Nunc). Prior to lysis cells were gently washed with a minimum amount of ice-cold 1×PBS (Greiner Bio-one). Ice-cold lysis buffer (1x RIPA buffer (ThermoFisher) supplemented with EDTA-free protease inhibitor (SLS)) was added to the cells which were subsequently scraped, transferred onto a 15 mL tube and incubated on ice for 10 minutes. The cell suspension was sonicated (50% amplitude, 1 bursts of 2 seconds). Lysates were incubated on ice for further 10 minutes on a rocker and then clarified by centrifugation at 13000 rpm in a table-top centrifuge at 4 °C for 30 min. Lysate protein was quantified by Pierce BCA protein assay following the manufacturer's protocol (Thermofisher). Lysates were aliquoted and stored at -80 °C.

A.4.6 Modified cell lysis protocol for mAPXmEGFP quantification in HEK293-mAPXmEGFP by immunoblotting

Cells were cultured in either a 6-well plate (Greiner Bio-one) or 10 cm dishes (Nunc). Prior to lysis cells were gently washed with PBS, detached using TrypLE (Gibco), and resuspended in PBS. Cells were counted using a Countess™ automated cell counter (Invitrogen) and 2.5 million cells were transferred in a 1.5 mL microcentrifuge tube and centrifuged (1200 rpm, 5 min). The supernatant was discarded and the cell pellet re-suspended in ice-cold lysis buffer (1x RIPA buffer (ThermoFisher)

supplemented with EDTA-free protease inhibitor (SLS)). Cells were lysed by incubation on ice for 15 min followed by sonication (50% amplitude, 1 bursts of 2 seconds). Lysates were incubated on ice for further 15 minutes on a rocker and then clarified by centrifugation at 13000 rpm in a table-top centrifuges at 4 °C for 15 min. Lysate protein were quantified by Pierce BCA protein assay in a 96-well plate (Greiner) following the manufacturer's protocol (Thermofisher) and using a CLARIOstar Plus fluorescence microplate reader. Lysates were stored at -80 °C.

A.5 Immunoblotting

Typically, 5-25 μg of lysate protein was prepared in a final volume of 10 μL of loading buffer using 4× Laemmli buffer (250 mM Tris pH 6.8, 8% SDS, 40% glycerol, 1.4 M β-mercaptoethanol, 0.02% bromophenol blue). Samples were boiled at 100 °C for 5 min. The lysate samples were loaded onto a 17-well NuPAGE 4-12% BisTris gel (11.0 mm x 17 well; Invitrogen) and electrophoresed at a constant voltage of 160 V for 1 h. Gels were transferred onto a low-fluorescence PVDF membrane using the XCell II Blot module (Invitrogen) for a wet transfer at a constant voltage of 30 V for 1 h. Membranes were blocked with 5% Blotto dry milk in Tris Buffered Saline-Tween, TBST (0.1% Tween) for 1 h at room temperature. ALAS-1, HO-1, HO-2, GAPDH, and mAPXmEGFP were separately probed by overnight primary antibody incubation at 4 °C using rabbit anti-ALAS-1, rabbit anti-HO-1, rabbit anti-HO-2, rabbit anti-GAPDH, and rabbit anti-GFP. Each detection was accompanied with the measurement of β-actin as internal control, which was probed with a 1:2000 dilution of mouse anti-β-actin (antibodies.com A85272).

ALAS-1 was probed with a 1:1500 dilution of rabbit anti-ALAS-1 (antibodies.com A8855), and HO-1 was probed with a 1:2500 dilution of rabbit anti-HO-1 (Bethyl Laboratories A305-354). HO-2 was probed with 1:2000 dilution of rabbit anti-HO-2 (Bethyl Laboratories A303-662). GAPDH was probed with a 1:20000 dilution of rabbit anti-GAPDH (antibodies.com A85377), and mAPXmEGFP was probed 1:1000 with rabbit anti GFP (antibodies.com A87774).

Following primary antibody incubation membranes were washed 3× with TBST on a rocker (5-min wash each). Membranes were incubated and gently rocked for 1 h at room temperature with goat anti-mouse secondary antibody (Biotium 20344) conjugated to a 680 nm fluorophore and donkey anti-rabbit secondary antibody (Biotium 20065) conjugated to a 790 nm fluorophore. Secondary antibodies were diluted 1:20000 in blocking buffer. After secondary antibody incubation membranes were washed 3× with TBST on a rocker (5 min wash each). Membrane images were acquired using a Licor Odyssey Fc imager with 2 min acquisition on the 700 and 800 channels. Images were analysed using Empiria Studio® Software.

Representative immunoblot detection of ALAS-1, GAPDH, HO-1, and HO-2 for the siRNA experiments

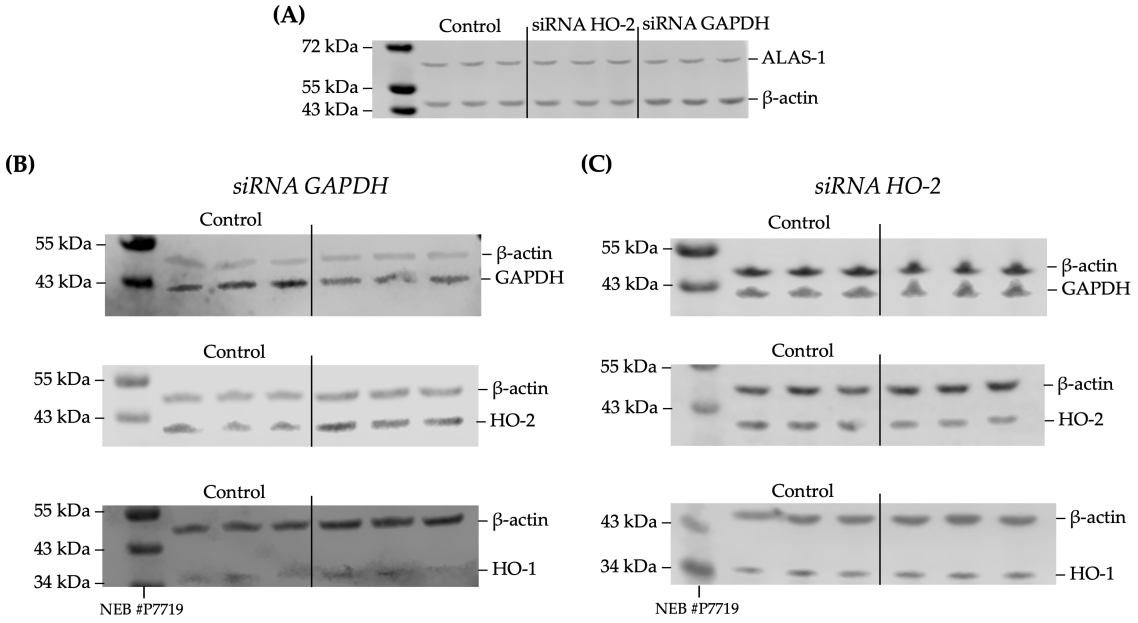

Figure A.8: Representative immunoblots showing a comparison between the band intensities detected in triplicate for whole-cell lysates of HEK293-mAPXmEGFP where HO-2 and GAPDH were knocked down by siRNA, respectively. (A) Comparison between the bands intensities of ALAS-1 for the two knockdown experiments. (B) Bands intensities of, respectively, GAPDH, HO-1, and HO-2 in HEK293-mAPXmEGFP where GAPDH was knocked-down by approximately 42%. (C) Band intensities of, respectively, GAPDH, HO-1, and HO-2 in HEK293-mAPXmEGFP where HO-2 was knocked-down. Membranes were imaged using a Licor Odyssey Fc. Analysis of bands intensities was carried out with Empiria Studio® Software using β-actin detection as an internal control to normalise the signal. The control shown in the figure corresponds to untreated cells. Results are discussed in Section 3.4.

A.6 Confocal microscopy

Cells were seeded into CELLview dishes (Greiner Bio-One) in the presence of 2 μg/mL poly-D-lysine for improved cell attachment [314] and were grown in phenol red–free α-MEM medium supplemented with 1% penicillin-streptomycin solution (αα), 200 μM geneticin, and 10% fetal bovine serum with the exeption of the siRNA experiments, where phenol red–free α-MEM was used with no further additives to minimise cytotoxicity. Separate compartments on cell dishes were treated either 24 h (1 mM SA, 10 μM hemin, 10 μM ZnPP) or 48 h (siRNA experiments) prior to imaging.

A.6.1 Staining of HEK293-mAPXmEGFP with Hoechst and Mitotracker, respectively

HEK293 cells stably or transiently transfected to express mAPXmEGFP were cultured in a microscopy dish (Greiner Bio-one) until 80% confluent. Cells were stained with Hoechst 33342 (Invitrogen; $\lambda_{Ex} = 361$ nm; $\lambda_{Em} = 486$ nm) or Mitotracker Deep Red FM (ThermoFischer; $\lambda_{Ex} = 641$ nm; $\lambda_{Em} = 662$ nm) following manufacturer's protocol. Images were taken on a Leica SP5II confocal microscope using a 63× oil immersion lens. For Hoechst 33342 detection, an excitation filter was used with a band pass centered at 405 nm, and fluorescence emission was collected between 410 and 440 nm. For mAPXmEGFP detection, an excitation filter was used with a band pass centered at 488 nm, and fluorescence emission was collected between 505 and 530 nm. For Mitotracker Deep Red FM, an excitation filter was used with a band pass centered at 633 nm, and fluorescence emission was collected between 649 and 709 nm.

A.6.2 Time-resolved measurements

Live-cell time-resolved measurements were performed on a laser-scanning confocal microscope (Leica SP8X; University of Bristol, Wolfson Bioimaging Facility) using a

63×/1.20 water immersion lens equipped with a pulsed white light laser, Picoquant electronics that allow Time Correlated Single Photon Counting (TCSPC) fluorescence lifetime data acquisition and fluorescence correlation spectroscopy measurements, and a SymPhoTime software (PicoQuant).

FLIM

For mAPXmEGFP lifetime detection, an excitation filter was used with a band pass centered at 488 nm, and fluorescence emission was collected between 495 and 551 nm. For Mitotracker DeepRed FM lifetime detection, an excitation filter was used with a band pass centered at 633 nm, and fluorescence emission was collected between 640 and 716 nm (Repetition rate: 40 MHz; image format: 256×256). Cells were maintained at 37 °C, with 5% CO_2. Typically, 10 images per condition explored were acquired. For every image acquired, six replicates of 30 second-acquisitions were performed. A global-fitting algorithm for multiexponential models was applied in FLIMfit to analyze all the pixel decay profiles in images recorded from HEK293-mAPXmEGFP [315]. If the photon count was below 200 for a single pixel in an image, then a black colour was assigned to that pixel in the image. Segmentation images were created using a custom pipeline for the plugin Modular Image Analysis (MIA) in FiJi. The custom pipeline to obtain segmented images to isolate mitochondrial signals was developed by Dr. Dominic Alibhai (Wolfson Bioimaging facility, University of Bristol).

FCS

Prior to live-cell FCS measurements conducted at 37 °C and 5% CO_2, the confocal volume was calibrated using the PicoQuant calibration script (available at: https://www.tcspc.com/doku.php/howto:calibrate_the_confocal_volume_for_fcs_using_the_fcs_calibration_script; last accessed: 06/23) and aqueous solutions of Rhodamine 6G (Rh6G) in the 1-20 nM range (Figure A.9) (measured confocal volume: V_{eff} = 0.93 fL).

An adjusted diffusion coefficient of Rh6G in water at 37 °C (5.5×10^{-6} cm^2s^{-1})

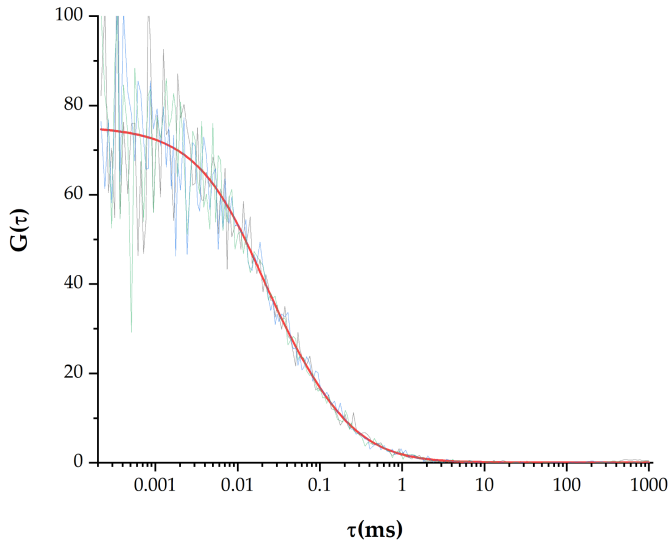

Figure A.9: Representative autocorrelation traces of a triplicate measurement of 20 nM Rh6G in $d\mathrm{H_2O}$ using the PicoQuant FCS calibration script. Grouped fitting of the traces was performed in SymPhoTime64 using a pure diffusion model (red trace).

was obtained by using a tabulated value at 25 °C (4.14×10^6 $\mathrm{cm^2s^{-1}}$ [284]) and by taking into account that the diffusion coefficient is temperature dependent according to the Stokes-Einstein relationship (Equation A.1).

$$D(T) = \frac{kT}{6\pi\eta(T)r} \tag{A.1}$$

Where η(T) is the viscosity of the solvent at a given temperature, k is the Boltzmann constant ($1.38\times10^{-23}\mathrm{J{\cdot}K^{-1}}$) and r is the hydrodynamic radius. If the calibration experiment is not performed at T=25 °C , the tabulated values should be recalculated using Equation A.2 (P. Kapusta, Absolute Diffusion Coefficients: Compilation of Reference Data for FCS Calibration, Rev. 1, PicoQuant GmbH., Berlin, 2010, https://www.picoquant.com/images/uploads/page/files/7353/appnote_diffusioncoefficients.pdf; last accessed: 06/23).

$$D(T) = D(273.15K) \times \frac{t + 273.15}{\eta(t)} \times 2.985 \cdot 10^{-6} Pa \cdot s \cdot K^{-1} \tag{A.2}$$

mAPXmEGFP was excited using white laser light with a band pass filter centered at 488 nm, and fluorescence emission was collected between 496 nm and 551 nm.

Triplicate measurements were acquired for each of the selected points in the confocal plane. The acquisition time duration for each measurement was set at 10 s.

The measured self-similarity traces were plotted using the SymPhoTime 64 software using the group FCS script and fitted therein. Dynamic processes in solution that affect the emission of fluorescence molecules causes fluctuations in their fluorescence signal $F(t)$ and are characterised by an autocorrelation function $G(\tau)$ (Equation A3; normalised) [136].

$$G(\tau) = \frac{\langle F(t) \cdot F(t+\tau) \rangle}{\langle F(t) \rangle^2} \tag{A.3}$$

Equation A.3, when applied to systems where the 3D diffusion of the fluorophore is obstructed - for example by highly crowded environments - takes the analytical form in Equation A.4 where N_s is the mean number of molecules in the confocal volume, τ_s is related to the beam waist and the diffusion coefficient d_w is an anomaly parameter equal to 2 for free diffusion but increases with increasing obstruction, and κ is related to the ratio between the beam waist and the axial radius of the focus. For a complete description of the model please refer to Wachsmuth *et al.* [283].

$$G(\tau) = \frac{1}{N_s} \left[\left(1 + \left(\frac{\tau}{\tau_s} \right)^{\frac{2}{d_w}} \right) \left(1 + \frac{1}{\kappa^2} \left(\frac{\tau}{\tau_s} \right)^{\frac{2}{d_w}} \right)^{\frac{1}{2}} \right]^{-1} \tag{A.4}$$

Equation A.4 was used to fit the measured auto-correlation traces. Equation A.4 represents the recommended model (indicated in SymPhoTime as "triplet extended (3D)" model) for fluorophores where the average photon count rate is not completely stable (commonly observed in cells) and/or the dye is diffusing in all three space directions through a crowded environment (see: https://www.tcspc.com/doku.php/howto:calculate_and_fit_fcs_traces_with_the_fcs_script; last accessed: 06/23).

Bibliography

[1] G. P. Moss, P. A. S. Smith, and D. Tavernier. Glossary of class names of organic compounds and reactivity intermediates based on structure (iupac recommendations 1995). *Pure Appl Chem*, 67(8-9):1307–1375, 1995.

[2] S. E. Martinez, D. Huang, A. Szczepaniak, W. A. Cramer, and J. L. Smith. Crystal structure of chloroplast cytochrome *f* reveals a novel cytochrome fold and unexpected heme ligation. *Structure*, 2(2):95–105, 1994.

[3] L. J. Smith, A. Kahraman, and J. M. Thornton. Heme proteins–diversity in structural characteristics, function, and folding. *Proteins*, 78(10):2349–68, 2010.

[4] J. C. Kendrew, H. C. Watson, B. E. Strandberg, R. E. Dickerson, D. C. Phillips, and V. C. Shore. The amino-acid sequence x-ray methods, and its correlation with chemical data. *Nature*, 190:666–70, 1961.

[5] M. F. Perutz. Relation between structure and sequence of haemoglobin. *Nature*, 194(0028-0836):914–7, 1962.

[6] T. L. Poulos. Heme enzyme structure and function. *Chem Rev*, 114(7):3919–62, 2014.

[7] J. Wang, F. Niemevz, L. Lad, L. Huang, D. E. Alvarez, G. Buldain, T. L. Poulos, and P. R. de Montellano. Human heme oxygenase oxidation of 5- and 15-phenylhemes. *J Biol Chem*, 279(41):42593–604, 2004.

[8] P. Ascenzi, A. Bellelli, M. Coletta, A. Colosimo, G. Falcioni, G. M. Giacometti, R. Ippoliti, L. Zolla, and B. Giardina. Multiple strategies for O_2 transport: from simplicity to complexity. *IUBMB Life*, 59(8-9):600–16, 2007.

[9] J. Breton, J. Lavergne, M. C. Wakeham, E. Nabedryk, and M. R. Jones. The unusually strong hydrogen bond between the carbonyl of Q_A and His M219 in the *Rhodobacter sphaeroides* reaction center is not essential for efficient electron transfer from Q_A^- to Q_B. *Biochemistry*, 46(22):6468–76, 2007.

[10] P. R. Jaschke, A. Hardjasa, E. L. Digby, C. N. Hunter, and J. T. Beatty. A BchD (magnesium chelatase) mutant of *Rhodobacter sphaeroides* synthesizes zinc bacteriochlorophyll through novel zinc-containing intermediates. *J Biol Chem*, 286(23):20313–22, 2011.

[11] R. Sobotka, M. Tichy, A. Wilde, and C. N. Hunter. Functional assignments for the carboxyl-terminal domains of the ferrochelatase from *Synechocystis* PCC

6803: the CAB domain plays a regulatory role, and region II is essential for catalysis. *Plant Physiol*, 155(4):1735–47, 2011.

[12] J. Kopecna, I. Cabeza de Vaca, N. B. P. Adams, P. A. Davison, A. A. Brindley, C. N. Hunter, V. Guallar, and R. Sobotka. Porphyrin binding to Gun4 protein, facilitated by a flexible loop, controls metabolite flow through the chlorophyll biosynthetic pathway. *J Biol Chem*, 290(47):28477–28488, 2015.

[13] J. W. Chidgey, P. J. Jackson, M. J. Dickman, and C. N. Hunter. PufQ regulates porphyrin flux at the haem/bacteriochlorophyll branchpoint of tetrapyrrole biosynthesis via interactions with ferrochelatase. *Mol Microbiol*, 106(6):961–975, 2017.

[14] P. C. E. Moody and E. L. Raven. The nature and reactivity of ferryl heme in compounds I and II. *Acc Chem Res*, 51(2):427–435, 2018.

[15] D. J. Stuehr and M. M. Haque. Nitric oxide synthase enzymology in the 20 years after the nobel prize. *Br J Pharmacol*, 176(2):177–188, 2019.

[16] C. A. Rouzer and L. J. Marnett. Cyclooxygenases: structural and functional insights. *J Lipid Res*, 50 Suppl:S29–34, 2009.

[17] L. Zhao, H. Xie, Y. Kang, Y. Lin, G. Liu, M. Sakato-Antoku, R. S. Patel-King, B. Wang, C. Wan, S. M. King, C. Zhao, and K. Huang. Heme-binding protein CYB5D1 is a radial spoke component required for coordinated ciliary beating. *Proc Natl Acad Sci U S A*, 118(17), 2021.

[18] T. Shimizu. Binding of cysteine thiolate to the Fe(III) heme complex is critical for the function of heme sensor proteins, 2012.

[19] E. A. Sweeny, S. Schlanger, and D. J. Stuehr. Dynamic regulation of NADPH oxidase 5 by intracellular heme levels and cellular chaperones. *Redox Biol*, 36:101656, 2020.

[20] M. Nishinaga, H. Sugimoto, Y. Nishitani, S. Nagai, S. Nagatoishi, N. Muraki, T. Tosha, K. Tsumoto, S. Aono, Y. Shiro, and H. Sawai. Heme controls the structural rearrangement of its sensor protein mediating the hemolytic bacterial survival. *Commun Biol*, 4(1):467, 2021.

[21] T. Shimizu, A. Lengalova, V. Martinek, and M. Martinkova. Heme: emergent roles of heme in signal transduction, functional regulation and as catalytic centres. *Chem Soc Rev*, 48(24):5624–5657, 2019.

[22] T. Shimizu, D. Huang, F. Yan, M. Stranava, M. Bartosova, V. Fojtikova, and M. Martinkova. Gaseous O_2, NO, and CO in signal transduction: structure and function relationships of heme-based gas sensors and heme-redox sensors. *Chem Rev*, 115(13):6491–533, 2015.

[23] J. Shen, X. Sheng, Z. Chang, Q. Wu, S. Wang, Z. Xuan, D. Li, Y. Wu, Y. Shang, X. Kong, L. Yu, L. Li, K. Ruan, H. Hu, Y. Huang, L. Hui, D. Xie, F. Wang, and R. Hu. Iron metabolism regulates p53 signaling through direct heme-p53 interaction and modulation of p53 localization, stability, and function. *Cell Rep*, 7(1):180–93, 2014.

[24] E. L. Carter, Y. Ramirez, and S. W. Ragsdale. The heme-regulatory motif of nuclear receptor Rev-erbβ is a key mediator of heme and redox signaling in circadian rhythm maintenance and metabolism. *Journal of Biological Chemistry*, 292(27):11280–11299, 2017.

[25] E. L. Carter, N. Gupta, and S. W. Ragsdale. High affinity heme binding to a heme regulatory motif on the nuclear receptor Rev-erbβ leads to its degradation and indirectly regulates its interaction with nuclear receptor corepressor. *Journal of Biological Chemistry*, 291(5):2196–2222, 2016.

[26] N. Gupta and S. W. Ragsdale. Thiol-disulfide redox dependence of heme binding and heme ligand switching in nuclear hormone receptor Rev-erbβ. *J Biol Chem*, 286(6):4392–403, 2011.

[27] S. Raghuram, K. R. Stayrook, P. Huang, P. M. Rogers, A. K. Nosie, D. B. McClure, L. L. Burris, S. Khorasanizadeh, T. P. Burris, and F. Rastinejad. Identification of heme as the ligand for the orphan nuclear receptors REV-ERBα and REV-ERBβ. *Nat Struct Mol Biol*, 14(12):1207–13, 2007.

[28] K. Kitanishi, J. Igarashi, K. Hayasaka, N. Hikage, I. Saiful, S. Yamauchi, T. Uchida, K. Ishimori, and T. Shimizu. Heme-binding characteristics of the isolated PAS-A domain of mouse Per2, a transcriptional regulatory factor associated with circadian rhythms. *Biochemistry*, 47(23):6157–6168, 2008.

[29] S. L. Freeman, H. Kwon, N. Portolano, G. Parkin, U. Venkatraman Girija, J. Basran, A. J. Fielding, L. Fairall, D. A. Svistunenko, P. C. E. Moody, J. W. R. Schwabe, C. P. Kyriacou, and E. L. Raven. Heme binding to human CLOCK affects interactions with the E-box. *Proc Natl Acad Sci U S A*, 116(40):19911–19916, 2019.

[30] M. V. Airola, J. Du, J. H. Dawson, and B. R. Crane. Heme binding to the mammalian circadian clock protein Period 2 is nonspecific. *Biochemistry*, 49(20):4327–4338, 2010.

[31] K. Hayasaka, K. Kitanishi, J. Igarashi, and T. Shimizu. Heme-binding characteristics of the isolated PAS-B domain of mouse Per2, a transcriptional regulatory factor associated with circadian rhythms. *Biochimica Et Biophysica Acta-Proteins and Proteomics*, 1814(2):326–333, 2011.

[32] E. M. Dioum, J. Rutter, J. R. Tuckerman, G. Gonzalez, M. A. Gilles-Gonzalez, and S. L. McKnight. NPAS2: A gas-responsive transcription factor. *Science*, 298(5602):2385–2387, 2002.

[33] G. S. Lukat-Rodgers, C. Correia, M. V. Botuyan, G. Mer, and K. R. Rodgers. Heme-based sensing by the mammalian circadian protein clock. *Inorg Chem*, 49(14):6349–65, 2010.

[34] A. Sarkar, E. L. Carter, J. B. Harland, A. L. Speelman, N. Lehnert, and S. W. Ragsdale. Ferric heme as a CO/NO sensor in the nuclear receptor Rev-Erbβ by coupling gas binding to electron transfer. *Proc Natl Acad Sci U S A*, 118(3):e2016717118, 2021.

[35] S. A. Mosure, T. S. Strutzenberg, J. Shang, P. Munoz-Tello, L. A. Solt, P. R. Griffin, and D. J. Kojetin. Structural basis for heme-dependent NCoR binding to the transcriptional repressor REV-ERBβ. *Sci Adv*, 7(5):eabc6479, 2021.

[36] P. M. Rogers, L. Ying, and T. P. Burris. Relationship between circadian oscillations of Rev-erbα expression and intracellular levels of its ligand, heme. *Biochem Biophys Res Commun*, 368(4):955–8, 2008.

[37] L. Yin, N. Wu, J. C. Curtin, M. Qatanani, N. R. Szwergold, R. A. Reid, G. M. Waitt, D. J. Parks, K. H. Pearce, G. B. Wisely, and M. A. Lazar. Rev-erbα, a heme sensor that coordinates metabolic and circadian pathways. *Science*, 318(5857):1786–9, 2007.

[38] Y. Mukaiyama, T. Uchida, E. Sato, A. Sasaki, Y. Sato, J. Igarashi, H. Kurokawa, I. Sagami, T. Kitagawa, and T. Shimizu. Spectroscopic and DNA-binding characterization of the isolated heme-bound basic helix-loop-helix-PAS-A domain of neuronal PAS protein 2 (NPAS2), a transcription activator protein associated with circadian rhythms. *FEBS J*, 273(11):2528–39, 2006.

[39] T. Uchida, I. Sagami, T. Shimizu, K. Ishimori, and T. Kitagawa. Effects of the bHLH domain on axial coordination of heme in the PAS-A domain of neuronal PAS domain protein 2 (NPAS2): conversion from His119/Cys170 coordination to His119/His171 coordination. *J Inorg Biochem*, 108:188–95, 2012.

[40] R. Koudo, H. Kurokawa, E. Sato, J. Igarashi, T. Uchida, I. Sagami, T. Kitagawa, and T. Shimizu. Spectroscopic characterization of the isolated heme-bound PAS-B domain of neuronal PAS domain protein 2 associated with circadian rhythms. *FEBS J*, 272(16):4153–62, 2005.

[41] M. Ishida, T. Ueha, and I. Sagami. Effects of mutations in the heme domain on the transcriptional activity and DNA-binding activity of NPAS2. *Biochem Biophys Res Commun*, 368(2):292–7, 2008.

[42] S. Minegishi, I. Sagami, S. Negi, K. Kano, and H. Kitagishi. Circadian clock disruption by selective removal of endogenous carbon monoxide. *Sci Rep*, 8(1):11996, 2018.

[43] R. Klemz, S. Reischl, T. Wallach, N. Witte, K. Jurchott, S. Klemz, V. Lang, S. Lorenzen, M. Knauer, S. Heidenreich, M. Xu, J. A. Ripperger, M. Schupp, R. Stanewsky, and A. Kramer. Reciprocal regulation of carbon monoxide metabolism and the circadian clock. *Nat Struct Mol Biol*, 24(1):15–22, 2016.

[44] K. Sudan, V. Vijayan, K. Madyaningrana, F. Gueler, K. Igarashi, R. Foresti, R. Motterlini, and S. Immenschuh. TLR4 activation alters labile heme levels to regulate BACH1 and heme oxygenase-1 expression in macrophages. *Free Radic Biol Med*, 137:131–142, 2019.

[45] K. van Wijk, T. Akabane, T. Kimura, S. Saitoh, S. Okano, V. P. Kelly, M. Takagi, K. Kodama, K. Takahashi, T. Tanaka, M. Nakajima, and O. Nakajima. Heterozygous disruption of ALAS1 in mice causes an accelerated age-dependent reduction in free heme, but not total heme, in skeletal muscle and liver. *Arch Biochem Biophys*, 697:108721, 2021.

[46] X. D. Tang, Mark F. Xu R Fau Reynolds, Maria L. Reynolds Mf Fau Garcia, Stefan H. Garcia Ml Fau Heinemann, Toshinori Heinemann Sh Fau Hoshi, and T. Hoshi. Haem can bind to and inhibit mammalian calcium-dependent Slo1 BK channels. *Nature*, 425(6957):531–535, 2003.

[47] S. Wang, S. Publicover, and Y. Gu. An oxygen-sensitive mechanism in regulation of epithelial sodium channel. *Proc Natl Acad Sci U S A*, 106(8):2957–62, 2009.

[48] M. J. Burton, S. M. Kapetanaki, T. Chernova, A. G. Jamieson, P. Dorlet, J. Santolini, P. C. Moody, J. S. Mitcheson, N. W. Davies, R. Schmid, E. L. Raven, and N. M. Storey. A heme-binding domain controls regulation of ATP-dependent potassium channels. *Proc Natl Acad Sci U S A*, 113(14):3785–90, 2016.

[49] M. J. Burton, J. Cresser-Brown, M. Thomas, N. Portolano, J. Basran, S. L. Freeman, H. Kwon, A. R. Bottrill, M. J. Llansola-Portoles, A. A. Pascal, R. Jukes-Jones, T. Chernova, R. Schmid, N. W. Davies, N. M. Storey, P. Dorlet, P. C. E. Moody, J. S. Mitcheson, and E. L. Raven. Discovery of a heme-binding domain in a neuronal voltage-gated potassium channel. *J Biol Chem*, 295(38):13277–13286, 2020.

[50] S. M. Kapetanaki, M. J. Burton, J. Basran, C. Uragami, P. C. E. Moody, J. S. Mitcheson, R. Schmid, N. W. Davies, P. Dorlet, M. H. Vos, N. M. Storey, and E. Raven. A mechanism for CO regulation of ion channels. *Nat Commun*, 9(1):907, 2018.

[51] J. H. Jaggar, A. Li, H. Parfenova, J. Liu, E. S. Umstot, A. M. Dopico, and C. W. Leffler. Heme is a carbon monoxide receptor for large-conductance Ca_2^+-activated K^+ channels. *Circ Res*, 97(8):805–12, 2005.

[52] S. E. Williams, S. P. Brazier, N. Baban, V. Telezhkin, C. T. Muller, D. Riccardi, and P. J. Kemp. A structural motif in the C-terminal tail of slo1 confers carbon monoxide sensitivity to human BK Ca channels. *Pflugers Arch*, 456(3):561–72, 2008.

[53] P. J. Kemp. Hemeoxygenase-2 as an O_2 sensor in K^+ channel-dependent chemotransduction. *Biochem Biophys Res Commun*, 338(1):648–52, 2005.

[54] S. Hou, S. H. Heinemann, and T. Hoshi. Modulation of BK_{Ca} channel gating by endogenous signaling molecules. *Physiology (Bethesda)*, 24:26–35, 2009.

[55] G. Wang. Mechanistic insight into the heme-independent interplay between iron and carbon monoxide in CFTR and Slo1 BK_{Ca} channels. *Metallomics*, 9(6):634–645, 2017.

[56] C. Peers, M. L. Dallas, and J. L. Scragg. Ion channels as effectors in carbon monoxide signaling. *Commun Integr Biol*, 2(3):241–2, 2009.

[57] R. Motterlini and L. E. Otterbein. The therapeutic potential of carbon monoxide. *Nat Rev Drug Discov*, 9(9):728–43, 2010.

[58] C. Peers. Modulation of ion channels and transporters by carbon monoxide: causes for concern? *Front Physiol*, 3:477, 2012.

[59] J. Y. Wu, H. Y. Qu, Z. L. Shang, S. T. Tao, G. H. Xu, J. Wu, H. Q. Wu, and S. L. Zhang. Reciprocal regulation of Ca_2^+-activated outward K^+ channels of pyrus pyrifolia pollen by heme and carbon monoxide. *New Phytol*, 189(4):1060–1068, 2011.

[60] G. Gessner, P. Ruhl, M. Westerhausen, T. Hoshi, and S. H. Heinemann. Fe_2^+-mediated activation of bk_{Ca} channels by rapid photolysis of CORM-S1 releasing CO and Fe_2^+. *ACS Chem Biol*, 15(8):2098–2106, 2020.

[61] G. Layer, J. Reichelt, D. Jahn, and D. W. Heinz. Structure and function of enzymes in heme biosynthesis. *Protein Sci*, 19(6):1137–61, 2010.

[62] T. Matsui, M. Unno, and M. Ikeda-Saito. Heme oxygenase reveals its strategy for catalyzing three successive oxygenation reactions. *Acc Chem Res*, 43(2):240–7, 2010.

[63] A. Wissbrock and D. Imhof. A tough nut to crack: Intracellular detection and quantification of heme in malaria parasites by a genetically encoded protein sensor. *Chembiochem*, 18(16):1561–1564, 2017.

[64] A. Aich, M. Freundlich, and P. G. Vekilov. The free heme concentration in healthy human erythrocytes. *Blood Cells Mol Dis*, 55(4):402–9, 2015.

[65] Y. Song, M. Yang, S. V. Wegner, J. Zhao, R. Zhu, Y. Wu, C. He, and P. R. Chen. A genetically encoded FRET sensor for intracellular heme. *ACS Chem Biol*, 10(7):1610–5, 2015.

[66] G. C. Leung, S. S. Fung, A. E. Gallio, R. Blore, D. Alibhai, E. L. Raven, and A. J. Hudson. Unravelling the mechanisms controlling heme supply and demand. *Proc Natl Acad Sci U S A*, 118(22):E2104008118.

[67] J. R. Abshire, C. J. Rowlands, S. M. Ganesan, P. T. So, and J. C. Niles. Quantification of labile heme in live malaria parasites using a genetically encoded biosensor. *Proc Natl Acad Sci U S A*, 114(11):E2068–E2076, 2017.

[68] D. A. Hanna, R. M. Harvey, O. Martinez-Guzman, X. Yuan, B. Chandrasekharan, G. Raju, F. W. Outten, I. Hamza, and A. R. Reddi. Heme dynamics and trafficking factors revealed by fluorescent heme sensors. *Proc Natl Acad Sci U S A*, 113(27):7539–44, 2016.

[69] H. L. Bonkovsky, J. T. Guo, W. Hou, T. Li, T. Narang, and M. Thapar. Porphyrin and heme metabolism and the porphyrias. *Compr Physiol*, 3(1):365–401, 2013.

[70] H. L. Bonkovsky, J. F. Healey, A. N. Lourie, and G. G. Gerron. Intravenous heme-albumin in acute intermittent porphyria: evidence for repletion of hepatic hemoproteins and regulatory heme pools. *Am J Gastroenterol*, 86(8):1050–6, 1992.

[71] T. Hunt, G. Vanderhoff, and I. M. London. Control of globin synthesis: the role of heme. *J Mol Biol*, 66(3):471–81, 1972.

[72] A. Lodola and O.T.G. Jones. Evidence for a rapidly turned over pool of haem in isolated hepatocytes. *FEBS Letters*, 90(2):250–254, 1978.

[73] G. Kikuchi and N. Hayashi. Regulation by heme of synthesis and intracellular translocation of δ-aminolevulinate synthase in the liver. *Mol Cell Biochem*, 37(1):27–41, 1981.

[74] S. I. Woodard and H. A. Dailey. Regulation of heme biosynthesis in *Escherichia coli*. *Arch Biochem Biophys*, 316(1):110–5, 1995.

[75] S. Granick, P. Sinclair, S. Sassa, and G. Grieninger. Effects by heme, insulin, and serum albumin on heme and protein synthesis in chick embryo liver cells cultured in a chemically defined medium, and a spectrofluorometric assay for porphyrin composition. *J Biol Chem*, 250(24):9215–25, 1975.

[76] L. Eriksen. So-called free erythrocyte protoporphyrin and its possible role in hemoglobin formation. *Acta Physiol Scand*, 53:288–99.

[77] R. B. van Huystee. Relationship of the heme moiety of peroxidase and the free heme pool in cultured peanut cells. *Zeitschrift für Pflanzenphysiologie*, 84(5):427–433, 1977.

[78] A. Tangeras and T. Flatmark. In vitro binding of protoheme IX and protoporphyrin IX to components in the matrix of rat liver mitochondria. *Biochim Biophys Acta*, 588(2):201–10, 1979.

[79] S. Granick and S. I. Beale. Hemes, chlorophylls, and related compounds: biosynthesis and metabolic regulation. *Adv Enzymol Relat Areas Mol Biol*, 46:33–203, 1978.

[80] H. L. Bonkowsky, P. R. Sinclair, and J. F. Sinclair. Hepatic heme metabolism and its control. *The Yale journal of biology and medicine*, 52(1):13–37, 1979.

[81] J. Thomas and J. D. Weinstein. Measurement of heme efflux and heme content in isolated developing chloroplasts. *Plant Physiol*, 94(3):1414–23, 1990.

[82] C. Celier and T. Cresteil. Control of cytochromes P450 expression in Gunn rat liver: implication of the intracellular heme pool. *Arch Biochem Biophys*, 290(2):407–10, 1991.

[83] H. Atamna. Heme, iron, and the mitochondrial decay of ageing. *Ageing Res Rev*, 3(3):303–18, 2004.

[84] S. Kumar and U. Bandyopadhyay. Free heme toxicity and its detoxification systems in human. *Toxicol Lett*, 157(3):175–88, 2005.

[85] M. A. Correia, P. R. Sinclair, and F. De Matteis. Cytochrome P450 regulation: the interplay between its heme and apoprotein moieties in synthesis, assembly, repair, and disposal. *Drug Metab Rev*, 43(1):1–26, 2011.

[86] A. A. Khan and J. G. Quigley. Control of intracellular heme levels: heme transporters and heme oxygenases. *Biochim Biophys Acta*, 1813(5):668–82, 2011.

[87] D. Garcia-Santos, M. Schranzhofer, M. Horvathova, M. M. Jaberi, J. A. Bogo Chies, A. D. Sheftel, and P. Ponka. Heme oxygenase 1 is expressed in murine erythroid cells where it controls the level of regulatory heme. *Blood*, 123(14):2269–77, 2014.

[88] D. Chiabrando, F. Vinchi, V. Fiorito, S. Mercurio, and E. Tolosano. Heme in pathophysiology: a matter of scavenging, metabolism and trafficking across cell membranes. *Front Pharmacol*, 5:61, 2014.

[89] H. Atamna, M. Brahmbhatt, W. Atamna, G. A. Shanower, and J. M. Dhahbi. ApoHRP-based assay to measure intracellular regulatory heme. *Metallomics*, 7(2):309–321, 2015.

[90] P. Ponka, A. D. Sheftel, A. M. English, D. Scott Bohle, and D. Garcia-Santos. Do mammalian cells really need to export and import heme? *Trends Biochem Sci*, 42(5):395–406, 2017.

[91] L. G. Israels, B. Yoda, and B. A. Schacter. Heme binding and its possible significance in heme movement and availability in the cell. *Ann N Y Acad Sci*, 244(0077-8923):651–61, 1975.

[92] Prem Ponka. Tissue-specific regulation of iron metabolism and heme synthesis: Distinct control mechanisms in erythroid cells. *Blood*, 89(1):1–25, 1997.

[93] S. W. Ryter and R. M. Tyrrell. The heme synthesis and degradation pathways: role in oxidant sensitivity. Heme oxygenase has both pro- and antioxidant properties. *Free Radic Biol Med*, 28(2):289–309, 2000.

[94] E. R. H. Walter, Y. Ge, J. C. Mason, J. J. Boyle, and N. J. Long. A coumarin-porphyrin FRET break-apart probe for heme oxygenase-1. *J Am Chem Soc*, 143(17):6460–6469, 2021.

[95] S. Sassa. Why heme needs to be degraded to iron, biliverdin IXα, and carbon monoxide? *Antioxid Redox Signal*, 6(5):819–24, 2004.

[96] M. Sachar, K. E. Anderson, and X. Ma. Protoporphyrin IX: the good, the bad, and the ugly. *J Pharmacol Exp Ther*, 356(2):267–75, 2016.

[97] O. T. Gbotosho, M. G. Kapetanaki, and G. J. Kato. The worst things in life are free: The role of free heme in sickle cell disease. *Front Immunol*, 11:561917, 2021.

[98] A. R. Reddi and I. Hamza. Heme mobilization in animals: A metallolipid's journey. *Acc Chem Res*, 49(6):1104–10, 2016.

[99] N. Shioda, Y. Yabuki, K. Yamaguchi, M. Onozato, Y. Li, K. Kurosawa, H. Tanabe, N. Okamoto, T. Era, H. Sugiyama, T. Wada, and K. Fukunaga. Targeting G-quadruplex DNA as cognitive function therapy for ATR-X syndrome. *Nat Med*, 24(6):802–813, 2018.

[100] D. Kuter, V. Streltsov, N. Davydova, G. A. Venter, K. J. Naidoo, and T. J. Egan. Molecular structures and solvation of free monomeric and dimeric ferriheme in aqueous solution: insights from molecular dynamics simulations and extended X-ray absorption fine structure spectroscopy. *Inorg Chem*, 53(20):10811–24, 2014.

[101] K. A. de Villiers, C. H. Kaschula, T. J. Egan, and H. M. Marques. Speciation and structure of ferriprotoporphyrin IX in aqueous solution: spectroscopic and diffusion measurements demonstrate dimerization, but not μ-oxo dimer formation. *JBIC Journal of Biological Inorganic Chemistry*, 12(1):101–117, 2007.

[102] M. P. Soares and M. T. Bozza. Red alert: labile heme is an alarmin. *Curr Opin Immunol*, 38:94–100, 2016.

[103] D. A. Hanna, O. Martinez-Guzman, and A. R. Reddi. Heme gazing: Illuminating eukaryotic heme trafficking, dynamics, and signaling with fluorescent heme sensors. *Biochemistry*, 56(13):1815–1823, 2017.

[104] R. K. Donegan, C. M. Moore, D. A. Hanna, and A. R. Reddi. Handling heme: The mechanisms underlying the movement of heme within and between cells. *Free Radic Biol Med*, 133:88–100, 2019.

[105] D. A. Hanna, R. Hu, H. Kim, O. Martinez-Guzman, M. P. Torres, and A. R. Reddi. Heme bioavailability and signaling in response to stress in yeast cells. *J Biol Chem*, 293(32):12378–12393, 2018.

[106] E. A. Sweeny, A. B. Singh, R. Chakravarti, O. Martinez-Guzman, A. Saini, M. M. Haque, G. Garee, P. D. Dans, L. Hannibal, A. R. Reddi, and D. J. Stuehr. Glyceraldehyde-3-phosphate dehydrogenase is a chaperone that allocates labile heme in cells. *J Biol Chem*, 293(37):14557–14568, 2018.

[107] Y. Dai, E. A. Sweeny, S. Schlanger, A. Ghosh, and D. J. Stuehr. GAPDH delivers heme to soluble guanylyl cyclase. *J Biol Chem*, 295(24):P8145–8154, 2020.

[108] A. S. Fleischhacker and S. W. Ragsdale. An unlikely heme chaperone confirmed at last. *J Biol Chem*, 293(37):14569–14570, 2018.

[109] L. Wang, V. Vijayan, M. S. Jang, A. Thorenz, R. Greite, S. Rong, R. Chen, N. Shushakova, I. Tudorache, K. Derlin, P. Pradhan, K. Madyaningrana, N. Madrahimov, J. H. Brasen, R. Lichtinghagen, C. van Kooten, M. Huber-Lang, H. Haller, S. Immenschuh, and F. Gueler. Labile heme aggravates renal inflammation and complement activation after ischemia reperfusion injury. *Front Immunol*, 10:2975, 2019.

[110] S. Xu, H. W. Liu, L. Chen, J. Yuan, Y. Liu, L. Teng, S. Y. Huan, L. Yuan, X. B. Zhang, and W. Tan. Learning from artemisinin: Bioinspired design of a reaction-based fluorescent probe for the selective sensing of labile heme in complex biosystems. *J Am Chem Soc*, 142(5):2129–2133, 2020.

[111] A. S. Fleischhacker, A. L. Gunawan, B. A. Kochert, L. Liu, T. E. Wales, M. C. Borowy, J. R. Engen, and S. W. Ragsdale. The heme regulatory motifs of heme oxygenase-2 contribute to the transfer of heme to the catalytic site for degradation. *J Biol Chem*, 295(16):5177–5191, 2020.

[112] S. Dastpeyman, R. Godin, G. Cosa, and A. M. English. Quantifying heme-protein maturation from ratiometric fluorescence lifetime measurements on the single fluorophore in its gfp fusion. *J Phys Chem A*, 124(4):746–754, 2020.

[113] R. O'Keeffe, G. O. Latunde-Dada, Y. L. Chen, X. L. Kong, A. Cilibrizzi, and R. C. Hider. Glutathione and the intracellular labile heme pool. *Biometals*, 2020.

[114] G. R. Greenberg and M. M. Wintrobe. A labile iron pool. *J Biol Chem*, 165(1):397, 1946.

[115] I. Chorkendorff and J. W. Niemantsverdriet. *Concepts of modern catalysis and kinetics*. Wiley-VCH, Weinheim, 2003.

[116] R. G. Wilkins. *Kinetics and mechanism of reactions of transition metal complexes*. VCH Publishers, Weinheim; New York, 1991.

[117] C. H. Langford and H. B. Gray. *Ligand substitution processes*. W.A. Benjamin, New York, 1966.

[118] A. E. Gallio, S. S. P. Fung, A. Cammack-Najera, A. J. Hudson, and E. L. Raven. Understanding the logistics for the distribution of heme in cells. *JACS Au*, 1(10):1541–1555, 2021.

[119] K. A. de Villiers and T. J. Egan. Heme detoxification in the malaria parasite: A target for antimalarial drug development. *Acc Chem Res*, 54(11):2649–2659, 2021.

[120] H. A. Dailey, T. A. Dailey, S. Gerdes, D. Jahn, M. Jahn, M. R. O'Brian, and M. J. Warren. Prokaryotic heme biosynthesis: Multiple pathways to a common essential product. *Microbiol Mol Biol Rev*, 81(1), 2017.

[121] Z. Qi and M. R. O'Brian. Interaction between the bacterial iron response regulator and ferrochelatase mediates genetic control of heme biosynthesis. *Molecular Cell*, 9(1):155–162, 2002.

[122] I. U. Heinemann, M. Jahn, and D. Jahn. The biochemistry of heme biosynthesis. *Arch Biochem Biophys*, 474(2):238–51, 2008.

[123] M. Unno, T. Matsui, and M. Ikeda-Saito. Structure and catalytic mechanism of heme oxygenase. *Nat Prod Rep*, 24(3):553–70, 2007.

[124] G. R. Morrison. Fluorometric microdetermination of heme protein. *Anal Chem*, 37:1124–6, 1965.

[125] T. Masuda and S. Takahashi. Chemiluminescent-based method for heme determination by reconstitution with horseradish peroxidase apo-enzyme. *Anal Biochem*, 355(2):307–9, 2006.

[126] M. T. Hopp, B. F. Schmalohr, T. Kuhl, M. S. Detzel, A. Wissbrock, and D. Imhof. Heme determination and quantification methods and their suitability for practical applications and everyday use. *Anal Chem*, 92(14):9429–9440, 2020.

[127] S. Takeda, N. Kamiya, and T. Nagamune. A novel protein-based heme sensor consisting of green fluorescent protein and apocytochrome $b_5$62. *Anal Biochem*, 317(1):116–119, 2003.

[128] J. A. Arpino, H. Czapinska, A. Piasecka, W. R. Edwards, P. Barker, M. J. Gajda, M. Bochtler, and D. D. Jones. Structural basis for efficient chromophore communication and energy transfer in a constructed didomain protein scaffold. *J Am Chem Soc*, 134(33):13632–40.

[129] X. Yuan, N. Rietzschel, H. Kwon, A. B. Walter Nuno, D. A. Hanna, J. D. Phillips, E. L. Raven, A. R. Reddi, and I. Hamza. Regulation of intracellular heme trafficking revealed by subcellular reporters. *Proc Natl Acad Sci U S A*, 113(35):E5144–52, 2016.

[130] S. Koga, S. Yoshihara, H. Bando, K. Yamasaki, Y. Higashimoto, M. Noguchi, S. Sueda, H. Komatsu, and H. Sakamoto. Development of a heme sensor using fluorescently labeled heme oxygenase-1. *Anal Biochem*, 433(1):2–9, 2013.

[131] J. Taira, Y. Nakashima, S. Yoshihara, S. Koga, S. Sueda, H. Komatsu, Y. Higashimoto, T. Takahashi, N. Tanioka, H. Shimizu, H. Morimatsu, and H. Sakamoto. Improvement of heme oxygenase-1-based heme sensor for quantifying free heme in biological samples. *Anal Biochem*, 489:50–2, 2015.

[132] O. Martinez-Guzman, M. M. Willoughby, A. Saini, J. V. Dietz, I. Bohovych, A. E. Medlock, O. Khalimonchuk, and A. R. Reddi. Mitochondrial-nuclear heme trafficking in budding yeast is regulated by GTPases that control mitochondrial dynamics and ER contact sites. *J Cell Sci*, 133(10):jcs237917, 2020.

[133] I. G. Chambers, M. M. Willoughby, I. Hamza, and A. R. Reddi. One ring to bring them all and in the darkness bind them: The trafficking of heme without deliverers. *Biochim Biophys Acta Mol Cell Res*, 1868(1):118881, 2021.

[134] Y. Hisamatsu, N. Umezawa, H. Yagi, K. Kato, and T. Higuchi. Design and synthesis of a 4-aminoquinoline-based molecular tweezer that recognizes protoporphyrin IX and iron(III) protoporphyrin IX and its application as a supramolecular photosensitizer. *Chem Sci*, 9(38):7455–7467, 2018.

[135] L. D. Newton, S. I. Pascu, R. M. Tyrrell, and I. M. Eggleston. Development of a peptide-based fluorescent probe for biological heme monitoring. *Org Biomol Chem*, 17(3):467–471, 2019.

[136] J. R. Lakowicz. *Principles of fluorescence spectroscopy*. Springer, New York, 2006.

[137] A. Periasamy and R. M. Clegg. *FLIM Microscopy in Biology and Medicine*. Chapman and Hall/CRC, 2009.

[138] D. M. Jameson and J. A. Ross. Fluorescence polarization/anisotropy in diagnostics and imaging. *Chem Rev*, 110(5):2685–708, 2010.

[139] G. Weber. Polarization of the fluorescence of macromolecules. 1. Theory and experimental method. *Biochem J*, 51(2):145–55, 1952.

[140] K. Kwapiszewska, K. Szczepanski, T. Kalwarczyk, B. Michalska, P. Patalas-Krawczyk, J. Szymanski, T. Andryszewski, M. Iwan, J. Duszynski, and R. Holyst. Nanoscale viscosity of cytoplasm is conserved in human cell lines. *J Phys Chem Lett*, 11(16):6914–6920, 2020.

[141] K. Wang, X. H. Sun, Y. Zhang, T. Zhang, Y. Zheng, Y. C. Wei, P. Zhao, D. Y. Chen, H. A. Wu, W. H. Wang, R. Long, J. B. Wang, and J. Chen. Characterization of cytoplasmic viscosity of hundreds of single tumour cells based on micropipette aspiration. *R Soc Open Sci*, 6(3):181707, 2019.

[142] T. Liu, X. Liu, D. R. Spring, X. Qian, J. Cui, and Z. Xu. Quantitatively mapping cellular viscosity with detailed organelle information via a designed pet fluorescent probe. *Sci Rep*, 4:5418, 2014.

[143] K. H. Sharp, M. Mewies, P. C. Moody, and E. L. Raven. Crystal structure of the ascorbate peroxidase-ascorbate complex. *Nat Struct Biol*, 10(4):303–7, 2003.

[144] J. A. Arpino, P. J. Rizkallah, and D. D. Jones. Crystal structure of enhanced green fluorescent protein to 1.35 Å resolution reveals alternative conformations for Glu222. *PLoS One*, 7(10):e47132, 2012.

[145] D. P. Barondeau, C. D. Putnam, C. J. Kassmann, J. A. Tainer, and E. D. Getzoff. Mechanism and energetics of green fluorescent protein chromophore synthesis revealed by trapped intermediate structures. *Proc Natl Acad Sci U S A*, 100(21):12111–6, 2003.

[146] E. Raven and B. Dunford. *Heme peroxidases*. Royal Society of Chemistry, Cambridge, 2016.

[147] C. M. Casadei, A. Gumiero, C. L. Metcalfe, E. J. Murphy, J. Basran, M. G. Concilio, S. C. Teixeira, T. E. Schrader, A. J. Fielding, A. Ostermann, M. P. Blakeley, E. L. Raven, and P. C. Moody. Heme enzymes. neutron cryo-crystallography captures the protonation state of ferryl heme in a peroxidase. *Science*, 345(6193):193–7, 2014.

[148] V. Hung, P. Zou, H. W. Rhee, N. D. Udeshi, V. Cracan, T. Svinkina, S. A. Carr, V. K. Mootha, and A. Y. Ting. Proteomic mapping of the human mitochondrial intermembrane space in live cells via ratiometric APEX tagging. *Mol Cell*, 55(2):332–41, 2014.

[149] G. C. Leung, S. S. Fung, N. R. B. Dovey, E. L. Raven, and A. J. Hudson. Precise determination of heme binding affinity in proteins. *Anal Biochem*, 572:45–51, 2019.

[150] O. Shimomura, F. H. Johnson, and Y. Saiga. Extraction, purification and properties of aequorin, a bioluminescent protein from the luminous hydromedusan, *Aequorea*. *J Cell Comp Physiol*, 59:223–39, 1962.

[151] M. Chalfie and S. Kain. *Green fluorescent protein: properties, applications, and protocols*. Wiley-Interscience, Hoboken, N.J., 2006.

[152] R. Y. Tsien. The green fluorescent protein. *Annu Rev Biochem*, 67:509–44, 1998.

[153] A. E. Palmer, Y. Qin, J. G. Park, and J. E. McCombs. Design and application of genetically encoded biosensors. *Trends Biotechnol*, 29(3):144–52, 2011.

[154] B. P. Cormack, R. H. Valdivia, and S. Falkow. FACS-optimized mutants of the green fluorescent protein (GFP). *Gene*, 173(1):33–38, 1996.

[155] J. D. Martell, T. J. Deerinck, Y. Sancak, T. L. Poulos, V. K. Mootha, G. E. Sosinsky, M. H. Ellisman, and A. Y. Ting. Engineered ascorbate peroxidase as a genetically encoded reporter for electron microscopy. *Nat Biotechnol*, 30(11):1143–8, 2012.

[156] D. A. Zacharias, J. D. Violin, A. C. Newton, and R. Y. Tsien. Partitioning of lipid-modified monomeric GFPs into membrane microdomains of live cells. *Science*, 296(5569):913–6.

[157] G. H. Patterson, S. M. Knobel, W. D. Sharif, S. R. Kain, and D. W. Piston. Use of the green fluorescent protein and its mutants in quantitative fluorescence microscopy. *Biophys J*, 73(5):2782–90.

[158] D. C. Prasher, V. K. Eckenrode, W. W. Ward, F. G. Prendergast, and M. J. Cormier. Primary structure of the aequorea victoria green-fluorescent protein. *Gene*, 111(2):229–33.

[159] C. W. Cody, D. C. Prasher, W. M. Westler, F. G. Prendergast, and W. W. Ward. Chemical structure of the hexapeptide chromophore of the aequorea green-fluorescent protein. *Biochemistry*, 32(5):1212–8.

[160] Jr. Phillips, G. N. Structure and dynamics of green fluorescent protein. *Curr Opin Struct Biol*, 7(6):821–7.

[161] K. S. Sarkisyan, A. S. Goryashchenko, P. V. Lidsky, D. A. Gorbachev, N. G. Bozhanova, A. Y. Gorokhovatsky, A. R. Pereverzeva, A. P. Ryumina, V. V. Zherdeva, A. P. Savitsky, K. M. Solntsev, A. S. Bommarius, G. V. Sharonov, J. R. Lindquist, M. Drobizhev, T. E. Hughes, A. Rebane, K. A. Lukyanov, and A. S. Mishin. Green fluorescent protein with anionic tryptophan-based chromophore and long fluorescence lifetime. *Biophys J*, 109(2):380–9.

[162] R. Heim, A. B. Cubitt, and R. Y. Tsien. Improved green fluorescence. *Nature*, 373(6516):663–4.

[163] R. Heim and R. Y. Tsien. Engineering green fluorescent protein for improved brightness, longer wavelengths and fluorescence resonance energy transfer. *Curr Biol*, 6(2):178–82.

[164] D. P. Myatt, L. Hatter, S. E. Rogers, A. E. Terry, and L. A. Clifton. Monomeric green fluorescent protein as a protein standard for small angle scattering. *Biomedical Spectroscopy and Imaging*, 6(3-4):123–134, 2017.

[165] P. S. Ebert, R. A. Hess, B. C. Frykholm, and D. P. Tschudy. Succinylacetone, a potent inhibitor of heme biosynthesis: Effect on cell growth, heme content and δ-aminolevulinic acid dehydratase activity of malignant murine erythroleukemia cells. *Biochemical and Biophysical Research Communications*, 88(4):1382–1390, 1979.

[166] K. Suhling, J. Siegel, D. Phillips, P. M. W. French, S. Lévêque-Fort, S. E. D. Webb, and D. M. Davis. Imaging the environment of green fluorescent protein. *Biophysical Journal*, 83(6):3589–3595, 2002.

[167] M. Cotlet, J. Hofkens, M. Maus, T. Gensch, M. Van der Auweraer, J. Michiels, G. Dirix, M. Van Guyse, J. Vanderleyden, A. J. W. G. Visser, and F. C. De Schryver. Excited-state dynamics in the enhanced green fluorescent protein mutant probed by picosecond time-resolved single photon counting spectroscopy. *The Journal of Physical Chemistry B*, 105(21):4999–5006, 2001.

[168] M. T. Nelp, P. A. Kates, J. T. Hunt, J. A. Newitt, A. Balog, D. Maley, X. Zhu, L. Abell, A. Allentoff, R. Borzilleri, H. A. Lewis, Z. Lin, S. P. Seitz, C. Yan, and J. T. Groves. Immune-modulating enzyme indoleamine 2,3-dioxygenase is effectively inhibited by targeting its apo-form. *Proc Natl Acad Sci U S A*, 115(13):3249–3254, 2018.

[169] F. Petrat, H. de Groot, R. Sustmann, and U. Rauen. The chelatable iron pool in living cells: a methodically defined quantity. *Biol Chem*, 383(3-4):489–502, 2002.

[170] A. Egyed and P. Saltman. Iron is maintained as Fe(II) under aerobic conditions in erythroid cells. *Biol Trace Elem Res*, 6(4):357–64, 1984.

[171] R. J. P. Williams. Free manganese(II) and iron(II) cations can act as intracellular cell controls. *FEBS Letters*, 140(1):3–10, 1982.

[172] D. A. Hanna, C. M. Moore, L. Liu, X. Yuan, I. M. Dominic, A. S. Fleischhacker, I. Hamza, S. W. Ragsdale, and A. R. Reddi. Heme oxygenase-2 (HO-2) binds and buffers labile ferric heme in human embryonic kidney cells. *J Biol Chem*, 298(2):101549, 2022.

[173] M. J. Warren and A. I. Scott. Tetrapyrrole assembly and modification into the ligands of biologically functional cofactors. *Trends Biochem Sci*, 15(12):486–91, 1990.

[174] Junli Zhang, Zhen Kang, Jian Chen, and Guocheng Du. Optimization of the heme biosynthesis pathway for the production of 5-aminolevulinic acid in *Escherichia coli*. *Scientific Reports*, 5(1):8584, 2015.

[175] D. J. Stuehr, Y. Dai, P. Biswas, E. A. Sweeny, and A. Ghosh. New roles for GAPDH, Hsp90, and NO in regulating heme allocation and hemeprotein function in mammals. *Biol Chem*, 2022.

[176] A. Colell, D. R. Green, and J. E. Ricci. Novel roles for GAPDH in cell death and carcinogenesis. *Cell Death Differ*, 16(12):1573–81, 2009.

[177] C. Tristan, N. Shahani, T. W. Sedlak, and A. Sawa. The diverse functions of GAPDH: views from different subcellular compartments. *Cell Signal*, 23(2):317–23, 2010.

[178] K. C. Chinta, H. T. Pacl, A. Agarwal, and A. J. C. Steyn. Heme oxygenase-1 as a pharmacological target for host-directed therapy to limit tuberculosis associated immunopathology. *Antioxidants (Basel)*, 10(2), 2021.

[179] R. C. M. Costa Silva and L. H. T. Correa. Heme oxygenase 1 in vertebrates: Friend and foe. *Cell Biochem Biophys*, 2021.

[180] M. D. Maines. Heme oxygenase: function, multiplicity, regulatory mechanisms, and clinical applications. *FASEB J*, 2(10):2557–68, 1988.

[181] M. D. Maines. The heme oxygenase system: a regulator of second messenger gases. *Annu Rev Pharmacol Toxicol*, 37:517–54, 1997.

[182] A. S. Fleischhacker, A. Sarkar, L. Liu, and S. W. Ragsdale. Regulation of protein function and degradation by heme, heme responsive motifs, and CO. *Crit Rev Biochem Mol Biol*, pages 1–32, 2021.

[183] D. A. Bryant, C. N. Hunter, and M. J. Warren. Biosynthesis of the modified tetrapyrroles-the pigments of life. *J Biol Chem*, 295(20):6888–6925, 2020.

[184] S. Kolluri, T. J. Sadlon, B. K. May, and H. L. Bonkovsky. Haem repression of the housekeeping 5-aminolaevulinic acid synthase gene in the hepatoma cell line LMH. *Biochem J*, 392(Pt 1):173–80, 2005.

[185] R. D. Riddle, M. Yamamoto, and J. D. Engel. Expression of delta-aminolevulinate synthase in avian cells: separate genes encode erythroid-specific and nonspecific isozymes. *Proc Natl Acad Sci U S A*, 86(3):792–6, 1989.

[186] B. K. May, S. C. Dogra, T. J. Sadlon, C. R. Bhasker, T. C. Cox, and S. S. Bottomley. Molecular regulation of heme biosynthesis in higher vertebrates. *Prog Nucleic Acid Res Mol Biol*, 51:1–51, 1995.

[187] J. T. Lathrop and M. P. Timko. Regulation by heme of mitochondrial protein transport through a conserved amino acid motif. *Science*, 259(5094):522–5, 1993.

[188] K. Nomura, Y. Kitagawa, M. Aihara, Y. Ohki, K. Furuyama, and T. Hirokawa. Heme-dependent recognition of 5-aminolevulinate synthase by the human mitochondrial molecular chaperone ClpX. *FEBS Lett*, 2021.

[189] S. J. Wolfson, A. Bartczak, and J. R. Bloomer. Effect of endogenous heme generation on delta-aminolevulinic acid synthase activity in rat liver mitochondria. *Journal of Biological Chemistry*, 254(9):3543–3546, 1979.

[190] M. A. Sirover. New insights into an old protein: the functional diversity of mammalian glyceraldehyde-3-phosphate dehydrogenase. *Biochim Biophys Acta*, 1432(2):159–84, 1999.

[191] M. A. Sirover. The role of posttranslational modification in moonlighting glyceraldehyde-3-phosphate dehydrogenase structure and function. *Amino Acids*, 53(4):507–515, 2021.

[192] C. M. Mulvey, L. M. Breckels, O. M. Crook, D. J. Sanders, A. L. R. Ribeiro, A. Geladaki, A. Christoforou, N. K. Britovsek, T. Hurrell, M. J. Deery, L. Gatto, A. M. Smith, and K. S. Lilley. Spatiotemporal proteomic profiling of the pro-inflammatory response to lipopolysaccharide in the THP-1 human leukaemia cell line. *Nat Commun*, 12(1):5773, 2021.

[193] Q. A. Albakri and D. J. Stuehr. Intracellular assembly of inducible NO synthase is limited by nitric oxide-mediated changes in heme insertion and availability. *J Biol Chem*, 271(10):5414–21, 1996.

[194] L. Hannibal, D. Collins, J. Brassard, R. Chakravarti, R. Vempati, P. Dorlet, J. Santolini, J. H. Dawson, and D. J. Stuehr. Heme binding properties of glyceraldehyde-3-phosphate dehydrogenase. *Biochemistry*, 51(43):8514–29, 2012.

[195] S. M. Waheed, A. Ghosh, R. Chakravarti, A. Biswas, M. M. Haque, K. Panda, and D. J. Stuehr. Nitric oxide blocks cellular heme insertion into a broad range of heme proteins. *Free Radic Biol Med*, 48(11):1548–58, 2010.

[196] P. Biswas, Y. Dai, and D. J. Stuehr. Indoleamine dioxygenase and tryptophan dioxygenase activities are regulated through GAPDH- and Hsp90-dependent control of their heme levels. *Free Radic Biol Med*, 180:179–190, 2022.

[197] P. Biswas and D. J. Stuehr. Indoleamine dioxygenase and tryptophan dioxygenase activities are regulated through control of cell heme allocation by nitric oxide. *J Biol Chem*, 299(6):104753, 2023.

[198] B. Tupta, E. Stuehr, M. P. Sumi, E. A. Sweeny, B. Smith, D. J. Stuehr, and A. Ghosh. GAPDH is involved in the heme-maturation of myoglobin and hemoglobin. *FASEB J*, 36(2):e22099, 2022.

[199] Y. Dai, A. S. Fleischhacker, L. Liu, S. Fayad, A. L. Gunawan, D. J. Stuehr, and S. W. Ragsdale. Heme delivery to heme oxygenase-2 involves glyceraldehyde-3-phosphate dehydrogenase. *Biol Chem*, 403(11-12):1043–1053, 2022.

[200] C. M. Bianchetti, L. Yi, S. W. Ragsdale, and Jr. Phillips, G. N. Comparison of apo- and heme-bound crystal structures of a truncated human heme oxygenase-2. *J Biol Chem*, 282(52):37624–31, 2007.

[201] L. Lad, D. J. Schuller, H. Shimizu, J. Friedman, H. Li, P. R. Ortiz de Montellano, and T. L. Poulos. Comparison of the heme-free and -bound crystal structures of human heme oxygenase-1. *J Biol Chem*, 278(10):7834–43, 2002.

[202] B. A. Kochert, A. S. Fleischhacker, T. E. Wales, D. F. Becker, J. R. Engen, and S. W. Ragsdale. Dynamic and structural differences between heme oxygenase-1 and-2 are due to differences in their C-terminal regions. *Journal of Biological Chemistry*, 294(20):8259–8272, 2019.

[203] M. F. Rubio, P. V. Agostino, G. A. Ferreyra, and D. A. Golombek. Circadian heme oxygenase activity in the hamster suprachiasmatic nuclei. *Neurosci Lett*, 353(1):9–12, 2003.

[204] Krista Kaasik and Cheng Chi Lee. Reciprocal regulation of haem biosynthesis and the circadian clock in mammals. *Nature*, 430(6998):467–471, 2004.

[205] L. Liu, A. B. Dumbrepatil, A. S. Fleischhacker, E. N. G. Marsh, and S. W. Ragsdale. Heme oxygenase-2 is post-translationally regulated by heme occupancy in the catalytic site. *J Biol Chem*, 295(50):17227–17240, 2020.

[206] F. Sun, Z. Zhao, M. M. Willoughby, S. Shen, Y. Zhou, Y. Shao, J. Kang, Y. Chen, M. Chen, X. Yuan, I. Hamza, A. R. Reddi, and C. Chen. HRG-9 homologues regulate haem trafficking from haem-enriched compartments. *Nature*, 610(7933):768–774, 2022.

[207] P. Podkalicka, O. Mucha, A. Jozkowicz, J. Dulak, and A. Loboda. Heme oxygenase inhibition in cancers: possible tools and targets. *Contemp Oncol (Pozn)*, 22(1A):23–32, 2018.

[208] J. J. Leonard, T. Yonetani, and J. B. Callis. A fluorescence study of hybrid hemoglobins containing free base and zinc protoporphyrin IX. *Biochemistry*, 13(7):1460–4, 1974.

[209] *RNA interference: from biology to clinical applications*, volume Volume 30. Humana Press, 2010.

[210] S. E. Williams, P. Wootton, H. S. Mason, J. Bould, D. E. Iles, D. Riccardi, C. Peers, and P. J. Kemp. Hemoxygenase-2 is an oxygen sensor for a calcium-sensitive potassium channel. *Science*, 306(5704):2093–7, 2004.

[211] A. Wissbrock, A. A. Paul George, H. H. Brewitz, T. Kuhl, and D. Imhof. The molecular basis of transient heme-protein interactions: analysis, concept and implementation. *Biosci Rep*, 39(1), 2019.

[212] A. Grant Mauk and G. R. Moore. Control of metalloprotein redox potentials: what does site-directed mutagenesis of hemoproteins tell us? *JBIC Journal of Biological Inorganic Chemistry*, 2(1):119–125, 1997.

[213] A. S. Fleischhacker, A. Sharma, M. Choi, A. M. Spencer, I. Bagai, B. M. Hoffman, and S. W. Ragsdale. The C-terminal heme regulatory motifs of heme oxygenase-2 are redox-regulated heme binding sites. *Biochemistry*, 54(17):2709–18, 2015.

[214] A. S. Fleischhacker, A. Sarkar, L. Liu, and S. W. Ragsdale. Regulation of protein function and degradation by heme, heme responsive motifs, and co. *Critical Reviews in Biochemistry and Molecular Biology*, 57(1):16–47, 2022.

[215] V. C. Tsolaki, S. K. Georgiou-Siafis, A. I. Tsamadou, S. A. Tsiftsoglou, M. Samiotaki, G. Panayotou, and A. S. Tsiftsoglou. Hemin accumulation and identification of a heme-binding protein clan in K562 cells by proteomic and computational analysis. *J Cell Physiol*, 2021.

[216] P. Lukacik, C. D. Owen, G. Harris, J. R. Bolla, S. Picaud, I. Alibay, J. E. Nettleship, L. E. Bird, R. J. Owens, P. C. Biggin, P. Filippakopoulos, C. V. Robinson, and M. A. Walsh. The structure of nontypeable *Haemophilus influenzae* SapA in a closed conformation reveals a constricted ligand-binding cavity and a novel RNA binding motif. *PLoS One*, 16(10):e0256070, 2021.

[217] S. Che, Y. Liang, Y. Chen, W. Wu, R. Liu, Q. Zhang, and M. Bartlam. Structure of *Pseudomonas aeruginosa* spermidine dehydrogenase: a polyamine oxidase with a novel heme-binding fold. *FEBS J*, 2021.

[218] K. W. Min, S. H. Lee, and S. J. Baek. Moonlighting proteins in cancer. *Cancer Lett*, 370(1):108–16, 2016.

[219] R. Liu and J. Hu. Hemebind: a novel method for heme binding residue prediction by combining structural and sequence information. *BMC Bioinformatics*, 12:207, 2011.

[220] Y. Xiong, J. Liu, W. Zhang, and T. Zeng. Prediction of heme binding residues from protein sequences with integrative sequence profiles. *Proteome Sci*, 10 Suppl 1:S20, 2012.

[221] D. J. Yu, J. Hu, J. Yang, H. B. Shen, J. Tang, and J. Y. Yang. Designing template-free predictor for targeting protein-ligand binding sites with classifier ensemble and spatial clustering. *IEEE/ACM Trans Comput Biol Bioinform*, 10(4):994–1008, 2013.

[222] J. Zhang, H. Chai, B. Gao, G. Yang, and Z. Ma. HEMEsPred: Structure-based ligand-specific heme binding residues prediction by using fast-adaptive ensemble learning scheme. *IEEE/ACM Trans Comput Biol Bioinform*, 15(1):147–156, 2016.

[223] A. A. Paul George, M. Lacerda, B. F. Syllwasschy, M. T. Hopp, A. Wissbrock, and D. Imhof. HeMoQuest: a webserver for qualitative prediction of transient heme binding to protein motifs. *BMC Bioinformatics*, 21(1):124, 2020.

[224] X. Chen, W. Lu, M. Y. Tsai, S. Jin, and P. G. Wolynes. Exploring the folding energy landscapes of heme proteins using a hybrid awsem-heme model. *J Biol Phys*, 2022.

[225] R. A. Laskowski, J. D. Watson, and J. M. Thornton. ProFunc: a server for predicting protein function from 3d structure. *Nucleic Acids Res*, 33(2):W89–93, 2005.

[226] J. Jumper, R. Evans, A. Pritzel, T. Green, M. Figurnov, O. Ronneberger, K. Tunyasuvunakool, R. Bates, A. Zidek, A. Potapenko, A. Bridgland, C. Meyer, S. A. A. Kohl, A. J. Ballard, A. Cowie, B. Romera-Paredes, S. Nikolov, R. Jain, J. Adler, T. Back, S. Petersen, D. Reiman, E. Clancy,

M. Zielinski, M. Steinegger, M. Pacholska, T. Berghammer, S. Bodenstein, D. Silver, O. Vinyals, A. W. Senior, K. Kavukcuoglu, P. Kohli, and D. Hassabis. Highly accurate protein structure prediction with AlphaFold. *Nature*, 596(7873):583–589, 2021.

[227] M. Varadi, S. Anyango, M. Deshpande, S. Nair, C. Natassia, G. Yordanova, D. Yuan, O. Stroe, G. Wood, A. Laydon, A. Zidek, T. Green, K. Tunyasuvunakool, S. Petersen, J. Jumper, E. Clancy, R. Green, A. Vora, M. Lutfi, M. Figurnov, A. Cowie, N. Hobbs, P. Kohli, G. Kleywegt, E. Birney, D. Hassabis, and S. Velankar. AlphaFold protein structure database: massively expanding the structural coverage of protein-sequence space with high-accuracy models. *Nucleic Acids Res*, 50(D1):D439–D444, 2022.

[228] A. Perrakis and T. K. Sixma. AI revolutions in biology: The joys and perils of AlphaFold. *EMBO Rep*, 22(11):e54046, 2021.

[229] H. M. Berman, J. Westbrook, Z. Feng, G. Gilliland, T. N. Bhat, H. Weissig, I. N. Shindyalov, and P. E. Bourne. The Protein Data Bank. *Nucleic Acids Res*, 28(1):235–42, 2000.

[230] The UniProt Consortium. UniProt: a worldwide hub of protein knowledge. *Nucleic Acids Res*, 47(D1):D506–D515, 2019.

[231] T. Paysan-Lafosse, M. Blum, S. Chuguransky, T. Grego, B. L. Pinto, G. A. Salazar, M. L. Bileschi, P. Bork, A. Bridge, L. Colwell, J. Gough, D. H. Haft, I. Letunic, A. Marchler-Bauer, H. Mi, D. A. Natale, C. A. Orengo, A. P. Pandurangan, C. Rivoire, C. J. A. Sigrist, I. Sillitoe, N. Thanki, P. D. Thomas, S. C. E. Tosatto, C. H. Wu, and A. Bateman. InterPro in 2022. *Nucleic Acids Res*, 51(D1):D418–D427, 2023.

[232] A. C. Wallace, R. A. Laskowski, and J. M. Thornton. Derivation of 3D coordinate templates for searching structural databases: application to Ser-His-Asp catalytic triads in the serine proteinases and lipases. *Protein Sci*, 5(6):1001–13, 1996.

[233] W. Oosterheert and P. Gros. Cryo-electron microscopy structure and potential enzymatic function of human six-transmembrane epithelial antigen of the prostate 1 (STEAP1). *J Biol Chem*, 295(28):9502–9512, 2020.

[234] Y. Kabe, T. Nakane, I. Koike, T. Yamamoto, Y. Sugiura, E. Harada, K. Sugase, T. Shimamura, M. Ohmura, K. Muraoka, A. Yamamoto, T. Uchida, S. Iwata, Y. Yamaguchi, E. Krayukhina, M. Noda, H. Handa, K. Ishimori, S. Uchiyama, T. Kobayashi, and M. Suematsu. Haem-dependent dimerization of PGRMC1/Sigma-2 receptor facilitates cancer proliferation and chemoresistance. *Nat Commun*, 7:11030, 2016.

[235] K. Igarashi, T. Kurosaki, and R. Roychoudhuri. BACH transcription factors in innate and adaptive immunity. *Nat Rev Immunol*, 17(7):437–450, 2017.

[236] S. Hira, T. Tomita, T. Matsui, K. Igarashi, and M. Ikeda-Saito. Bach1, a heme-dependent transcription factor, reveals presence of multiple heme binding sites with distinct coordination structure. *IUBMB Life*, 59(8-9):542–51, 2007.

[237] J. Shen, X. Sheng, Z. Chang, Q. Wu, D. Xie, F. Wang, and R. Hu. The heme-p53 interaction: Linking iron metabolism to p53 signaling and tumorigenesis. *Mol Cell Oncol*, 3(1):e965642, 2016.

[238] J. Yang, K. D. Kim, A. Lucas, K. E. Drahos, C. S. Santos, S. P. Mury, D. G. Capelluto, and C. V. Finkielstein. A novel heme-regulatory motif mediates heme-dependent degradation of the circadian factor period 2. *Mol Cell Biol*, 28(15):4697–711, 2008.

[239] Y. Nishitani, H. Okutani, Y. Takeda, T. Uchida, K. Iwai, and K. Ishimori. Specific heme binding to heme regulatory motifs in iron regulatory proteins and its functional significance. *J Inorg Biochem*, 198:110726, 2019.

[240] A. T. Smith, S. Pazicni, K. A. Marvin, D. J. Stevens, K. M. Paulsen, and J. N. Burstyn. Functional divergence of heme-thiolate proteins: a classification based on spectroscopic attributes. *Chem Rev*, 115(7):2532–58, 2015.

[241] A. W. Foster, T. R. Young, P. T. Chivers, and N. J. Robinson. Protein metalation in biology. *Curr Opin Chem Biol*, 66:102095, 2021.

[242] D. Osman, M. A. Martini, A. W. Foster, J. Chen, A. J. P. Scott, R. J. Morton, J. W. Steed, E. Lurie-Luke, T. G. Huggins, A. D. Lawrence, E. Deery, M. J. Warren, P. T. Chivers, and N. J. Robinson. Bacterial sensors define intracellular free energies for correct enzyme metalation. *Nat Chem Biol*, 15(3):241–249, 2019.

[243] T. R. Young, M. A. Martini, A. W. Foster, A. Glasfeld, D. Osman, R. J. Morton, E. Deery, M. J. Warren, and N. J. Robinson. Calculating metalation in cells reveals CobW acquires Co(ii) for vitamin B12 biosynthesis while related proteins prefer Zn(II). *Nat Commun*, 12(1):1195, 2021.

[244] I. Hamza and H. A. Dailey. One ring to rule them all: trafficking of heme and heme synthesis intermediates in the metazoans. *Biochim Biophys Acta*, 1823(9):1617–32, 2012.

[245] C. Andreini, I. Bertini, G. Cavallaro, G. L. Holliday, and J. M. Thornton. Metal ions in biological catalysis: from enzyme databases to general principles. *J Biol Inorg Chem*, 13(8):1205–18, 2008.

[246] M. R. Bleackley and R. T. Macgillivray. Transition metal homeostasis: from yeast to human disease. *Biometals*, 24(5):785–809, 2011.

[247] L. A. Finney and T. V. O'Halloran. Transition metal speciation in the cell: insights from the chemistry of metal ion receptors. *Science*, 300(5621):931–6, 2003.

[248] A. W. Foster, D. Osman, and N. J. Robinson. Metal preferences and metallation. *J Biol Chem*, 289(41):28095–103, 2014.

[249] C. E. Outten and A. N. Albetel. Iron sensing and regulation in saccharomyces cerevisiae: Ironing out the mechanistic details. *Curr Opin Microbiol*, 16(6):662–8, 2013.

[250] C. E. Outten and T. V. O'Halloran. Femtomolar sensitivity of metalloregulatory proteins controlling zinc homeostasis. *Science*, 292(5526):2488–92, 2001.

[251] T. D. Rae, P. J. Schmidt, R. A. Pufahl, V. C. Culotta, and T. V. O'Halloran. Undetectable intracellular free copper: the requirement of a copper chaperone for superoxide dismutase. *Science*, 284(5415):805–8, 1999.

[252] L. Banci, I. Bertini, F. Cantini, and S. Ciofi-Baffoni. Cellular copper distribution: a mechanistic systems biology approach. *Cell Mol Life Sci*, 67(15):2563–89, 2010.

[253] D. L. Huffman and T. V. O'Halloran. Function, structure, and mechanism of intracellular copper trafficking proteins. *Annu Rev Biochem*, 70:677–701, 2001.

[254] A. C. Rosenzweig and T. V. O'Halloran. Structure and chemistry of the copper chaperone proteins. *Curr Opin Chem Biol*, 4(2):140–7, 2000.

[255] D. Osman, A. W. Foster, J. Chen, K. Svedaite, J. W. Steed, E. Lurie-Luke, T. G. Huggins, and N. J. Robinson. Fine control of metal concentrations is necessary for cells to discern zinc from cobalt. *Nat Commun*, 8(1):1884, 2017.

[256] S. Tottey, D. R. Harvie, and N. J. Robinson. Understanding how cells allocate metals using metal sensors and metallochaperones. *Acc Chem Res*, 38(10):775–83, 2005.

[257] K. J. Waldron, J. C. Rutherford, D. Ford, and N. J. Robinson. Metalloproteins and metal sensing. *Nature*, 460(7257):823–30, 2009.

[258] L. A. Ba, M. Doering, T. Burkholz, and C. Jacob. Metal trafficking: from maintaining the metal homeostasis to future drug design. *Metallomics*, 1(4):292–311.

[259] Z. Ma, F. E. Jacobsen, and D. P. Giedroc. Coordination chemistry of bacterial metal transport and sensing. *Chem Rev*, 109(10):4644–81, 2009.

[260] G. T. Antelo, A. J. Vila, D. P. Giedroc, and D. A. Capdevila. Molecular evolution of transition metal bioavailability at the host-pathogen interface. *Trends Microbiol*, 29(5):441–457, 2021.

[261] C. A. Blindauer. Bacterial metallothioneins: past, present, and questions for the future. *J Biol Inorg Chem*, 16(7):1011–24.

[262] C. A. Blindauer and O. I. Leszczyszyn. Metallothioneins: unparalleled diversity in structures and functions for metal ion homeostasis and more. *Nat Prod Rep*, 27(5):720–41, 2010.

[263] O. Daltrop, J. M. Stevens, C. W. Higham, and S. J. Ferguson. The CcmE protein of the *c*-type cytochrome biogenesis system: unusual in vitro heme incorporation into apo-CcmE and transfer from holo-CcmE to apocytochrome. *Proc Natl Acad Sci U S A*, 99(15):9703–8, 2002.

[264] L. Thony-Meyer. A heme chaperone for cytochrome *c* biosynthesis. *Biochemistry*, 42(45):13099–105, 2003.

[265] R. G. Kranz, C. Richard-Fogal, J. S. Taylor, and E. R. Frawley. Cytochrome *c* biogenesis: mechanisms for covalent modifications and trafficking of heme and for heme-iron redox control. *Microbiol Mol Biol Rev*, 73(3):510–28, Table of Contents, 2009.

[266] Y. Huang, P. Zhang, Z. Yang, P. Wang, H. Li, and Z. Gao. Interaction of glyceraldehyde-3-phosphate dehydrogenase and heme: The relevance of its biological function. *Arch Biochem Biophys*, 619:54–61, 2017.

[267] A. Rosa, V. E. Pye, C. Graham, L. Muir, J. Seow, K. W. Ng, N. J. Cook, C. Rees-Spear, E. Parker, M. S. Dos Santos, C. Rosadas, A. Susana, H. Rhys, A. Nans, L. Masino, C. Roustan, E. Christodoulou, R. Ulferts, A. G. Wrobel, C. E. Short, M. Fertleman, R. W. Sanders, J. Heaney, M. Spyer, S. Kjaer, A. Riddell, M. H. Malim, R. Beale, J. I. MacRae, G. P. Taylor, E. Nastouli, M. J. van Gils, P. B. Rosenthal, M. Pizzato, M. O. McClure, R. S. Tedder, G. Kassiotis, L. E. McCoy, K. J. Doores, and P. Cherepanov. SARS-CoV-2 can recruit a heme metabolite to evade antibody immunity. *Sci Adv*, 7(22), 2021.

[268] E. L. Raven. A short history of heme dioxygenases: rise, fall and rise again. *J Biol Inorg Chem*, 22(2-3):175–183, 2017.

[269] I. Efimov, J. Basran, S. J. Thackray, S. Handa, C. G. Mowat, and E. L. Raven. Structure and reaction mechanism in the heme dioxygenases. *Biochemistry*, 50(14):2717–24, 2011.

[270] E. S. Millett, I. Efimov, J. Basran, S. Handa, C. G. Mowat, and E. L. Raven. Heme-containing dioxygenases involved in tryptophan oxidation. *Curr Opin Chem Biol*, 16(1-2):60–6, 2012.

[271] A. Lewis-Ballester, K. N. Pham, D. Batabyal, S. Karkashon, J. B. Bonanno, T. L. Poulos, and S. R. Yeh. Structural insights into substrate and inhibitor binding sites in human indoleamine 2,3-dioxygenase 1. *Nat Commun*, 8(1):1693, 2017.

[272] K. K. Srivastava, E. E. Cable, S. E. Donohue, and H. L. Bonkovsky. Molecular basis for heme-dependent induction of heme oxygenase in primary cultures of chick embryo hepatocytes. demonstration of acquired refractoriness to heme. *Eur J Biochem*, 213(3):909–17, 1993.

[273] W. R. Light 3rd and J. S. Olson. The effects of lipid composition on the rate and extent of heme binding to membranes. *J Biol Chem*, 265(26):15632–7, 1990.

[274] W. R. Light 3rd and J. S. Olson. Transmembrane movement of heme. *J Biol Chem*, 265(26):15623–31, 1990.

[275] M. Y. Rose, R. A. Thompson, W. R. Light, and J. S. Olson. Heme transfer between phospholipid-membranes and uptake by apohemoglobin. *J Biol Chem*, 260(11):6632–6640, 1985.

[276] D. Chiabrando, S. Marro, S. Mercurio, C. Giorgi, S. Petrillo, F. Vinchi, V. Fiorito, S. Fagoonee, A. Camporeale, E. Turco, G. R. Merlo, L. Silengo, F. Altruda, P. Pinton, and E. Tolosano. The mitochondrial heme exporter FLVCR1b mediates erythroid differentiation. *J Clin Invest*, 122(12):4569–79, 2012.

[277] L. Tian, N. Martin, P. G. Bassindale, A. J. Patil, M. Li, A. Barnes, B. W. Drinkwater, and S. Mann. Spontaneous assembly of chemically encoded two-dimensional coacervate droplet arrays by acoustic wave patterning. *Nat Commun*, 7:13068, 2016.

[278] M. S. Hargrove, E. W. Singleton, M. L. Quillin, L. A. Ortiz, Jr. Phillips, G. N., J. S. Olson, and A. J. Mathews. His64(E7)–>Tyr apomyoglobin as a reagent for measuring rates of hemin dissociation. *J Biol Chem*, 269(6):4207–14, 1994.

[279] D. S. Culbertson and J. S. Olson. Role of heme in the unfolding and assembly of myoglobin. *Biochemistry*, 49(29):6052–6063, 2010.

[280] J. Enderlein, I. Gregor, D. Patra, T. Dertinger, and U. B. Kaupp. Performance of fluorescence correlation spectroscopy for measuring diffusion and concentration. *Chemphyschem*, 6(11):2324–36, 2005.

[281] S. A. Kim, K. G. Heinze, and P. Schwille. Fluorescence correlation spectroscopy in living cells. *Nat Methods*, 4(11):963–73, 2007.

[282] J. Ries, M. Bayer, G. Csucs, R. Dirkx, M. Solimena, H. Ewers, and P. Schwille. Automated suppression of sample-related artifacts in fluorescence correlation spectroscopy. *Opt Express*, 18(11):11073–82, 2010.

[283] M. Wachsmuth, W. Waldeck, and J. Langowski. Anomalous diffusion of fluorescent probes inside living cell nuclei investigated by spatially-resolved fluorescence correlation spectroscopy. *J Mol Biol*, 298(4):677–89, 2000.

[284] C. B. Müller, A. Loman, V. Pacheco, F. Koberling, D. Willbold, W. Richtering, and J. Enderlein. Precise measurement of diffusion by multi-color dual-focus fluorescence correlation spectroscopy. *EPL (Europhysics Letters)*, 83(4), 2008.

[285] N. L. Hindul, A. Jhita, D. G. Oprea, T. A. Hussain, O. Gonchar, M. A. M. Campillo, L. O'Regan, M. T. Kanemaki, A. M. Fry, K. Hirota, and K. Tanaka. Construction of a human hTERT RPE-1 cell line with inducible Cre for editing of endogenous genes. *Biol Open*, 11(2), 2022.

[286] J. A. Vara, A. Portela, J. Ortin, and A. Jimenez. Expression in mammalian cells of a gene from *Streptomyces alboniger* conferring puromycin resistance. *Nucleic Acids Res*, 14(11):4617–24, 1986.

[287] T. Natsume, T. Kiyomitsu, Y. Saga, and M. T. Kanemaki. Rapid protein depletion in human cells by auxin-inducible degron tagging with short homology donors. *Cell Rep*, 15(1):210–218, 2016.

[288] A. T. Das, L. Tenenbaum, and B. Berkhout. Tet-On systems for doxycycline-inducible gene expression. *Curr Gene Ther*, 16(3):156–67, 2016.

[289] X. Zhou, M. Vink, B. Klaver, B. Berkhout, and A. T. Das. Optimization of the Tet-On system for regulated gene expression through viral evolution. *Gene Ther*, 13(19):1382–90, 2006.

[290] A. Ghosh, Y. Dai, P. Biswas, and D. J. Stuehr. Myoglobin maturation is driven by the hsp90 chaperone machinery and by soluble guanylyl cyclase. *FASEB J*, 33(9):9885–9896, 2019.

[291] K. Ogawa, J. Sun, S. Taketani, O. Nakajima, C. Nishitani, S. Sassa, N. Hayashi, M. Yamamoto, S. Shibahara, H. Fujita, and K. Igarashi. Heme mediates derepression of Maf recognition element through direct binding to transcription repressor Bach1. *EMBO J*, 20(11):2835–43, 2001.

[292] Q. Ma. Role of Nrf2 in oxidative stress and toxicity. *Annu Rev Pharmacol Toxicol*, 53:401–26, 2013.

[293] J. Alam, E. Killeen, P. Gong, R. Naquin, B. Hu, D. Stewart, J. R. Ingelfinger, and K. A. Nath. Heme activates the heme oxygenase-1 gene in renal epithelial cells by stabilizing Nrf2. *Am J Physiol Renal Physiol*, 284(4):F743–52, 2003.

[294] Y. Dai, E. M. Faul, A. Ghosh, and D. J. Stuehr. NO rapidly mobilizes cellular heme to trigger assembly of its own receptor. *Proc Natl Acad Sci U S A*, 119(4).

[295] A. Ghosh, M. P. Sumi, B. Tupta, T. Okamoto, K. Aulak, M. Tsutsui, H. Shimokawa, S. C. Erzurum, and D. J. Stuehr. Low levels of nitric oxide promotes heme maturation into several hemeproteins and is also therapeutic. *Redox Biol*, 56:102478, 2022.

[296] R. Chakravarti, K. S. Aulak, P. L. Fox, and D. J. Stuehr. GAPDH regulates cellular heme insertion into inducible nitric oxide synthase. *Proc Natl Acad Sci U S A*, 107(42):18004–9, 2010.

[297] A. Ghosh, M. Chawla-Sarkar, and D. J. Stuehr. Hsp90 interacts with inducible NO synthase client protein in its heme-free state and then drives heme insertion by an ATP-dependent process. *FASEB J*, 25(6):2049–60, 2011.

[298] R. Chakravarti and D. J. Stuehr. Thioredoxin-1 regulates cellular heme insertion by controlling S-nitrosation of glyceraldehyde-3-phosphate dehydrogenase. *J Biol Chem*, 287(20):16179–86, 2012.

[299] Y. Adachi, M. Umeda, A. Kawazoe, T. Sato, Y. Ohkawa, S. Kitajima, S. Izawa, I. Sagami, and S. Taketani. The novel heme-dependent inducible protein, SRRD regulates heme biosynthesis and circadian rhythms. *Arch Biochem Biophys*, 631:19–29, 2017.

[300] L. R. Artinian, J. M. Ding, and M. U. Gillette. Carbon monoxide and nitric oxide: interacting messengers in muscarinic signaling to the brain's circadian clock. *Exp Neurol*, 171(2):293–300, 2001.

[301] S. Panda, M. P. Antoch, B. H. Miller, A. I. Su, A. B. Schook, M. Straume, P. G. Schultz, S. A. Kay, J. S. Takahashi, and J. B. Hogenesch. Coordinated

transcription of key pathways in the mouse by the circadian clock. *Cell*, 109(3):307–20, 2002.

[302] B. Tunctan, Y. Weigl, A. Dotan, L. Peleg, H. Zengil, I. Ashkenazi, and N. Abacioglu. Circadian variation of nitric oxide synthase activity in mouse tissue. *Chronobiol Int*, 19(2):393–404, 2002.

[303] T. A. Takeda, A. Mu, T. T. Tai, S. Kitajima, and S. Taketani. Continuous de novo biosynthesis of haem and its rapid turnover to bilirubin are necessary for cytoprotection against cell damage. *Sci Rep*, 5:10488, 2015.

[304] A. F. McDonagh, L. A. Palma, and D. A. Lightner. Blue light and bilirubin excretion. *Science*, 208(4440):145–51, 1980.

[305] A. Kumagai, R. Ando, H. Miyatake, P. Greimel, T. Kobayashi, Y. Hirabayashi, T. Shimogori, and A. Miyawaki. A bilirubin-inducible fluorescent protein from eel muscle. *Cell*, 153(7):1602–11, 2013.

[306] C. L. Nobles, J. R. Clark, S. I. Green, and A. W. Maresso. A dual component heme biosensor that integrates heme transport and synthesis in bacteria. *J Microbiol Methods*, 118:7–17, 2015.

[307] D. G. Glanville, C. Mullineaux-Sanders, C. J. Corcoran, B. T. Burger, S. Imam, T. J. Donohue, and A. T. Ulijasz. A high-throughput method for identifying novel genes that influence metabolic pathways reveals new iron and heme regulation in pseudomonas aeruginosa. *mSystems*, 6(1):e00933–20, 2021.

[308] S. Mourino, B. J. Giardina, H. Reyes-Caballero, and A. Wilks. Metabolite-driven regulation of heme uptake by the biliverdin ixbeta/delta-selective heme oxygenase (hemo) of pseudomonas aeruginosa. *J Biol Chem*, 291(39):20503–15, 2016.

[309] M. Shum, C. A. Shintre, T. Althoff, V. Gutierrez, M. Segawa, A. D. Saxberg, M. Martinez, R. Adamson, M. R. Young, B. Faust, R. Gharakhanian, S. Su, K. Chella Krishnan, K. Mahdaviani, M. Veliova, D. M. Wolf, J. Ngo, L. Nocito, L. Stiles, J. Abramson, A. J. Lusis, A. L. Hevener, M. E. Zoghbi, E. P. Carpenter, and M. Liesa. ABCB10 exports mitochondrial biliverdin, driving metabolic maladaptation in obesity. *Sci Transl Med*, 13(594), 2021.

[310] B. A. Springer and S. G. Sligar. High-level expression of sperm whale myoglobin in *Escherichia coli*. *Proc Natl Acad Sci U S A*, 84(24):8961–5, 1987.

[311] F. W. J. Teale. Cleavage of the haem-protein link by acid methylethylketone. *Biochimica et Biophysica Acta*, 35, 1959.

[312] L. Lad, M. Mewies, and E. L. Raven. Substrate binding and catalytic mechanism in ascorbate peroxidase: evidence for two ascorbate binding sites. *Biochemistry*, 41(46):13774–81, 2002.

[313] F. Gorrec. The morpheus protein crystallization screen. *J Appl Crystallogr*, 42(Pt 6):1035–1042, 2009.

[314] A. Faussner, M. M. Deininger, C. Weber, and S. Steffens. Direct addition of poly-lysine or poly-ethylenimine to the medium: A simple alternative to plate pre-coating. *PLoS One*, 17(7):e0260173, 2022.

[315] S. C. Warren, A. Margineanu, D. Alibhai, D. J. Kelly, C. Talbot, Y. Alexandrov, I. Munro, M. Katan, C. Dunsby, and P. M. French. Rapid global fitting of large fluorescence lifetime imaging microscopy datasets. *PLoS One*, 8(8):e70687, 2013.

Part IV

Publications and list of activities

List of activities

Presented below is a list of publications and activities pertaining to the work presented in this thesis and carried out between September 2019 and March 2023.

Publications

PNAS, 2021 - *Leung, C.-H.; Fung, S.-P; Gallio, A.E..; Blore, R.; Alibhai, D.; Raven, E.L.; Hudson; A.J.*, 118, 22, e2104008118. Unravelling the mechanisms controlling heme supply and demand.

JACS Au, 2021 - *Gallio, A.E.; Fung, S.-P.; Cammack-Najera, A.; Hudson, A.J.; Raven, E.L.*. Understanding the Logistics for the Distribution of Heme in Cells.

J Biol Chem, 2023 - *manuscript submitted* - *Freeman, S.L.; Oliveira, S.F; Gallio, A.E.; Rosa, A.; Simitakou, M.K.; Arthur, C.J.; Mulholland, A.J.; Cherepanov, P.; Raven, E.L.*. Heme binding to the SARS-Cov-2 spike glycoprotein.

Conferences and relevant experiences

Harnessing and mimicking the reactivity of biological metals for a healthy and sustainable future – Gordon Research Conference - January 2023 - *Ventura, CA, USA*, poster contribution.

Inorganic Insights into Fundamental Life Processes – Gordon Research Seminar - January 2023 - *Ventura, CA, USA*, poster contribution.

The roles of tetrapyrroles in catalysis, regulation, metabolism, and disease – Gordon Research Conference - July 2022 - *Newport, RI, USA*, talk and poster contribution.

Christmas Bioenergetics Meeting, University of Sheffield – December 2021 - *online*, talk.

Dalton 2021 – Inorganic Biochemistry Discussion Group of the Royal Society of Chemistry - July 2021 - *online*, poster contribution.

Tetrapyrrole discussion group - September 2019 - *University of Bristol, UK*, poster contribution.

Other relevant experience

13th International course on "Time-Resolved Microscopy and Correlation Spectroscopy" - March 2021 - *online*, organised by PicoQuant (Berlin).

Unravelling the mechanisms controlling heme supply and demand

Galvin C.-H. Leung[a,b], Simon S.-P. Fung[a,b], Andrea E. Gallio[c], Robert Blore[a,b], Dominic Alibhai[d], Emma L. Raven[c,1], and Andrew J. Hudson[a,b,1]

[a]School of Chemistry, University of Leicester, LE1 7RH Leicester, United Kingdom; [b]Leicester Institute of Structural & Chemical Biology, University of Leicester, LE1 7HB Leicester, United Kingdom; [c]School of Chemistry, University of Bristol, BS8 1TS Bristol, United Kingdom; and [d]Wolfson Bioimaging Facility, Faculty of Life Sciences, University of Bristol, BS8 1TD Bristol, United Kingdom

Edited by John T. Groves, Princeton University, Princeton, NJ, and approved April 15, 2021 (received for review March 3, 2021)

In addition to heme's role as the prosthetic group buried inside many different proteins that are ubiquitous in biology, there is new evidence that heme has substantive roles in cellular signaling and regulation. This means that heme must be available in locations distant from its place of synthesis (mitochondria) in response to transient cellular demands. A longstanding question has been to establish the mechanisms that control the supply and demand for cellular heme. By fusing a monomeric heme-binding peroxidase (ascorbate peroxidase, mAPX) to a monomeric form of green-fluorescent protein (mEGFP), we have developed a heme sensor (mAPXmEGFP) that can respond to heme availability. By means of fluorescence lifetime imaging, this heme sensor can be used to quantify heme concentrations; values of the mean fluorescence lifetime (τ_{Mean}) for mAPX-mEGFP are shown to be responsive to changes in free (unbound) heme concentration in cells. The results demonstrate that concentrations are typically limited to one molecule or less within cellular compartments. These miniscule amounts of free heme are consistent with a system that sequesters the heme and is able to buffer changes in heme availability while retaining the capability to mobilize heme when and where it is needed. We propose that this exchangeable supply of heme can operate using mechanisms for heme transfer that are analogous to classical ligand-exchange mechanisms. This exquisite control, in which heme is made available for transfer one molecule at a time, protects the cell against the toxic effect of excess heme and offers a simple mechanism for heme-dependent regulation in single-molecule steps.

heme biology | fluorescence lifetime imaging | biosensing

Heme is essential for the survival of virtually all living systems—from bacteria, fungi, and yeast, through plants to animals. The family of heme proteins is vast, and heme proteins are responsible for a multitude of functions that are essential for the survival of the cell. To meet the needs of supply and demand for heme in cells, most organisms need to synthesize it. Biosynthesis of the heme cofactor is, therefore, one of the most important metabolic processes in biology; it occurs as an eight-step enzymatic pathway, the last three steps of which occur in the mitochondria (1). Surplus heme, on the other hand, is removed by heme oxygenase located in the endoplasmic reticulum (2). However, while the machinery for heme synthesis and degradation is well known, a decades-old question has been to establish precisely how heme is transported between its place of synthesis and subsequently made available to other regions of the cell where heme is in demand. Recent published work has hypothesized that membrane structures (3) and membrane contacts (4) are involved in the heme trafficking mechanism. Nevertheless, the scarcity of information in this area stands in stark contrast to the extensive efforts that have been directed toward understanding the structures and reactivities of many different heme proteins (e.g., refs. 5–8). An answer to this long-standing question on heme transport has recently become even more pressing because it is now established that heme has a regulatory/signaling role in the cell that goes well beyond the existing known requirements for heme in the housekeeping proteins that are essential for cell survival. These regulatory roles include transcriptional regulation and gas sensing, regulation of the circadian clock, and the gating of numerous ion channels (9–11). Deficiencies or excesses in cellular heme concentration also have widespread implications in health and disease [aging (12, 13), cardiovascular disease (14–16), inflammation (17–19), and immune response (17, 19–21)], and thus there is a need to understand the logistics of heme supply and demand.

The absolute requirement that heme, once synthesized, is then made available around the cell raises a number of fundamental questions that currently have no complete answers. One idea is that there is a pool of free heme to respond to cellular demands, and this has been discussed as far back as the 1970s (22, 23). However, the concept of a "heme pool" is problematic from both a chemical and biochemical perspective. The first is that heme is cytotoxic because it promotes the formation of free radicals through Fenton chemistry. So, if free heme is present in uncontrolled concentrations—for example, in a pool—then it would be a nuisance to the cell. A second problem is that heme is a hydrophobic molecule by virtue of its conjugated tetrapyrrole ring structure and is therefore insoluble; it also dimerizes extensively in aqueous solution (24) and in this form cannot be delivered to proteins that require only one molecule of heme per binding site. A free molecule of heme can therefore only exist transiently, and if a large reserve of heme is present, the heme molecules would presumably need to be exchanged rapidly between binding partners to remain solubilized, in the same way that heme is solubilized within the interior of other well-known

Significance

Heme is essential for the survival of virtually all living systems and is involved in many fundamental biological processes. It is also implicated as a signaling/regulatory molecule and must be mobilized in response to cellular demands. This presents a complex logistical problem: heme cannot simply diffuse around cells because it is both insoluble and cytotoxic. We show that the cell exhibits exquisite control over release of heme by limiting its availability to one molecule or less within cellular compartments. We suggest an exchange mechanism between protein partners to control supply and demand. Such a mechanism would provide an in-built buffering capacity for heme, enable cells to hoard supplies of heme, and protect the cell against the undesirable effects of heme.

Author contributions: E.L.R. and A.J.H. conceived research; E.L.R. and A.J.H. designed research; G.C.-H.L., S.S.-P.F., R.B., and D.A. performed research; S.S.-P.F., A.E.G., E.L.R., and A.J.H. analyzed data; and E.L.R. and A.J.H. wrote the paper.

The authors declare no competing interest.

This article is a PNAS Direct Submission.

[1]To whom correspondence may be addressed. Email: emma.raven@bristol.ac.uk or andrew.hudson@leicester.ac.uk.

This article contains supporting information online at https://www.pnas.org/lookup/suppl/doi:10.1073/pnas.2104008118/-/DCSupplemental.

Published May 25, 2021.

heme proteins (e.g., hemoglobin). A third unknown is that while the need for availability of heme around the cell is undisputed with the exception of certain pathogenic bacteria [which do not synthesize heme and instead acquire it from the host (25)] and the CcmE chaperones for cytochrome *c* [in itself a special case as cytochrome *c* binds heme covalently (26, 27)], very few heme transporters have been identified (28–31).

New, more sensitive, and more sophisticated approaches are needed to develop a better understanding of the dynamics of cellular heme availability and the mechanisms that control it. Using fluorescence lifetime imaging (FLIM), we have probed the availability of heme in different locations of live cells via its interaction with a genetically encoded sensor. While extremely low concentrations of free heme have been determined quantitatively using this approach, the response of the sensor indicates the existence of a larger reserve of heme, which provides an exchangeable supply that can be mobilized between heme-binding partners. These results indicate that heme availability is not linked to a

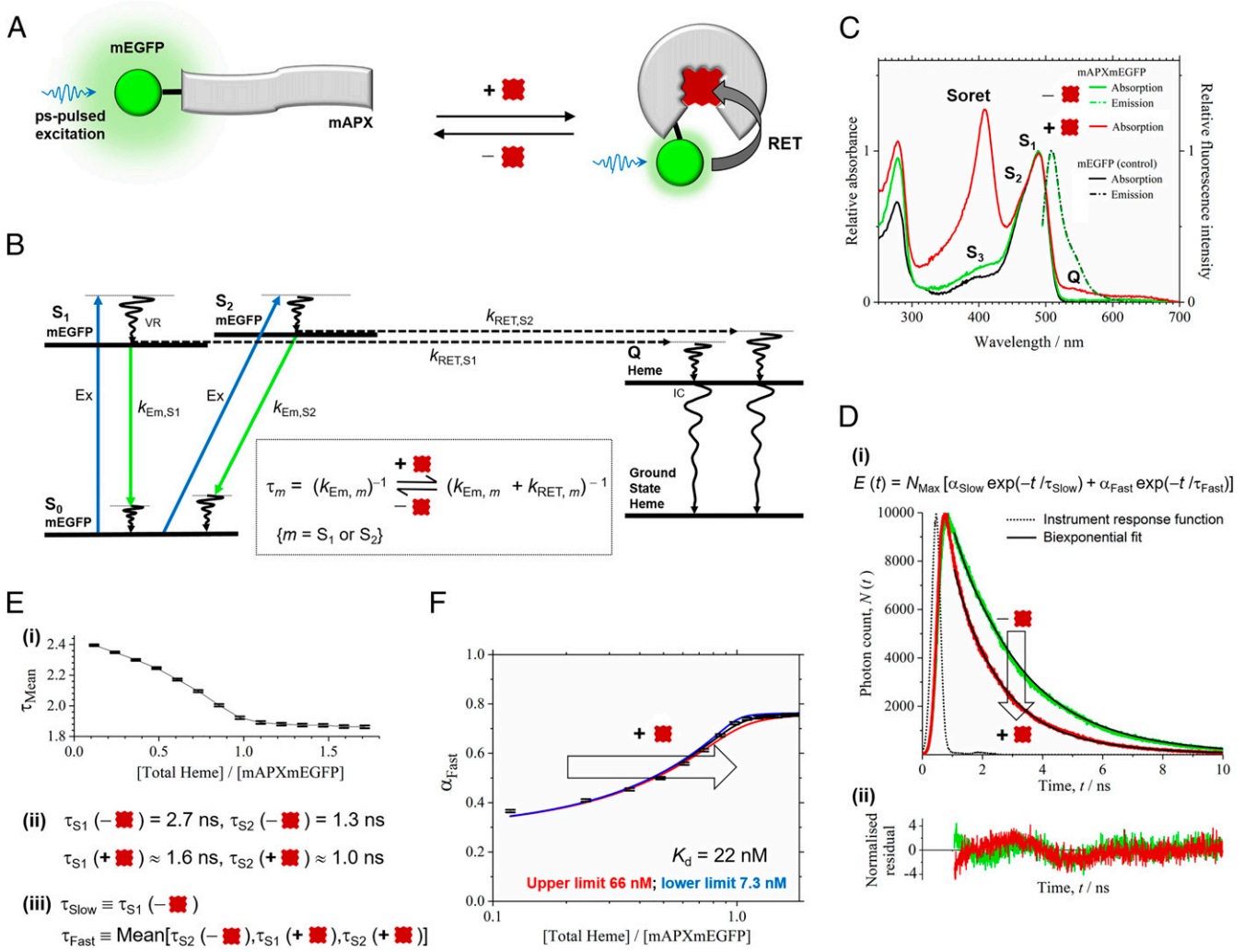

Fig. 1. Heme sensing in cells. (*A*) The sensor is mAPX (gray) conjugated to mEGFP (green). Binding of heme (dark red) to mAPX results in RET from photoexcited mEGFP, with concomitant reduction in emission lifetime. (*B*) The principle of the sensor operation is based on different decay pathways from excited states of mEGFP in the presence and absence of heme. Excitation (Ex, blue) of mEGFP from the ground state, S_0, to excited-vibronic states, S_1 and S_2, is followed by vibrational relaxation (VR). Decay pathways from S_1 and S_2 are either (*A*) fluorescence emission (green) with rate constants, $k_{Em,S1}$ and $k_{Em,S2}$, respectively, or (*B*) RET to an electronic-excited state of heme (c.f. mEGFP emission and heme Q band for overlap) with rate constants, $k_{RET,S1}$ and $k_{RET,S2}$, respectively, followed by VR and internal conversion (IC) to the ground state of heme. (*Inset*) Equations for fluorescence lifetimes, τ_{S1} and τ_{S2}, in the presence and absence of heme. (*C*) Absorption and fluorescence spectra for mAPXmEGFP and mEGFP (λ_{Ex}, 488 nm). Partially resolved bands (centered at 490 nm) for mEGFP are assigned to S_1 and S_2; a further weak absorption band for mEGFP (S_3) and, on addition of heme, Soret and Q bands (408 and 541 nm) are observed. (*D*) (i) Time-correlated single-photon counting, $N(t)$, from *apo*- (green) and *holo*-mAPXmEGFP (red) (λ_{Ex}, 475 nm; λ_{Em}, 510 nm; 37 °C) fitted to a biexponential-decay function, $E(t)$, with time constants of 2.7 (τ_{Slow}) and 1.3 ns (τ_{Fast}). (ii) Normalized residuals for fitting to the decay profiles, $(N(t) - E(t)) / \sqrt{E(t)}$. χ^2 values were between 0.8 and 1.7 for biexponential fitting to the reported decay data. Significant improvement in χ^2 cannot be achieved by inclusion of >2 decay terms. $\chi^2 = (1 / h) \times \Sigma (N - E)^2 / E$ {h time bins}. (*E*) (i) Sequential additions of heme to *apo*-mAPXmEGFP lead to a gradual increase in the amplitude of the fast (α_{Fast}) relative to the slow (α_{Slow}) component and a decrease in the mean lifetime, τ_{Mean}. (ii) τ_{S1} and τ_{S2} for *apo*-mAPXmEGFP are the same as the optimized values of τ_{Slow} and τ_{Fast} from $E(t)$. Both τ_{S1} and τ_{S2} are reduced in *holo*-mAPXmEGFP (see *B*, *Inset*), and estimates have been made for these values by assuming that $k_{RET,S1} = k_{RET,S2}$ (*SI Appendix*). (iii) The biexponential model, $E(t)$, for mixtures of *apo*- and *holo*- mAPXmEGFP has a slow-decay component, τ_{Slow}, equal to τ_{S1} (*apo*) and a fast-decay component, τ_{Fast}, equal to the mean of τ_{S2} (*apo*), τ_{S1} (*holo*), and τ_{S2} (*holo*). (*F*) A theoretical single-site binding model fitted to the amplitude, α_{Fast}, in decay profiles obtained by sequential additions of heme to *apo*-mAPXmEGFP at 37 °C. The estimation of error bars in *E* and *F* is described in *SI Appendix*, section 2.

dedicated heme pool nor is controlled solely by specific heme chaperones. Instead, we propose that an exchangeable (buffered) reservoir of heme is present in the cell to provide not only a flexible supply of heme but also protection against the undesirable cytotoxic consequences of excess heme concentrations.

Results

A heme sensor was constructed comprising the *apo* form (i.e., without heme) of a monomeric form of ascorbate peroxidase (APX), referred to here as *apo*-mAPX, fused to a monomeric form of green fluorescent protein (mEGFP) (as in Fig. 1*A*; further details of the construct designs are given in *Materials and Methods*). APX is a heme-dependent peroxidase (32). Its catalytic activity has been used for proteomic mapping in cells (33) and to identify the accumulation of heme in cellular compartments (34); EGFP has also been fused to APX in order to identify the cellular location of the enzyme (34). It is a homodimer in solution (34), and the monomeric (mutant) form was used in this work with mEGFP to avoid complexities arising from dimerization of either APX or GFP in the FLIM experiments below. This heme sensor (referred to as mAPXmEGFP) is able to quantify precisely heme concentration in live cells via measurement of the fluorescence lifetime of mEGFP. By recording the decay at a single emission wavelength, the ratio of *apo* to *holo* forms of mAPXmEGFP, and hence the heme concentration, can be determined precisely in our FLIM experiments. A major advantage of FLIM of mAPXmEGFP is that neither inner filtering of the fluorescence emission nor the partial inactivation of the fluorescent protein by photobleaching have an effect on photon emission times from mEGFP (35). Hence the two major limitations of previous designs for fluorescent heme sensors (4, 36–43) will not affect our experimental studies. Inner filtering and photobleaching does have a significant effect on the measured intensity of fluorescence emission, and all previous sensor designs comprising a heme-binding protein and one or more fluorescent proteins have relied on the measurement of fluorescent emission intensity to determine heme concentrations. In the work presented here, mAPXmEGFP uses a single fluorophore for lifetime studies; the decay parameters of mAPXmEGFP can be recorded accurately, and heme concentration can be determined more precisely.

Under irradiation from a picosecond-pulsed laser (at 475 to 488 nm), the fluorescence decay from *apo*-mAPXmEGFP contains two components derived from excitation to, and subsequently emission from, a pair of noninteracting excited states, S_1 and S_2 (Fig. 1 *B* and *C*) (44). The principle of the design is that binding of heme to the sensor facilitates resonance-energy transfer (RET; Fig. 1*B*) from these excited states of mEGFP to the heme chromophore and, subsequently, internal conversion and vibrational relaxation to the ground state. Hence, heme binding leads to a decrease in the emission lifetimes, τ_1 and τ_2, from each of the excited states of mEGFP (Fig. 1*B*, *Inset*).

In initial in vitro experiments, the *apo*-mAPXmEGFP protein was isolated and purified from *Escherichia coli* cultured in media supplemented with succinylacetone (*Materials and Methods*). Succinylacetone inhibits the second step of the eight-step heme synthesis pathway and thus limits the amount of heme available to the cells (45). mAPXmEGFP, expressed in *E. coli* under these growth conditions, is isolated 97% in the *apo* form (*Materials and Methods*). The absorption spectrum (green solid line in Fig. 1*C*) accordingly shows strong peaks only for mEGFP (i.e., 470 and 490 nm). On addition of heme to *apo*-mAPXmEGFP, a further absorption band is observed, as expected, in the heme Soret region (408 nm). Where mEGFP was expressed in *E.coli*, under the same conditions as for mAPXmEGFP (with the exception of the addition of succinylacetone), the absorption spectrum for mEGFP alone (black solid line in Fig. 1*C*) is similar to that for *apo*-mAPXmEGFP. The fluorescence emission spectrum of mEGFP is unchanged by fusion to mAPX (peak maximum at 509 nm; as shown in green and black dot-dash lines in Fig. 1*C*).

Fluorescence decay profiles for emission were measured for *apo*-mAPXmEGFP in the presence of varying amounts of heme and hence with different ratios of *apo* to *holo* (i.e., heme bound) forms of the sensor (Fig. 1*D*). The entire set of decay profiles ($n = 14$) can be fitted to a biexponential decay with fixed time constants of 2.7 (τ_{Slow}) and 1.3 ns (τ_{Fast}). The amplitude of the fast-decay component (α_{Fast}) increases relative to the slow-decay component (α_{Slow}) with sequential additions of heme leading to a decline in the intensity-weighted mean lifetime, τ_{Mean} (Fig. 1*E*, *i*; where $\tau_{Mean} = (\Sigma_m\, \alpha_m \times \tau_m^2) / (\Sigma_m\, \alpha_m \times \tau_m)$ {m = Slow, Fast}; $\alpha_{Slow} + \alpha_{Fast} = 1$). The emission lifetimes τ_{S1} and τ_{S2} for *apo*- and *holo*-mAPXmEGFP correspond to the fitted time constants τ_{Slow} and τ_{Fast}. Both τ_{S1} and τ_{S2} are reduced in *holo*-mAPXmEGFP compared to *apo*-mAPXmEGFP due to the competing nonradiative RET pathway (Fig. 1*B*, *Inset* and Fig. 1*E*, *ii*). Indirect evidence suggests that the emission spectra from S_1 and S_2 are near perfectly superimposed (*SI Appendix*, Fig. S1*B*). Because rate constants for RET depend on overlap between the emission spectrum of the donor and the absorption spectrum of the acceptor, $k_{RET,S1}$ and $k_{RET,S2}$, are expected to be approximately equal. Resonance energy transfer will make the values of τ_{S1} and τ_{S2} for *holo*-mAPXmEGFP higher and lower, respectively, than τ_{S2} for *apo*-mAPXmEGFP (*SI Appendix*, section 1 and Table S1). Hence it is possible to apply a biexponential decay model for all measurements containing different ratios of *apo*- and *holo*-mAPXmEGFP, where one of the components has a time constant (τ_{Slow}) equal to the long decay lifetime (i.e., τ_{S1} in *apo*-mAPXmEGFP) and another component has a time constant (τ_{Fast}) equal to the mean of the three short decay lifetimes (i.e., τ_{S2} in *apo*-mAPXmEGFP and both τ_{S1} and τ_{S2} in *holo*-mAPXmEGFP (Fig. 1*E*, *iii*)]. In this way, it is possible to determine the ratio of the concentrations of *apo*- to *holo*-mAPXmEGFP from the relative amplitudes of these fitted-exponential terms, α_{Slow} and α_{Fast} (*SI Appendix*, Eq. **S8**). A 1:1 binding model can be used to rationalize the changes in α_{Slow} and α_{Fast} observed following sequential additions of heme to *apo*-mAPXmEGFP (Fig. 1*F*, full details given in *SI Appendix*, section 2). The precision for the fitting of a 1:1 binding model to the lifetime data supports the proposed model given in Fig. 1*E*. Using this approach, the heme-dissociation constant for mAPXmEGFP has been determined (K_d = 22 nM; lower limit, 7 nM; upper limit, 66 nM). The K_d of mAPXmEGFP was found to be independent of both pH and ionic strength (*SI Appendix*, Fig. S3).

Subsequent to these in vitro experiments above, both mEGFP (alone) and *apo*-mAPXmEGFP were expressed in separate HEK293 cell lines. The total concentration of expressed mAPXmEGFP was estimated to be ca. 1 μM (*SI Appendix*, Fig. S4). Expression of mEGFP in HEK cells allows α_{Slow} and α_{Fast} to be determined in the absence of RET (as the latter requires heme in close proximity to mEGFP, Fig. 1*B*). The fluorescence decay was measured at different locations in HEK cells by confocal FLIM. The measured decays were fitted to separate biexponential functions, and the resulting amplitudes and lifetimes of the decay components were used to calculate intensity-weighted mean lifetimes, $\tau_{Mean} = (\Sigma_m\, \alpha_m \times \tau_m^2) / (\Sigma_m\, \alpha_m \times \tau_m)$ {m = Slow, Fast}. Fig. 2 shows color maps of τ_{Mean} for cells expressing both mEGFP (alone) and *apo*-mAPXmEGFP. Each of the color maps is accompanied by a histogram showing the frequencies for which particular values of τ_{Mean} occur in the spatial distribution of pixels for the images of cells under different conditions. While the concentration of the sensor is highest in the cytosol, there is still a sufficient concentration of the sensor in the nucleus and other parts of the cell. In the presence of high concentrations of free heme, there is substantial quenching of the sensor fluorescence in the nucleus (*SI Appendix*, Fig. S6). The time constants obtained for a biexponential function using a global-fitting algorithm to the imaging data for both mEGFP and mAPXmEGFP were 2.5 (τ_{Slow}) and 1.2 ns (τ_{Fast}). Fluorescence lifetimes for the sensor were expected to be marginally shorter in HEK cells (in vivo) than those observed for the purified protein (in vitro; Fig. 1*D*) due to the inverse dependence of fluorescence

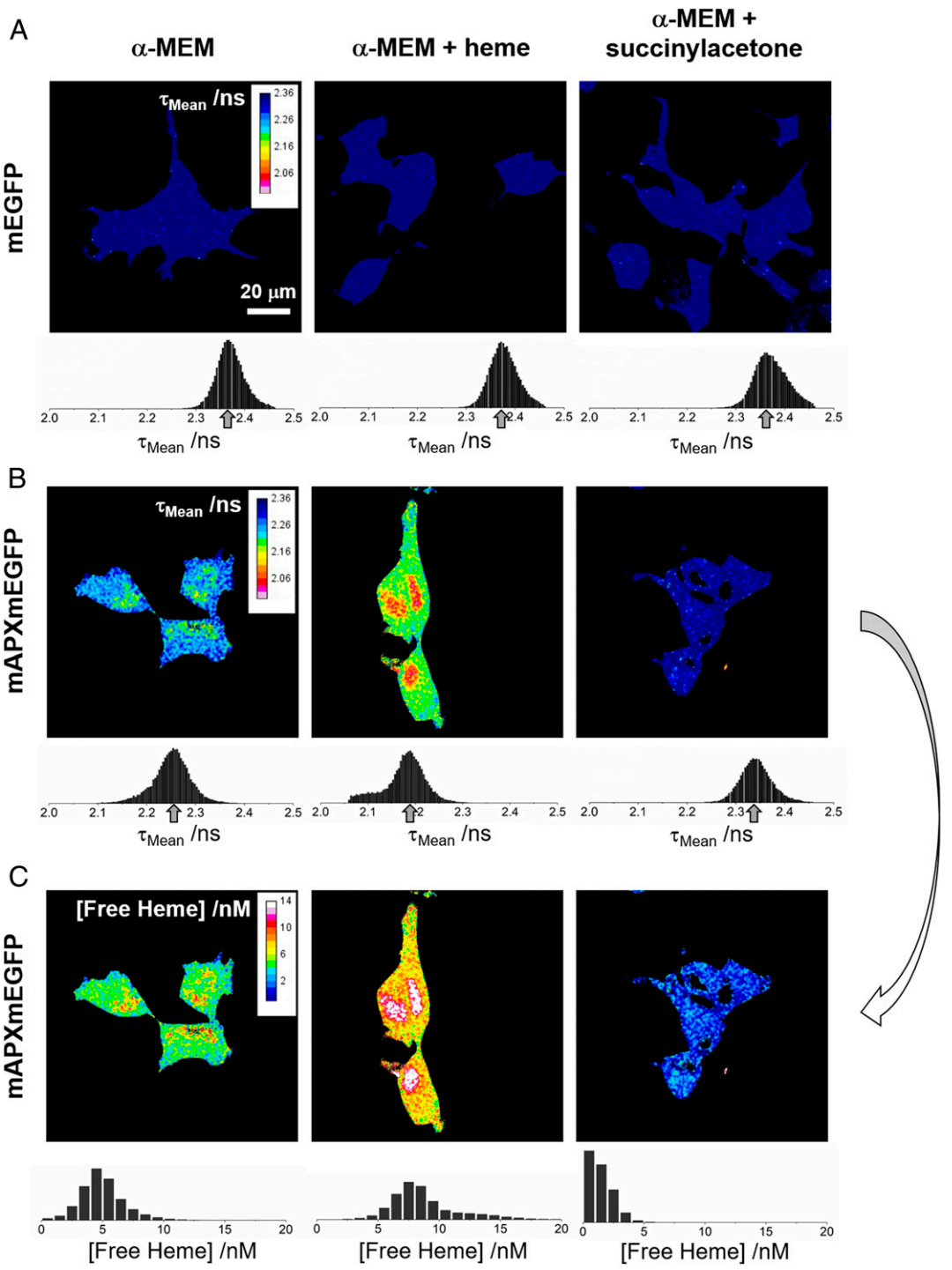

Fig. 2. Color maps of intensity-weighted mean fluorescence lifetime and free heme concentration. The intensity-weighted mean fluorescence lifetime, τ_{Mean}, for HEK293 cells expressing either (*A*) mEGFP alone or (*B*) mAPXmEGFP and cultured under different conditions (λ_{Ex}, 488 nm; λ_{Em} > 495 nm). (*Left*) α-MEM (with 10% fetal bovine serum); (*Middle*) α-MEM supplemented with heme (10 μM; 24 h prior to imaging); (*Right*) α-MEM depleted of heme following addition of succinylacetone (1 mM; 24 h prior to imaging). If the photon count was below a value of 200 for an individual pixel, then a black color was assigned to that pixel in the color map (this is the threshold criteria used in the FLIM experiments for the estimation of the decay parameters; *Materials and Methods*). Each of the color maps in *A* and *B* are accompanied by a histogram showing the frequencies for which particular values of τ_{Mean} occur in the spatial distribution of pixels for the images of cells under different conditions. An arrow indicates the modal pixel value of τ_{Mean}. (*C*) The concentration of free heme calculated from the relative amplitudes, α_{Slow} and α_{Fast}, in the images shown in *B* using the heme-dissociation constant, K_d, for mAPXmEGFP determined in Fig. 1*F* (22 nM at 37 °C). The full calculation is outlined in *SI Appendix*, section 3. The detection limit for [Free Heme] is <1 nM (0.6 molecule per fL). Each of the color maps for free heme concentration is accompanied by a histogram showing the frequencies for which particular values of [Free Heme] occur in the spatial distribution of pixels for the images of cells under different conditions. The black color has been used to represent pixels for which the photon count was below the threshold of 200. All colors other than black represent reliable measurements of [Free Heme]. For the images in the *Left* column of *A* and *B*, the time-correlated single-photon counting data and the fitted-biexponential decay curves are shown in *SI Appendix*, Fig. S6.

lifetime on the square of the refractive index (27, 29). The average χ^2 value for biexponential modeling of the pixel data in a single image was 0.99 (*SI Appendix*, Fig. S6 and section 6).

For both mEGFP and mAPXmEGFP, separate images were obtained for HEK293 cells grown in α-minimum essential medium (α-MEM; Fig. 2, *Left*), in α-MEM supplemented with heme (Fig. 2, *Middle*), and in α-MEM supplemented with succinylacetone to deplete heme from cells (Fig. 2, *Right*). For mEGFP, the modal value for τ_{Mean} does not change in the images recorded under the three different conditions—this is evident as the peak in the histogram is between 2.36 and 2.37 ns (Fig. 2*A*, *Left*, *Middle*, and *Right*). In each example for mEGFP, the distribution of τ_{Mean} is approximately symmetrical with a narrow full-width half-maximum of 0.06 to 0.07 ns. In contrast, for mAPXmEGFP, the modal value for τ_{Mean} does change significantly in the images recorded under the three different cell culture conditions. In α-MEM, the modal value for τ_{Mean} of mAPXmEGFP was 2.25 ns (Fig. 2*B*, *Left*), which is significantly lower than the value measured for mEGFP above due to RET from the excited mEGFP chromophore within the subpopulation of mAPXmEGFP that contains a bound molecule of heme (refer to Fig. 1*B*). Under heme-supplemented conditions, the modal value of τ_{mean} was further reduced to 2.19 ns (Fig. 2*B*, *Middle*). There is a considerable tail in the distribution toward shorter lifetimes, which indicates that there are regions of the cell with much higher concentrations of heme. Under heme-depleted conditions, the modal value for τ_{Mean} of mAPXmEGP was 2.33 ns (Fig. 2*B*, *Right*), which is close to that observed in the cell lines expressing mEGFP alone (Fig. 2*A*). This is consistent with there being no heme bound to mAPXmEGP under these heme-depleted conditions. All of the images shown in Fig. 2 contain multiple cells (>2, up to 5 cells). The modal value and the spatial distribution of values for τ_{Mean} is consistent among the discrete numbers of cells in each image recorded under the different conditions.

These FLIM experiments show that values of τ_{Mean} are lowered in mAPXmEGFP when a heme molecule bound to mAPX is located in close proximity to mEGFP (<10-nm distance). In the case of the HEK cell lines expressing mEGFP on its own (Fig. 2*A*), the absence of a heme-binding domain fused to the fluorescent protein means that there is little variation in τ_{Mean} even when there are significant changes in cellular concentrations of heme. In contrast, for the HEK cells lines expressing mAPXmEGFP (Fig. 2*B*), there are substantive differences in modal values of τ_{Mean} measured under conditions of different heme concentration. Using the results from the in vitro studies (Fig. 1), it is possible to transform the imaging data from live cells (Fig. 2*B*) to construct a map illustrating the concentration of free heme in the cell (Fig. 2*C*; *SI Appendix*, Eqs. **S17** and **S18**—the full calculation is described in *SI Appendix*, section 3). Free heme will be a small fraction of the total heme present in cells. There will be considerably larger fractions associated with known hemoproteins and bound reversibly to other heme-binding partners. In free heme, the iron ion exists in a square planar complex with protoporphyrin IX only (the axial coordinate positions could be occupied by water molecules). Each of the color maps for free heme concentration, in Fig. 2*C*, are accompanied by a histogram showing the frequencies for which particular values of concentration exist in the spatial distribution of pixels for the images of cells under different conditions. The breadth of the distribution shown in the histogram plots indicate how the spatial distribution of free heme varies within the discrete number of cells in each of the images. The free heme concentration determined here has a modal value of 4 to 5 nM under normal conditions, reducing to <1 nM under heme-depleted conditions. These concentrations correspond to 2.4 to 3.0 molecules of heme per fL (control conditions) to <1.0 molecule per fL (under heme-depleted conditions).

We have explored the possibility that the presence of the sensor can perturb the concentration of free heme in cells. A model has been constructed, in which the sensor (A = mAPXmEGFP in Fig. 3) competes with the *apo*-proteins (B in Fig. 3) for the available heme in the cell. At the measured expression level for the sensor of ca. 1 μM (*SI Appendix*, Fig. S4), the sensor will not perturb the cellular biochemistry by depleting the availability of heme (forming a complex AH) as long as the total concentration of heme exceeds or equals 3 μM (the value reported in ref. 46 from denatured cell lysates). In this model, the total concentration of heme will include a minute fraction of free heme (estimated to be 5 nM; as in Fig. 2*C*, *Left*) and a larger fraction associated with reversible binding partners, BH.

Discussion

The quantitative maps of free heme concentration derived from the FLIM experiments demonstrate very low amounts of free heme (ca. 5 nM). We interpret this to mean that free heme represents a minute fraction of the entire amount of heme present in the cell. Indeed, this concentration of free heme stands in sharp contrast to the much higher concentration of 3 μM measured in ref. 46 following the denaturing of cell lysates; this much higher concentration would be dominated by contributions from the population of heme molecules that are bound to proteins rather than the small amounts of free heme. Our in vivo measurement of free heme in HEK293 cells is also one to two orders of magnitude lower than

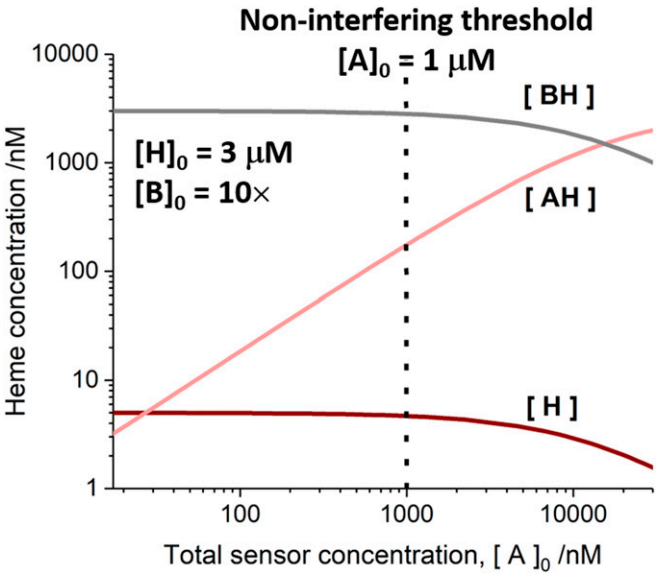

Fig. 3. A computational model illustrating how the concentration of exchangeable heme varies as a function of the total concentration of the expressed sensor, $[A]_0$; A = mAPXmEGFP. Exchangeable heme will be mostly associated with binding partners, B (where [BH], in gray, represents the concentration of heme bound to B). A minute proportion of the exchangeable heme exists as free molecules, H (with the concentration, [H], shown in dark red). At higher values of $[A]_0$, a larger proportion of exchangeable heme will be transferred to the sensor. The concentration of the *holo* form of the heme sensor, [AH], is shown in light red), where the total concentration of the expressed sensor, $[A]_0$ = [A] + [AH] is given on the horizontal axis ([A] = concentration of the *apo* form of the sensor). The model has been created by assuming that the total concentration of heme, $[H]_0$ = [H] + [BH] + [AH], is 3 μM (46); the concentration of free heme, [H], in the absence of a sensor or acceptor protein is 5 nM (as observed in Fig. 2, *Lower Left*); and the K_d for heme dissociation from the sensor is 22 nM (Fig. 1*F*). The total concentration of heme-binding partners, $[B]_0$ = [B] + [BH], has been assumed to be 10 × $[H]_0$ to achieve effective buffering of heme concentration. We have determined an experimental value of 1 μM for the cellular concentration of the sensor (dotted line, *SI Appendix*, Fig. S4). At and below these concentrations, the expression of the sensor does not interfere with the availability of heme in cells, and the concentration of exchangeable heme (both [BH] and [H]) is unaffected, as shown in the plot.

the reported values in other cell lines: HeLa (42), yeast (41), and IMR90 (11). These authors have described the concentrations as representing labile heme (41, 42) and regulatory heme (11) but, in these earlier publications, the exact identity of the heme species in labile heme and regulatory heme has not been described.

Numerous substantive conclusions derive from this quantitative measurement reported in Fig. 2. Perhaps the most obvious is that the long-held concept of a pool of free heme (22, 23) becomes immediately irrelevant because there are too few molecules of heme available to support a dedicated pool. By restricting free heme to such miniscule concentrations, the problems associated with heme-dependent cytotoxicity are also solved because the probability of free heme reacting with oxygen or other reactive oxygen species is much reduced.

Thinking more widely, these minute and presumably transient concentrations of free heme will be dwarfed by the total heme complement within the cell, which will be incorporated into multiple housekeeping and other proteins that are essential for cellular function. For a proportion of this total heme complement, heme binding to a respective protein is so tight as to be practically irreversible—with the heme only released upon enzymatic degradation and not available for movement around the cell or for interaction with the sensor in our experiments. However, for the experiments in Fig. 2*B* to be viable, at least some proportion of the total heme complement—that which is not bound irreversibly to housekeeping proteins—must be available for exchange. Our experiments are thus consistent with the idea that there is a population of the total heme complement that is bound more weakly and therefore reversibly to heme-binding partner proteins or to other molecules (which might include free amino acids) that can buffer against changes in the heme concentration. The changes in concentration of free heme observed in the imaging experiments are relatively small (<0.6 to 2.4 molecules per fL; Fig. 2*C*), which is consistent with a buffering mechanism. These heme molecules that are weakly bound to buffer molecules, along with the miniscule population of free heme, would constitute a body of exchangeable heme in the cell.

A model that is consistent with the sensor measurements is outlined in mechanistic form in Fig. 4. The foundation for the model is an exchange mechanism for managing heme supply and demand in cells involving a body of reversible heme-binding partners, which might be known heme proteins or other proteins (see legend). In earlier publications, the existence of what was termed a regulatory heme pool (48, 49) or intracellular heme pool (50) was proposed to account for varied observations in blood disorders such as porphyria (51, 52), gene expression (22, 53, 54), heme protein levels (23), and heme biosynthesis (55, 56). More recently, the weakly bound fraction of the total heme complement has been referred to as labile heme (41, 42, 57) and regulatory heme (11). While the model presented in Fig. 4 can still be reconciled with earlier work, it uses the concept of exchangeable heme, as introduced above, to account for both the presence of weakly bound heme (to act as a buffer against changes in heme concentration) and the transient existence of free heme (which is measured precisely by the FLIM experiment). The model in Fig. 4 also describes a mechanism for heme exchange. We see clear advantages of such an exchange mechanism between protein partners, designed for the purpose of managing heme supply and demand. It would provide a powerful buffering capacity for the cell to mitigate changes in heme concentration. This heme-buffering capacity would be useful to manage changes in the supply and demand of heme that require immediate adjustment and that cannot be mitigated in a timely manner by up-regulation of heme oxygenase or heme synthesis. A supply of exchangeable heme, to be made available on demand in this highly controlled fashion as shown in Fig. 4 *A* and *B*, could also be utilized for precise and tightly regulated heme-dependent signaling control.

This process of heme exchange as described above is analogous to classical mechanisms for ligand and solvent exchange that have long been established in transition metal chemistry (58). Exchange of heme between partners in cells is simple in concept, as outlined in Fig. 4, but by analogy with the versatile ligand exchange mechanisms that are known in metal complexes could conceivably proceed by several different routes (e.g., associative, dissociative, or interchange mechanisms). It would avoid the need for specific heme chaperones which, aside from exceptional examples [such as GAPDH (31)], have persistently eluded identification over decades. Note, however, that our data do not rule out the use of chaperones altogether, and they might be useful in mammalian systems in cases where more directed heme transfers or allocations are required. We expect that a cell will take advantage of all possible mechanisms for transfer of heme from the exchangeable reservoir, but one example is illustrated in Fig. 4*C*. A dissociative pathway, as shown in Fig. 4*C*, provides a mechanism by which the release of at least a single molecule of heme has a finite probability. Even transient release of a free molecule of heme into the aqueous medium of the cell would be sufficient for its capture by another protein (such as a regulatory or signaling heme protein) or, as in this work, by a sensor. Free heme concentrations in the region of 1 molecule per fL, as identified here, in the vicinity of a signaling site are still sufficient to ensure its population with heme by this exchange process, although dissociation of heme might present an activation energy barrier (Fig. 4*D*). The concentration of free heme is controlled by the relative rates of association and dissociation of heme from reversible-binding partners. While the former process dominates leading to only a few molecules of free heme per fL (or a transient existence for an individual molecule of free heme), the binding partners have sequestered a much larger concentration of exchangeable heme. We speculate that the total concentration of exchangeable heme will remain relatively constant in the cell; however, the transiency of free heme (i.e., the free heme concentration) could be controlled by changes in the relative composition of the buffering ensemble, which is expected to differ in various compartments of the cell to meet specific local demands for heme. An alternative mechanism might involve association of exchange partners [as suggested for exchange of metal ions in cells (59), *SI Appendix*, Fig. S7].

In the mechanism shown in Fig. 4*C*, the abundance of heme-binding partners dictates both the overall buffering capacity and hence the free heme concentration in the cell (as shown in *SI Appendix*, Fig. S5*A*). Fixing the availability of heme within a defined range allows the cell to exclusively supply heme to proteins possessing a K_d value below the threshold of free heme concentration which is thus generated (this concept is illustrated in *SI Appendix*, Fig. S5*B* using a simple competitive binding model). This exquisite control also provides a mechanism for heme-dependent signaling and regulation, as heme can be supplied discretely, leading to the switching on of proteins in single-molecule steps. Since changes in the availability of heme could be deleterious due to switching on/off of heme dependent functions, the control of heme supply is vital to the cell.

Armed with a better understanding of heme localization and mobilization across compartments in cells, the future holds the possibility to establish how deficiencies or excesses of heme affect the regulation of numerous functions known to have heme dependencies [e.g., regulatory proteins involved in gene expression and circadian response (60–62)]. Our model of heme availability will lead to a more complete understanding of the activities and consequences of these regulatory proteins and various immune pathologies for which heme homeostasis is a key driver (20). Since heme concentrations are known to increase during hypoxia and after thrombosis/stroke, there are important consequences for cardiovascular disease (14), as well as in neuronal survival and aging which are also dependent on heme (12).

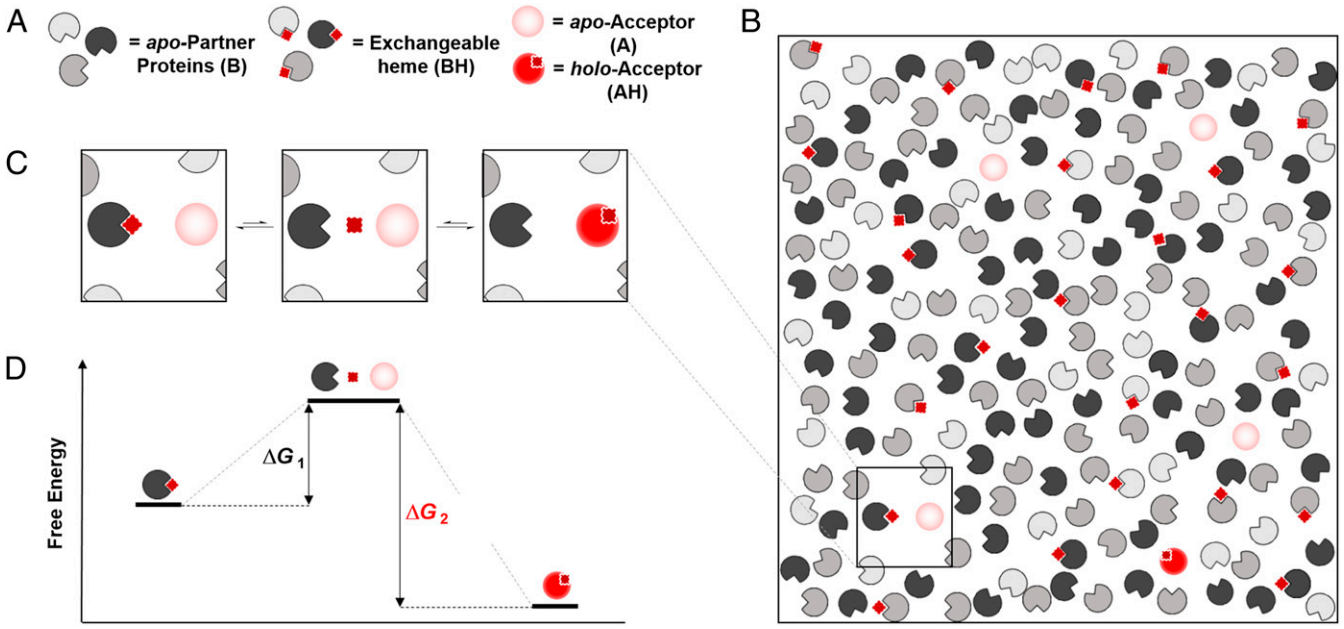

Fig. 4. An exchange mechanism for managing heme supply and demand in cells. (*A* and *B*) We envisage a body of reversible heme-binding partners, represented by pacmans in different shades of gray (referred to as B in Fig. 3), along with potential heme-acceptor proteins (shaded light red pacmans; these might also be the sensor, referred to as A in Fig. 3). These heme-binding partners could be known heme proteins [indoleamine 2,3-dioxygenase, for example, is known to lose its heme under certain conditions (47)] or other proteins such as GAPDH (28, 29, 31). Heme is shown as a dark red square or diamond (referred to as H in Fig. 3). (*C*) Heme exchanges between heme-binding partners via dynamic chemical equilibria. (*Left*) Heme in the cell is bound to a heme-binding protein: we refer to this as exchangeable heme. (*Middle*) Dissociation of heme from a heme protein is typically a rare event; it results in an *apo*-partner protein and a molecule of free heme. These free heme molecules are presumed to be transiently formed and may be ligated with weak, easily dissociated ligands (e.g., H_2O) or otherwise solvated (24). (*Right*) The heme thus released then binds to other heme-acceptor proteins (light red) (or is picked up by a sensor). The free heme reported by our sensors (Fig. 2) measures the likelihood that heme will dissociate from a partner protein, with higher concentrations describing a more frequent event. Thus, the free heme in each region of a cell is controlled by the dissociation constants and the relative abundance of all heme-binding partner proteins in that region. (*D*) A consequence of the thermodynamic reversibility of heme binding is that the transfer of heme can be facilitated between the exchangeable pool and another protein. The energy profile of this heme exchange mechanism is indicated.

Materials and Methods

Protein Expression and Purification for In Vitro Characterization of mEGFP and mAPXmEGFP. mAPX was created from the wild-type protein by incorporation of the K14D and E112K mutations and then expressed recombinantly as a fusion protein with mEGFP (63) in a pLEICS-45 vector carrying ampicillin resistance and a N-terminal His tag. This fusion protein—containing the double mutation (K14D/E112K)—is referred to as mAPXmEGFP in this work. mEGFP was inserted into a pLEICS-01 vector carrying ampicillin resistance and a N-terminal His tag. For in vitro characterization experiments, mEGFP alone and the mAPXmEGFP sensor were expressed in *E. coli* BL21(DE3). In both cases, cells were grown in lysogeny broth (LB) at 37 °C until the optical density at 600 nm was 0.6 to 1.0. Protein expression was induced with 250 μM isopropyl-β-D-thio-galactoside and incubated at 23 °C overnight. For expression of mAPXmEGFP in *E. coli*, the LB media was supplemented with succinylacetone (1 mM; Sigma Aldrich); otherwise, the protocols for expression of mAPXmEGFP and mEGFP were the same. Cells were pelleted by centrifugation (3,000 *g*, 30 min, 4 °C) and resuspended in a buffer solution containing 10 mM potassium phosphate (pH = 7) and 150 mM KCl followed by addition of lysozyme (2 mg/mL; Sigma Aldrich), DNase (0.1 mg/mL; Sigma Aldrich), and protease inhibitor mixture (Roche). The solution was then sonicated on ice in cycles of 30 s (on)/ 30 s (off) for 30 min. The lysate was clarified by centrifugation (20,000 *g*, 30 min, 4 °C). Both mEGFP and mAPXmEGFP were purified from the supernatant by loading onto a nickel affinity column (Ni-NTA Agarose, Qiagen), washing with 100 mM imidazole, and elution with 300 mM imidazole. The eluate was desalted with a PD10-G25 (GE Healthcare) column and further purified on a HiLoad Superdex 200-pg column (GE Healthcare) in 10 mM phosphate buffered saline (pH = 7) containing 150 mM KCl (64). The concentration of the protein was estimated using an absorption coefficient for EGFP of 53,000 $M^{-1} \cdot cm^{-1}$ at 514 nm (65). The absorption coefficient for *holo*-APX is 107,000 $M^{-1} \cdot cm^{-1}$ at 410 nm (66). Using this value to estimate the amount of *holo*-mAPXmEGFP, the percentage of protein isolated in the *apo* form (97%; see main text) was determined.

Others have reported on the multimeric nature of APX (67) and EGFP (68). By utilizing monomeric forms of these proteins and avoiding the possibility of the fused construct oligomerizing through association of either heme-binding or fluorescent protein domains, a precise quantitative measurement of heme via fluorescence lifetime is possible. If one or both of the protein domains dimerizes in an APX + GFP construct, there will exist alternative pathways for nonradiative energy transfer between the fluorescent protein if there is more than one bound heme molecule. This will have an impact on the number of decay components and the intensity-weighted mean lifetime for the fluorescence emission. Hence, a monomeric sensor is essential to ensure a 1:1 stoichiometric interaction between the reporter and heme for quantitative mapping via lifetime measurements of heme concentrations in live cells. The sensor used in our experiments comprises the monomeric forms of both the heme-binding protein (the K14D/E112K variant of APX, referred to as mAPX), and mEGFP.

In Vitro Time-Correlated Single-Photon Counting of Fluorescence Emission from mEGFP and mAPXmEGFP. Time-correlated single-photon counting decay curves measured from in vitro protein samples (1 μM concentration of protein, in 10 mM potassium phosphate (pH = 7)), were measured using a Horiba Jobin Yvon fluorimeter (Fluorolog & Fluorohub) with pulsed laser excitation (478 nm; <200-ns pulse duration). Data sets of decay profiles were fitted globally to a multiexponential function using the FLIMfit software (69). Unless otherwise stated, all measurements were made at 37 °C.

Mammalian Cell Transfection. HEK293 cells purchased from the European Collection of Authenticated Cell Cultures were maintained in α-MEM (Gibco) supplemented with 10% fetal bovine serum (Gibco) at 37 °C and 5% CO_2. Cells were transfected with mAPXmEGFP in pLEICS-138 vector or mEGFP in pLEICS-12. Transfection was performed with Lipofectamine 3000 reagent (Thermo Fischer Scientific) according with the manufacturer's protocol. Stable cell lines were generated by selection with 500 μg/mL Geneticin (G418, Thermo Fischer Scientific) over a period of 3 wk. A Western blot was performed on lysates to estimate the concentration of mAPXmEGFP from

HEK293–pLEICS-138–mAPX cells using known quantities of recombinant protein spiked into wild-type HEK293 as a protein standard (*SI Appendix*, Fig. S4).

FLIM of Mammalian Cell Lines. Cells were seeded into CELLview dishes (Greiner Bio-One) and were grown in phenol red–free α-MEM media supplemented with 10% fetal bovine serum. Separate compartments on cell dishes were treated 24 h prior to imaging with either 1 mM succinylacetone or 10 μM heme (iron protoporphyrin IX chloride, hemin). FLIM was performed on a laser-scanning confocal microscope equipped with a pulsed white light laser (Leica SP8X; University of Bristol, Wolfson Bioimaging Facility). An excitation filter was used with a band pass centered at 488 nm, and fluorescence emission was collected between 495 and 550 nm. Cells were maintained at 37 °C, with 5% CO_2. A global-fitting algorithm for multiexponential models was applied to analyze all the pixel decay profiles in images recorded from cell lines expressing mEGFP or mAPXmEGFP (69). Individual values for the amplitudes and lifetimes of the decay components were used for both the calculation of free heme concentration (*SI Appendix*, section 3) and the calculation of the intensity-weighed mean lifetime, τ_{mean}, in order to generate color maps of the heme distribution in cells (see *Results*). If the photon count was below 200 for a single pixel in an image, then a black color was assigned to that pixel in the color maps. Any assigned color other than black reports a reliable value for τ_{mean}; a photon count of 200 was the threshold criteria in the FLIM experiments for the estimation of the decay parameters. Even in spatial locations of the cell in which the concentration of the sensor is low (i.e., in the nucleus, where photon counts were between 200 and 500), a consistent measurement of τ_{mean} was obtained across the pixels in these regions of a cell (see the white and red areas in Fig. 2*B*). As long as reliable and consistent values for the decay parameters could be determined, then it has been possible to report values for the concentration of free heme.

Data Availability. All study data are included in the article and/or *SI Appendix*.

ACKNOWLEDGMENTS. We would like to acknowledge Professor David Stephens (Department of Biochemistry, University of Bristol) for support in cell culturing and helpful discussions. We thank Dipti Vashi and Sharon Munday in the Protein Expression Laboratory (PROTEX-University of Leicester) for preparing the expression clones. We gratefully acknowledge the Wolfson Bioimaging Facility for their support and assistance in this work and BrisSynBio, a BBSRC/EPSRC-funded Synthetic Biology Research Centre (Grant Number: L01386X) for funding the FLIM microscope. The research was supported by the Leverhulme Trust (RPG-2016-397) awarded to A.J.H. and E.L.R.; G.C.-H.L. is grateful to the College of Science and Engineering, University of Leicester for a PhD studentship; and A.E.G. is grateful to the Engineering and Physical Sciences Research Council for a PhD studentship.

1. H. A. Dailey, *Biosynthesis of Heme and Cholorophylls* (McGraw-Hill, New York, 1990).
2. T. Matsui, M. Unno, M. Ikeda-Saito, Heme oxygenase reveals its strategy for catalyzing three successive oxygenation reactions. *Acc. Chem. Res.* **43**, 240–247 (2010).
3. R. O'Keeffe *et al*., Glutathione and the intracellular labile heme pool. *Biometals* **34**, 221–228 (2020).
4. O. Martinez-Guzman *et al*., Mitochondrial-nuclear heme trafficking in budding yeast is regulated by GTPases that control mitochondrial dynamics and ER contact sites. *J. Cell Sci.* **133**, jcs237917 (2020).
5. J. T. Groves, Enzymatic C-H bond activation: Using push to get pull. *Nat. Chem.* **6**, 89–91 (2014).
6. J. T. Groves, N. C. Boaz, Biochemistry. Fishing for peroxidase protons. *Science* **345**, 142–143 (2014).
7. K. D. Karlin, Bioinorganic chemistry: Model offers intermediate insight. *Nature* **463**, 168–169 (2010).
8. S. G. Sligar, Chemistry. Glimpsing the critical intermediate in cytochrome P450 oxidations. *Science* **330**, 924–925 (2010).
9. T. Shimizu *et al*., Gaseous O2, NO, and CO in signal transduction: Structure and function relationships of heme-based gas sensors and heme-redox sensors. *Chem. Rev.* **115**, 6491–6533 (2015).
10. T. Shimizu, A. Lengalova, V. Martínek, M. Martínková, Heme: Emergent roles of heme in signal transduction, functional regulation and as catalytic centres. *Chem. Soc. Rev.* **48**, 5624–5657 (2019).
11. H. Atamna, M. Brahmbhatt, W. Atamna, G. A. Shanower, J. M. Dhahbi, ApoHRP-based assay to measure intracellular regulatory heme. *Metallomics* **7**, 309–321 (2015).
12. A. G. Smith, E. L. Raven, T. Chernova, The regulatory role of heme in neurons. *Metallomics* **3**, 955–962 (2011).
13. H. Atamna, Heme, iron, and the mitochondrial decay of ageing. *Ageing Res. Rev.* **3**, 303–318 (2004).
14. K. R. Wagner, B. E. Dwyer, Hematoma removal, heme, and heme oxygenase following hemorrhagic stroke. *Ann. N. Y. Acad. Sci.* **1012**, 237–251 (2004).
15. K. T. Sawicki, H. C. Chang, H. Ardehali, Role of heme in cardiovascular physiology and disease. *J. Am. Heart Assoc.* **4**, e001138 (2015).
16. V. Jeney, G. Balla, J. Balla, Red blood cell, hemoglobin and heme in the progression of atherosclerosis. *Front. Physiol.* **5**, 379 (2014).
17. F. F. Dutra, M. T. Bozza, Heme on innate immunity and inflammation. *Front. Pharmacol.* **5**, 115 (2014).
18. J. D. Belcher, J. D. Beckman, G. Balla, J. Balla, G. Vercellotti, Heme degradation and vascular injury. *Antioxid. Redox Signal.* **12**, 233–248 (2010).
19. P. Pradhan, V. Vijayan, F. Gueler, S. Immenschuh, Interplay of heme with macrophages in homeostasis and inflammation. *Int. J. Mol. Sci.* **21**, 740 (2020).
20. G. Canesin, S. M. Hejazi, K. D. Swanson, B. Wegiel, Heme-derived metabolic signals dictate immune responses. *Front. Immunol.* **11**, 66 (2020).
21. R. Martins, S. Knapp, Heme and hemolysis in innate immunity: Adding insult to injury. *Curr. Opin. Immunol.* **50**, 14–20 (2018).
22. T. Hunt, G. Vanderhoff, I. M. London, Control of globin synthesis: The role of heme. *J. Mol. Biol.* **66**, 471–481 (1972).
23. A. Lodola, O. T. Jones, Evidence for a rapidly turned over pool of haem in isolated hepatocytes. *FEBS Lett.* **90**, 250–254 (1978).
24. D. Kuter, G. A. Venter, K. J. Naidoo, T. J. Egan, Experimental and time-dependent density functional theory characterization of the UV-visible spectra of monomeric and μ-oxo dimeric ferriprotoporphyrin IX. *Inorg. Chem.* **51**, 10233–10250 (2012).
25. W. Huang, A. Wilks, Extracellular heme uptake and the challenge of bacterial cell membranes. *Annu. Rev. Biochem.* **86**, 799–823 (2017).
26. J. M. Stevens, O. Daltrop, J. W. A. Allen, S. J. Ferguson, C-type cytochrome formation: Chemical and biological enigmas. *Acc. Chem. Res.* **37**, 999–1007 (2004).
27. R. G. Kranz, C. Richard-Fogal, J. S. Taylor, E. R. Frawley, Cytochrome c biogenesis: mechanisms for covalent modifications and trafficking of heme and for heme-iron redox control. *Microbiol. Mol. Biol. Rev.* **73**, 510–528 (2009).
28. Y. Dai, E. A. Sweeny, S. Schlanger, A. Ghosh, D. J. Stuehr, GAPDH delivers heme to soluble guanylyl cyclase. *J. Biol. Chem.* **295**, 8145–8154 (2020).
29. E. A. Sweeny *et al*., Glyceraldehyde-3-phosphate dehydrogenase is a chaperone that allocates labile heme in cells. *J. Biol. Chem.* **293**, 14557–14568 (2018).
30. A. Galmozzi *et al*., PGRMC2 is an intracellular haem chaperone critical for adipocyte function. *Nature* **576**, 138–142 (2019).
31. R. Chakravarti, K. S. Aulak, P. L. Fox, D. J. Stuehr, GAPDH regulates cellular heme insertion into inducible nitric oxide synthase. *Proc. Natl. Acad. Sci. U.S.A.* **107**, 18004–18009 (2010).
32. C. M. Casadei *et al*., Heme enzymes. Neutron cryo-crystallography captures the protonation state of ferryl heme in a peroxidase. *Science* **345**, 193–197 (2014).
33. H. W. Rhee *et al*., Proteomic mapping of mitochondria in living cells via spatially restricted enzymatic tagging. *Science* **339**, 1328–1331 (2013).
34. X. Yuan *et al*., Regulation of intracellular heme trafficking revealed by subcellular reporters. *Proc. Natl. Acad. Sci. U.S.A.* **113**, E5144–E5152 (2016).
35. S. Dastpeyman, R. Godin, G. Cosa, A. M. English, Quantifying heme-protein maturation from ratiometric fluorescence lifetime measurements on the single fluorophore in its GFP fusion. *J. Phys. Chem. A* **124**, 746–754 (2020).
36. S. Takeda, N. Kamiya, R. Arai, T. Nagamune, Design of an artificial light-harvesting unit by protein engineering: Cytochrome b(562)-green fluorescent protein chimera. *Biochem. Biophys. Res. Commun.* **289**, 299–304 (2001).
37. S. Takeda, N. Kamiya, T. Nagamune, A novel protein-based heme sensor consisting of green fluorescent protein and apocytochrome b(562). *Anal. Biochem.* **317**, 116–119 (2003).
38. J. A. Arpino *et al*., Structural basis for efficient chromophore communication and energy transfer in a constructed didomain protein scaffold. *J. Am. Chem. Soc.* **134**, 13632–13640 (2012).
39. S. Koga *et al*., Development of a heme sensor using fluorescently labeled heme oxygenase-1. *Anal. Biochem.* **433**, 2–9 (2013).
40. J. R. Abshire, C. J. Rowlands, S. M. Ganesan, P. T. So, J. C. Niles, Quantification of labile heme in live malaria parasites using a genetically encoded biosensor. *Proc. Natl. Acad. Sci. U.S.A.* **114**, E2068–E2076 (2017).
41. D. A. Hanna *et al*., Heme dynamics and trafficking factors revealed by genetically encoded fluorescent heme sensors. *Proc. Natl. Acad. Sci. U.S.A.* **113**, 7539–7544 (2016).
42. Y. Song *et al*., A genetically encoded FRET sensor for intracellular heme. *ACS Chem. Biol.* **10**, 1610–1615 (2015).
43. Y. Hisamatsu, N. Umezawa, H. Yagi, K. Kato, T. Higuchi, Design and synthesis of a 4-aminoquinoline-based molecular tweezer that recognizes protoporphyrin IX and iron(iii) protoporphyrin IX and its application as a supramolecular photosensitizer. *Chem. Sci. (Camb.)* **9**, 7455–7467 (2018).
44. K. Suhling *et al*., Imaging the environment of green fluorescent protein. *Biophys. J.* **83**, 3589–3595 (2002).
45. P. S. Ebert, R. A. Hess, B. C. Frykholm, D. P. Tschudy, Succinylacetone, a potent inhibitor of heme biosynthesis: Effect on cell growth, heme content and delta-aminolevulinic acid dehydratase activity of malignant murine erythroleukemia cells. *Biochem. Biophys. Res. Commun.* **88**, 1382–1390 (1979).
46. L. Liu, A. B. Dumbrepatil, A. S. Fleischhacker, E. N. G. Marsh, S. W. Ragsdale, Heme oxygenase-2 is post-translationally regulated by heme occupancy in the catalytic site. *J. Biol. Chem.* **295**, 17227–17240 (2020).
47. M. T. Nelp *et al*., Immune-modulating enzyme indoleamine 2,3-dioxygenase is effectively inhibited by targeting its apo-form. *Proc. Natl. Acad. Sci. U.S.A.* **115**, 3249–3254 (2018).
48. D. Garcia-Santos *et al*., Heme oxygenase 1 is expressed in murine erythroid cells where it controls the level of regulatory heme. *Blood* **123**, 2269–2277 (2014).
49. M. Sachar, K. E. Anderson, X. Ma, Protoporphyrin IX: The good, the bad, and the ugly. *J. Pharmacol. Exp. Ther.* **356**, 267–275 (2016).
50. P. Ponka, A. D. Sheftel, A. M. English, D. Scott Bohle, D. Garcia-Santos, Do mammalian cells really need to export and import heme? *Trends Biochem. Sci.* **42**, 395–406 (2017).

51. H. L. Bonkovsky *et al*., Porphyrin and heme metabolism and the porphyrias. *Compr. Physiol.* **3**, 365–401 (2013).
52. H. L. Bonkovsky, J. F. Healey, A. N. Lourie, G. G. Gerron, Intravenous heme-albumin in acute intermittent porphyria: Evidence for repletion of hepatic hemoproteins and regulatory heme pools. *Am. J. Gastroenterol.* **86**, 1050–1056 (1991).
53. C. Celier, T. Cresteil, Control of cytochromes P450 expression in gunn rat liver: Implication of the intracellular heme pool. *Arch. Biochem. Biophys.* **290**, 407–410 (1991).
54. T. V. O'Halloran, Transition metals in control of gene expression. *Science* **261**, 715–725 (1993).
55. S. I. Woodard, H. A. Dailey, Regulation of heme biosynthesis in Escherichia coli. *Arch. Biochem. Biophys.* **316**, 110–115 (1995).
56. S. Granick, P. Sinclair, S. Sassa, G. Grieninger, Effects by heme, insulin, and serum albumin on heme and protein synthesis in chick embryo liver cells cultured in a chemically defined medium, and a spectrofluorometric assay for porphyrin composition. *J. Biol. Chem.* **250**, 9215–9225 (1975).
57. R. K. Donegan, C. M. Moore, D. A. Hanna, A. R. Reddi, Handling heme: The mechanisms underlying the movement of heme within and between cells. *Free Radic. Biol. Med.* **133**, 88–100 (2019).
58. C. H. Langford, H. B. Gray, *Ligand Substitution Processes* (W. A. Benjamin, Inc., New York, 1965).
59. A. W. Foster, D. Osman, N. J. Robinson, Metal preferences and metallation. *J. Biol. Chem.* **289**, 28095–28103 (2014).
60. S. Hira, T. Tomita, T. Matsui, K. Igarashi, M. Ikeda-Saito, Bach1, a heme-dependent transcription factor, reveals presence of multiple heme binding sites with distinct coordination structure. *IUBMB Life* **59**, 542–551 (2007).
61. E. L. Carter, N. Gupta, S. W. Ragsdale, High affinity heme binding to a heme regulatory motif on the nuclear receptor rev-erbβ leads to its degradation and indirectly regulates its interaction with nuclear receptor corepressor. *J. Biol. Chem.* **291**, 2196–2222 (2016).
62. E. Jaumouillé, P. Machado Almeida, P. Stähli, R. Koch, E. Nagoshi, Transcriptional regulation via nuclear receptor crosstalk required for the Drosophila circadian clock. *Curr. Biol.* **25**, 1502–1508 (2015).
63. D. A. Zacharias, J. D. Violin, A. C. Newton, R. Y. Tsien, Partitioning of lipid-modified monomeric GFPs into membrane microdomains of live cells. *Science* **296**, 913–916 (2002).
64. H. Kwon *et al*., Direct visualization of a Fe(IV)-OH intermediate in a heme enzyme. *Nat. Commun.* **7**, 13445 (2016).
65. G. H. Patterson, S. M. Knobel, W. D. Sharif, S. R. Kain, D. W. Piston, Use of the green fluorescent protein and its mutants in quantitative fluorescence microscopy. *Biophys. J.* **73**, 2782–2790 (1997).
66. D. K. Jones, D. A. Dalton, F. I. Rosell, E. L. Raven, Class I heme peroxidases: Characterization of soybean ascorbate peroxidase. *Arch. Biochem. Biophys.* **360**, 173–178 (1998).
67. D. Mandelman, F. P. Schwarz, H. Li, T. L. Poulos, The role of quaternary interactions on the stability and activity of ascorbate peroxidase. *Protein Sci.* **7**, 2089–2098 (1998).
68. R. Y. Tsien, The green fluorescent protein. *Annu. Rev. Biochem.* **67**, 509–544 (1998).
69. S. C. Warren *et al*., Rapid global fitting of large fluorescence lifetime imaging microscopy datasets. *PLoS One* **8**, e70687 (2013).

JACS Au
AN OPEN ACCESS JOURNAL OF THE AMERICAN CHEMICAL SOCIETY

pubs.acs.org/jacsau

Perspective

Understanding the Logistics for the Distribution of Heme in Cells

Andrea E. Gallio, Simon S.-P. Fung, Ana Cammack-Najera, Andrew J. Hudson,* and Emma L. Raven*

Cite This: *JACS Au* 2021, 1, 1541−1555

Read Online

ACCESS | Metrics & More | Article Recommendations

ABSTRACT: Heme is essential for the survival of virtually all living systems—from bacteria, fungi, and yeast, through plants to animals. No eukaryote has been identified that can survive without heme. There are thousands of different proteins that require heme in order to function properly, and these are responsible for processes such as oxygen transport, electron transfer, oxidative stress response, respiration, and catalysis. Further to this, in the past few years, heme has been shown to have an important regulatory role in cells, in processes such as transcription, regulation of the circadian clock, and the gating of ion channels. To act in a regulatory capacity, heme needs to move from its place of synthesis (in mitochondria) to other locations in cells. But while there is detailed information on how the heme lifecycle begins (heme synthesis), and how it ends (heme degradation), what happens in between is largely a mystery. Here we summarize recent information on the quantification of heme in cells, and we present a discussion of a mechanistic framework that could meet the logistical challenge of heme distribution.

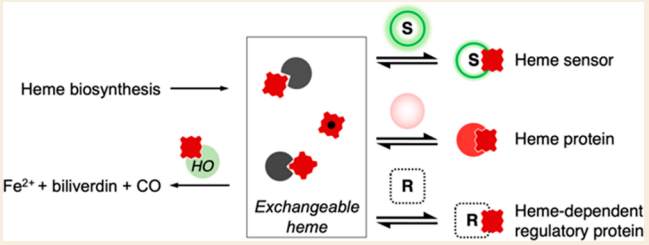

KEYWORDS: *heme, heme quantification, heme trafficking, heme homeostasis, heme sensors*

INTRODUCTION

Heme is a macrocyclic complex of iron, with the metal ion coordinated equatorially to the four nitrogen atoms of an electronically delocalized protoporphyrin IX ring (Figure 1A) and to one or two axial ligands. Broadly following an IUPAC convention that defines heme as a complex of iron coordinated to a porphyrin and to one or two axial ligands,[1] the term heme is used widely, and often interchangeably, to refer to different types of iron protoporphyrin IX where the precise heme structure (e.g., heme *a*, heme *b*, heme *c*, heme *d*, etc.) is not always elaborated. When one of these heme structures is bound to a protein, the two axial ligation positions are normally occupied by donor ligands provided by protein amino acids. Heme ligation to the side chains of His, Cys, Met, Tyr, Lys, Glu residues and even the N-terminus is known.[2,3] In binding to a protein in this way, the heme becomes either 5- or 6-coordinated, Figure 1B. By convention, the proximal position, which is most commonly a histidine, is assigned as the fifth ligand and is normally shown underneath the heme when visualizing heme structures. The sixth ligand, if there is one, is then drawn above the heme on the so-called distal side. This proximal/distal terminology dates back at least as far as the crystallography studies of Kendrew and Perutz.[4,5] The distal position can be occupied by a protein amino acid; by a diatomic gas (e.g., O_2, NO, CO); by water, hydroxide, or another small molecule ligand (e.g., H_2S, CN^-); or it can be vacant giving a 5-coordinate heme species. The reactivity of the heme is controlled in part by the number and identity of these

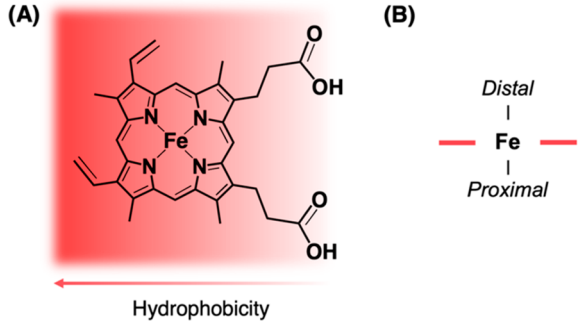

Figure 1. (A) The structure of iron protoporphyrin IX, also known as heme *b*. While heme is mostly hydrophobic, the carboxylate groups enable hydrogen-bonding interactions between the heme group and other molecules, including assisting the binding of heme to a protein. (B) The heme group is classified as containing distal and proximal sides, which are conventionally drawn above and below the plane of the ring, respectively. In heme proteins, the proximal side is usually bound to an amino acid residue provided by the protein; this helps to control its reactivity as a redox center[190,191] and its properties as a gas-binding molecule for storage and signaling.[11]

Received: June 25, 2021
Published: August 10, 2021

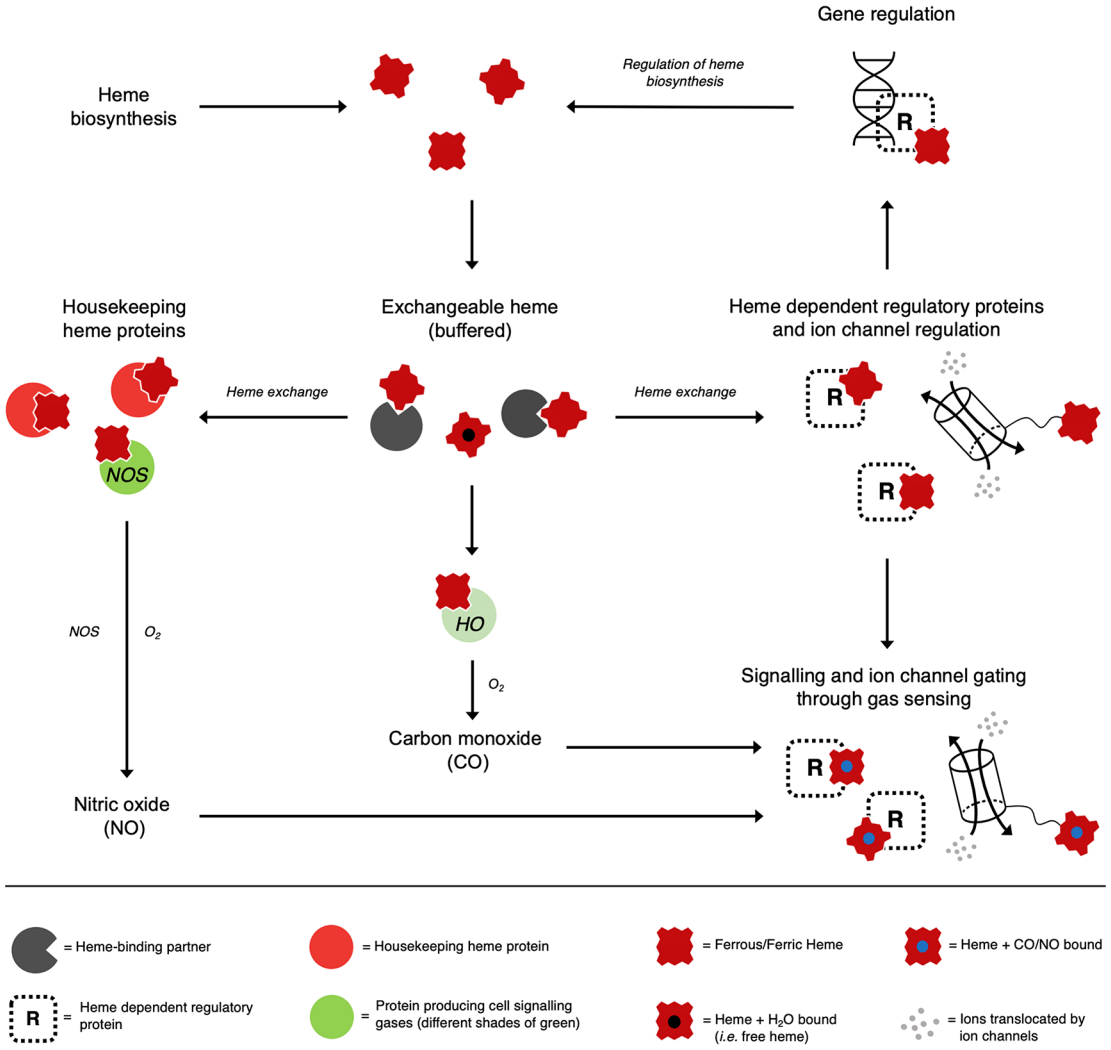

Figure 2. The possible interconnected pathways for the movements of heme in cells, and the links to signaling gases such as CO and NO. From the total heme synthesized in the cell (top), a proportion is bound irreversibly to heme-binding housekeeping proteins (red circles) that are essential for cell survival. A body of exchangeable heme is envisaged as being mostly weakly bound, soon after heme biosynthesis, to heme-binding partners (dark gray pacmans in this and other figures, which could be heme proteins or non-heme proteins) and available for exchange to heme dependent regulatory proteins (R, right). These heme-binding partners constitute an exchangeable, buffered, reservoir that can provide a flexible supply of heme and protect against changes in heme concentration. Once formed, these heme-bound proteins can serve in regulatory roles by, for example, binding to DNA for transcriptional control (top right; including the regulation of heme biosynthesis[17,21,28,37,192−194]) or to ion channels (middle and bottom right[54,195]). In green circles are shown the proteins that produce cell signaling gases—nitric oxide synthase (NOS, left) and heme oxygenase (NOS, middle). The synthesis of NO by NOS, and the production of CO by the heme degrading HO enzyme, adds multiple layers of complexity by coupling the formation of cell signaling gases to the heme-binding process. This would allow both CO and NO to bind to any heme protein with a regulatory function (bottom right) but could equally well occur for other heme dependent regulatory processes. It is worth noting that, while the binding of π-acid ligands like CO is traditionally associated exclusively with heme in its ferrous form, ferric heme has also been shown capable of binding CO/NO.[41] For the purposes of this review, movement of ferric/ferrous heme is presumed to mean heme *b*.

ligands at the proximal and distal positions, while stabilization of the heme molecule is further controlled by the heme-binding pocket via hydrophobic interactions with the porphyrin ring and vinyl groups, and hydrogen bonds between the propionate groups and the solvent.[6]

The role of the protein can thus be envisaged as solubilizing the hydrophobic and thus poorly soluble heme molecule, and in doing so controlling the reactivity of the heme group for biological purposes. Over the past several decades, most of what has been learned about the role of heme in biology relates to binding of heme to individual proteins such as those involved in oxygen transport (e.g., myoglobin, hemoglobin) and sensing (e.g., cytoglobin, neuroglobin),[7] bioenergetics (e.g., cytochrome *c*, cytochrome *c* oxidase),[6] metabolism and catalysis driven by the insertion of oxygen (e.g., cytochrome P450, indoleamine 2,3-dioxygenase),[6] peroxidase catalysis,[8] formation of nitric oxide,[9] and lipid metabolism (e.g., COX-2).[10]

In addition to these widely known roles for heme in biology, there is now a substantial body of evidence that identifies heme as a regulator of various cellular activities.[11−16] The first report, to our knowledge, of heme as a regulator was as far back as 1975, when heme was observed as regulating the synthesis of δ-aminolevulinic acid synthase which catalyzes the first step of the 8-step heme biosynthesis pathway.[17] We see chemical logic in the concept of regulatory mechanisms in cells that are linked to heme binding, but the idea of heme as a regulator laid dormant in the literature for many years. Despite its toxicity

https://doi.org/10.1021/jacsau.1c00288
JACS Au 2021, 1, 1541−1555

and lack of solubility, heme has a number of redeeming features that make it easier to understand why it could regulate cellular functions. The first is that heme is redox active and can respond to the redox status of the cell by modulating its oxidation state. The concentration of heme in cells is controlled by the balance of heme biosynthesis (to increase heme concentrations) and heme oxygenase activity (which degrades heme and produces CO as a byproduct). Cell signaling gases, such as O_2, NO, and CO, can bind rapidly and sometimes reversibly to heme—this could be exploited alongside the association of heme with a protein to create a second layer of regulatory control. CO is itself produced via degradation of heme by the O_2-dependent heme oxygenase enzyme,[18−20] and NO is produced by the heme- and O_2-dependent NO synthase enzyme;[9] i.e., the production of cell signaling gases also depends on the presence of heme. We envisage that the redox state of the cell, the oxidation state of the heme, the balance between heme synthesis and degradation, and the relative concentrations of O_2, NO, and CO may all be interconnected as outlined in Figure 2. This could be used as a versatile mechanism for cell signaling. Examples of heme-dependent regulation are beyond the scope of this review but have been summarized recently.[11,12] They include, among others, transcriptional regulation and gas sensing,[11,12,15] degradation of the p53 protein,[21] regulation of the circadian clock,[22−42] immune response,[43,44] aging,[45] and the gating of numerous ion channels.[46−69]

THE BIOLOGICAL NEED FOR HEME DISTRIBUTION

The fundamental requirement for heme across virtually all organisms—both in catalytic and regulatory roles as outlined above—means that cells need mechanisms to manage heme supply and distribution. Supply of heme is regulated by the well-studied heme biosynthesis pathway.[70] At the other end of the heme lifecycle, surplus heme (when it exists) is degraded by the O_2-dependent heme oxygenase enzyme.[18,19] But while the enzymatic machinery for making heme−heme synthesis—and removing heme−heme degradation—is well established, what happens in between is almost completely unknown. It has been recognized as far back as the 1970s[71,72] that cells need a supply of heme to respond to cellular demands, but until quite recently tools to examine this question have been lacking. In this review, we outline recent advances in the development of methods for measuring heme in cells, and we present ideas on, and possible mechanisms for, heme mobilization consistent with quantitative determinations of heme concentration.

TERMINOLOGY

To begin the discussion, we describe and define the terminology. For the purposes of this review, we take heme (in the context of heme transport) to mean heme *b*. Literature on the role and distributions of heme in cells has used a bewildering, and at times imprecise, range of terminologies. Phrases such as "labile heme", "regulatory heme", "free heme", and "heme pool" are all used in the literature, often interchangeably.[73] While the need to discriminate between these types of heme in cells is obvious, it is challenging to provide a precise description of each. What does "labile heme" mean? How can "free heme" exist in the cell, given that heme is cytotoxic and poorly soluble? Does the phrase "regulatory heme" describe a supply of heme dedicated *exclusively* for regulatory purposes, or might it be used for other purposes? Given its insolubility and cytotoxicity, does it actually make sense to talk about "pools" of heme when current estimates for heme concentration are in the nM to μM range?[74−79] The lack of precise descriptions for the nature of different types of heme can lead to confusing or contradictory interpretations. Below we provide a summary and offer some suggestions, which we hope will be helpful in future discussions for both specialists and newcomers to the field.

Regulatory Heme

In disciplines that vary from blood disorder (e.g., porphyria),[80,81] gene expression,[71,72] and heme biosynthesis,[82,83] a small portion of the total heme content of the cell has been referred to over many years as being present in a regulatory or intracellular heme pool. These terms originate from early papers[71,72,83−86] where it was also suggested that the nature of heme was a free molecule (see below). The existence of a form of regulatory heme is conceptually useful, and because of this the nature of regulatory heme has been debated as long ago as 1975 when new roles for heme—above and beyond the traditional roles in oxygen binding, electron transfer, and catalysis—were identified by Granick.[83] In Granick's work, the regulation of heme biosynthesis was proposed as being controlled by fluctuations in the concentrations of heme in a dedicated heme pool where heme was envisaged as being weakly associated with an ensemble of cytosolic proteins.[83,87] These weak binding interactions were considered important for heme to be readily exchangeable.[83,86] The terms were then later adopted by scientists in multiple fields.[46,80,88−98] Hence, since Granick's initial studies, the phrases "regulatory heme" and "free heme" have been widely used although not precisely defined.

Free Heme

To the best of our knowledge, the term free heme was introduced in the 1970s[72,85,99] and was interpreted as an intracellular population of free heme molecules either on their own (free) or all together (in a pool). These early papers noted the difficulties associated with the idea of a pool of free heme, but, nevertheless, the concept and the terms "free heme" and "pool of free heme" became ingrained in the literature.[85,92,94,95,100,101] The term "free heme" has never been precisely defined—broadly speaking it has been taken to mean a heme molecule that is not bound to anything else. There are difficulties with that idea, however, and the concept of large amounts of free heme, because heme is cytotoxic through Fenton chemistry and radical formation.[92,94,96,102−104] So if heme is free in the cells, it would cause problems. Heme is also a hydrophobic molecule and poorly soluble, so presumably cannot exist in cells without being solubilized by binding to a protein, cellular membranes,[105] or even nucleic acids.[45,106] Moreover, heme needs to be ligated at the fifth and sixth ligation position, otherwise, it will stack to form dimers, or higher multimers, in solution.[107,108] This is problematic for cellular handing because, in a dimeric or multimeric form, heme could not be delivered to proteins that require only one molecule per binding site.

We envisage that a "free" molecule of heme can therefore only exist transiently in cells. In this review, we will use the term "free heme" to indicate molecules of iron protoporphyrin IX, in the ferrous or ferric oxidation state, existing in the absence of any protein binding partner but weakly associated with water molecules as ligands at the fifth and sixth coordination sites.

https://doi.org/10.1021/jacsau.1c00288
JACS Au 2021, 1, 1541−1555

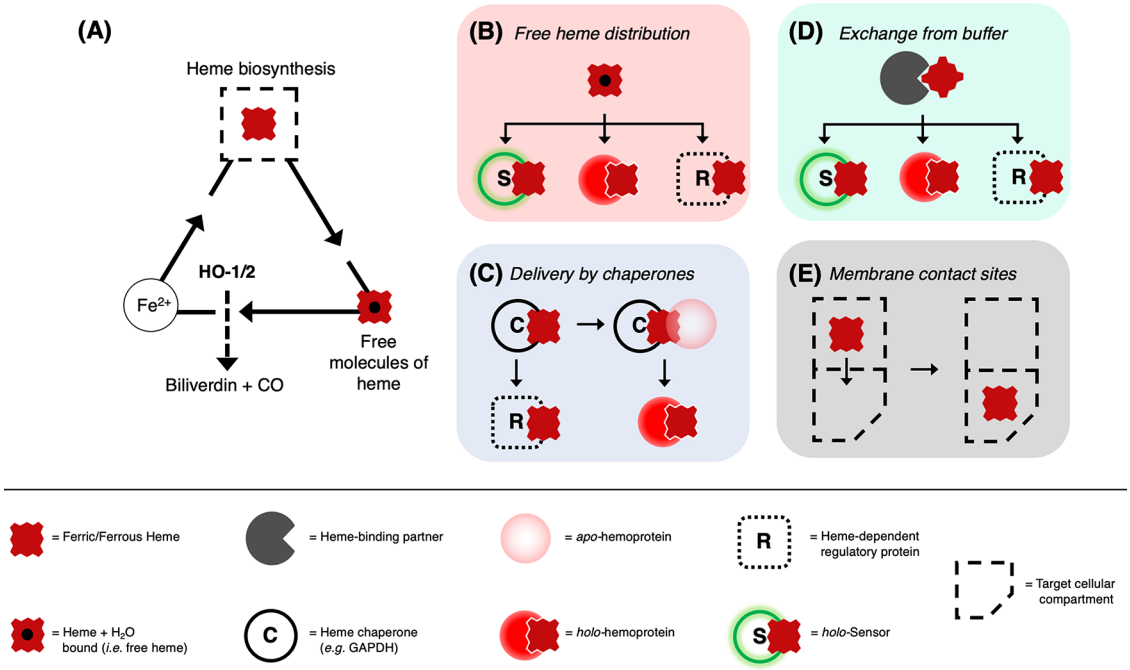

Figure 3. Representation of possible mechanisms for distribution and delivery of heme across the cell. (A) The life cycle of heme in cells starts with its biosynthesis in the mitochondria (full dashed square) and ends with its degradation by heme oxygenase (HO-1/2). Heme oxygenase generates Fe^{2+} which can be recycled for the synthesis of new heme molecules. A balance between synthesis and degradation contributes to the controlling heme concentrations in cells. (B–E) The supply of heme to the locations where it is in demand is suggested as occurring via four possible mechanisms (colored panels). In (B), direct distribution of free heme into a heme protein (red circle), a heme-dependent regulatory function (R, white box), or a genetically encoded/synthetic heme sensor for quantification studies (S, green circle). Free heme (either ferrous or ferric) is envisaged as being present in minuscule concentrations but will still represent a mechanism for heme to be made available in cells.[77] In (C), chaperone-mediated heme delivery to an *apo*-heme protein (pale red circle), for example by GAPDH.[113−115] In (D), heme bound to heme-binding partners (dark gray pacman) constitutes a body of exchangeable heme readily available for downstream applications, in the same way as in (B). Possible candidates for heme-binding proteins are IDO, HBP22/23, SOUL, and albumin.[111,163,196] In (E), distribution of heme via membrane contact sites between mitochondria—where heme is synthesized—to target cellular compartments which bypasses the need for transporters to mediate the delivery of heme.[171]

Labile Heme

In recent years the term "labile heme" has appeared.[44,78,96,105,109−120] The use of this term allows a distinction to be made between the proportion of the total heme content that is available for mobilization, and the proportion that is unavailable (or, more precisely, inert for exchange) because it is bound with a high affinity, and therefore irreversibly, to proteins. Ideas on what the concepts of labile heme actually means mimic the early ideas on free heme.[83,87] Labile heme is envisaged as being continuously engaged in transient binding to intracellular proteins that exist to actively buffer heme concentrations in the cell. Since some heme is unavailable for distribution in cells, labile heme is thus envisaged as a intermediary through which heme can move and be distributed through the cell.[105,110−112] The term labile heme probably finds its origins as an adaptation of "labile iron pool" that predated it.[121]

Exchangeable Heme

The use of the term lability to distinguish a more mobile fraction of the total heme from that which is permanently (irreversibly) embedded into heme proteins is similar in concept to the kinetic lability of ligands in inorganic metal complexes.[122−124] Labile ligands exchange very fast, and inert ligands exchange slowly. But the availability and distribution of heme will be defined not just by the kinetic lability of the ligands bound to the heme, but also by thermodynamics. This is because cascades of heme exchange events down a thermodynamic gradient (dictated by heme binding affinity) will control the overall distribution of heme. Hence, our opinion is that "exchangeable heme"—which has been adopted in a limited number of examples[77,86,97,125]—is a more precise term to convey the concept that both kinetic and thermodynamic processes are relevant when considering the bioavailability of heme.

Definitions Used in This Review

We propose here a working set of definitions.

Total Heme (H_t). The total heme content of a cell. This includes the fraction of heme that is bound irreversibly to proteins and thus not available for other purposes (defined here as H_h), and the fraction of exchangeable heme (which includes small quantities of free heme, see below).

Exchangeable Heme (H_e). A fraction of the total heme that is reversibly bound to proteins or small ligand molecules (e.g., free amino acids, H_2O). Exchangeable heme can be considered as a reservoir that provides an accessible supply of heme to the cell.

Free Heme (H_f). Molecules of heme that are not bound to a protein but weakly coordinated with water molecules. We expect free heme to exist in vanishingly small quantities. Long and co-workers[126] have recently offered a definition for free heme which is similar to that proposed here.

https://doi.org/10.1021/jacsau.1c00288
JACS Au 2021, 1, 1541−1555

In principle, $H_t = H_h + H_e + H_f$, where H_h is the amount of heme that is bound irreversibly to heme proteins (including membrane and cytosolic proteins).

THE LOGISTICS OF HEME SUPPLY AND DEMAND

Given the need to move heme from its place of synthesis (in the mitochondria) to other regions of the cell, how can cells control the balance of supply and demand and what mechanisms are in place to do this?

Controlling Supply and Demand

The balance between heme biosynthesis and degradation is part of the regulatory control that the cell needs to maintain heme availability below the cytotoxic threshold (Figure 3A).[94,102,127] Heme oxygenase, whose mechanism of degradation of heme into biliverdin and CO is well-known,[18,19] plays a crucial role in maintaining this balance. Heme oxygenase-1 is transcriptionally regulated and induced by infection, inflammation, oxidative stress or increasing concentrations of heme.[128,129] Interestingly, the post-transcriptional regulation of heme oxygenase-2 (abundant in the brain, testes, and neural tissue) has been shown to be controlled by heme occupancy in the active site.[130] Specifically, heme oxygenase-2 appears to be destabilized and more likely to be degraded when heme is not bound, which is the likely situation under conditions of heme deficiency and when high heme oxygenase activity is undesirable. This regulation would help to keep heme concentrations within a suitable physiological range under conditions of cellular heme deficiency.[130]

The Involvement of Heme Chaperones

The existence of biological chaperone systems is documented for other redox active transition metal ions (e.g., iron, copper, molybdenum, cobalt, nickel).[131−134] Cells adopt strategies to tightly regulate the concentrations of different metals ions, ensuring suitable levels of bioavailability, effective physiological responses, and prevention of cytotoxicity.[133−149] The concentration of transition metal ions in cells is kept at very low levels to avoid inappropriate activation of signaling pathways. For instance, the intracellular free copper concentration in *S. cerevisiae* is limited to less than one molecule per cell.[133,137] Similarly, free zinc is estimated in the low femtomolar range in *E. coli*.[133,136] Instead of being free to circulate around the cell, metal ions are stored, locked in an inaccessible state, and released to a network of chaperones or chelators that control their delivery, repurposing, and ensure fidelity in metalation when two competitive metals can bind to the same site.[134,138−144] By comparison, it is reasonable to presume that cells use similar principles for the movement and distribution of free heme (Figure 3C,D).

The identification of heme chaperones with the specific role of transporting and selectively delivering heme to downstream proteins would thus clarify the picture considerably. But very few heme chaperones have been identified over the years. A notable example is the CcmE chaperone, part of the multi component Ccm membrane heme maturation machinery for heme translocation to cytochrome *c* in most proteobacteria, archaea, deinococcales, and plant mitochondria.[150−153] However, this is a special case as it speaks only to the need for formation of covalent links to heme in the specialized *c*-type cytochromes. GAPDH is perhaps the most compelling example of a heme chaperone so far identified.[113−115,154] The interaction between GAPDH and heme was initially thought to occur to protect heme from degradation during its transport (which at the same time reduces its cytotoxicity).[155] But GAPDH has since been found to be responsible for the delivery of heme to the nuclear transcription factor Hap1[156] in *S. cerevisiae*, to cytosolic iNOS in mouse macrophage cells,[113] and to soluble guanylate cyclase in HEK293 cells.[114]

The involvement of GAPDH in heme delivery in both yeast and mammalian systems is indicative of a broadly conserved strategy for heme transport.[113] GAPDH is primarily a glycolytic enzyme, and, therefore, its function as a heme chaperone looks to be opportunistic as far as the cell is concerned. This begs the question as to whether there are other as-yet unidentified heme chaperones lurking about the cell in disguise. Certainly, if heme chaperones are used at all then more than one could be required to create an effective supply chain. Arguably, chaperones of chaperones might even exist.[115] But if heme binding can be opportunistic and does not need a specific heme-binding motif—as GAPDH seems to indicate—then identification of heme chaperones becomes an incredibly demanding task which would need to take into account noncanonical heme-binding motifs in addition to the large number of proteins with known heme-binding sites.[3,157]

All of this leads us to the conclusion that existing, well-known heme-binding proteins could be repurposed for the task of cellular heme delivery under certain conditions. For example, indoleamine 2,3-dioxygenase, whose mechanism and structure is well-documented,[158−162] has recently been shown to lose its heme under certain conditions,[163] which suggests the possibility that it could be used as a source of heme in specific regions of cells. In all likelihood, there may be other cellular proteins that can similarly masquerade as heme chaperones.

Possible Limitations on the Utility of Chaperones for the Distribution of Heme

The distribution of heme via chaperones can be used to explain how heme moves from the mitochondria to other locations, and then subsequently to the endoplasmic reticulum for degradation by heme oxygenase. But the chaperone mechanism is ill-equipped to deal with rapid changes in heme availability. If increases or decreases in heme concentration are required, then the rate-limiting steps are heme synthesis and degradation. Upregulation of heme synthesis, by expression of the ALA synthase enzyme, in response to low heme availability could take at least 30 min,[164] while induction of heme oxygenase-1 for heme degradation could take hours.[165] Both of these mechanisms are too slow by far if rapid control of heme concentration is required, for example in the case of ion channel regulation which is necessary for appropriate cardiac function.[54] Hence, if the cell is solely reliant on heme chaperones, then it runs the risk of spikes in heme availability should there be a mismatch in timings between the delivery and the removal of heme. Taken together, and bearing in mind the failure (so far) to identify large numbers of heme chaperones, we suggest that complementary mechanisms will be required to regulate heme distribution. We elaborate on this below.

Buffering of Free Heme Concentration as a Mechanism of Control

An ability to store heme in cells would decrease the reliance of cells on heme synthesis and degradation and could be coupled to mechanisms to make heme more or less available, on-demand and at speed (Figure 3D). To date, there have been no proteins identified that have the dedicated function of

https://doi.org/10.1021/jacsau.1c00288
JACS Au 2021, 1, 1541−1555

Table 1. Summary of Reported Cellular Heme Concentrations from Known Heme Reporters or Fluorescent Heme Sensors

reporter	heme probe	fluorescent tag(s)	$K_{d,heme}$ (nM)[a,b]	measured heme concentration (nM)	quantitation method	tested in	ref.
CYSDY-9	IsdX1, IsdC	ECFP, EYFP	63.5 ± 14.3	Cytosol 25.6 ± 5.5 Mitochondria 23.3 ± 4.9 Nucleus 31.0 ± 7.0 ER 5.4 ± 1.4[c]	FRET	HeLa	76
HS1	Cytochrome b_{562}	EGFP, mKATE2	3 (ferric), <1 (ferrous)	Cytosol 20−40 Nucleus <2.5 Mitochondria <2.5	FRET	*S. cerevisiae*	79
CHY	*P. falciparum* Histidine rich protein	ECFP, EYFP	∼250	Cytosol 1600	FRET	*P. falciparum*	78
apo-HRP	Horseradish peroxidase	–	–	600	peroxidase activity[d]	Human lung fibroblasts (IRM90)	73,97
apo-HRP	Horseradish peroxidase	–	–	2100 ± 2	Reconstitution of catalytic activity[d]	Human erythrocytes	74
apo-HRP	Horseradish peroxidase	–	270 ± 40	433 ± 125	Reconstitution of catalytic activity[d]	HEK293	75
mAPXmEGFP[e]	Ascorbate peroxidase	mEGFP	22	Cytosol 4	RET	HEK293	77

[a]The heme affinity, or conversely the dissociation constant $K_{d,heme}$, is a key parameter in heme quantitation. $K_{d,heme}$ values should be close to the physiological concentrations of heme (in the nM to μM range), to ensure prompt response of the sensor to changes in [heme] but also avoiding the sensor becoming either fully saturated or fully unsaturated (which is essential to study dynamic cellular processes). $K_{d,heme}$ defines the fraction of total cellular heme which is available for donor−acceptor heme exchange (acceptor = *apo*-heme sensor). Heme sensors with the highest heme affinities will accept heme from a larger ensemble of heme donors, and vice versa. Caution is needed when comparing heme concentrations obtained with different sensors, as the sensors with lower $K_{d,heme}$ will draw heme from a larger number of donors. [b]For ferric heme unless otherwise stated. [c]A relatively low concentration of heme was measured in the endoplasmic reticulum of HeLa cells compared to other cell lines (mouse melanoma B16, human HCT116 colon cancer cell, human PANC-1, hamster kidney fibroblast BHK-21, and CHO), which was interpreted as due to the high expression levels of heme oxygenase-1 in the endoplasmic reticulum surface of HeLa cells. [d]*holo*-HRP was formed by mixing *apo*-HRP with HEK293 lysates. The reconstitution of the catalytic activity of the HRP reporter by its binding to cellular heme was then used to measure heme concentration. [e]mAPX = monomeric APX; mEGFP = monomeric EGFP.

storing heme, but there is evidence, from recent work,[77] of a buffering capacity within cells that can accommodate changes in either the total concentration of heme (i.e., $[H_t]$), or the concentration of exchangeable heme (i.e., $[H_e]$), while maintain the capability to mobilize heme as and when necessary. As indicated above, it is entirely possible that known heme proteins (such as indoleamine 2,3-dioxygenase, and GAPDH) participate in the buffering of free heme concentration ($[H_f]$) and protect the cell against increases or decreases in total, or exchangeable, heme concentration. In this scenario for heme buffering, the ability of any given protein to acquire heme is based on how well it competes for heme (i.e., the heme affinity) against other proteins. Hence the availability of heme in the cell would be dependent entirely on the K_d, and abundance, of these heme-binding partners. In this way, the concentration of free heme is buffered—or, in other words, the availability of heme is kept within a limited range—by the many heme-binding proteins in the buffer and would be distributed among those proteins according to their relative heme affinities.

Crucially, in this buffering model the hierarchy of heme-binding affinity would be responsive to changes in the composition of the buffering proteins. As an example, upregulation of proteins in the buffer with high heme affinity (e.g., a globin, or a cytochrome) would deplete the capacity of the exchangeable heme reservoir to release heme, as heme was dragged to thermodynamically inaccessible sites. As well as providing a reservoir of exchangeable heme able to meet the localized and instantaneous demands of the cell, such a buffering system would, along with the heme degradation pathways, prevent heme-induced cytotoxicity by limiting the concentrations of free heme within the cell. The interplay between heme biosynthesis, degradation, transcriptional and post-transcriptional regulation of heme buffering proteins, are all envisaged as jointly contributing to the buffering of heme in cells.

Trafficking through Membranes

Evidence is emerging for the involvement of biological membranes as important factors in the trafficking of cellular heme. Heme has been shown to be capable of diffusing or even being retained by cellular lipid bilayers[166−168] and examples of putative membrane heme transporters have been identified, most notably the mitochondrial exporter Flvcr1b, which have been reviewed elsewhere.[94,169] But while heme may or may not necessitate membrane transporters for its movement across compartments, the contribution of lipid bilayers to heme trafficking is still not completely clarified. A recent study has proposed that the trafficking of heme through membranes does not rely on transporters and is, in contrast, a chaperone-less pathway made possible by interorganellar contact sites. This provides an elegant solution for the exchange of heme between compartments (Figure 3E).[170,171]

QUANTIFYING HEME CONCENTRATIONS IN CELLS

Early Estimation of Heme Concentration

Granick speculated in the 1970s[83,87] that the concentration of exchangeable heme in the cytosol was in the range 10−100 nM. This value is, in fact, remarkably close to recent measurements (Table 1). In the past, the cellular heme concentration has had to be inferred from the amount of heme measured in soluble cell lysis extracts determined using either fluorometric approaches[172] or enzymatic reconstitution

https://doi.org/10.1021/jacsau.1c00288
JACS Au 2021, 1, 1541−1555

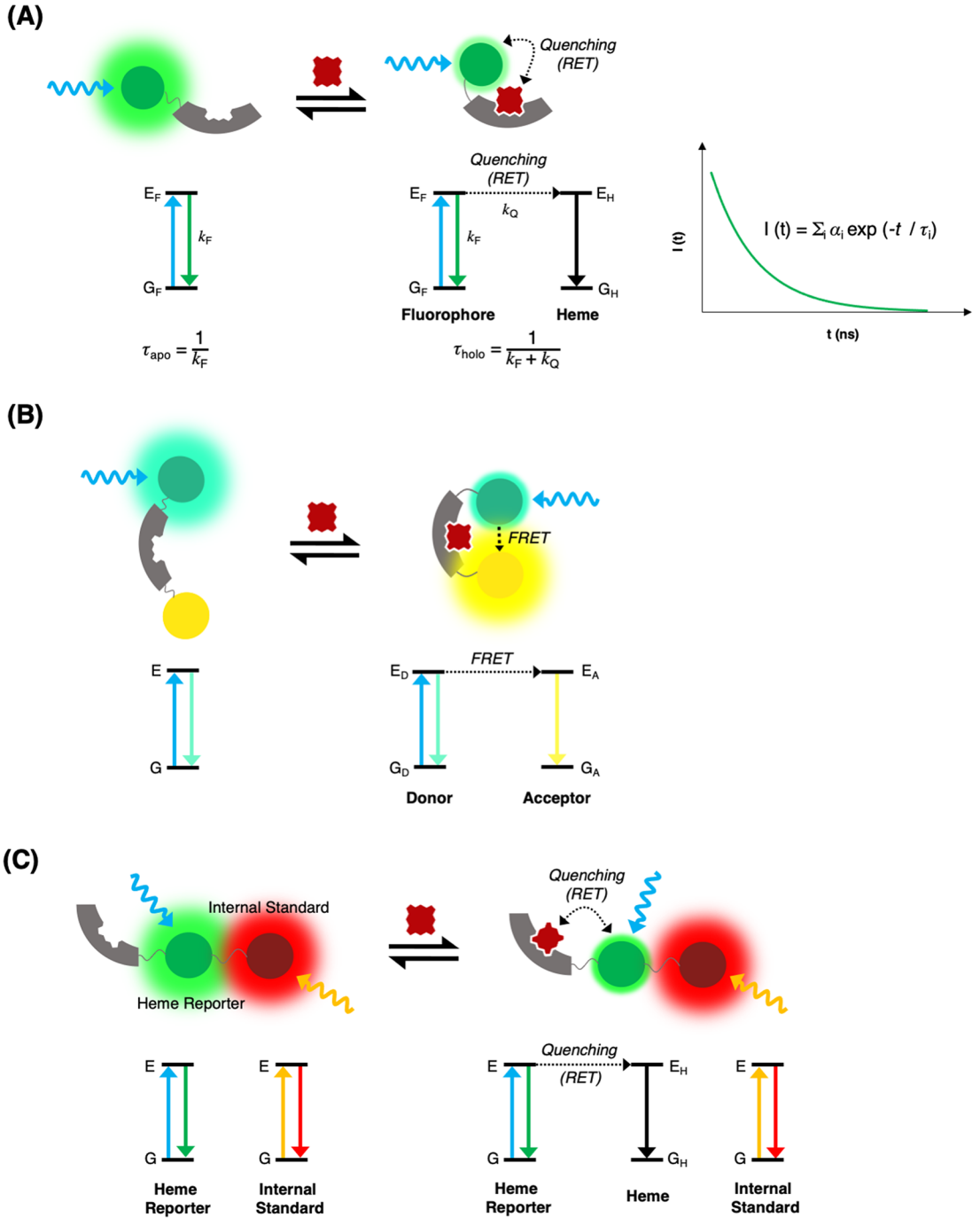

Figure 4. Basic principles of heme sensor designs. (A) RET sensors: Heme-binding to this type of sensor introduces an additional relaxation pathway for the electronic excited state of the fluorophore. The mean fluorescence lifetime of the probe changes between the limiting values of τ_{apo} to τ_{holo} for the pure *apo* and *holo* forms of the sensor dependent on heme concentration.[77] (B) FRET sensors: The heme-binding domain of the sensor undergoes a conformational change that brings two fluorophores into close proximity to one another. In this example, Förster energy transfer results in a decrease in the emission of a green fluorophore and an increase in emission of a yellow fluorophore. Hence changes in the relative emission intensities of the two fluorophores can be used to determine heme concentration.[76] Multiple heme-binding sites may be present in the heme-binding domain.[78] (C) A RET sensor (similar to that shown in (A)) that incorporates an additional fluorophore in order to measure a ratiometric intensity. The sensor is composed of two fluorophores, but heme-binding triggers the selective quenching of the fluorescence of only one of them. The unperturbed tag can then be used as an internal reference to monitor the changes in the intensity of emission for the quenched fluorophore, providing a method for precise heme quantitation.[79,112]

techniques.[74,89,97,173] These methods are likely to report a concentration that lies somewhere between that for exchangeable heme ($[H_e]$) and the total amount of heme present in the cell ($[H_t]$) because the denaturing methods lead to release of heme from many heme proteins. In order to selectively measure concentrations of exchangeable heme, it is necessary to use a method that is compatible with in vivo fluorescence imaging or spectroscopy of live cells.[174] Such an approach is possible by the design and application of genetically encoded

https://doi.org/10.1021/jacsau.1c00288
JACS Au 2021, 1, 1541−1555

heme sensors which can be expressed recombinantly in different cell lines.

The Development of Cellular Heme Sensors

Genetically encoded sensors comprise a heme-binding protein conjugated to one or more fluorescent proteins. For the sensor to report on the presence and quantify the concentration of heme, the fluorescence output must be modulated by heme binding. There are different mechanisms that can lead to suitable modulation of the fluorescence output.

a. Förster Resonance-Energy Transfer between the Fluorescent Protein and a Bound Molecule of Heme. The heme-binding pocket of the sensor must be located in close proximity to the chromophore-forming amino acids in the fluorescent protein, and the emission of the fluorescent protein must have spectral overlap with either the Soret or Q absorption bands of heme.[175] In this case, resonance-energy transfer provides a nonradiative decay pathway for the photoexcited state of the chromophore, via the heme moiety, that competes with the radiative-decay pathway responsible for the fluorescence signal (Figure 4A,C).

b. Förster Resonance-Energy Transfer between a Pair of Fluorescent Proteins. Unlike in (a), the heme-binding pocket must be distant from both fluorescent proteins, and, instead, the binding of heme to the sensor must lead to a conformational change that brings the chromophore-forming amino acids on each of the fluorescent proteins (i.e., the donor and acceptor sites) into close proximity; see Figure 4B. In this case, resonance-energy transfer between the donor and acceptor leads to subsequent radiative decay from the acceptor. Hence the binding of a molecule of heme is detected by the attenuation of the short wavelength emission band of one the fluorescent proteins (the donor), and the appearance of the long wavelength emission band of the other fluorescent protein (the acceptor).

In order to distinguish between the mode of operation of these two different designs for heme sensors, we will refer to the mechanism described in (a) as just resonance-energy transfer (RET) and the mechanism described in (b) as fluorescence resonance-energy transfer (FRET).

Further consideration is given here to the heme sensor design comprising a heme-binding domain and a single fluorescent protein (i.e., that shown in Figure 4A). If the distance between the chromophore-forming amino acids on the fluorescent protein and the heme-binding pocket, r, is much less than the Förster distance, R_0 (calculated from the spectral overlap integral[175]), then the efficiency of RET in the *holo*-sensor will be near to 100%. The fluorescence quantum yield of the *holo*-sensor (i.e., the sensor with heme bound to it) will be near to 0%, and the presence of heme can be inferred from the quenching of the intensity of the fluorescence emission. Alternatively, if the distance r is close to the R_0, then there will be an intermediate efficiency for RET in the *holo*-sensor (given by $100\% \times 1/(1 + (r/R_0)^6)$. The fluorescence quantum yield of the *holo*-sensor will be reduced (but will not equal zero), and the presence of heme can be inferred from either the reduction in the emission intensity or from a reduction in the fluorescence lifetime.

A change in the fluorescence lifetime can be observed by time-correlated single photon counting, where the proportions of the *apo*- and *holo*-forms of the sensor can also be deduced by determining the relative amplitudes of functions in the fitting of a multiexponential decay model, Figure 4A. For a genetically encoded heme sensor, a measurement of a fluorescence decay profile has significant advantages over a measurement of fluorescence intensity: (i) The fluorescence decay can be used to determine the ratio of *holo*- to *apo*-forms of the sensor, but the intensity can only be used to detect the *apo*-form of the sensor (because the *holo*-form of the sensor is quenched). Sensor designs that rely on measurements of fluorescence quenching require an additional tag (distant from the heme-binding pocket and the other chromophore site) to normalize the signal intensity. (ii) The quantitative accuracy of fluorescence lifetime imaging or spectroscopy is independent of the inner filter effect or partial photobleaching of the fluorescent protein.

Another property of the emission of a fluorescent protein is the anisotropy (polarization), which might be modulated by changes in the rotational diffusion between the *apo*- and *holo*-forms of the sensor. The sensitivity of a polarization measurement will be highly dependent on the local viscosity and, as yet, it has not been exploited in the context of heme sensing.

Maintaining Homeostasis in the Presence of Heme Sensors

The in vivo deployment of a heme sensor in cells introduces an additional heme-binding species into the cellular milieu. Hence the sensor will compete with other heme-binding proteins in the cell for molecules of exchangeable heme. While there would be no issue with the sensor competing for heme with either heme-binding proteins, or small molecules, whose roles are to buffer the concentration of free heme, it is critical that this competition does not extend to bona fide heme proteins that require heme either for their function or to adjust their properties. To accurately measure the availability of heme in cellular compartments, the expressed sensor must integrate into the network of buffering partners, and its presence must not result in a significant change either to the amount of exchangeable heme (H_e) associated with these heme-binding partners, or to the miniscule amount of free heme (H_f) in the cell. For a certain concentration of exchangeable heme, it is fairly straightforward to estimate an appropriate range of concentrations for the sensor that will preserve heme homeostasis in the cell.[77] On the basis of measurements in the cytosol of HEK293 cells,[77] a sensor concentration of up to 1 μM would not be expected to alter the availability of heme for exchangeable heme concentrations equal to, or in excess of, 3 μM. It is realistic to assume that, if a sensor is deployed in a localized area of the cell (e.g., directed specifically to the nucleus), then the sensor concentration may exceed 1 μM. Hence, we anticipate that, in future, controlling the concentration of expressed sensor will be increasingly important.

Summary of Known RET and FRET-Based Heme Sensors

There are a number of reports of different fluorescent heme sensors in the literature. We summarize them briefly below. Heme concentrations reported from the studies of these sensors are given in Table 1.

In the early 2000s, Takeda et al. provided the first proof-of-concept for a heme sensor. The sensor comprised an EGFP-cytochrome b_{562} fusion protein,[176] and it was subsequently optimized for enhanced RET.[177] Fluorescently labeled variants of heme oxygenase-1 (K18C[178] and D140H[179] variants) have also been used to detect heme in vitro. These sensors were a step forward in terms of heme quantification, but were not

https://doi.org/10.1021/jacsau.1c00288
JACS Au 2021, 1, 1541−1555

deployed in cells for real-time monitoring of heme concentrations.

The first genetically encoded heme sensor was CYSDY-9.[76] CISDY-9 was designed to exploit the natural dimerization of a pair of bacterial chaperones (IsdX1 and IsdC). Tagging each chaperone with a fluorescent probe and linking them with a short peptide tether produced an intracellular FRET reporter which was used to analyze heme population in HeLa cells, Table 1. With the exception of the endoplasmic reticulum, heme concentrations were found to be evenly distributed across the cytosol, the mitochondria and the nucleus, which is different from the observations in yeast (see above and ref 79). It may be the case that results from different sensor systems cannot be directly compared, see Table 1.

Cytochrome b_{562} was later engineered with EGFP and mKATE2 fluorescent tags. This created a sensor that could be deployed in cells[79] in which the fluorescence intensity of EGFP was quenched (via RET) on heme-binding; the intensity of mKATE2 was unchanged providing a means of assessing heme concentration by ratiometric analysis. A somewhat heterogeneous distribution of heme throughout yeast cells was reported, Table 1, and the behavior of the sensor in cells[112] supported the concept of a (buffered) reservoir of exchangeable heme that is readily available for regulatory roles and crucial in the overall physiology of yeast. The same sensor was then utilized to demonstrate that heme delivery from mitochondria—the place of heme biosynthesis—to the nucleus was 25% faster than to the cytosol and the mitochondrial inner matrix. The authors suggested direct membrane contacts between mitochondria and the ER as a possible pathway for heme delivery to the nucleus.[170,171]

A genetically encoded (FRET-based) heme sensor based on histidine rich protein 2 has been used to quantify heme concentrations in the parasite *P. falciparum*.[78] In this case, heme concentrations are higher (ca. 1.6 μM), but this is not completely unexpected considering that 80% of the amount of heme contained in a human body is synthesized by red blood cells.[73]

Peroxidase-based fluorescent sensors, based on horseradish peroxidase and ascorbate peroxidase, were first used to measure dynamic heme fluxes in *C. elegans*.[75] Ascorbate peroxidase has also been used recently to monitor heme concentrations and distributions in live cells[77] using fluorescence lifetime imaging microscopy. In this work, miniscule concentrations (a few nM) of free heme were identified—corresponding to one molecule or less per cellular compartment. These observations are consistent with a system that sequesters free heme.

The Use of Heme Sensors to Study Heme Protein Maturation

Applications of heme sensors can extend beyond the determination of heme concentrations. A GFP-labeled version of cytochrome *c* peroxidase has been recently developed and used to study heme protein maturation by heme insertion.[119] In this design, the percentage of the heme-bound sensor in yeast cells was revealed by the relative amplitudes of exponential-decay components in the emission measured by fluorescence lifetime imaging. This provides a forward-looking approach to establish in real-time the dynamic processes involved in the folding process that accompanies the formation of heme proteins.

Alternative Approaches

There are other technological approaches to heme quantification, including the use of the antimalarial 4-aminoquinoline probe[180] and peptide-based fluorescent probes.[181] The use of heme catabolites—biliverdin and bilirubin—as a way of tracking and studying heme biochemistry is also promising and is starting to provide interesting insights into the interplay between the biochemistry of heme and other biological pathways.[182−189]

POSSIBLE MECHANISMS OF HEME TRANSFER

Detailed information on the mechanism to transfer heme from one place to another—for example between protein partners—is as yet poorly defined. It has been suggested[77] that an exchange mechanism between protein partners might play a role, as shown in Figure 5. This is envisaged as heme exchange between a donor, which could be a buffering molecule or a chaperone, and an acceptor such as a heme protein or a heme sensor. This heme exchange could take place by a range of different pathways (corresponding to dissociative or associative mechanisms) for delivery of heme to specific acceptors. The existence of such a mechanism, as outlined in Figure 5, would account for the buffering of the concentration of free heme, changes in heme availability, and how cells are able to hoard supplies of heme despite the undesirable effects of heme. It

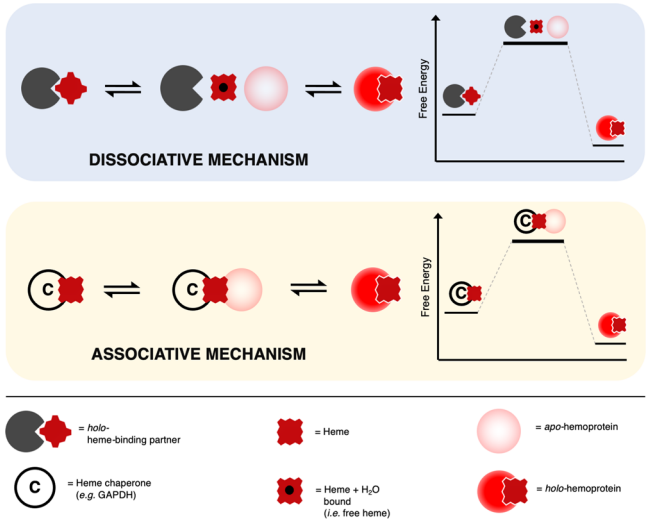

Figure 5. Possible mechanisms for exchange of heme. Heme-binding partners (dark gray pacmans) are envisaged as transferring heme to heme proteins (red circles) by dissociative (pale gray box) or associative (pale yellow box) pathways, resembling classical ligand exchange mechanisms in coordination chemistry. In a dissociative pathway, a free molecule of heme (assumed to be coordinated by a water molecule) is formed transiently following dissociation from a heme-binding partner, and is intercepted by an *apo*-heme protein (faded red circles). Alternatively, an associative exchange of heme is possible and is shown here for the example of heme delivery by chaperones (C, circles). This latter mechanism may provide better selectivity toward the target heme protein. However, we do not envisage this as being exclusive to chaperones, but a mechanism which, in principle, is available to be used by heme-binding partners as well in delivering heme to apo heme proteins. The different mechanisms of heme exchange may help to fine-tune the delivery of heme to specific acceptors.

https://doi.org/10.1021/jacsau.1c00288
JACS Au 2021, 1, 1541−1555

would also provide a responsive capability for mobilization of heme when and where needed.

SUMMARY AND FUTURE OUTLOOK

The logistics for the distribution of heme in cells have yet to be fully discovered. In practice, the dynamic requirements of cellular supply and demand may be complex, and perhaps there is no single mechanism for movement of heme within cells that dominates. Chaperones, heme-binding partners, membranes, and transporters may well work together in a concerted way and could provide contingencies for heme supply under conditions where the cell needs to react quickly to changes in heme demand. We see the role of a buffered reservoir of heme-binding proteins, potentially in large numbers, as being important. This could allow heme to travel from one place to another, where molecules of heme hitchhike across the cell by binding to whichever protein(s) they can find en route to their final destination.

AUTHOR INFORMATION

Corresponding Authors

Andrew J. Hudson − *Department of Chemistry and Leicester Institute of Structural and Chemical Biology, University of Leicester, Leicester LE1 7RH, U.K.;* orcid.org/0000-0003-1849-9666; Email: andrew.hudson@leicester.ac.uk

Emma L. Raven − *School of Chemistry, University of Bristol, Bristol BS8 1TS, U.K.;* orcid.org/0000-0002-1643-8694; Email: emma.raven@bristol.ac.uk

Authors

Andrea E. Gallio − *School of Chemistry, University of Bristol, Bristol BS8 1TS, U.K.;* orcid.org/0000-0003-3094-681X

Simon S.-P. Fung − *Department of Chemistry and Leicester Institute of Structural and Chemical Biology, University of Leicester, Leicester LE1 7RH, U.K.;* orcid.org/0000-0003-0789-7765

Ana Cammack-Najera − *School of Chemistry, University of Bristol, Bristol BS8 1TS, U.K.;* orcid.org/0000-0001-5043-5940

Complete contact information is available at: https://pubs.acs.org/10.1021/jacsau.1c00288

Notes

The authors declare no competing financial interest.

ACKNOWLEDGMENTS

The research was supported by the Leverhulme Trust (RPG-2016- 397) awarded to A.J.H. and E.L.R.; A.E.G. is grateful to the Engineering and Physical Sciences Research Council for a PhD studentship.

REFERENCES

(1) Moss, G. P.; Smith, P. A. S.; Tavernier, D. Glossary of class names of organic compounds and reactivity intermediates based on structure (IUPAC Recommendations 1995). *Pure Appl. Chem.* **1995**, *67* (8−9), 1307−1375.

(2) Martinez, S. E.; Huang, D.; Szczepaniak, A.; Cramer, W. A.; Smith, J. L. Crystal structure of chloroplast cytochrome f reveals a novel cytochrome fold and unexpected heme ligation. *Structure* **1994**, *2* (2), 95−105.

(3) Smith, L. J.; Kahraman, A.; Thornton, J. M. Heme proteins–diversity in structural characteristics, function, and folding. *Proteins: Struct., Funct., Genet.* **2010**, *78* (10), 2349−68.

(4) Perutz, M. F. Relation between structure and sequence of haemoglobin. *Nature* **1962**, *194* (4832), 914−917.

(5) Kendrew, J. C.; Watson, H. C.; Strandberg, B. E.; Dickerson, R. E.; Phillips, D. C.; Shore, V. C. A Partial Determination by X-ray Methods, and its Correlation with Chemical Data. *Nature* **1961**, *190* (4777), 666−670.

(6) Poulos, T. L. Heme enzyme structure and function. *Chem. Rev.* **2014**, *114* (7), 3919−62.

(7) Ascenzi, P.; Bellelli, A.; Coletta, M.; Colosimo, A.; Falcioni, G.; Giacometti, G. M.; Ippoliti, R.; Zolla, L.; Giardina, B. Multiple strategies for O2 transport: from simplicity to complexity. *IUBMB Life* **2007**, *59* (8−9), 600−16.

(8) Moody, P. C. E.; Raven, E. L. The Nature and Reactivity of Ferryl Heme in Compounds I and II. *Acc. Chem. Res.* **2018**, *51* (2), 427−435.

(9) Stuehr, D. J.; Haque, M. M. Nitric oxide synthase enzymology in the 20 years after the Nobel Prize. *Br. J. Pharmacol.* **2019**, *176* (2), 177−188.

(10) Rouzer, C. A.; Marnett, L. J. Cyclooxygenases: structural and functional insights. *J. Lipid Res.* **2009**, *50*, S29−S34.

(11) Shimizu, T.; Lengalova, A.; Martinek, V.; Martinkova, M. Heme: emergent roles of heme in signal transduction, functional regulation and as catalytic centres. *Chem. Soc. Rev.* **2019**, *48* (24), 5624−5657.

(12) Shimizu, T.; Huang, D.; Yan, F.; Stranava, M.; Bartosova, M.; Fojtikova, V.; Martinkova, M. Gaseous O2, NO, and CO in signal transduction: structure and function relationships of heme-based gas sensors and heme-redox sensors. *Chem. Rev.* **2015**, *115* (13), 6491−533.

(13) Shimizu, T. Binding of cysteine thiolate to the Fe(III) heme complex is critical for the function of heme sensor proteins. *J. Inorg. Biochem.* **2012**, *108*, 171−7.

(14) Sweeny, E. A.; Schlanger, S.; Stuehr, D. J. Dynamic regulation of NADPH oxidase 5 by intracellular heme levels and cellular chaperones. *Redox Biol.* **2020**, *36*, 101656.

(15) Nishinaga, M.; Sugimoto, H.; Nishitani, Y.; Nagai, S.; Nagatoishi, S.; Muraki, N.; Tosha, T.; Tsumoto, K.; Aono, S.; Shiro, Y.; Sawai, H. Heme controls the structural rearrangement of its sensor protein mediating the hemolytic bacterial survival. *Commun. Biol.* **2021**, *4* (1), 467.

(16) Zhao, L.; Xie, H.; Kang, Y.; Lin, Y.; Liu, G.; Sakato-Antoku, M.; Patel-King, R. S.; Wang, B.; Wan, C.; King, S. M.; Zhao, C.; Huang, K. Heme-binding protein CYB5D1 is a radial spoke component required for coordinated ciliary beating. *Proc. Natl. Acad. Sci. U. S. A.* **2021**, *118* (17), e2015689118.

(17) Layer, G.; Reichelt, J.; Jahn, D.; Heinz, D. W. Structure and function of enzymes in heme biosynthesis. *Protein Sci.* **2010**, *19* (6), 1137−61.

(18) Matsui, T.; Unno, M.; Ikeda-Saito, M. Heme oxygenase reveals its strategy for catalyzing three successive oxygenation reactions. *Acc. Chem. Res.* **2010**, *43* (2), 240−7.

(19) Unno, M.; Matsui, T.; Ikeda-Saito, M. Structure and catalytic mechanism of heme oxygenase. *Nat. Prod. Rep.* **2007**, *24* (3), 553−70.

(20) Siracusa, R.; Schaufler, A.; Calabrese, V.; Fuller, P. M.; Otterbein, L. E. Carbon Monoxide: from Poison to Clinical Trials. *Trends Pharmacol. Sci.* **2021**, *42* (5), 329−339.

(21) Shen, J.; Sheng, X.; Chang, Z.; Wu, Q.; Wang, S.; Xuan, Z.; Li, D.; Wu, Y.; Shang, Y.; Kong, X.; Yu, L.; Li, L.; Ruan, K.; Hu, H.; Huang, Y.; Hui, L.; Xie, D.; Wang, F.; Hu, R. Iron metabolism regulates p53 signaling through direct heme-p53 interaction and modulation of p53 localization, stability, and function. *Cell Rep.* **2014**, *7* (1), 180−93.

(22) Carter, E. L.; Ramirez, Y.; Ragsdale, S. W. The heme-regulatory motif of nuclear receptor Rev-erbbeta is a key mediator of heme and redox signaling in circadian rhythm maintenance and metabolism. *J. Biol. Chem.* **2017**, *292* (27), 11280−11299.

(23) Carter, E. L.; Gupta, N.; Ragsdale, S. W. High Affinity Heme Binding to a Heme Regulatory Motif on the Nuclear Receptor Rev-erbbeta Leads to Its Degradation and Indirectly Regulates Its

Interaction with Nuclear Receptor Corepressor. *J. Biol. Chem.* **2016**, *291* (5), 2196−222.
(24) Gupta, N.; Ragsdale, S. W. Thiol-disulfide redox dependence of heme binding and heme ligand switching in nuclear hormone receptor rev-erb{beta}. *J. Biol. Chem.* **2011**, *286* (6), 4392−403.
(25) Wu, N.; Yin, L.; Hanniman, E. A.; Joshi, S.; Lazar, M. A. Negative feedback maintenance of heme homeostasis by its receptor, Rev-erbalpha. *Genes Dev.* **2009**, *23* (18), 2201−9.
(26) Rogers, P. M.; Ying, L.; Burris, T. P. Relationship between circadian oscillations of Rev-erbalpha expression and intracellular levels of its ligand, heme. *Biochem. Biophys. Res. Commun.* **2008**, *368* (4), 955−8.
(27) Yin, L.; Wu, N.; Curtin, J. C.; Qatanani, M.; Szwergold, N. R.; Reid, R. A.; Waitt, G. M.; Parks, D. J.; Pearce, K. H.; Wisely, G. B.; Lazar, M. A. Rev-erbalpha, a heme sensor that coordinates metabolic and circadian pathways. *Science* **2007**, *318* (5857), 1786−9.
(28) Raghuram, S.; Stayrook, K. R.; Huang, P.; Rogers, P. M.; Nosie, A. K.; McClure, D. B.; Burris, L. L.; Khorasanizadeh, S.; Burris, T. P.; Rastinejad, F. Identification of heme as the ligand for the orphan nuclear receptors REV-ERBalpha and REV-ERBbeta. *Nat. Struct. Mol. Biol.* **2007**, *14* (12), 1207−13.
(29) Kitanishi, K.; Igarashi, J.; Hayasaka, K.; Hikage, N.; Saiful, I.; Yamauchi, S.; Uchida, T.; Ishimori, K.; Shimizu, T. Heme-binding characteristics of the isolated PAS-A domain of mouse Per2, a transcriptional regulatory factor associated with circadian rhythms. *Biochemistry* **2008**, *47* (23), 6157−68.
(30) Airola, M. V.; Du, J.; Dawson, J. H.; Crane, B. R. Heme binding to the Mammalian circadian clock protein period 2 is nonspecific. *Biochemistry* **2010**, *49* (20), 4327−38.
(31) Hayasaka, K.; Kitanishi, K.; Igarashi, J.; Shimizu, T. Heme-binding characteristics of the isolated PAS-B domain of mouse Per2, a transcriptional regulatory factor associated with circadian rhythms. *Biochim. Biophys. Acta, Proteins Proteomics* **2011**, *1814* (2), 326−33.
(32) Mukaiyama, Y.; Uchida, T.; Sato, E.; Sasaki, A.; Sato, Y.; Igarashi, J.; Kurokawa, H.; Sagami, I.; Kitagawa, T.; Shimizu, T. Spectroscopic and DNA-binding characterization of the isolated heme-bound basic helix-loop-helix-PAS-A domain of neuronal PAS protein 2 (NPAS2), a transcription activator protein associated with circadian rhythms. *FEBS J.* **2006**, *273* (11), 2528−39.
(33) Dioum, E. M.; Rutter, J.; Tuckerman, J. R.; Gonzalez, G.; Gilles-Gonzalez, M. A.; McKnight, S. L. NPAS2: a gas-responsive transcription factor. *Science* **2002**, *298* (5602), 2385−7.
(34) Uchida, T.; Sagami, I.; Shimizu, T.; Ishimori, K.; Kitagawa, T. Effects of the bHLH domain on axial coordination of heme in the PAS-A domain of neuronal PAS domain protein 2 (NPAS2): conversion from His119/Cys170 coordination to His119/His171 coordination. *J. Inorg. Biochem.* **2012**, *108*, 188−95.
(35) Koudo, R.; Kurokawa, H.; Sato, E.; Igarashi, J.; Uchida, T.; Sagami, I.; Kitagawa, T.; Shimizu, T. Spectroscopic characterization of the isolated heme-bound PAS-B domain of neuronal PAS domain protein 2 associated with circadian rhythms. *FEBS J.* **2005**, *272* (16), 4153−62.
(36) Ishida, M.; Ueha, T.; Sagami, I. Effects of mutations in the heme domain on the transcriptional activity and DNA-binding activity of NPAS2. *Biochem. Biophys. Res. Commun.* **2008**, *368* (2), 292−7.
(37) Freeman, S. L.; Kwon, H.; Portolano, N.; Parkin, G.; Venkatraman Girija, U.; Basran, J.; Fielding, A. J.; Fairall, L.; Svistunenko, D. A.; Moody, P. C. E.; Schwabe, J. W. R.; Kyriacou, C. P.; Raven, E. L. Heme binding to human CLOCK affects interactions with the E-box. *Proc. Natl. Acad. Sci. U. S. A.* **2019**, *116* (40), 19911−19916.
(38) Lukat-Rodgers, G. S.; Correia, C.; Botuyan, M. V.; Mer, G.; Rodgers, K. R. Heme-based sensing by the mammalian circadian protein CLOCK. *Inorg. Chem.* **2010**, *49* (14), 6349−65.
(39) Minegishi, S.; Sagami, I.; Negi, S.; Kano, K.; Kitagishi, H. Circadian clock disruption by selective removal of endogenous carbon monoxide. *Sci. Rep.* **2018**, *8* (1), 11996.
(40) Klemz, R.; Reischl, S.; Wallach, T.; Witte, N.; Jurchott, K.; Klemz, S.; Lang, V.; Lorenzen, S.; Knauer, M.; Heidenreich, S.; Xu, M.; Ripperger, J. A.; Schupp, M.; Stanewsky, R.; Kramer, A. Reciprocal regulation of carbon monoxide metabolism and the circadian clock. *Nat. Struct. Mol. Biol.* **2017**, *24* (1), 15−22.
(41) Sarkar, A.; Carter, E. L.; Harland, J. B.; Speelman, A. L.; Lehnert, N.; Ragsdale, S. W. Ferric heme as a CO/NO sensor in the nuclear receptor Rev-Erbss by coupling gas binding to electron transfer. *Proc. Natl. Acad. Sci. U. S. A.* **2021**, *118* (3), e2016717118.
(42) Mosure, S. A.; Strutzenberg, T. S.; Shang, J.; Munoz-Tello, P.; Solt, L. A.; Griffin, P. R.; Kojetin, D. J. Structural basis for heme-dependent NCoR binding to the transcriptional repressor REV-ERBbeta. *Sci. Adv.* **2021**, *7* (5), eabc6479.
(43) Janciauskiene, S.; Vijayan, V.; Immenschuh, S. TLR4 Signaling by Heme and the Role of Heme-Binding Blood Proteins. *Front. Immunol.* **2020**, *11*, 1964.
(44) Sudan, K.; Vijayan, V.; Madyaningrana, K.; Gueler, F.; Igarashi, K.; Foresti, R.; Motterlini, R.; Immenschuh, S. TLR4 activation alters labile heme levels to regulate BACH1 and heme oxygenase-1 expression in macrophages. *Free Radical Biol. Med.* **2019**, *137*, 131−142.
(45) van Wijk, K.; Akabane, T.; Kimura, T.; Saitoh, S.; Okano, S.; Kelly, V. P.; Takagi, M.; Kodama, K.; Takahashi, K.; Tanaka, T.; Nakajima, M.; Nakajima, O. Heterozygous disruption of ALAS1 in mice causes an accelerated age-dependent reduction in free heme, but not total heme, in skeletal muscle and liver. *Arch. Biochem. Biophys.* **2021**, *697*, 108721.
(46) Tang, X. D.; Xu, R.; Reynolds, M. F.; Garcia, M. L.; Heinemann, S. H.; Hoshi, T. Haem can bind to and inhibit mammalian calcium-dependent Slo1 BK channels. *Nature* **2003**, *425* (6957), 531−5.
(47) Sahoo, N.; Goradia, N.; Ohlenschlager, O.; Schonherr, R.; Friedrich, M.; Plass, W.; Kappl, R.; Hoshi, T.; Heinemann, S. H. Heme impairs the ball-and-chain inactivation of potassium channels. *Proc. Natl. Acad. Sci. U. S. A.* **2013**, *110* (42), E4036−44.
(48) Wang, S.; Publicover, S.; Gu, Y. An oxygen-sensitive mechanism in regulation of epithelial sodium channel. *Proc. Natl. Acad. Sci. U. S. A.* **2009**, *106* (8), 2957−62.
(49) Burton, M. J.; Kapetanaki, S. M.; Chernova, T.; Jamieson, A. G.; Dorlet, P.; Santolini, J.; Moody, P. C.; Mitcheson, J. S.; Davies, N. W.; Schmid, R.; Raven, E. L.; Storey, N. M. A heme-binding domain controls regulation of ATP-dependent potassium channels. *Proc. Natl. Acad. Sci. U. S. A.* **2016**, *113* (14), 3785−90.
(50) Augustynek, B.; Kudin, A. P.; Bednarczyk, P.; Szewczyk, A.; Kunz, W. S. Hemin inhibits the large conductance potassium channel in brain mitochondria: a putative novel mechanism of neuro-degeneration. *Exp. Neurol.* **2014**, *257*, 70−5.
(51) Horrigan, F. T.; Heinemann, S. H.; Hoshi, T. Heme regulates allosteric activation of the Slo1 BK channel. *J. Gen. Physiol.* **2005**, *126* (1), 7−21.
(52) Burton, M. J.; Cresser-Brown, J.; Thomas, M.; Portolano, N.; Basran, J.; Freeman, S. L.; Kwon, H.; Bottrill, A. R.; Llansola-Portoles, M. J.; Pascal, A. A.; Jukes-Jones, R.; Chernova, T.; Schmid, R.; Davies, N. W.; Storey, N. M.; Dorlet, P.; Moody, P. C. E.; Mitcheson, J. S.; Raven, E. L. Discovery of a heme-binding domain in a neuronal voltage-gated potassium channel. *J. Biol. Chem.* **2020**, *295* (38), 13277−13286.
(53) Wilkinson, W. J.; Kemp, P. J. Carbon monoxide: an emerging regulator of ion channels. *J. Physiol.* **2011**, *589* (13), 3055−3062.
(54) Kapetanaki, S. M.; Burton, M. J.; Basran, J.; Uragami, C.; Moody, P. C. E.; Mitcheson, J. S.; Schmid, R.; Davies, N. W.; Dorlet, P.; Vos, M. H.; Storey, N. M.; Raven, E. A mechanism for CO regulation of ion channels. *Nat. Commun.* **2018**, *9* (1), 907.
(55) Peers, C.; Boyle, J. P.; Scragg, J. L.; Dallas, M. L.; Al-Owais, M. M.; Hettiarachichi, N. T.; Elies, J.; Johnson, E.; Gamper, N.; Steele, D. S. Diverse mechanisms underlying the regulation of ion channels by carbon monoxide. *Br. J. Pharmacol.* **2015**, *172* (6), 1546−56.
(56) Hou, S.; Xu, R.; Heinemann, S. H.; Hoshi, T. The RCK1 high-affinity Ca2+ sensor confers carbon monoxide sensitivity to Slo1 BK channels. *Proc. Natl. Acad. Sci. U. S. A.* **2008**, *105* (10), 4039−43.

https://doi.org/10.1021/jacsau.1c00288
JACS Au 2021, 1, 1541−1555

(57) Yi, L.; Morgan, J. T.; Ragsdale, S. W. Identification of a thiol/disulfide redox switch in the human BK channel that controls its affinity for heme and CO. *J. Biol. Chem.* **2010**, *285* (26), 20117−27.
(58) Kuhl, T.; Wissbrock, A.; Goradia, N.; Sahoo, N.; Galler, K.; Neugebauer, U.; Popp, J.; Heinemann, S. H.; Ohlenschlager, O.; Imhof, D. Analysis of Fe(III) heme binding to cysteine-containing heme-regulatory motifs in proteins. *ACS Chem. Biol.* **2013**, *8* (8), 1785−93.
(59) Jaggar, J. H.; Li, A.; Parfenova, H.; Liu, J.; Umstot, E. S.; Dopico, A. M.; Leffler, C. W. Heme is a carbon monoxide receptor for large-conductance Ca2+-activated K+ channels. *Circ. Res.* **2005**, *97* (8), 805−12.
(60) Williams, S. E.; Brazier, S. P.; Baban, N.; Telezhkin, V.; Muller, C. T.; Riccardi, D.; Kemp, P. J. A structural motif in the C-terminal tail of slo1 confers carbon monoxide sensitivity to human BK Ca channels. *Pfluegers Arch.* **2008**, *456* (3), 561−72.
(61) Kemp, P. J. Hemeoxygenase-2 as an O2 sensor in K+ channel-dependent chemotransduction. *Biochem. Biophys. Res. Commun.* **2005**, *338* (1), 648−52.
(62) Williams, S. E.; Wootton, P.; Mason, H. S.; Bould, J.; Iles, D. E.; Riccardi, D.; Peers, C.; Kemp, P. J. Hemoxygenase-2 is an oxygen sensor for a calcium-sensitive potassium channel. *Science* **2004**, *306* (5704), 2093−7.
(63) Hou, S.; Heinemann, S. H.; Hoshi, T. Modulation of BKCa channel gating by endogenous signaling molecules. *Physiology* **2009**, *24*, 26−35.
(64) Wang, G. Mechanistic insight into the heme-independent interplay between iron and carbon monoxide in CFTR and Slo1 BKCa channels. *Metallomics* **2017**, *9* (6), 634−645.
(65) Peers, C.; Dallas, M. L.; Scragg, J. L. Ion channels as effectors in carbon monoxide signaling. *Commun. Integr. Biol.* **2009**, *2* (3), 241−2.
(66) Motterlini, R.; Otterbein, L. E. The therapeutic potential of carbon monoxide. *Nat. Rev. Drug Discovery* **2010**, *9* (9), 728−43.
(67) Peers, C. Modulation of ion channels and transporters by carbon monoxide: causes for concern? *Front. Physiol.* **2012**, *3*, 477.
(68) Wu, J. Y.; Qu, H. Y.; Shang, Z. L.; Tao, S. T.; Xu, G. H.; Wu, J.; Wu, H. Q.; Zhang, S. L. Reciprocal regulation of Ca(2)+-activated outward K+ channels of Pyrus pyrifolia pollen by heme and carbon monoxide. *New Phytol.* **2011**, *189* (4), 1060−1068.
(69) Gessner, G.; Ruhl, P.; Westerhausen, M.; Hoshi, T.; Heinemann, S. H. Fe(2+)-Mediated Activation of BKCa Channels by Rapid Photolysis of CORM-S1 Releasing CO and Fe(2). *ACS Chem. Biol.* **2020**, *15* (8), 2098−2106.
(70) Dailey, H. A. *Biosynthesis of Heme and Cholorophylls*; McGraw-Hill: New York, 1990.
(71) Hunt, T.; Vanderhoff, G.; London, I. M. Control of globin synthesis: the role of heme. *J. Mol. Biol.* **1972**, *66* (3), 471−81.
(72) Lodola, A.; Jones, O. T. G. Evidence for a rapidly turned over pool of haem in isolated hepatocytes. *FEBS Lett.* **1978**, *90* (2), 250−254.
(73) Wissbrock, A.; Imhof, D. A Tough Nut to Crack: Intracellular Detection and Quantification of Heme in Malaria Parasites by a Genetically Encoded Protein Sensor. *ChemBioChem* **2017**, *18* (16), 1561−1564.
(74) Aich, A.; Freundlich, M.; Vekilov, P. G. The free heme concentration in healthy human erythrocytes. *Blood Cells, Mol., Dis.* **2015**, *55* (4), 402−9.
(75) Yuan, X.; Rietzschel, N.; Kwon, H.; Walter Nuno, A. B.; Hanna, D. A.; Phillips, J. D.; Raven, E. L.; Reddi, A. R.; Hamza, I. Regulation of intracellular heme trafficking revealed by subcellular reporters. *Proc. Natl. Acad. Sci. U. S. A.* **2016**, *113* (35), E5144−52.
(76) Song, Y.; Yang, M.; Wegner, S. V.; Zhao, J.; Zhu, R.; Wu, Y.; He, C.; Chen, P. R. A Genetically Encoded FRET Sensor for Intracellular Heme. *ACS Chem. Biol.* **2015**, *10* (7), 1610−5.
(77) Leung, G. C.; Fung, S. S.; Gallio, A. E.; Blore, R.; Alibhai, D.; Raven, E. L.; Hudson, A. J. Unravelling the mechanisms controlling heme supply and demand. *Proc. Natl. Acad. Sci. U. S. A.* **2021**, *118* (22), E2104008118.
(78) Abshire, J. R.; Rowlands, C. J.; Ganesan, S. M.; So, P. T.; Niles, J. C. Quantification of labile heme in live malaria parasites using a genetically encoded biosensor. *Proc. Natl. Acad. Sci. U. S. A.* **2017**, *114* (11), E2068−E2076.
(79) Hanna, D. A.; Harvey, R. M.; Martinez-Guzman, O.; Yuan, X.; Chandrasekharan, B.; Raju, G.; Outten, F. W.; Hamza, I.; Reddi, A. R. Heme dynamics and trafficking factors revealed by genetically encoded fluorescent heme sensors. *Proc. Natl. Acad. Sci. U. S. A.* **2016**, *113* (27), 7539−44.
(80) Bonkovsky, H. L.; Guo, J. T.; Hou, W.; Li, T.; Narang, T.; Thapar, M. Porphyrin and heme metabolism and the porphyrias. *Compr Physiol* **2013**, *3* (1), 365−401.
(81) Bonkovsky, H. L.; Healey, J. F.; Lourie, A. N.; Gerron, G. G. Intravenous heme-albumin in acute intermittent porphyria: evidence for repletion of hepatic hemoproteins and regulatory heme pools. *Am. J. Gastroenterol.* **1991**, *86* (8), 1050−1056.
(82) Woodard, S. I.; Dailey, H. A. Regulation of heme biosynthesis in Escherichia coli. *Arch. Biochem. Biophys.* **1995**, *316* (1), 110−5.
(83) Granick, S.; Sinclair, P.; Sassa, S.; Grieninger, G. Effects by heme, insulin, and serum albumin on heme and protein synthesis in chick embryo liver cells cultured in a chemically defined medium, and a spectrofluorometric assay for porphyrin composition. *J. Biol. Chem.* **1975**, *250* (24), 9215−25.
(84) Eriksen, L. So-called free erythrocyte protoporphyrin and its possible role in hemoglobin formation. *Acta Physiol. Scand.* **1961**, *53*, 288−99.
(85) van Huystee, R. B. Relationship of the Heme Moiety of Peroxidase and the Free Heme Pool in Cultured Peanut Cells. *Z. Pflanzenphysiol.* **1977**, *84* (5), 427−433.
(86) Tangeras, A.; Flatmark, T. In vitro binding of protoheme IX and protoporphyrin IX to components in the matrix of rat liver mitochondria. *Biochim. Biophys. Acta, Gen. Subj.* **1979**, *588* (2), 201−10.
(87) Granick, S.; Beale, S. I. Hemes, chlorophylls, and related compounds: biosynthesis and metabolic regulation. *Adv. Enzymol. Relat. Areas Mol. Biol.* **2006**, *46*, 33−203.
(88) Bonkowsky, H. L.; Sinclair, P. R.; Sinclair, J. F. Hepatic heme metabolism and its control. *Yale J. Biol. Med.* **1979**, *52* (1), 13−37.
(89) Thomas, J.; Weinstein, J. D. Measurement of heme efflux and heme content in isolated developing chloroplasts. *Plant Physiol.* **1990**, *94* (3), 1414−23.
(90) Celier, C.; Cresteil, T. Control of cytochromes P450 expression in Gunn rat liver: implication of the intracellular heme pool. *Arch. Biochem. Biophys.* **1991**, *290* (2), 407−10.
(91) Atamna, H. Heme, iron, and the mitochondrial decay of ageing. *Ageing Res. Rev.* **2004**, *3* (3), 303−18.
(92) Kumar, S.; Bandyopadhyay, U. Free heme toxicity and its detoxification systems in human. *Toxicol. Lett.* **2005**, *157* (3), 175−88.
(93) Correia, M. A.; Sinclair, P. R.; De Matteis, F. Cytochrome P450 regulation: the interplay between its heme and apoprotein moieties in synthesis, assembly, repair, and disposal. *Drug Metab. Rev.* **2011**, *43* (1), 1−26.
(94) Khan, A. A.; Quigley, J. G. Control of intracellular heme levels: heme transporters and heme oxygenases. *Biochim. Biophys. Acta, Mol. Cell Res.* **2011**, *1813* (5), 668−82.
(95) Garcia-Santos, D.; Schranzhofer, M.; Horvathova, M.; Jaberi, M. M.; Bogo Chies, J. A.; Sheftel, A. D.; Ponka, P. Heme oxygenase 1 is expressed in murine erythroid cells where it controls the level of regulatory heme. *Blood* **2014**, *123* (14), 2269−77.
(96) Chiabrando, D.; Vinchi, F.; Fiorito, V.; Mercurio, S.; Tolosano, E. Heme in pathophysiology: a matter of scavenging, metabolism and trafficking across cell membranes. *Front. Pharmacol.* **2014**, *5*, 61.
(97) Atamna, H.; Brahmbhatt, M.; Atamna, W.; Shanower, G. A.; Dhahbi, J. M. ApoHRP-based assay to measure intracellular regulatory heme. *Metallomics* **2015**, *7* (2), 309−321.
(98) Ponka, P.; Sheftel, A. D.; English, A. M.; Scott Bohle, D.; Garcia-Santos, D. Do Mammalian Cells Really Need to Export and Import Heme? *Trends Biochem. Sci.* **2017**, *42* (5), 395−406.

https://doi.org/10.1021/jacsau.1c00288
JACS Au 2021, 1, 1541−1555

(99) Israels, L. G.; Yoda, B.; Schacter, B. A. Heme binding and its possible significance in heme movement and availability in the cell. *Ann. N. Y. Acad. Sci.* **1975**, *244*, 651−61.
(100) Ponka, P. Tissue-Specific Regulation of Iron Metabolism and Heme Synthesis: Distinct Control Mechanisms in Erythroid Cells. *Blood* **1997**, *89* (1), 1−25.
(101) Ryter, S. W.; Tyrrell, R. M. The heme synthesis and degradation pathways: role in oxidant sensitivity. Heme oxygenase has both pro- and antioxidant properties. *Free Radical Biol. Med.* **2000**, *28* (2), 289−309.
(102) Sassa, S. Why heme needs to be degraded to iron, biliverdin IXalpha, and carbon monoxide? *Antioxid. Redox Signaling* **2004**, *6* (5), 819−824.
(103) Sachar, M.; Anderson, K. E.; Ma, X. Protoporphyrin IX: the Good, the Bad, and the Ugly. *J. Pharmacol. Exp. Ther.* **2016**, *356* (2), 267−75.
(104) Gbotosho, O. T.; Kapetanaki, M. G.; Kato, G. J. The Worst Things in Life are Free: The Role of Free Heme in Sickle Cell Disease. *Front. Immunol.* **2021**, *11*, 561917.
(105) Reddi, A. R.; Hamza, I. Heme Mobilization in Animals: A Metallolipid's Journey. *Acc. Chem. Res.* **2016**, *49* (6), 1104−10.
(106) Shioda, N.; Yabuki, Y.; Yamaguchi, K.; Onozato, M.; Li, Y.; Kurosawa, K.; Tanabe, H.; Okamoto, N.; Era, T.; Sugiyama, H.; Wada, T.; Fukunaga, K. Targeting G-quadruplex DNA as cognitive function therapy for ATR-X syndrome. *Nat. Med.* **2018**, *24* (6), 802−813.
(107) de Villiers, K. A.; Kaschula, C. H.; Egan, T. J.; Marques, H. M. Speciation and structure of ferriprotoporphyrin IX in aqueous solution: spectroscopic and diffusion measurements demonstrate dimerization, but not mu-oxo dimer formation. *JBIC, J. Biol. Inorg. Chem.* **2007**, *12* (1), 101−17.
(108) Kuter, D.; Streltsov, V.; Davydova, N.; Venter, G. A.; Naidoo, K. J.; Egan, T. J. Molecular structures and solvation of free monomeric and dimeric ferriheme in aqueous solution: insights from molecular dynamics simulations and extended X-ray absorption fine structure spectroscopy. *Inorg. Chem.* **2014**, *53* (20), 10811−24.
(109) Soares, M. P.; Bozza, M. T. Red alert: labile heme is an alarmin. *Curr. Opin. Immunol.* **2016**, *38*, 94−100.
(110) Hanna, D. A.; Martinez-Guzman, O.; Reddi, A. R. Heme Gazing: Illuminating Eukaryotic Heme Trafficking, Dynamics, and Signaling with Fluorescent Heme Sensors. *Biochemistry* **2017**, *56* (13), 1815−1823.
(111) Donegan, R. K.; Moore, C. M.; Hanna, D. A.; Reddi, A. R. Handling heme: The mechanisms underlying the movement of heme within and between cells. *Free Radical Biol. Med.* **2019**, *133*, 88−100.
(112) Hanna, D. A.; Hu, R.; Kim, H.; Martinez-Guzman, O.; Torres, M. P.; Reddi, A. R. Heme bioavailability and signaling in response to stress in yeast cells. *J. Biol. Chem.* **2018**, *293* (32), 12378−12393.
(113) Sweeny, E. A.; Singh, A. B.; Chakravarti, R.; Martinez-Guzman, O.; Saini, A.; Haque, M. M.; Garee, G.; Dans, P. D.; Hannibal, L.; Reddi, A. R.; Stuehr, D. J. Glyceraldehyde-3-phosphate dehydrogenase is a chaperone that allocates labile heme in cells. *J. Biol. Chem.* **2018**, *293* (37), 14557−14568.
(114) Dai, Y.; Sweeny, E. A.; Schlanger, S.; Ghosh, A.; Stuehr, D. J. GAPDH Delivers Heme to Soluble Guanylyl Cyclase. *J. Biol. Chem.* **2020**, *295* (24), 8145.
(115) Fleischhacker, A. S.; Ragsdale, S. W. An unlikely heme chaperone confirmed at last. *J. Biol. Chem.* **2018**, *293* (37), 14569−14570.
(116) Wang, L.; Vijayan, V.; Jang, M. S.; Thorenz, A.; Greite, R.; Rong, S.; Chen, R.; Shushakova, N.; Tudorache, I.; Derlin, K.; Pradhan, P.; Madyaningrana, K.; Madrahimov, N.; Brasen, J. H.; Lichtinghagen, R.; van Kooten, C.; Huber-Lang, M.; Haller, H.; Immenschuh, S.; Gueler, F. Labile Heme Aggravates Renal Inflammation and Complement Activation After Ischemia Reperfusion Injury. *Front. Immunol.* **2019**, *10*, 2975.
(117) Xu, S.; Liu, H. W.; Chen, L.; Yuan, J.; Liu, Y.; Teng, L.; Huan, S. Y.; Yuan, L.; Zhang, X. B.; Tan, W. Learning from Artemisinin: Bioinspired Design of a Reaction-Based Fluorescent Probe for the Selective Sensing of Labile Heme in Complex Biosystems. *J. Am. Chem. Soc.* **2020**, *142* (5), 2129−2133.
(118) Fleischhacker, A. S.; Gunawan, A. L.; Kochert, B. A.; Liu, L.; Wales, T. E.; Borowy, M. C.; Engen, J. R.; Ragsdale, S. W. The heme regulatory motifs of heme oxygenase-2 contribute to the transfer of heme to the catalytic site for degradation. *J. Biol. Chem.* **2020**, *295* (16), 5177−5191.
(119) Dastpeyman, S.; Godin, R.; Cosa, G.; English, A. M. Quantifying Heme-Protein Maturation from Ratiometric Fluorescence Lifetime Measurements on the Single Fluorophore in Its GFP Fusion. *J. Phys. Chem. A* **2020**, *124* (4), 746−754.
(120) O'Keeffe, R.; Latunde-Dada, G. O.; Chen, Y. L.; Kong, X. L.; Cilibrizzi, A.; Hider, R. C. Glutathione and the intracellular labile heme pool. *BioMetals* **2021**, *34* (2), 221−228.
(121) Greenberg, G. R.; Wintrobe, M. M. A labile iron pool. *J. Biol. Chem.* **1946**, *165* (1), 397.
(122) Chorkendorff, I.; Niemantsverdriet, J. W. *Concepts of Modern Catalysis and Kinetics*; Wiley-VCH: Weinheim, Germany, 2003.
(123) Wilkins, R. G.; Wilkins, R. G. *Kinetics and Mechanism of Reactions of Transition Metal Complexes*; VCH Publishers: Weinheim, New York, 1991.
(124) Langford, C. H.; Gray, H. B. *Ligand Substitution Processes*; W.A. Benjamin: New York, 1966.
(125) de Villiers, K. A.; Egan, T. J. Heme Detoxification in the Malaria Parasite: A Target for Antimalarial Drug Development. *Acc. Chem. Res.* **2021**, *54* (11), 2649−2659.
(126) Walter, E. R. H.; Ge, Y.; Mason, J. C.; Boyle, J. J.; Long, N. J. A Coumarin-Porphyrin FRET Break-Apart Probe for Heme Oxygenase-1. *J. Am. Chem. Soc.* **2021**, *143* (17), 6460−6469.
(127) Ponka, P.; Sheftel, A. D.; English, A. M.; Scott Bohle, D.; Garcia-Santos, D. Do Mammalian Cells Really Need to Export and Import Heme? *Trends Biochem. Sci.* **2017**, *42* (5), 395−406.
(128) Maines, M. D. The heme oxygenase system: a regulator of second messenger gases. *Annu. Rev. Pharmacol. Toxicol.* **1997**, *37*, 517−54.
(129) Maines, M. D. Heme oxygenase: function, multiplicity, regulatory mechanisms, and clinical applications. *FASEB J.* **1988**, *2* (10), 2557−68.
(130) Liu, L.; Dumbrepatil, A. B.; Fleischhacker, A. S.; Marsh, E. N. G.; Ragsdale, S. W. Heme oxygenase-2 is post-translationally regulated by heme occupancy in the catalytic site. *J. Biol. Chem.* **2020**, *295* (50), 17227−17240.
(131) Andreini, C.; Bertini, I.; Cavallaro, G.; Holliday, G. L.; Thornton, J. M. Metal ions in biological catalysis: from enzyme databases to general principles. *JBIC, J. Biol. Inorg. Chem.* **2008**, *13* (8), 1205−18.
(132) Bleackley, M. R.; Macgillivray, R. T. Transition metal homeostasis: from yeast to human disease. *BioMetals* **2011**, *24* (5), 785−809.
(133) Finney, L. A.; O'Halloran, T. V. Transition metal speciation in the cell: insights from the chemistry of metal ion receptors. *Science* **2003**, *300* (5621), 931−6.
(134) Foster, A. W.; Osman, D.; Robinson, N. J. Metal preferences and metallation. *J. Biol. Chem.* **2014**, *289* (41), 28095−103.
(135) Outten, C. E.; Albetel, A. N. Iron sensing and regulation in Saccharomyces cerevisiae: Ironing out the mechanistic details. *Curr. Opin. Microbiol.* **2013**, *16* (6), 662−8.
(136) Outten, C. E.; O'Halloran, T. V. Femtomolar sensitivity of metalloregulatory proteins controlling zinc homeostasis. *Science* **2001**, *292* (5526), 2488−92.
(137) Rae, T. D.; Schmidt, P. J.; Pufahl, R. A.; Culotta, V. C.; O'Halloran, T. V. Undetectable intracellular free copper: the requirement of a copper chaperone for superoxide dismutase. *Science* **1999**, *284* (5415), 805−8.
(138) Banci, L.; Bertini, I.; Cantini, F.; Ciofi-Baffoni, S. Cellular copper distribution: a mechanistic systems biology approach. *Cell. Mol. Life Sci.* **2010**, *67* (15), 2563−89.

https://doi.org/10.1021/jacsau.1c00288
JACS Au 2021, 1, 1541−1555

(139) Huffman, D. L.; O'Halloran, T. V. Function, structure, and mechanism of intracellular copper trafficking proteins. *Annu. Rev. Biochem.* **2001**, *70*, 677−701.
(140) Rosenzweig, A. C.; O'Halloran, T. V. Structure and chemistry of the copper chaperone proteins. *Curr. Opin. Chem. Biol.* **2000**, *4* (2), 140−7.
(141) Osman, D.; Martini, M. A.; Foster, A. W.; Chen, J.; Scott, A. J. P.; Morton, R. J.; Steed, J. W.; Lurie-Luke, E.; Huggins, T. G.; Lawrence, A. D.; Deery, E.; Warren, M. J.; Chivers, P. T.; Robinson, N. J. Bacterial sensors define intracellular free energies for correct enzyme metalation. *Nat. Chem. Biol.* **2019**, *15* (3), 241−249.
(142) Osman, D.; Foster, A. W.; Chen, J.; Svedaite, K.; Steed, J. W.; Lurie-Luke, E.; Huggins, T. G.; Robinson, N. J. Fine control of metal concentrations is necessary for cells to discern zinc from cobalt. *Nat. Commun.* **2017**, *8* (1), 1884.
(143) Tottey, S.; Harvie, D. R.; Robinson, N. J. Understanding how cells allocate metals using metal sensors and metallochaperones. *Acc. Chem. Res.* **2005**, *38* (10), 775−83.
(144) Waldron, K. J.; Rutherford, J. C.; Ford, D.; Robinson, N. J. Metalloproteins and metal sensing. *Nature* **2009**, *460* (7257), 823−30.
(145) Ba, L. A.; Doering, M.; Burkholz, T.; Jacob, C. Metal trafficking: from maintaining the metal homeostasis to future drug design. *Metallomics* **2009**, *1* (4), 292−311.
(146) Ma, Z.; Jacobsen, F. E.; Giedroc, D. P. Coordination chemistry of bacterial metal transport and sensing. *Chem. Rev.* **2009**, *109* (10), 4644−81.
(147) Antelo, G. T.; Vila, A. J.; Giedroc, D. P.; Capdevila, D. A. Molecular Evolution of Transition Metal Bioavailability at the Host-Pathogen Interface. *Trends Microbiol.* **2021**, *29* (5), 441−457.
(148) Blindauer, C. A. Bacterial metallothioneins: past, present, and questions for the future. *JBIC, J. Biol. Inorg. Chem.* **2011**, *16* (7), 1011−24.
(149) Blindauer, C. A.; Leszczyszyn, O. I. Metallothioneins: unparalleled diversity in structures and functions for metal ion homeostasis and more. *Nat. Prod. Rep.* **2010**, *27* (5), 720−41.
(150) Daltrop, O.; Stevens, J. M.; Higham, C. W.; Ferguson, S. J. The CcmE protein of the c-type cytochrome biogenesis system: unusual in vitro heme incorporation into apo-CcmE and transfer from holo-CcmE to apocytochrome. *Proc. Natl. Acad. Sci. U. S. A.* **2002**, *99* (15), 9703−8.
(151) Thony-Meyer, L. A heme chaperone for cytochrome c biosynthesis. *Biochemistry* **2003**, *42* (45), 13099−105.
(152) Kranz, R. G.; Richard-Fogal, C.; Taylor, J. S.; Frawley, E. R. Cytochrome c biogenesis: mechanisms for covalent modifications and trafficking of heme and for heme-iron redox control. *Microbiol. Mol. Biol. Rev.* **2009**, *73* (3), 510−28. Table of Contents.
(153) Brausemann, A.; Zhang, L.; Ilcu, L.; Einsle, O. Architecture of the membrane-bound cytochrome c heme lyase CcmF. *Nat. Chem. Biol.* **2021**, *17*, 800−805.
(154) Hannibal, L.; Collins, D.; Brassard, J.; Chakravarti, R.; Vempati, R.; Dorlet, P.; Santolini, J.; Dawson, J. H.; Stuehr, D. J. Heme binding properties of glyceraldehyde-3-phosphate dehydrogenase. *Biochemistry* **2012**, *51* (43), 8514−29.
(155) Huang, Y.; Zhang, P.; Yang, Z.; Wang, P.; Li, H.; Gao, Z. Interaction of glyceraldehyde-3-phosphate dehydrogenase and heme: The relevance of its biological function. *Arch. Biochem. Biophys.* **2017**, *619*, 54−61.
(156) O'Halloran, T. Transition metals in control of gene expression. *Science* **1993**, *261* (5122), 715−725.
(157) *Handbook of Porphyrin Science*; World Scientific Publishing Company, 2012; Vol. *30*, p 512.
(158) Raven, E. L. A short history of heme dioxygenases: rise, fall and rise again. *JBIC, J. Biol. Inorg. Chem.* **2017**, *22* (2−3), 175−183.
(159) Efimov, I.; Basran, J.; Thackray, S. J.; Handa, S.; Mowat, C. G.; Raven, E. L. Structure and reaction mechanism in the heme dioxygenases. *Biochemistry* **2011**, *50* (14), 2717−24.
(160) Millett, E. S.; Efimov, I.; Basran, J.; Handa, S.; Mowat, C. G.; Raven, E. L. Heme-containing dioxygenases involved in tryptophan oxidation. *Curr. Opin. Chem. Biol.* **2012**, *16* (1−2), 60−6.
(161) Lewis-Ballester, A.; Pham, K. N.; Batabyal, D.; Karkashon, S.; Bonanno, J. B.; Poulos, T. L.; Yeh, S. R. Structural insights into substrate and inhibitor binding sites in human indoleamine 2,3-dioxygenase 1. *Nat. Commun.* **2017**, *8* (1), 1693.
(162) Geng, J.; Liu, A. Heme-dependent dioxygenases in tryptophan oxidation. *Arch. Biochem. Biophys.* **2014**, *544*, 18−26.
(163) Nelp, M. T.; Kates, P. A.; Hunt, J. T.; Newitt, J. A.; Balog, A.; Maley, D.; Zhu, X.; Abell, L.; Allentoff, A.; Borzilleri, R.; Lewis, H. A.; Lin, Z.; Seitz, S. P.; Yan, C.; Groves, J. T. Immune-modulating enzyme indoleamine 2,3-dioxygenase is effectively inhibited by targeting its apo-form. *Proc. Natl. Acad. Sci. U. S. A.* **2018**, *115* (13), 3249−3254.
(164) Kikuchi, G.; Hayashi, N. Regulation by heme of synthesis and intracellular translocation of delta-aminolevulinate synthase in the liver. *Mol. Cell. Biochem.* **1981**, *37* (1), 27−41.
(165) Srivastava, K. K.; Cable, E. E.; Donohue, S. E.; Bonkovsky, H. L. Molecular basis for heme-dependent induction of heme oxygenase in primary cultures of chick embryo hepatocytes. Demonstration of acquired refractoriness to heme. *Eur. J. Biochem.* **1993**, *213* (3), 909−17.
(166) Light, W. R., 3rd; Olson, J. S. The effects of lipid composition on the rate and extent of heme binding to membranes. *J. Biol. Chem.* **1990**, *265* (26), 15632−7.
(167) Light, W. R., 3rd; Olson, J. S. Transmembrane movement of heme. *J. Biol. Chem.* **1990**, *265* (26), 15623−31.
(168) Rose, M. Y.; Thompson, R. A.; Light, W. R.; Olson, J. S. Heme Transfer between Phospholipid-Membranes and Uptake by Apohemoglobin. *J. Biol. Chem.* **1985**, *260* (11), 6632−6640.
(169) Chiabrando, D.; Marro, S.; Mercurio, S.; Giorgi, C.; Petrillo, S.; Vinchi, F.; Fiorito, V.; Fagoonee, S.; Camporeale, A.; Turco, E.; Merlo, G. R.; Silengo, L.; Altruda, F.; Pinton, P.; Tolosano, E. The mitochondrial heme exporter FLVCR1b mediates erythroid differentiation. *J. Clin. Invest.* **2012**, *122* (12), 4569−79.
(170) Martinez-Guzman, O.; Willoughby, M. M.; Saini, A.; Dietz, J. V.; Bohovych, I.; Medlock, A. E.; Khalimonchuk, O.; Reddi, A. R. Mitochondrial-nuclear heme trafficking in budding yeast is regulated by GTPases that control mitochondrial dynamics and ER contact sites. *J. Cell Sci.* **2020**, *133* (10), jcs237917.
(171) Chambers, I. G.; Willoughby, M. M.; Hamza, I.; Reddi, A. R. One ring to bring them all and in the darkness bind them: The trafficking of heme without deliverers. *Biochim. Biophys. Acta, Mol. Cell Res.* **2021**, *1868* (1), 118881.
(172) Morrison, G. R. Fluorometric Microdetermination of Heme Protein. *Anal. Chem.* **1965**, *37*, 1124−6.
(173) Masuda, T.; Takahashi, S. Chemiluminescent-based method for heme determination by reconstitution with horseradish peroxidase apo-enzyme. *Anal. Biochem.* **2006**, *355* (2), 307−9.
(174) Hopp, M. T.; Schmalohr, B. F.; Kuhl, T.; Detzel, M. S.; Wissbrock, A.; Imhof, D. Heme Determination and Quantification Methods and Their Suitability for Practical Applications and Everyday Use. *Anal. Chem.* **2020**, *92* (14), 9429−9440.
(175) Lakowicz, J. R. *Principles of Fluorescence Spectroscopy*; Springer: New York, 2006.
(176) Takeda, S.; Kamiya, N.; Nagamune, T. A novel protein-based heme sensor consisting of green fluorescent protein and apocytochrome b562. *Anal. Biochem.* **2003**, *317* (1), 116−119.
(177) Arpino, J. A.; Czapinska, H.; Piasecka, A.; Edwards, W. R.; Barker, P.; Gajda, M. J.; Bochtler, M.; Jones, D. D. Structural basis for efficient chromophore communication and energy transfer in a constructed didomain protein scaffold. *J. Am. Chem. Soc.* **2012**, *134* (33), 13632−40.
(178) Koga, S.; Yoshihara, S.; Bando, H.; Yamasaki, K.; Higashimoto, Y.; Noguchi, M.; Sueda, S.; Komatsu, H.; Sakamoto, H. Development of a heme sensor using fluorescently labeled heme oxygenase-1. *Anal. Biochem.* **2013**, *433* (1), 2−9.

https://doi.org/10.1021/jacsau.1c00288
JACS Au 2021, 1, 1541−1555

(179) Taira, J.; Nakashima, Y.; Yoshihara, S.; Koga, S.; Sueda, S.; Komatsu, H.; Higashimoto, Y.; Takahashi, T.; Tanioka, N.; Shimizu, H.; Morimatsu, H.; Sakamoto, H. Improvement of heme oxygenase-1-based heme sensor for quantifying free heme in biological samples. *Anal. Biochem.* **2015**, *489*, 50−2.
(180) Hisamatsu, Y.; Umezawa, N.; Yagi, H.; Kato, K.; Higuchi, T. Design and synthesis of a 4-aminoquinoline-based molecular tweezer that recognizes protoporphyrin IX and iron(iii) protoporphyrin IX and its application as a supramolecular photosensitizer. *Chem. Sci.* **2018**, *9* (38), 7455−7467.
(181) Newton, L. D.; Pascu, S. I.; Tyrrell, R. M.; Eggleston, I. M. Development of a peptide-based fluorescent probe for biological heme monitoring. *Org. Biomol. Chem.* **2019**, *17* (3), 467−471.
(182) Takeda, T. A.; Mu, A.; Tai, T. T.; Kitajima, S.; Taketani, S. Continuous de novo biosynthesis of haem and its rapid turnover to bilirubin are necessary for cytoprotection against cell damage. *Sci. Rep.* **2015**, *5*, 10488.
(183) McDonagh, A. F.; Palma, L. A.; Lightner, D. A. Blue light and bilirubin excretion. *Science* **1980**, *208* (4440), 145−51.
(184) Kumagai, A.; Ando, R.; Miyatake, H.; Greimel, P.; Kobayashi, T.; Hirabayashi, Y.; Shimogori, T.; Miyawaki, A. A bilirubin-inducible fluorescent protein from eel muscle. *Cell* **2013**, *153* (7), 1602−11.
(185) Nobles, C. L.; Clark, J. R.; Green, S. I.; Maresso, A. W. A dual component heme biosensor that integrates heme transport and synthesis in bacteria. *J. Microbiol. Methods* **2015**, *118*, 7−17.
(186) Glanville, D. G.; Mullineaux-Sanders, C.; Corcoran, C. J.; Burger, B. T.; Imam, S.; Donohue, T. J.; Ulijasz, A. T. A High-Throughput Method for Identifying Novel Genes That Influence Metabolic Pathways Reveals New Iron and Heme Regulation in Pseudomonas aeruginosa. *mSystems* **2021**, *6* (1), e00933-20.
(187) Mourino, S.; Giardina, B. J.; Reyes-Caballero, H.; Wilks, A. Metabolite-driven Regulation of Heme Uptake by the Biliverdin IXbeta/delta-Selective Heme Oxygenase (HemO) of Pseudomonas aeruginosa. *J. Biol. Chem.* **2016**, *291* (39), 20503−15.
(188) Rosa, A.; Pye, V. E.; Graham, C.; Muir, L.; Seow, J.; Ng, K. W.; Cook, N. J.; Rees-Spear, C.; Parker, E.; Dos Santos, M. S.; Rosadas, C.; Susana, A.; Rhys, H.; Nans, A.; Masino, L.; Roustan, C.; Christodoulou, E.; Ulferts, R.; Wrobel, A. G.; Short, C. E.; Fertleman, M.; Sanders, R. W.; Heaney, J.; Spyer, M.; Kjaer, S.; Riddell, A.; Malim, M. H.; Beale, R.; MacRae, J. I.; Taylor, G. P.; Nastouli, E.; van Gils, M. J.; Rosenthal, P. B.; Pizzato, M.; McClure, M. O.; Tedder, R. S.; Kassiotis, G.; McCoy, L. E.; Doores, K. J.; Cherepanov, P. SARS-CoV-2 can recruit a heme metabolite to evade antibody immunity. *Sci. Adv.* **2021**, *7* (22), eabg7607.
(189) Shum, M.; Shintre, C. A.; Althoff, T.; Gutierrez, V.; Segawa, M.; Saxberg, A. D.; Martinez, M.; Adamson, R.; Young, M. R.; Faust, B.; Gharakhanian, R.; Su, S.; Chella Krishnan, K.; Mahdaviani, K.; Veliova, M.; Wolf, D. M.; Ngo, J.; Nocito, L.; Stiles, L.; Abramson, J.; Lusis, A. J.; Hevener, A. L.; Zoghbi, M. E.; Carpenter, E. P.; Liesa, M. ABCB10 exports mitochondrial biliverdin, driving metabolic maladaptation in obesity. *Sci. Transl. Med.* **2021**, *13* (594), eabd1869.
(190) Dawson, J. H. Probing structure-function relations in heme-containing oxygenases and peroxidases. *Science* **1988**, *240* (4851), 433−9.
(191) Ortiz de Montellano, P. R. Control of the catalytic activity of prosthetic heme by the structure of hemoproteins. *Acc. Chem. Res.* **1987**, *20* (8), 289−294.
(192) Ogawa, K.; Sun, J.; Taketani, S.; Nakajima, O.; Nishitani, C.; Sassa, S.; Hayashi, N.; Yamamoto, M.; Shibahara, S.; Fujita, H.; Igarashi, K. Heme mediates derepression of Maf recognition element through direct binding to transcription repressor Bach1. *EMBO J.* **2001**, *20* (11), 2835−43.
(193) Ma, Q. Role of nrf2 in oxidative stress and toxicity. *Annu. Rev. Pharmacol. Toxicol.* **2013**, *53*, 401−26.
(194) Alam, J.; Killeen, E.; Gong, P.; Naquin, R.; Hu, B.; Stewart, D.; Ingelfinger, J. R.; Nath, K. A. Heme activates the heme oxygenase-1 gene in renal epithelial cells by stabilizing Nrf2. *Am. J. Physiol Renal Physiol* **2003**, *284* (4), F743−52.
(195) Burton, M. J.; Kapetanaki, S. M.; Chernova, T.; Jamieson, A. G.; Dorlet, P.; Santolini, J.; Moody, P. C. E.; Mitcheson, J. S.; Davies, N. W.; Schmid, R.; Raven, E. L.; Storey, N. M. A heme-binding domain controls regulation of ATP-dependent potassium channels. *Proc. Natl. Acad. Sci. U. S. A.* **2016**, *113* (14), 3785−3790.
(196) Hamza, I.; Dailey, H. A. One ring to rule them all: trafficking of heme and heme synthesis intermediates in the metazoans. *Biochim. Biophys. Acta, Mol. Cell Res.* **2012**, *1823* (9), 1617−32.

https://doi.org/10.1021/jacsau.1c00288
JACS Au 2021, 1, 1541−1555